Microfluidic Assays for the Characterization of Neutrophils in Biology and Clinical Research

By

Eric Karl-Heinz Sackmann

A dissertation submitted in partial fulfillment of

the requirements for the degree of

Doctor of Philosophy

(Materials Science)

at the

University of Wisconsin – Madison

2013

Date of final oral examination: 04/15/13

The dissertation is approved by the following members of the Final Oral committee:

David J. Beebe, Professor, Biomedical Engineering
Anna Huttenlocher, Professor, Pediatrics
William L. Murphy, Associate Professor, Biomedical Engineering
Patricia J. Keely, Professor, Cell and Regenerative Biology
Justin C. Williams, Associate Professor, Biomedical Engineering

"...there is nothing which can better deserve your patronage than the promotion of science and literature. Knowledge is in every country the surest basis of public happiness. In one in which the measures of government receive their impressions so immediately from the sense of the community as in ours, it is proportionably essential."

President George Washington in his first State of the Union address to Congress
January 8, 1790

"Everything I do depends on other members of our species and the shoulders that we stand on.
And a lot of us want to contribute something back to our species
and to add something to the flow."

Steve Jobs, 2011

Table of Contents

Acknowledgments

I would like to start by thanking my adviser, Dave Beebe, for providing me with the opportunity to shape my graduate studies while lending valuable insights and guidance throughout my time in the lab. It is no accident that your group is producing some of the most compelling work in our field, and your current and future successes are well-deserved. I know you and your students will continue to do great things. I would also like to thank the members of the Microtechnology, Medicine, and Biology lab for all the brainstorming sessions and valuable feedback throughout years. Our lab is highly collaborative, and the projects I have worked on received invaluable contributions from other members of the lab. In particular I would like to acknowledge Edmond Young, Scott Berry, Erwin Berthier, Lauren Bischel, Farsh Moussavi-Harami, John Guckenberger, Jolene Enge, and Adan Gutierrez. I have had the pleasure of working closely with all of you at some point during my graduate career and have benefited from your hard work, experience, and insight. I also wish to acknowledge Anna Huttenlocher and Sameer Mathur, and the researchers from your biology and clinical research labs that I have had the fortune of working with. Having such willing and complimentary partnerships has greatly increased the impact and quality of my work.

I would also like to thank the Materials Science Program and the University of Wisconsin—Madison for giving me the opportunity to join your exceptional cohort of students and faculty. I have never known a more wonderful and fulfilling place to live than Madison, and cannot imagine a better place to have spent the lion's share of my 20's. To Diana Rhoads and Ray Vanderby—you two keep a pretty great program running smoothly and should be proud.

I owe much of my happiness and success at the University of Wisconsin to the love of my life, Anna Fulton. Not only have you been my best friend and partner over my graduate career, but you were also a valuable resource for learning literature search methodologies in my day-to-day research. You and your family—Angus, Marjorie, Loris, Kelly, Elizabeth, Ross, and Sarah—have been a tremendous source of love and support. Thanks for agreeing to marry me.

And to all the other really good friends I have made here (you know who you are), thanks for all of the laughs and great company.

Lastly, I would like to acknowledge my family. To my parents, Peter and Afaf Sackmann, who always offered their full support and encouragement in my academic pursuits. You probably did not think I would end up taking a decade to get through my post-high school education, but I am thankful that you supported me throughout. To my sister Shereen and her husband Justin. I first heard about a great engineering school called Cal Poly from you two, which led me to my first academic stop. I also received convincing warnings from Shereen to stay in school for a while longer as I was completing my degree at Cal Poly, which helped lead me to Madison. Both were valuable pieces of advice that I am thankful I followed. Your six year head start has certainly awarded me some much appreciated wisdom and guidance over the years.

Many thanks and much love.

For my parents, Shereen, Justin,
and my dearest Anna

Abstract

Neutrophils are the most abundant type of white blood cell in the innate immune system, playing a central role in defending the body from pathogens during the initial stages of inflammation. When tissue becomes wounded or infected, neutrophils exit the blood stream and rapidly mobilize towards the site of infection in order to engulf and destroy harmful pathogens and prevent the spread of infection. The directed migration of neutrophils toward the site of inflammation is guided by biochemical changes in the neutrophils' extracellular microenvironment—a process called chemotaxis. Dysfunction in neutrophil chemotaxis is implicated in the pathophysiology of several diseases, including asthma, rheumatoid arthritis, and cancer. The causes of neutrophil chemotaxis dysfunction are complex and still not fully understood. Over the last 50 years, several useful *in vitro* tools have been developed to identify factors that stimulate neutrophil migration, and interrogate other aspects of neutrophil biology. However, currently macroscale chemotaxis assays limit the types of biological and clinical questions that can be addressed in important ways. For example, many macroscale chemotaxis assays cannot precisely control the formation and stability of chemokine concentration gradients throughout an experiment—a critical factor when assessing neutrophil chemotaxis.

To address technical limitations with traditional neutrophil chemotaxis assays, new microfluidic approaches have developed in recent years offering improvements in several key areas, such as lower sample volume requirements and precise control of biochemical gradients. However, these methods usually involve complex fluid handling protocols and technical expertise, which has limited their impact in mainstream biology research. The work presented in this document describes new techniques to assess neutrophil chemotaxis, as well as other important aspects of neutrophil biology. The assays emphasize user-friendly design and only require a micropipet to operate. Furthermore, all the techniques presented here only require a lancet puncture to perform the assay and can be setup within minutes, compared to milliliters of blood and over an hour of preparation time for analogous macroscale assays. These microfluidic technologies were applied to several research and clinical studies that were either difficult or impossible to perform in the past.

The content of my doctoral dissertation can be divided into four primary topics: (1) a review of the field of microfluidics, and more specifically macroscale and microscale chemotaxis assays; (2) the fabrication of microfluidic devices using multiple materials and methods; (3) the development and implementation of *in vitro* microfluidic tools that assay neutrophil biology to study and diagnose diseases; and (4) the development of a biomimetic microfluidic technology that aims to recapitulate the *in vivo* inflammatory response of neutrophils to wounded tissue.

Chapter 1

Contributions of microfluidics to biomedical research: where we are and where we should go

1.1 Introduction

A decade ago, our lab wrote that, "microfluidics has the potential to significantly change the way modern biology is performed."[1] Indeed, we were part of a chorus of researchers that envisioned the possibility of new microfluidic tools making significant contributions to biology and medical research.[2-6] The optimism surrounding microfluidics was well warranted because of the compelling advantages microfluidic approaches could possibly offer over traditional traditional assays used in cell biology. Conceptually, the idea of microfluidics is that fluids can be precisely manipulated using a microscale device that is fabricated using methods first developed by the semiconductor industry. These devices, commonly referred to as miniaturized total analysis system (μTAS)[7,8] or lab-on-a-chip (LoC) technologies, could be applied to applications in biology research to streamline complex assay protocols; require significantly less sample volume, reducing the cost of reagents and avoiding waste of precious samples; provide gains in scalability for screening applications and batch sample processing that is analogous to multi-well plates; and provide the investigator with significantly more control and predictability of the spatio-temporal dynamics of the cell's microenvironment.

This approach to developing comprehensive microfluidic solutions to address problems in biology and clinical research has been embraced by engineers. However, despite significant advancements in microfluidics as a technology platform, the adoption of novel μTAS techniques into mainstream biology research has not matched the initial enthusiasm surrounding the field.[9] Many argue the technology is still in search of a "killer application", where the sample-to-answer concept provides a solution that greatly outperforms current methods.[10,11] In this introductory chapter, we will examine the impact of microfluidic technologies on cell biology and medical research within the last decade. We will briefly review how fluid phenomena at the microscale can be leveraged to accomplish useful tasks that are not achievable at the macroscale. Then we will assess the adoption

rate of microfluidic techniques in mainstream biomedical research and explore what factors may be hindering this adoption process. Finally, we will discuss positive trends in the field and infer lessons that can be applied to future microfluidic technology development.

1.2 What is microfluidics and why is it useful?

The field of microfluidics is characterized by the study and manipulation of fluids at the sub-millimeter length scale. Fluid phenomena for micro- and nano-liter volumes of liquid change significantly compared to the macroscale (Box 1). For example, the role that the force of gravity plays at microscale dimensions is greatly reduced compared to its dominance at the macroscale. Conversely, surface tension and capillary forces are significantly more dominant forces at the microscale, which can be leveraged for a variety of tasks, such as passively pumping fluids in microchannels[12]; precisely patterning surfaces with user-defined substrates[13]; filtering various analytes[14]; and forming mono-disperse droplets[15] in multiphase fluid streams for a variety of applications. These represent a fraction of the myriad of problems that microfluidic technologies have attempted

Box 1: useful microfluidics concepts

Laminar vs. turbulent flow

The Reynolds number (Re) is a dimensionless quantity that describes the ratio of intertial to viscous forces of a fluid. Re is propotional to the characteristic velocity of the fluid and length scale of the system; and Re is inversely proportional to the fluid viscosity. High Re (> ~2,000) fluids have flow profiles that increasingly mix stochastically (turbulent flow). For microfluidic systems, Re is almost always in the laminar flow regime, allowing for highly predictable fluid dynamics. Molecular diffusion also dramatically changes at this scale since convective mixing does not occur, enabling predictable diffusion kinetics.

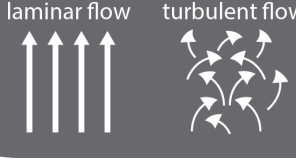

Surface and interfactial tension

Surface tension describes the tendancy of a fluid on a surface to reduce its free energy by contracting the fluid at the surface-air interface. Interfacial tension is a similar phenomenon, but is generally applied to two immiscible fluids (e.g. oil and water). These forces play more dominant roles on the microscale compared to gravity, which is much more dominant on the macro-scale. Researchers have leveraged these phenomena to conduct protein and cell sorting; perform nanoreactions for protein crystalization; and passively drive fluids through microchannels.

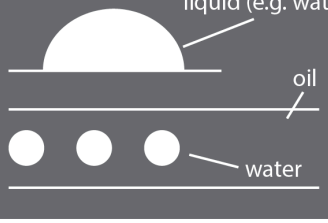

Capillary forces

Capillary action describes the movement of a fluids through a narrow constricution, such as a narrow tube or porous material. At the micro-scale, capillary action often dominates the gravity, allowing fluids to advance in opposition to the force of gravity. Capillary forces have been used to manipulate fluids in many applications, the most famous examples perhaps being the at-home pregnancy test and portable glucometers to monitor blood glucose levels.

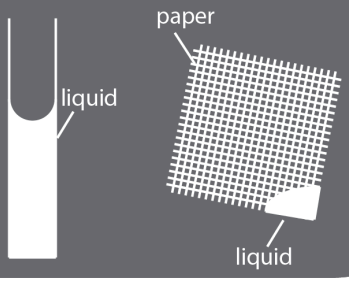

to address. How has the technological advancement and maturity of the microfluidics field translated to end-user adoption and impact?

1.3 The impact of microfluidics in biomedical research

A primary goal for much of the microfluidics community is to develop useful technologies that enhance the capabilities of investigators in biology and medical research. Many microfluidic studies describe methods that aim to replace traditional macroscale assays, and usually perform proof-of-concept (PoC) experiments that demonstrate the efficacy of the new approach. These novel microfluidic methods are usually published in journals that one might characterize as "engineering" journals, or publications whose readership is comprised largely of engineers and other members of the physical sciences (e.g. chemists and physicists). If publishing PoC studies in engineering journals represents the development phase for a novel biology assay, then adoption of the technique is when the technology is utilized and published in a biology or medical journal. After all, the stated goal of virtually all PoC studies is to demonstrate new technologies that enable biologists in their everyday research. So how are we doing so far?

We measured the adoption of microfluidic technologies in mainstream biomedical research within the last decade to assess their potential impact beyond the engineering community (Figure 1). In order to identify broad trends of what journals have published papers that use microfluidics, we defined three categories: (1) "engineering" journals (e.g. *Lab on a chip*, *Small, Analytical Chemistry*); (2) "biology and medical" journals (e.g. *Blood*, *Cell, Journal of Clinical Investigation*); and (3) "multidisciplinary" journals (e.g. *Nature, Science, PNAS*). The results reveal, unsurprisingly, that the overwhelming number of microfluidics papers are still being published in engineering journals (Figure 1a). These engineering journals have facilitated the technological development and growth of microfluidics over the last decade. Multidisciplinary journals helped to expose microfluidics to a broad readership, until about five years ago when the adoption of microfluidic techniques in biomedical research studies began outpacing publications in interdisciplinary journals. Today the share of microfluidics publications is dominated by engineering journals (85%) as the microfluidics community has grown significantly, and biomedical journals have taken some "publication share" from multidisciplinary journals (9% and 6%, respectively; Figure 1b). A closer examination of the authorship affiliations for studies published in biomedical

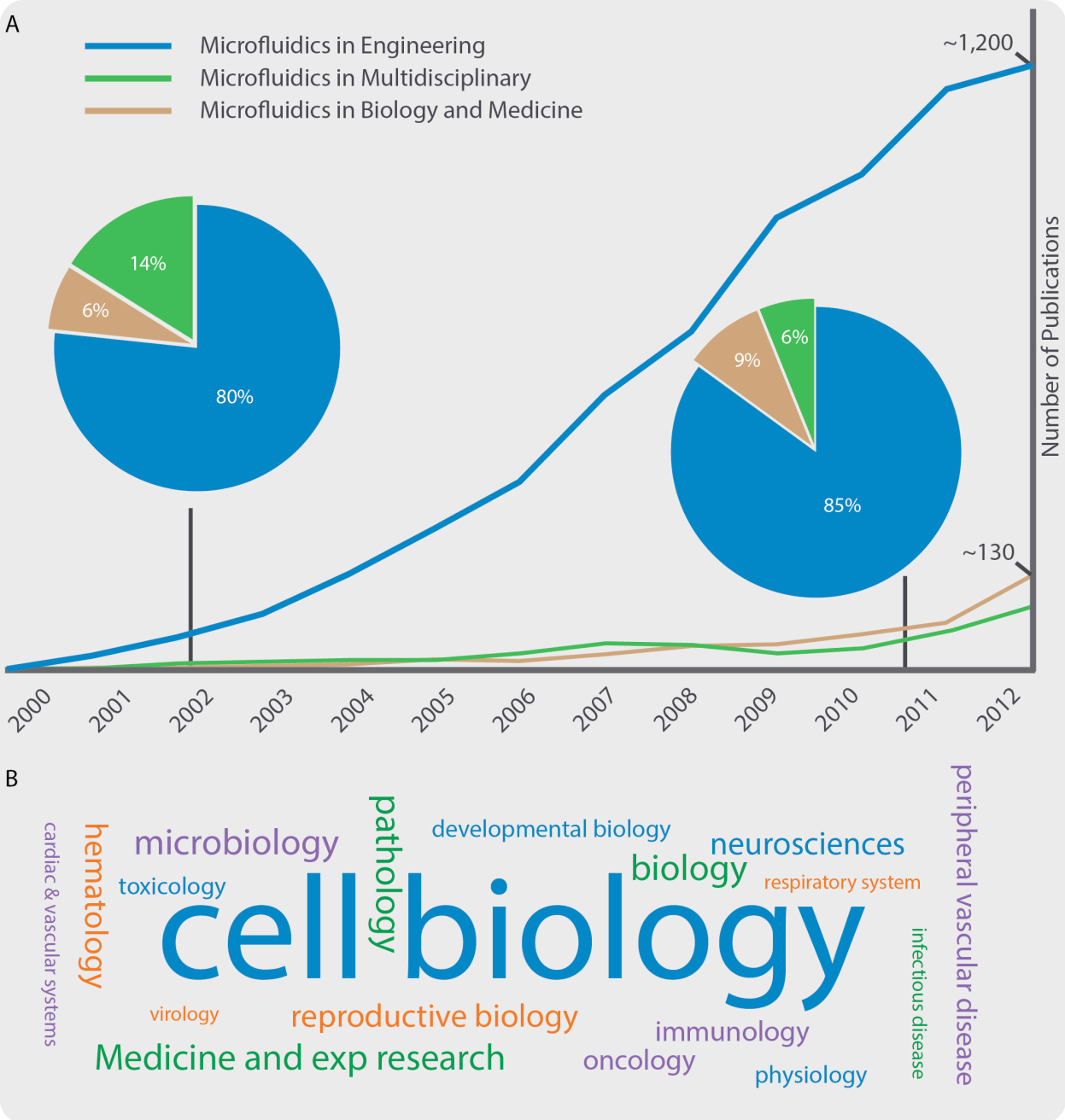

Figure 1.1 Microfluidic publications in engineering, biology, and medical journals from 2000-2012. (A) In 2012, there were roughly 10 times more publications in microfluidics journals compared to biomedical journals. However, the share of microfluidics papers being published in multidisciplinary journals decreased as publication share in biomedical and engineering journals increased. **(B)** Word cloud illustrating what fields most frequently utilized microfluidics. The size of the font is proportional to the cumulative number of publications in

the WoS category (2000-2012), with the exception of "cell biology", which would need to be ~5 times larger.

journals reveals that biology/clinical labs and engineering labs almost always appeared together as coauthors on these studies. This highlights the importance of engineers and biologists actively collaborating to help facilitate the adoption of new microfluidic technologies, rather than engineers designing new assays and passively hoping they get used someday.

Lastly, we analyzed what fields within the biology and clinical research communities are utilizing microfluidic technologies the most (Figure 1c). "Cell biology" and "Biology" encompass most of the microfluidics publications, possibly because these categories are somewhat generic and incorporate several subcategories. Following these categories, the most adoption is seen in "Hematology"; "Medicine and Experimental Research"; and "Immunology." Most of these publications are for diagnostic applications (in the case of Medicine and Experimental Research) and the manipulation of blood samples for biology research (Hematology and Immunology)—applications where microfluidics have compelling advantages over traditional methods.

1.4 A case study in chemotaxis assays

A reality that is perhaps lost on microfluidics engineers is that the state-of-the-art for most macroscale assays used in cell biology research is evolving and improving over time. Biologists understand better than anyone the deficiencies of the techniques they use, and they occasionally make modifications to these macroscale assays that get adopted by other biology researchers. An example of this technological evolution can be found in visual chemotaxis assays—techniques that measure the directional migration of a cell in response to a source of chemoattractant factors that change concentration in space and time.

Macroscale visual chemotaxis assays have improved significantly since their initial introduction in the 1970's (Figure 2). The most widely used chemotaxis assay is known as the "Boyden chamber" or "Transwell" assay, developed in 1962 by Stephen Boyden.[16] The Transwell assay works by creating a concentration gradient of chemoattractant compounds between two wells that are separated by a microporous membrane. Chemotactic cells located in the upper well sense the gradient in concentration and migrate across the membrane towards the solution in the lower well where the cells are counted. This method has been highly valuable over the last 50

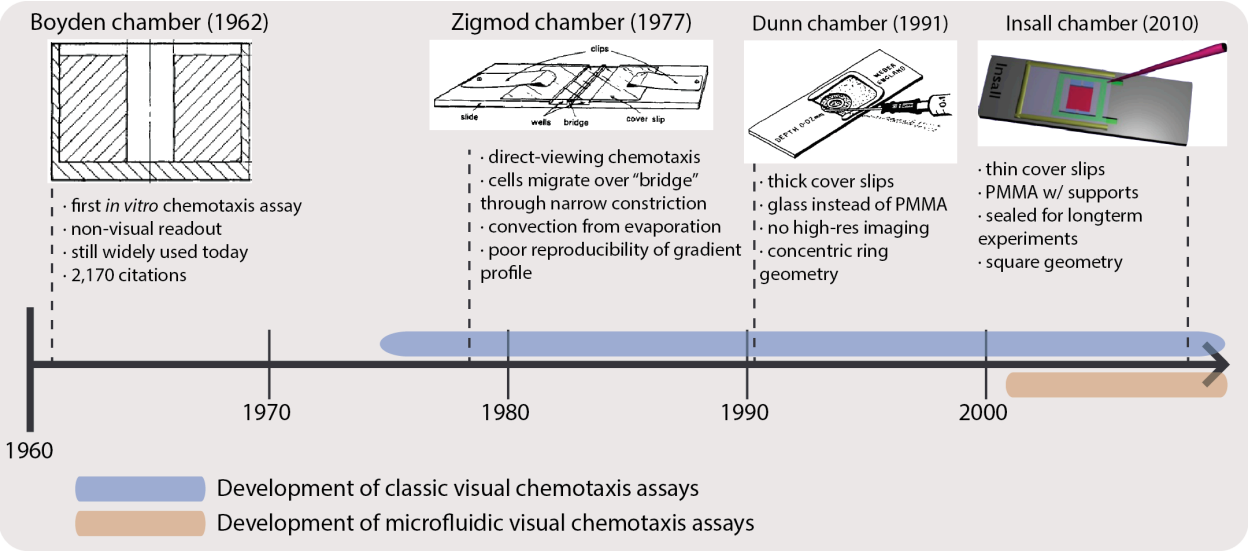

Figure 1.2 The development of visual chemotaxis assays over time. The Boyden chamber assay is also shown since it was the first popular *in vitro* chemotaxis technique. The Zigmond chamber design has undergone several evolutionary changes to address problems with previous versions of the assay. Note the relatively short time microfluidics techniques have been available in comparison to the classical visual chemotaxis assays.

years for identifying chemotactic factors for various cell types; however, the technique does not allow for observation of the cell migration path or cell morphology. This experimental limitation (along with others) led to the development of visual chemotaxis assays such as the Zigmond chamber.[17] In this system, cells can be observed visually with an optical microscope as they undergo chemotaxis on a coverslip across a narrow (tens of micrometers) constriction towards a source chemoattractant. Importantly, this technique allowed for clear phase contrast imaging of cell migration and morphology. However, users of the technique discovered that evaporation of the small volumes of liquid in this system, along with the use of the flexible material polymethly methacrylate (PMMA), led to short-lived and unstable chemical gradient profiles. In the early 90's, Zicha *et al.* designed a modification of the Zigmond chamber called the Dunn chamber.[18] This system used a concentric spherical geometry made of glass instead of PMMA, and used thick coverslips to mitigate the variability in the gap constriction (and therefore gradient profile) during the course of the experiment. This design enabled much more stable gradient profiles for up to ~30 hours, representing a significant advance for monitoring the

chemotaxis of more slowly moving cell types such as fibroblasts. One of the major drawbacks of the Dunn chamber design is that it required thick coverslips in order to minimize flexure of the system during a chemotaxis experiment, which helped to maintain stability of the gradient over time. While this design choice is acceptable for low magnification imaging, the thick coverslips make high-resolution oil immersion microscopy for mechanistic studies difficult. In an effort to improve upon the Dunn chamber, Muinonen-Martin *et al*. designed the Insall chamber, which used rigid support posts and a paraffin-vaseline seal, allowing for the use of thin coverslips that are required for high numerical aperture (NA), oil immersion microscopy.[19] The Insall chamber represents the most recent of a long evolution of direct-viewing chemotaxis chambers that have been developed over the course of three decades.

Microfluidics has offered many excellent solutions for next-generation chemotaxis assays (reviewed in references 20 and 21), however none of these methods have seen widespread adoption at the level of the aforementioned macroscale assays. The generation of chemical gradient profiles is an area where microfluidic technologies are uniquely qualified because of the highly predictable[22,23], diffusion-dominant characteristics of the fluid flow at this scale (Box 1; discussed in greater detail in Chapter 2). Yet macroscale assays are still predominantly used for chemotaxis studies in cell biology research. The low adoption rate of microfluidic chemotaxis assays may be due to the fluid handling expertise and infrastructure required in early designs[24,25], which may have acted as a barrier to entry for biologists.[26] Recently published microfluidic chemotaxis techniques are beginning to take usability requirements into consideration and designing simpler chemotaxis assays that do not require active pumping systems.[27-29] Another possibility is that biologists are more comfortable with using the existing direct-viewing macroscale chemotaxis assays that have been developed and vetted over nearly 40 years (Figure 2). Notably, each iterative improvement on the Zigmond chamber design was published by investigators with appointments in biology (Zigmond), experimental pathology (Boyden & Dunn); and cancer research (Insall)—none of the designs were produced from "engineering" disciplines. Clearly biology researchers understand their experimental needs and posses the ability to engineer new methods to meet those needs. Microfluidic engineers are relative newcomers to cell chemotaxis game—and generally speaking other types of cell biology assays—but have underlying technological and experimental advantages to build tools that

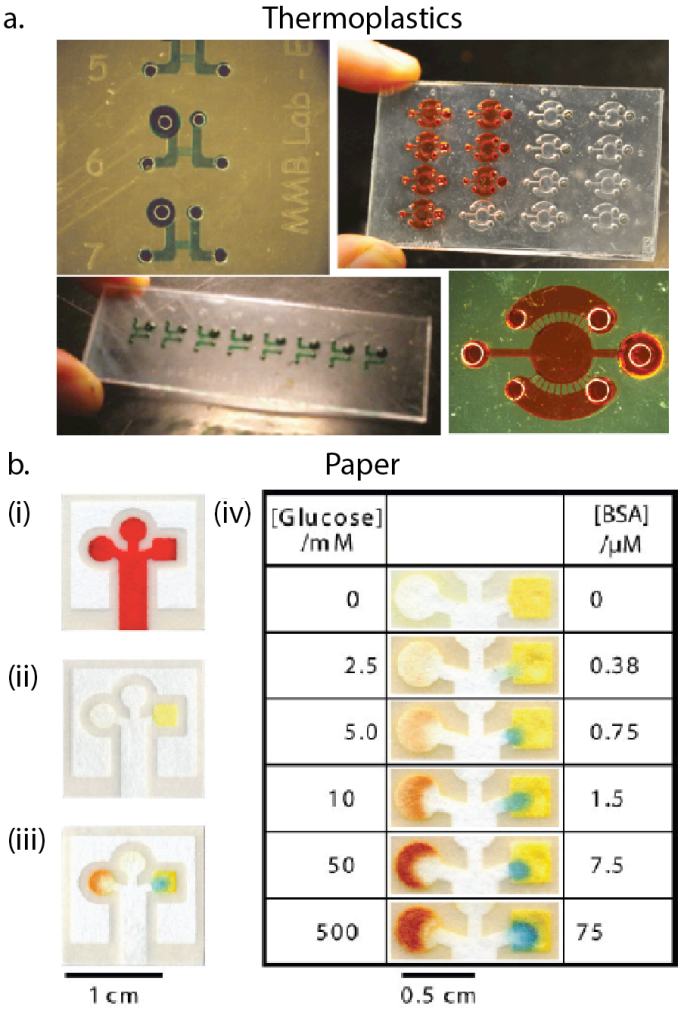

Figure 1.3 Materials other than PMDS are being used for microfluidic device design. (A) Several labs have demonstrated accessible methods of thermoplastic microfluidic device fabrication. **(B)** Paper, and to a lesser extent wax **(C)**, are being used in the developing world for diagnostic applications owing to benefits in device cost; operation; and destructibility with limited waste infrastructure. All images were reproduced with permission from original sources (see 1.11 Copyright permission).

should ultimately be too attractive to scientists in cell biology research. Going forward engineers and biologists should work in close collaboration during assay development, rather than each group continuing disparate, parallel engineering of microscale and macroscale methods.

1.5 Different materials tailored for specific applications

Unlike the semiconductor industry where silicon is the backbone material on which the technology has been built[30,31], the materials used for developing microfluidic devices have undergone significant transition over the years. Early µTAS devices were fabricated out of silicon[32-35] and glass[36-39] using cleanroom techniques that were translated to microfluidic device fabrication. This was largely a choice of convenience since the techniques and

facilities were already in place, but not a long-term solution for cell biology research. Silicon is opaque to visible and ultraviolet light, making this material incompatible with popular microscopy methods. Glass and silicon are both brittle materials; have non-trivial bonding protocols for closing microchannels; and in general have expensive, inaccessible fabrication methods. These materials were useful for demonstrating how μTAS systems could be designed and function, but were ultimately limited in their growth potential. Cheaper, more accessible materials and fabrication methods were needed to fuel the growth of microfluidic technology development and adoption.

In 1998, Whitesides proposed using polydimethylsiloxane (PDMS)—an optically transparent, gas and vapor permeable elastomer— for the fabrication of microfluidic devices[40], and this has become the most widely adopted method for fabricating microfluidic devices. These micromolding techniques built upon technology first developed by Bell Labs in the 1970s[41], and other advancements in the 1980s.[42] It would be hard to exaggerate how important and enabling PDMS has been for microfluidics, contributing to the growth of the field in both technological development and number of publications.[43] Adoption of the material can be attributed to several key factors, including (1) the relatively cheap and easy setup for fabricating devices using PDMS; (2) the hydrophobic surface properties can be tuned to become more hydrophilic[44,45]; (3) the ability to reversibly and (in some cases) irreversibly bond PDMS to glass, plastic, PDMS itself, and other materials; and (4) the elasticity of PMDS allows for easy removal from delicate silicon molds for feature replication. In addition to the practical fabrication considerations of using an elastomer, there are significant functional advantages as well. Researchers have used the elasticity of PDMS to create micropillar arrays that assay the mechanobiology of various cell types.[46,47] However, perhaps most importantly the elasticity of PMDS allows for valving and actuation[48,49], which has led to a plethora of microfluidic designs and publications. Fluidigm®—the largest commercial μTAS technology company currently in the market—builds their microfluidic systems using deformable elastomers (NanoFlex™ valves).

Despite all the beneficial properties of PDMS that enabled its rapid adoption amongst engineers, there are several limitations to using the material for biomedical research. For example, PDMS has been found to leach

uncrosslinked oligomers from the curing process into solution[50], requiring additional device preparation to mitigate this potentially harmful effect.[51] Additionally, PDMS has been shown to absorb small molecules[50,52], which can impact critical cell signaling dynamics. Furthermore, the vapor permeability of PDMS means that significant evaporation can occur during an experiment[53], which can be detrimental for cell microenvironments at micro- and nanoliter fluid volumes.[54,55] Strategies such as parylene coating the microchannel surface[56] and other techniques[57,58] have been developed to mitigate this problem, but these processes are consequences of deploying a non-ideal material for cell biology applications—the often cited "biocompatability" of PDMS appears to be somewhat of a misnomer. Finally, distributing PDMS devices to collaborators is not easily scalable. While making prototype devices for iterating on a new concept is easy, making many of these devices and packaging them in a user-friendly way for collaborators is often nontrivial. Given these limitations, it seems PDMS is not a one-size-fits-all material for certain microfluidic applications, and particularly for cell biology research.[59]

The limitations of PDMS have prompted researchers to explore alternative materials in recent years (Figure 3). In the microfluidics community there has been a push towards the use of thermoplastics such as polystyrene (PS) and cyclic olefin copolymer (COC)[60] for microfluidic devices (Figure 3a). Thermoplastic materials such as polymethyl methacrylate (PMMA) and polycarbonate (PC)[61,62] were popular for the fabrication of μTAS devices in the 90's, but lost favor with researchers because the fabrication methods were more difficult and expensive than PDMS. However, the microfluidics community has largely addressed this issue by developing more accessible fabrication methods for thermoplastic μTAS devices[63-65], although these techniques are not without limitations.[43,66] The use of polystyrene mitigates or eliminates many material property issues associated with PDMS, including the bulk absorption of small molecules; evaporation through the device; and PS makes handling and packaging easier for use in collaborations. Indeed, we have recently argued that PS should be used over PDMS for many cell biology applications, particularly since biologists have a long history of using PS for cell culture.[43]

In addition to thermoplastic materials, there has been significant progress in using destructible, cheap materials such as paper (Figure 3b), wax (Figure 3c) and cloth[67] for point-or-care applications in low-resource settings. These materials have the benefit of being cheap and easily incinerated[68], making them ideal choices for

settings where safe disposal of biological samples is challenging.[3,69] Currently there is tremendous activity in developing microfluidic paper-based analytical devices (μPAD). These μPAD devices operate by passively wicking biological samples through patterned hydrophilic regions using capillary forces, and often employ calorimetric readouts. The hydrophobic channel patterning can be accomplished using a variety of methods such as wax printing[70]; photolithographic patterning of photoresist[71]; inkjet printing of PMDS[72]; and flexographically printed polystyrene.[73] μPAD devices are becoming increasingly sophisticated, with a recent study demonstrating a single-step enzyme-linked immunosorbent assay (ELISA) for the detection of human chorionic gonadotropin (hCG).[74]

The movement beyond PDMS with the use of wax, thermoplastics, and paper is a positive development for the microfluidics community. Rather than solely relying on PDMS for device fabrication regardless of its limitations, researchers are beginning to consider new materials based on the requirements of an application. This shift to tailoring the choice of material frees researchers to invent elegant and creative solutions, particularly for point-of-care applications in the developing world.

1.6 When μTAS technologies are the only solution

Most of the microfluidic technologies that were developed for cell biology applications in the early 2000's sought to improve upon existing macroscale assays. Many of these technologies delivered on the promised performance improvements, yet were never adopted by mainstream biology researchers. Another possibility for this lack of adoption beyond those we have previously discussed is that these technologies are only improvements on already established techniques. Although microfluidic methods may have been technological superior in some cases, they were ultimately only iterative improvements upon methods that already existed. Are you interested in performing protein analysis? Conduct a western blot or ELISA. Are you interested studying cell chemotaxis? Perform a Boyden chamber assay. Are you interested in tissue regeneration after a wound? Scratch your cells with a micropipet tip and see what happens. Microfluidic techniques exist that perform all of these assays with equivalent or improved performance[26], but they do not offer fundamentally new capabilities compared to the current state-of-the-art.

Within the last several years there has been a growing number of microfluidic technologies that solve problems that have not yet been addressed by macroscale approaches. Two recognizable examples that embody this distinction can be found in the glucometer and the pregnancy test. Each test passively wicks bodily fluids into porous materials, either blood (glucometer) or urine (pregnancy test), and performs a complex biochemical assay to provide an immediate measurement. Benchtop assays exist that can certainly perform these tasks, but the portability and rapid feedback these assays provide is transformative for the end user. There are currently applications like these for which microfluidic methods appear to be the best, and possibly only, immediate solution. These various applications share overlapping qualities that make them useful techniques. However, for the purpose of this discussion we will break them into three categories: diagnostic devices for low-resource settings; the rapid processing of biofluids for research and clinical applications; and so called "organ-on-a-chip" devices for drug discovery and diagnostics.

1.6.1 Diagnostics for low-resource settings

The western model of centralized laboratories processing clinical samples with expensive equipment does not translate to the developing world. Many low-resource settings do not have the means or infrastructure to perform these tests and analyses, necessitating creative alternative solutions to meet this largely unsolved problem. Microfluidic methods are being developed to perform a variety diagnostic tests with builtin analysis capabilities that are compatible with the infrastructure in the developing world. As discussed earlier, new material systems such as paper, wax, and others are making major contributions in this area.[60,69] The common themes with these devices include being ultra-simple to operate; providing some qualitative or quantitative output that does not require sophisticated equipment to measure (e.g. cell phone camera or scanner); and ideally the materials used to make the devices are destructible, to avoid unsafe contamination, or scalable and cheap to manufacture. In a recent study, Chin *et al.* aimed to meet these requirements in a microfluidic chip that performed an ELISA-like assay within ~20 minutes using volumes of blood that can be obtained from a lancet puncture (Figure 4a). Importantly, the assay did not require external pumping systems; emphasized straightforward operation; and used cheap photodetectors for the rapid optical readout. The authors analyzed over 70 blood samples obtained from a hospital in Rwanda and successfully diagnosed human

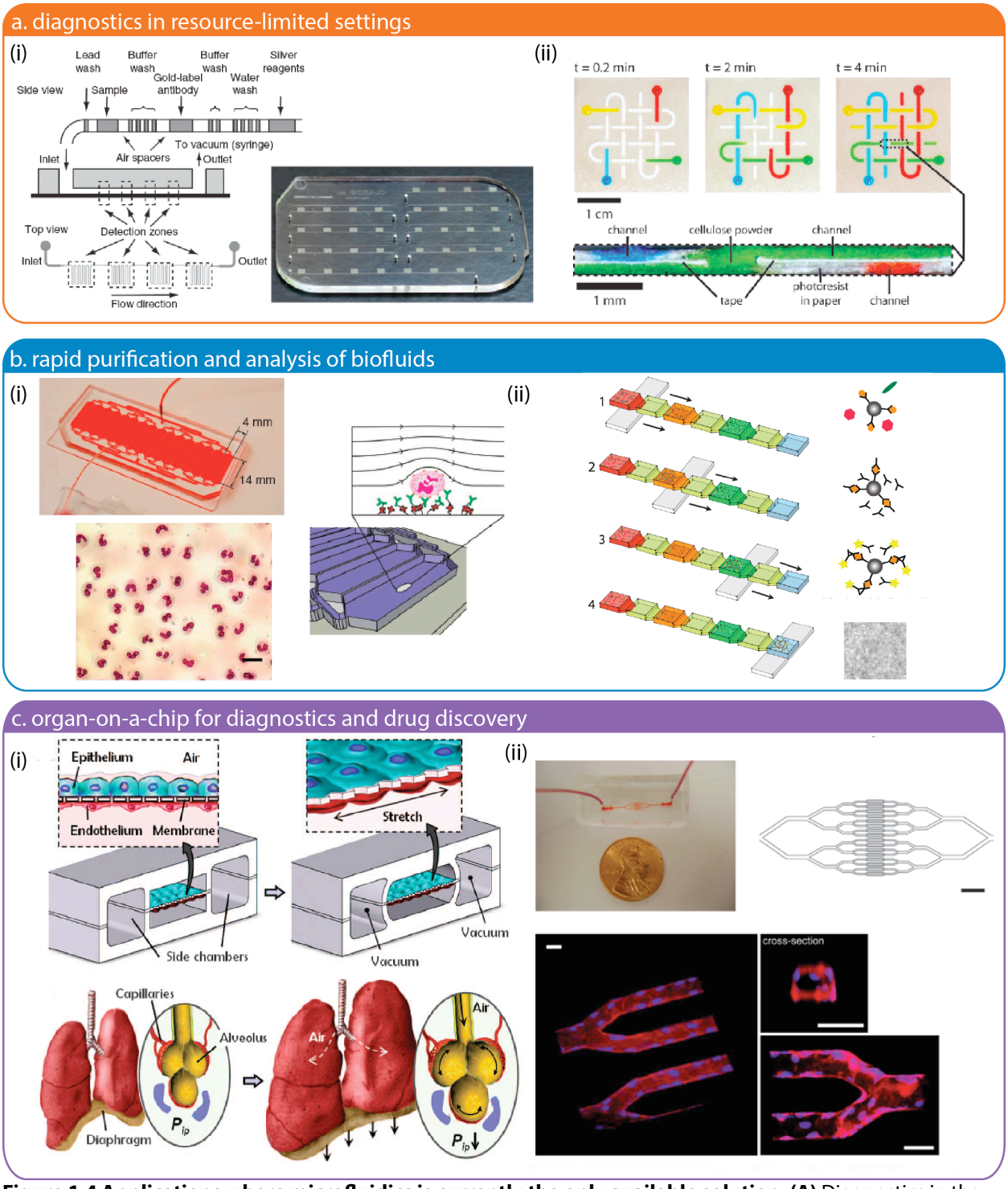

Figure 1.4 Applications where microfluidics is currently the only available solution. (A) Diagnostics in the developing world is an excellent example of leveraging the benefits of μTAS technologies where classical (Western) diagnostic paradigms fail. (i) A user-friendly cartridge to perform ELISA's for the diagnosis of HIV and

other diseases. (ii) 3D μPAD showing complex fluid handling operations that occur passively in a paper device for diagnostics in the developing world. **(B)** Rapid purification of (i) neutrophils using antibody based capture in cartridge device, or (ii) other target analyzes such as RNA, other cell types, and proteins. **(C)** Organ on a chip assays for drug development and specialized diagnostic applications. (i) Complex Microsystems can be developed to recreate organs physiology, such as the physiology of the lunch, directly on a microfluidic device.m (ii) biomimetic blood vessel and capillary networks can also be recreated *in vitro* to diagnosis SCD and other diseases involving blood vessel–whole blood interactions. All images reprinted with permission.

immunodeficiency virus (HIV) in all but one patient, achieving sensitivity and specificity values that rival a lab-based ELISA test. This study and others are promising indications that μTAS technologies could make significant contributions to healthcare in the develop world.

1.6.2 Rapidly assaying biofluids with microfluidics

Engineers have leveraged properties unique to the microscale that have enabled studies that are difficult or impossible using macroscale approaches (Figure 4b). These methods have largely been applied to clinical applications since they use ultra-low volumes of biofluids for the sample processing and can usually be accomplished rapidly and easily. To some degree these assays mimic what macroscale assays accomplish, but the methods offer fundamentally new approaches that enable fundamentally new applications. For example, the rapid purification and analysis of neutrophils—the phagocytotic cells that are first responders for the innate immune system—has been demonstrated in several studies in recent years for clinical and research applications.[28,75-77] These techniques cut down on blood processing times from roughly an hour using milliliters of blood[78], to a few minutes using only microliters of blood. These methods can be applied to measure neutrophil function for diagnostic and research purposes, enabling a new class of studies that have previously been beyond the capabilities of macroscale methods.[28] Other purification schemes have been developed that leverage the increased dominance of surface tension at the microscale to sort target analytes in biofluids across multiphase barriers (e.g. oil and water) using fast and simple procedures.[14,79,80] Not only is this purification scheme simpler and faster than most macroscale methods, but improved sensitivities for protein and genetic purifications may

be achievable due to a reduction in the number of wash cycles required to carry out an experiment. These applications are only some of the examples where microscale benefits are being leveraged to carry out experiments that are not reasonably achievable using macroscale methods.

1.6.3 *Organ-on-a-chip*

The pharmaceutical industry currently is faced with unsustainable research and development (R&D) costs[81,82] that require the industry to change how they pursue the development of new drugs.[83,84] The industry faces multiple headwinds, such as the exclusivity on blockbuster drugs for several companies soon expiring, and dramatically fewer new drugs being approved by the Food and Drug Administration (FDA) in recent years. These circumstances necessitate new strategies for drug development that increase R&D productivity in order to avoid a potential drought in innovative new drugs coming to market.

Microfluidics researchers are taking aim at this problem by developing potentially transformative technologies to mitigate the cost of new drug development. A new class of microfluidic devices seek to replicate *in vivo* organ function on a microchip (Figure 4c). This new class of so called "organ-on-a-chip" technologies integrates several well-understood microfluidic components into a single *in vitro* device, allowing researchers to more closely recapitulate *in vivo* function. This ambitious effort is still in its infancy, though several promising studies have shown examples of these biomimetic systems. Examples of organ-on-a-chip technologies include the gut-on-a-chip[85]; lung-on-a-chip[86]; blood vessel-on-a-chip[87-89]; and kidney-on-a-chip.[90] Furthermore, these modular systems could theoretically be combined into a complete "human-on-a-chip" model that mimics *in vivo* function of these organs working together in concert.[91] The result would be class a sophisticated *in vitro* assays where drugs could be tested, increasing the predictability of a new drug (i.e. hit rate) prior to animal testing or human clinical trials. In a tangential application, blood vessel-on-a-chip devices have already been utilized for the diagnosis of sickle cell disease (SCD) in the clinic.[87,89] For example, Tsai *et al.* described a microfluidic chip that recapitulated *in vivo* conditions of a blood vessel—such as blood flow rate; endothelial cell shear stress; and biochemical activation states—in order to reliably detect vasco-occlusions due to SCD. This system highlights how certain properties of microfluidic systems such as high resolution micropatterning and precise control of the hemodynamic and shear profiles in the microchip enabled the measurement of biophysical abnormalities in

a clinical setting. Significant work is still required before organ-on-a-chip methods can be adopted in mainstream drug R&D or clinical diagnostics, although early developments in this area are promising.

1.7 Where we go from here

The question of how to increase adoption of microfluidic technologies within mainstream biomedical research remains largely unanswered. We have shown that microfluidic technologies are being utilized for some studies in biology research and diagnostic applications, however the large majority of microfluidics publications are still in technical journals specific to the field (Figure 1). Adoption of new technologies that supplant or even compliment existing methods is often a slow process. For evidence of this, one needn't look further than the computer mouse, which took 20 years to appear in the Macintosh™ computer after its invention by Douglas Engelbart in the 1960's. But that does not mean microfluidics engineers should become disillusioned or discouraged. Researchers in the field must develop deliberate and thoughtful strategies that will best push the technology forward. We now have several decades of experience to draw upon, and there are some useful lessons we can apply.

1.7.1 Fostering mutually beneficial collaborations

During the early years of microfluidics the field had largely taken an, "if we build it, they will come" approach to developing and publishing microfluidic technologies. Perhaps the idea was that these fancy microfluidic chips would look so impressive, researchers from the biology community would rush to figure out how to make and use the new technologies themselves. Clearly this cliquey formula of engineers and biologists leading separate academic lives does not benefit either community. Fortunately researchers have acknowledged that a divide between the developers of the technology and the end-users is counterproductive. Most of the recent microfluidics papers published in "biology and medical journals" are co-authored by engineers, biologists, and clinicians. This evidence of increasing collaboration is a promising development for everyone involved. In order to sustain this trend, microfluidic researchers should aggressively court collaborators from biology and clinical laboratories (and vice versa). Direct interaction and feedback from the end-user is tremendously useful during technology development. Furthermore, new applications and ideas can be generated by biology collaborators that engineers—being non-experts in cell biology or clinical research—would never have considered.

1.7.2 The simplest solution is almost always best

All signs indicate that there is no silver bullet for accelerating the adoption process, however there are design choices engineers can make in order to lower the barrier to entry for biologists. How the end user interacts with a new technology is a critical aspect of whether the method is adopted. Microfluidics engineers have been attempting to simplify fluid handling methods in their designs with passive pumping approaches that only require a micropipet to operate.[12,14,27-29,79,92] Some microfluidic applications will always require the use of external pumps and pneumatic fluid handling systems; examples include most organ-on-a-chip devices and techniques that require continuous flow to generate specific shear profiles (e.g. biomimetic blood vessel models). However, engineers should limit the use of these external systems whenever possible. Creating a simpler approach often requires more creative solutions, but this can greatly improve the experience for the end-user. Paper diagnostic assays are an excellent example of single-step, automated, and user-friendly μTAS solutions where the technology completely disappears and the user can focus on interpreting the results[69]. We have recently developed a similarly straightforward, automated approach for general cell biology applications that does not require external pumping equipment or even a micropipet to perform complex assay protocols.[93] General problems of packaging and distributing microfluidic technologies to collaborators will also need to be addressed until microfluidic assays become more commercially viable in the academic research market. However these problems can also be viewed through the lens of user-friendly assay design.

1.8 Methods

A literature search was performed using Web of Science (WoS; provided by Thomson Reuters) to determine the number of microfluidics publications in various disciplines (Figure 1). The search was performed for the term "microfludic*" and "nanofluidic*". The results of the number of publications were obtained from the WoS analytics reporting system for each search term, and then summed before being presented in Figure 1. Three categories were characterized by the WoS search that capture the relevant journals for the years 2000-2012. The analysis of "Microfluidics in Engineering" reports the number of microfluidic publications in the "Nanoscience and Nanotechnology" WoS category. The analysis of "Microfluidics in Multidisciplinary" category corresponds to the "Multidisciplinary" WoS category. The analysis of "Microfluidics in Biology and Medicine" reports publications

from WoS categories shown in Figure 1b. The search explicitly excluded "reviews", "book chapters", "book reviews", "meeting abstracts", "meeting summaries", and included "articles." The data shown reflects the most recent literature search, performed on 3/21/2013. The following search general string was used: Topic=(microfluidic*) AND Year Published=(2000-2012) AND Document Types=(Article) NOT Document Types=(Book OR Book Chapter OR Book Review OR Meeting Abstract OR Meeting Summary OR Proceedings Paper OR Review). This string yielded the total "microfluidic*" publications in all WoS categories. The search was then refined by the WoS categories shown above (e.g. Web of Science Categories=(MULTIDISCIPLINARY).

1.9 Acknowledgments

I would like to acknowledge Anna Fulton and Dave Beebe for their contributions to this chapter. I also wish to thank Scott Berry, Peter Thomas, Lindsay Strotman, and Ben Casavant, for helpful discussions during the preparation of this chapter.

E.K.S. and D.J.B. wrote the content presented in this chapter. A.L.F. contributed to the design and execution of the literature searches that measured the quantity of microfluidic publications in biology and medical research.

1.10 Conflicts of interest

E.K.S. and D.J.B. have patent applications pending on technology cited in this work. D.J.B. has ownership in Bellbrook Labs, LLC, which has licensed technology cited in this work.

1.11 Copyright permission

Figures 2-4 have represented data that has previously been published with permission from the original sources. The content in this chapter is in preparation for submission, and therefore dose not require copyright permission to present in my dissertation.

Chapter 2

Microfluidic chemotaxis technologies for research and translational medicine

2.1 Introduction

The human body is made up of 100 trillion cells[94], with over 200 cell types that perform a variety important biological functions. Cell migration is one of the most critical functions for the proper execution of several physiological processes. For example, cell migration is central to wound healing in order to repair damaged tissue.[95] Cell migration is vital for mobilizing white blood cells in order mount an innate immune response and promptly fight off infection.[96] In some cases cell motility can be detrimental, as is the case when metastatic cancer cells spread rapidly throughout the body during cancer progression.[97-99] The migration of most cell types during these physiological processes is rarely random, but rather guided by extracellular cues that direct cell movement. There are several types extracellular cues that can direct cell migration, including gradients in cellular adhesion sites (haptotaxis); mechanical cues in the cell microenvironment (durotaxis); changes in the electrical field (electrotaxis); and the presence of soluble proteins (chemotaxis). For chemotaxis to occur, a cell senses an extracellular biochemical gradient and responds by migrating directionally towards, or away from, the increasing concentration of the attractant molecule. Cell chemotaxis has been an area of great interest to the cell biology community, and many chemotaxis assays have been developed in order to study this phenomenon in depth. This chapter will describe the physiology of eukaryotic cell chemotaxis; provide an overview of macroscale and microscale chemotaxis assays that have been developed over the last 50 years; and explore the potential of translating appropriately designed chemotaxis techniques beyond the research setting and into the clinic.

2.2 Eukaryotic cell chemotaxis

Cellular chemotaxis is a complex, multi-stage process by which receptors on the cell membrane recognize the presence of external biochemical cues, and then amplifying intracellular signaling pathways to polarize its cytoskeleton and migrate in response. Prokaryotic and eukaryotic cell types both have the ability to undergo chemotaxis, though prokaryotic chemotaxis is characterized by significantly different mechanisms and signaling

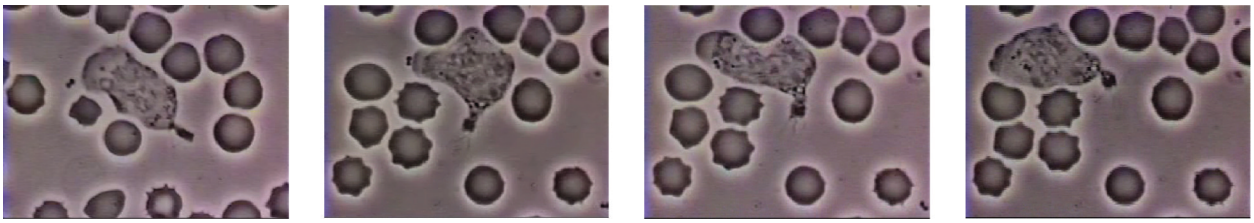

Figure 2.1 A famous example of neutrophil chemotaxis and phagocytosis. The neutrophil is seen migrating towards a bacterium as the bacterium secretes some kind of unknown chemoattractant (e.g. N-formyl peptides like fMLP). The neutrophil polarizes its cytoskeleton and extends lamellepodia towards an increasing concentration of proteins that guide the cell towards the bacterium. Note the ability of the neutrophil to rapidly change direction and polarization in response to movement of the bacterium, as well as its ability to navigate around red blood cells. In its final fate, the bacterium is engulfed by the neutrophil and killed during phagocytosis. (The above images were taken from a 16 mm video recorded by David Rogers of Vanderbilt University in the 1950's. Details can be found at ***www.biochemweb.org/neutrophil.shtml***.)

pathways. Two classic chemotaxis models that have been well-characterized in the literature include *Dictyostelium discoideum* amoebae and neutrophils, which capture many of the characteristics of eukaryotic cell chemotaxis. However, there are mechanistic differences between the various chemotactic cell types that cannot be covered in this chapter. For details on cell types that will not be discussed here, we refer readers to the following reviews on chemotaxis for bacteria[100]; *Dictyostelium discoideum*[101,102]; dendritic cells[103]; natural killer cells[104]; and macrophages.[105,106] In order to provide an example of the biology of chemotaxis in a cell type that is relevant to the context of translational medicine, we will focus on neutrophils–the most abundant cell type in the innate immune system and first responders during inflammation and wounding healing (Figure 1).

Neutrophil chemotaxis can be broken down into three primary interlaced stages: chemosensing, polarization, and locomotion (reviewed in 107,108). When a neutrophil senses a concentration gradient of external secreted proteins known as chemokines, the cell polarizes its cytoskeleton and engages in sustained directional migration towards the attractant molecules (i.e. chemoattractant). We will provide a brief overview of the biology of chemotaxis for neutrophils, and refer the reader to the aforementioned excellent reviews for a more in depth treatment of the subject.

2.2.1 Chemosensing

Prior to being activated by external cues, neutrophils stay in an inactive and immobile state. When chemoattractant is present, neutrophils extend and retract lamellipodia—protrusions of the cell membrane structured by actin filaments—to dynamically form pseudopods for roughly 60 second intervals. If a uniform chemoattractant is present, neutrophils migrate more or less randomly until the cell senses a gradient of chemoattractant and begins to migrate directionally. Neutrophils sense chemoattractants using transmembrane chemoattractant receptors (e.g. fMLP-R and C5a-R) that become occupied by extracellular chemokines, and these receptors activate heterotrimeric G-proteins that transduce the extracellular signals into an intracellular activation cascade. The chemoattractant receptors are relatively uniformly distributed on the cell membrane, and the local and temporary nature of the pseudopod formation allows neutrophils to rapidly change the extension of pseudopodia in reaction to location changes of the source of chemoattractant. Once the cell becomes polarized, neutrophils maintain the original leading edge of the cell and turns towards the new source of chemoattractant rather than forming new lamellapodia.

2.2.2 Polarization & Locomotion

Neutrophils can become polarized in a uniform concentration of chemoattractant, however polarization is much more likely when a gradient of concentration exists, leading to persistent migration towards the source of chemoattractant (chemotaxis). When there is a difference as little as 1-2% in the number of receptors on opposite ends of the cell occupied by chemoattractants, the neutrophil polarizes its cytoskeleton by increasing the number of advancing pseudopodia on the anterior portion of the cell and enriching retracting uropods with myosin in the posterior portion of the cell. Once activated and polarized, neutrophils have the ability to persistently migrate towards a site of inflammation that is sending inflammatory signals (chemokines), or chase down pathogens such as bacteria to phagocytose and clear the pathogen. The persistent migration of neutrophils is determined by a variety of factors such as type of chemoattractant, steepness and profile of the concentration gradient and other biophysical and biochemical factors in the neutrophils' extracellular microenvironment.

2.3 The role of chemotaxis in disease

In the introduction we described chemotaxis as being central to the pathophysiology of many diseases. Indeed, chemotaxis is relevant to the spread of metastatic cancer[99]; wound healing[95,109,110]; the inflammatory response by the innate immune system[111,112]; rheumatoid arthritis[113]; chronic obstructive pulmonary disorder (COPD, reference 114); and asthma.[115-117] The role that cell chemotaxis plays in the pathogenesis of these and many other diseases has been a topic of intense interest over the last 50 years. Researchers have made significant progress in identifying chemotactic cell types that are central to the pathogenesis of a disease, as well as the the identification of cytokines that are relevant to the orchestration of these mobile cells.

For example, the dissemination of metastatic cancer cells from a primary tumor site throughout the body is central to the pathophysiology of the disease. If a primary tumor is detected early, treatment regimens and prognosis are greatly improved compared to late-stage detection.[118] In other words, the cancer becomes much harder to treat if the cells have migrated away from the primary tumor site; entered the nearby bloodstream (created after angiogenisis has been initiated near the primary tumor); and extravasated from the blood stream to form a secondary site. If the cancer cells have not mobilized from the primary tumor site, the cancer can often be surgically removed or treated with local irradiation. Although directional migration is not necessary for this process, there is evidence that metastases form more efficiently when the cells migrate directionally.[119] Furthermore, researchers have shown that the chemotaxis of tumor cells towards macrophages is important for intravasation into the blood vessel, and for invasion into the tissue of a secondary site.[120] Thus, minimizing or disrupting the ability of cancer cells to undergo chemotaxis would likely lead to a reduction in the metastasis of cancer cells and improved prognostic outcomes for cancer patients.

Asthma is another disease where chemotaxis—in this case the dysfunctionally regulated chemotaxis of inflammatory cells—directly contributes to the pathogenesis of the syndrome. Asthma is a condition characterized by chronic inflammation of the lungs, which ultimately leads to obstruction of airflow and manifests in clinical symptoms such as wheezing, coughing, and shortness of breath. The condition has far-reaching impact, affecting more than 300 million people worldwide.[121] Furthermore, asthma prevalence has

increased significantly over the last 30 years in many regions, with some indications that prevalence may be reaching a plateau in the developed world.[117,122] Researchers have made significant progress uncovering the mechanisms and pathophysiology of asthma, leading to improved treatment and management. However, diagnosing asthma still remains a challenge for physicians[123-125], and misdiagnosis can lead to unnecessary treatment; greatly increased medical costs[126]; or more consequentially, missed treatment for vulnerable populations such as the elderly.[123,124] In this case, mitigating the hyperchemotactic activity of inflammatory cells could lead to improved clinical outcomes for asthmatic patients.

Cancer metastasis and asthma are two of many examples where chemotaxis plays a central role in the pathophysiology of a disease. Researchers have studied theses pathways in an attempt to not only understand the biology of a disease, but develop therapies that target areas of the pathway that may be vulnerable to interventions. For instance, a therapy blocking the production of Interleukin-5 (IL-5)—a cytokine that is implicated in mucus secretion; the recruitment of eosinophils to the lungs (leading to eosinophilia for asthmatic patients); and airway hyper-responsiveness (AHR)[127]—might decrease eosinophil and mast cell recruitment to the lungs resulting in symptom relief for the patient. Anti-IL-5 clinical trials are currently currently underway[128,129], and this is an example of how therapeutic interventions can be developed once the underlying pathway is uncovered. In order to understand the role of cell chemotaxis for various diseases and facilitate the development of drug therapies, researchers require robust *in vitro* assays to controllably and systematically study cell chemotaxis. In the following sections, we will explore both traditional macroscale chemotaxis assays and more recently developed microfluidic systems. Furthermore, we will explore how properly designed microfluidic chemotaxis devices can potentially be used in a clinical setting for diagnostic and therapeutic purposes.

2.4 Traditional methods for studying cell chemotaxis

Several assays have been developed that have made significant contributions to our understanding of cell chemotaxis (Figure 2). The first widely adopted *in vitro* assay for studying cell chemotaxis was developed by Stephen Boyden in 1962[16], known as the "Boyden chamber" or "Transwell" assay. The Transwell assay is a two-chamber system, with each chamber filled with media and separated by a microporous membrane (Figure 2A).

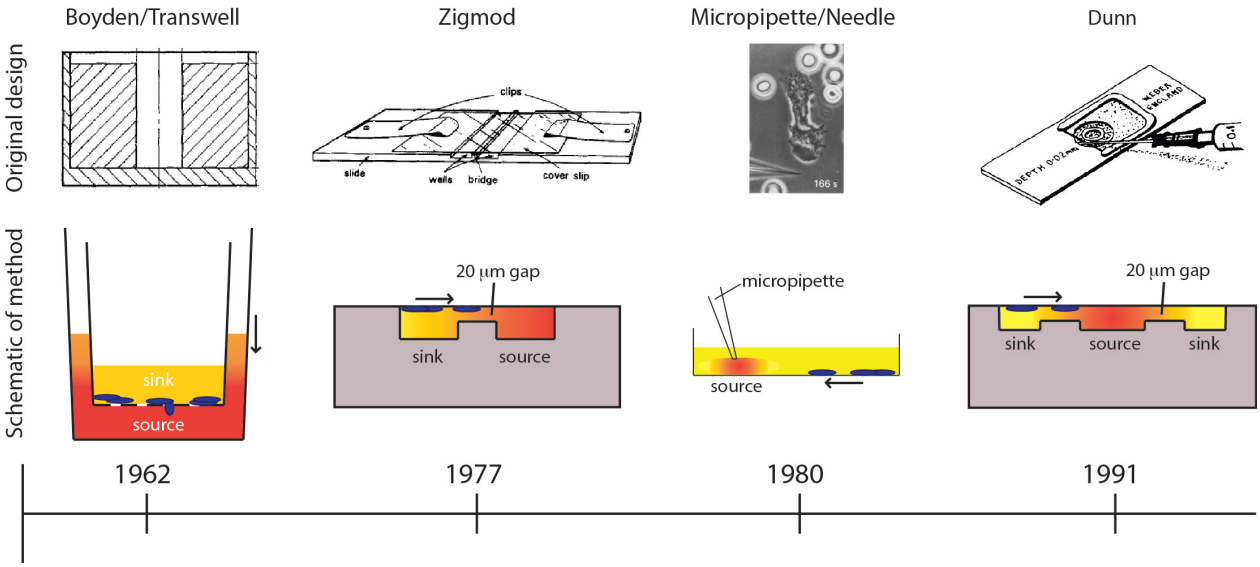

Figure 2.2 Overview of macroscale chemotaxis assays that have been developed over the years. The timeline below each assay indicates the date the technology was invented below each assay (not to scale). The direction of the arrow indicates the direction of cell chemotaxis. The color shading indicates the formation of the chemical gradient of chemoattractant.

The lower chamber contains a test substance of interest (e.g. chemoattractants), and the upper chamber contains cells that may or may not respond to the test substance. During the course of an experiment, the source compound diffuses across the porous membrane due to the concentration gradient that exists between the two chambers. As we discussed earlier, chemotactic cells can sense the spatial distribution of chemoattractants and, depending on the cell type and chemoattractant, migrate across the membrane and towards the source of the concentration gradient. Multiple wells can be studied at once and in parallel to introduce proper controls (i.e. no concentration gradient), or to test varying doses in order to comprehensively characterize the chemotactic response of the cell type-compound combination. Following the introduction of the Boyden chamber, several early studies demonstrated the utility of *in vitro* chemotaxis assays by characterizing the chemotactic response of several cell types under various experimental conditions.[16,130-132] Following the successes of the Boyden chamber, researchers sought to develop new designs that offered different approaches to measuring cell chemotaxis.

Alternative *in vitro* chemotaxis assays that have been utilized in the biology community include the Zigmond chamber[17]; the Dunn chamber, which is a modification of the Zigmond chamber design[18]; the under-agarose assay[133]; and micropipette-based[134] assays. A comparison of some of these chemotaxis techniques is shown in Figure 2. The Zigmond chamber consists of two etched wells—a chemoattractant (source) well and a well containing cells and media (sink)—that are separated by bridge that restricts convection of fluid from one well to the other (Figure 2B). The cells are placed on an inverted coverslip spanning the two wells, allowing the investigator to visually observe the cells undergo chemotaxis across the bridge as a chemical gradient is formed. However, the gradients are short-lived (~1 hour) and somewhat unstable due to the evaporation that occurs with this design. These drawbacks lead to the Dunn chamber design[18], where a spherical geometry was adopted so the wells can be completely encapsulated by the coverslip to limit evaporation (Figure 2D). The under-agarose assay is another early example of a technique that allowed the investigator to visually observe the migration of cells over time. In the under-agarose assay, holes are punched in agarose gel and a chemoattractant is placed in the holes to act as a source for the concentration gradient. Due to the concentration gradient that exists between the source and the surrounding gel, the compound diffuses into the gel and cells sense the changing spatial distribution of the source compound over time and migrate towards the source under the agarose gel. This method provides a relatively simple and robust technique for creating one or more chemical gradients, while visualizing the response of cells in a physically confined environment. Foxmann *et al.* utilized the multi-source capabilities of the under-agarose assay to characterize the neutrophil chemotactic function in competing gradients[135], and there are many other studies that utilize this technique.[136,137] However, as useful as these *in vitro* chemotaxis assays have been over the years, researchers have discovered several limitations that limit the types of biological questions that can be addressed.

Many of the technological limitations that arise from the assays are due to large sample volume requirements; unstable or unpredictable gradient profiles; or usability issues that make it difficult to run the desired experiment. For example, the most common macroscale chemotaxis assay in use today — the Transwell assay — develops unstable chemical gradient profiles[138]; filters cells by size and deformability due to the rigid microporous membrane the cells must cross[139]; and delivers ambiguous results as chemotaxis and chemokinesis

are difficult to differentiate in this system.[140] The under-agarose assay allows for visualization of the cell migration path, but has an unstable chemical gradient that forms in all directions.[138] Additionally, under-agarose assays has low spatial resolution with respect to source and cell placement because of the way the experiment is conducted. The user is required to define these locations with a micropipet and crude hole punching methods for the source of chemoattractant, both of which can be prone to significant variability. Therefore, while the method is relatively simple to perform and can be useful for visualizing cell migration paths, the under-agarose assay is not well-suited for reliable quantification of cell chemotaxis. Another popular and more modern visual chemotaxis assay is the Micropipette assay (also known as the "Needle assay"). This technique offers significant technical advances over these older techniques, such as high resolution real-time imaging (Figure 2C, reference 141). However, the method is also best suited for qualitative analysis because its onerous labor requirements limit investigators to low throughput sampling. Another significant limitation of most macroscale assays is that they require large sample volumes in order to isolate specific cell types of interest. For example, if one wishes to perform a neutrophil chemotaxis experiment using these common macroscale techniques, the sample preparation would require lengthy blood draws and cell purification protocols[78] that require tens of milliliters of blood. This sample volume requirement limits the number of times one can sample a subject to probe their neutrophil chemotactic function, thereby restricting the time resolution of the experiment. Additionally, the large blood volumes needed makes sampling infants or small animals (e.g. mice, rats, etc.) for neutrophil chemotaxis logistically complex, if not impossible.

Microfluidic technologies can play an important role in providing solutions to many of these limitations. Indeed, over the last decade microfluidic engineers have either solved or greatly improved upon the gradient stability and sample volume limitations of macroscale assays. In the following sections, we will explore why microfluidic technologies are particularly useful for chemotaxis assays by describing the physics of fluids at the microscale.

2.5 Microfluidic methods for studying cell chemotaxis

Microfluidic devices are ideally suited to perform chemotaxis assays and offer significant advantages over macroscale approaches. As we discussed earlier, chemotactic eukaryotic cells can sense spatial and temporal perturbations in their microenvironment, and respond by directionally migrating towards the increasing concentration of the stimulus. However, the cell cannot undergo chemotaxis if the changing concentration occurs so suddenly that the receptors on the cell membrane cannot discern a difference in soluble factors from one side of the cell versus the opposing side. Fortunately, the physics of fluids at the micro/nanoliter scale makes creating diffusion dominant mass transport a relatively trivial task. The fluids at this scale are often characterized by a series of dimensionless quantities[142]; the quantity that is most widely cited (and probably the least interesting), is the Reynolds number (Re, Equation 1):

(1) $$Re = \frac{\upsilon L_0}{\eta}$$

where *v* is the characteristic velocity of the fluid; L_0 is the characteristic length scale in which the fluid is traveling; and η is the kinematic viscosity of the fluid. For devices with dimensions on the micrometer scale that manipulate fluids with typical velocities (*v* << m/s) and kinematic viscosity (e.g. aqueous solutions, oils, etc.), the Reynolds number, Re << 1, is well under the transition from turbulent to laminar flow. Thus, the size scale of microfluidic technologies dictates that fluids generally operate in the laminar flow regime. The implications of this phenomenon for creating controllable gradients of soluble proteins are significant. Laminar fluids can be manipulated, combined, and separated in highly predictable and reproducible ways without stochastic convective currents (turbulence) disturbing the mass transport dynamics. Therefore, two or more neighboring microfluidic streams can run adjacently to each other without turbulent mixing; instead, molecular diffusion dominates the mass transport between the laminar fluids.

Diffusion a process characterized by Brownian motion, where molecules moving from a higher concentration to lower concentration (i.e. thermodynamically driven), and the kinetics of this process are

determined by the activation energy required to move the diffusing molecule (e.g. proteins) through a particular medium (e.g. aqueous solution). In one dimension, diffusion can be modeled by (Equation 2):

(2) $$d = \sqrt{2Dt}$$

Where *d* is the distance a molecule with diffusivity *D* travels in time *t*. There is another dimensionless quantity that describes the ratio of convection of a fluid compared to diffusion of a molecule within that fluid, known most commonly as the Peclet number (Equation 3):

(3) $$Pe = \frac{\upsilon L_0}{D}$$

where *v* and L_0 are still the characteristic velocity of the fluid and length-scale of the system, respectively; and *D* is still the diffusivity of a molecule from one fluid into the medium of an adjacent fluid. This number helps one determine the relative importance of diffusion compared to the convection of the fluid. In practice, the Pe number can be used to determine the necessary length of a microchannel to allow complete diffusion of a molecule from one fluid stream to another. For example, consider two fluids – Fluid A and Fluid B – flowing in adjacent laminar flow streams at 10 μm/s in a microchannel with width of 500 μm, and we wish to calculate the channel length required for a protein with diffusivity of 50 $\mu m^2/s$ to diffuse from Fluid B to the channel edge for Fluid A (Figure 3). Due to the lack of convective mixing on this scale, the protein B will take 20 channel widths, or 5 cm to diffuse across Fluid A (a distance a few times the diameter of a human hair). These numbers demonstrate that one can control diffusion well within

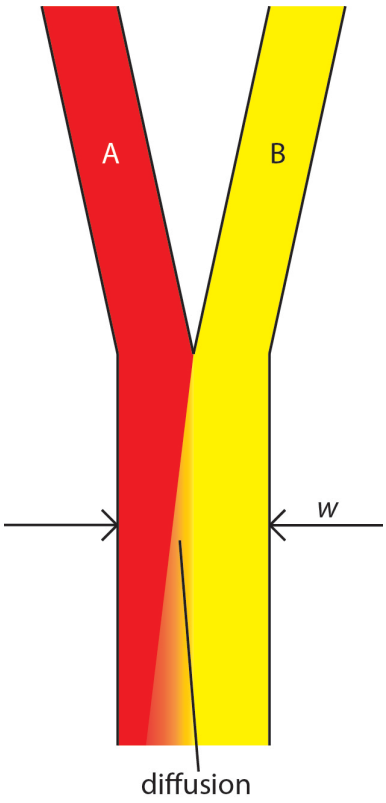

Figure 2.3 Generic design of two fluids flowing through a microchannel in the laminar flow regime. Diffusion of molecules from Fluid B occurs transverse to the fluid flow and down the concentration gradient towards Fluid A.

microchannels, but without convection, transporting molecules from one area of a microchannel to another takes considerable time.

Microfluidic engineers have leveraged the unique properties of fluids at the microscale to make significant advancements in the capabilities of chemotaxis assays (Figure 4). The control of the cellular microenvironment with highly predictable, diffusion-dominant fluid phenomena makes microfluidic devices ideally suited tools for chemotaxis assays. A classic example of a microfluidic chemotaxis device that leverages microfluidic fluid phenomena is the "christmas tree" design developed by George Whitesides' lab in 2000 (Figure 4A, reference 24). In this system, the authors created concentration gradients of various solutions by mixing fluid streams with different source concentrations in serpentine microchannels , and then recombined the fluids with different combinations of the source concentration after the serpentine channels meet downstream. The result of these mixing operations is a user-defined concentration gradient of the original source molecules (Figure 4B). This channel design both utilizes and contends with laminar flow phenomena in order to achieve highly reproducible concentration gradients that are difficult or impossible to replicate using macroscale techniques. The laminar flow properties of the system allow for the components of each source fluid to be separated and then recombined in a predictable and controllable fashion. However, the lack of convection in the system means a serpentine channel design must be utilized to allow for complete mixing due to the high Peclet number. This

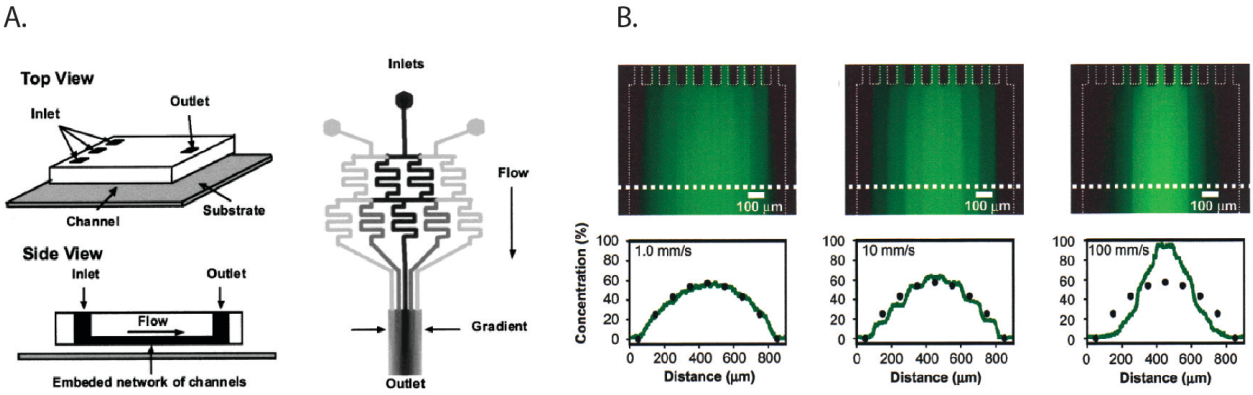

Figure 2.4 Schematic and data of the microfluidic "christmas tree" gradient generator. **A.** Design of the serpentine gradient generator that shows the splitting and recombination of multiple fluid streams to create a chemical gradient. **B.** Gradient profiles of fluorescent dye that show the versatility of the technique.

channel design has been used for developing chemical gradients for multiple cell types, including neutrophils[143]; neural stem cells[144]; *Dictyostelium discoideum*[145]; and metastatic breast cancer cells.[146]

The "christmas tree" design is one example of leveraging microfluidic phenomena to develop highly predictable chemical gradients, however many other gradient devices have been developed over the years using microfluidics. For example, Wong *et al.* describe a microfluidic system that utilizes hydrogel barriers to compartmentalize the source, sink, and cell channels.[147] Here, the authors utilize properties of the hydrogels that enable its use in cell culture—namely the high viscosity of the hydrogel that prevents convective mass transport; and the permeability of hydrogels so proteins can diffuse from on compartment to another (e.g. from the source, to the cells, to the sink). In another class of static, no-flow microfluidic gradient generators, engineers have taken advantage of the greatly increased resistance to fluid convection as microchannel height is decreased:

(4) $$Q = \frac{\Delta P}{R}$$

where Q is the flow rate of the fluid, $\mathbf{\Delta}P$ is the pressure drop across the microchannel, and R is the fluidic resistance of the microchannel. Equation 4 shows the that the convection rate of the fluid is inversely proportional to the resistance in of the microchannel. For a microchannel with rectangular cross-section and high aspect ratio (width of channel far greater/less than the height of the microchannel), the resistance in the microchannel is given by:

(5) $$R = \frac{12\mu L}{wh^3}$$

where h and w are the height and width of the channel, respectively; L is the length of the microchannel; and μ is the viscosity of the fluid.[1] From Equation 5, we see that the resistance of a microchannel with a high aspect ratio is inversely proportional to the cube of its height. Therefore, a devices can be engineered to be highly resistive to convection by decreasing the height of the microchannel (e.g. 7-15 μm) compared to the height of the cell, source, and sink channels. This technique of separating microchannels that contain cells and reagents by low-

height "diffusion channels" has been utilized to create no-flow gradient devices[27,148], and for microfluidic multi-culture systems.[149] This approach offers the benefits of highly controlled chemical gradients without requiring tubing or active pumping systems, and conserving intercellular signaling that would normally be removed with a convection-based design. Other microfluidic designs have been reported that emphasize user-friendly operation to facilitate adoption by biologists, while generating robust chemical gradient profiles. For example, our lab recently reported a two component chemotaxis device that sorts neutrophils within minutes[75], and can easily form a chemical gradient by placing a lid with chemoattractant onto a base where the neutrophils have been sorted.[28] This technique enabled a new set of applications that were difficult or impossible to conduct using macroscale chemotaxis assays, demonstrating how microfluidic systems can not only simplify, but enhance the capabilities of biomedical researchers. This technique and its applications will be discussed in great detail in subsequent chapters. The technological advancements in microfluidics combined with their demonstrated advantages over macroscale assays allowed for their implementation in several clinical applications.

2.6 Microfluidic chemotaxis for translational research

Assays that directly probe cellular chemotactic function have the potential to make valuable contributions to medicine. The concept of probing the function of a cell-type to characterize a patient's disease state is beginning to show promising results in medical research. This approach seeks to elicit information from the cell-type of interest in order to diagnose disease, or perhaps for monitoring drug therapies. However, the approach of using cell chemotaxis function as a readout for clinical medicine in an embryonic stage, with few studies demonstrating this approach to-date. These studies share several characteristics, such as superior control of the biochemical gradient compared to macroscale chemotaxis assays; user-friendly operation helped by utilizing passive pumping techniques[12] for fluid handling; and the use of visual readouts that track cell migration over time.

Neutrophils are a potential candidate cell-type for eliciting disease information based on chemotaxis function because of their central role in the pathophysiology of several diseases, as well as their robust ability to

undergo chemotaxis. Several studies have been conducted that probe neutrophils for diagnostic information.[27,76,77,148] For example, Butler *et al.* describe a neutrophil chemotaxis platform that analyzed neutrophils from burn patients in order to characterize their health status.[27] In this study, the authors found that the magnitude of the burn injury negatively correlated with the speed of neutrophils migrating towards the chemoattractant, and impaired neutrophil chemotaxis was observed as early as 24 hours after the patient was burned. This result validates trends that have been observed in previous studies using traditional chemotaxis techniques, such as the Transwell and Zigmond assays[150], although those studies did not observe changes in neutrophil function until 72 hours after the patient was burned. Additionally, the authors in this study found a correlation between total body surface area of the burn and neutrophil chemotaxis function of the patient, which earlier studies did

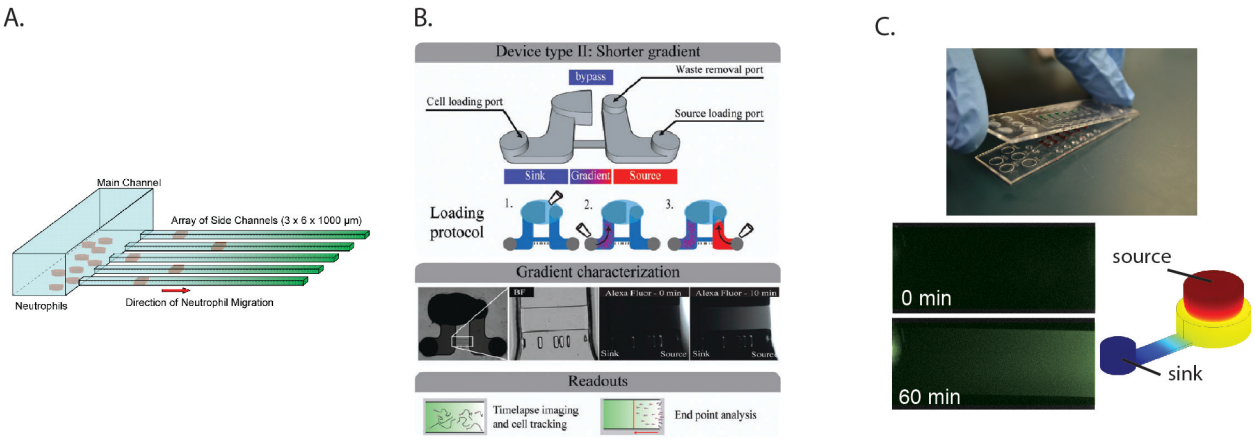

Figure 2.5 Recent user-friendly chemotaxis devices that have been utilized for clinical applications. A. Neutrophil chemotaxis through cell-sized microchannels (3 µm x 6 µm) that allow for easy quantification; robust persistent neutrophil chemotaxis; and precent convection from the source to the sink. **B.** A chemotaxis device that also utilizes a low-height "diffusion channel" to prevent convection, along with a low-resistance "bypass" to direct any potential convection in the diffusion channel. **C.** A neutrophil chemotaxis device that operates by placing a lid containing chemoattractant onto a base containing the cells. Once the connection is made, the chemoattractant can diffuse into the microchannel where the cells are visually tracked over time. Experimental and modeling data of the gradient development are shown. Importantly, all three of these methods can be operated using only a micropipette, and don't require complex fluid handling equipment of expertise.

not uncover. The improved detection of disease phenotypes for the burn patients compared to macroscale techniques is likely due to the improved sensitivity that microfluidic gradient generators can achieve. Keeping user-friendly design considerations in mind, the authors designed this microfluidic chemotaxis device to operate without any external fluid handling equipment (Figure 5A). In contrast, most traditional macroscale chemotaxis assays would be difficult to operate in a clinical setting. This study demonstrates how chemotactic function can provide rich, functional information that can potentially be used as a diagnostic, prognostic, and/or therapeutic biomarker.

In our research lab, we have also explored the possibility of using neutrophil chemotaxis for diagnostic applications.[148] Berthier *et al.* describe a microfluidic chemotaxis device that can easily setup biochemical gradients in a high-throughput screen and automatically track neutrophil chemotactic function (Figure 5B). This study analyzed the neutrophil chemotactic function from an infant who presented recurrent bacterial infections. The analysis showed a significantly retarded neutrophil chemotactic response for the patient compared to both healthy controls and the infant's parents (0.7 μm/s vs. 0.15-0.17 μm/s, respectively). The visual assay provided clear morphological information of the neutrophils and quantitative characterization of the neutrophil chemotaxis. Importantly, both pieces of information conveyed a signaling defect for the patient. Indeed, the patient was later diagnosed with a rare genetic mutation in a GTPase Rac2 (D57N) that has been previously reported in the literature for an infant with immunodeficiency.[151] This sort of rare immunodeficiency is difficult to diagnose clinically, but this study demonstrates that a functional readout based on cell chemotaxis could potentially aid in making the diagnosis. In another clinical study, we are employing an adaptation of a previously published chemotaxis platform (Figure 5C, reference 28) to study whether neutrophil chemotaxis can be used as a biomarker to characterize or diagnose asthma. In this study, we have utilized a microfluidic kit design, where all the reagents required to run the assay are assembled in a complete, user-friendly assay. Additionally, the method employs a neutrophil sorting technique[75] that can be performed in several minutes using blood obtained from a lancet puncture. These features make it simple to rapidly perform the chemotaxis assay and makes the system well-suited for implementation in a clinical setting. Preliminary results from this study indicate that neutrophil chemotactic function may be impaired for asthmatic patients compared to non-asthmatic, allergic rhinitis

patients (more details in Chapter 5). Although the results still need to be vetted with additional experiments and broader patient populations, the study illustrates how microfluidic solutions can provide significant advantages over macroscale assays for clinical applications. Furthermore, these works demonstrate that chemotaxis can be a useful readout in the clinic to assist physicians with diagnosis or management of a variety of diseases.

Currently there are few studies that use chemotactic readouts in a clinical setting, and other cell types beyond neutrophils have not been utilized for this purpose. However, given that there are migratory cell types that are central to the pathophysiology of many disease, there are no technical or biological reasons why the chemotactic function of other cell types could not be measured for clinical applications in the future. A new class of user-friendly chemotaxis assays that are combined with sophisticated automated tracking software have been published in recent years. These assays provide a compelling solution for physicians that wish to add additional tools when performing differential diagnostic procedures.

2.7 Future outlook

The use of microfluidic chemotaxis technologies in biology and translational research is still its infancy, and the likelihood of these techniques penetrating into mainstream clinical practice remains unclear. To-date, there have been proof-of-concept studies that demonstrate how cell chemotaxis can be used to characterize or diagnose clinical symptoms, and these functional readouts have the potential to yield highly personalized insights into the disease phenotype for patients. However, the adoption of these techniques will likely be determined by whether the chemotactic information can aid physicians in making diagnostic or therapeutic choices. This information needs to add to the characterization of the patient beyond the clinical symptoms the patient exhibits and the genetic/proteomic analysis that could be performed. Does the morphology of a migrating cell reveal information about the disease? Does directionality or chemotaxis velocity of a cell indicate hyperactivity that is useful for diagnostics or management of patient therapies? Recent studies have demonstrated that in some cases, the answer to these questions is "yes," but more studies are required in order to cement these techniques into mainstream clinical practice. What is clear is that the advantages of using microfluidic technologies for

personalized analysis of a patient is compelling, and microfluidics appears to offer the most promising technological platform on which to build these novel assays.

2.8 Copyright permission

This chapter has been taken an adapted from my contribution to a book chapter currently in preparation. Figures 2, 4, and 5 contain images that have been reprinted with permission from the original sources. Figure 2 from references 16, 17, 134, and 18. Figure 4 from reference 24. Figure 5 from references 27, 148, and 28.

Chapter 3

Fabrication of microfluidic devices with PDMS and polystyrene

3.1 Introduction

Microfluidic devices have been fabricated using a variety of techniques over the years using different material systems such as glass[36-39], silicon[32,33], thermoplastics[63-65], wax[152], paper[69], and an elastomer material called polydimethylsiloxane (PDMS; see Chapter 1 for more a more detailed treatment of this topic). The most common fabrication method that has emerged over the last 15 years utilizes photolithography methods taken from the semiconductor industry to rapid prototype (RPT) 3-D microfluidic molds on silicon wafers. Once the mold has been fabricated, PDMS can be poured over the mold and cured over time to form a solid microfluidic negative of the mold. This is the most common method utilized in our lab to create microfluidic devices, so this technique will be briefly reviewed in this chapter. Furthermore, this chapter will outline a method we developed for the fabrication of thermoplastic materials using hot embossing. The procedure enables investigators to create pressure- and temperature-resistant replicates of the silicon mold that can be pressed into thermoplastics to create microfluidic structures. Lastly, this chapter will explore some of the challenges associated with the fabrication of low-height or high aspect ratio (AR) thermoplastic devices and offer possible solutions.

3.2 Fabrication of PDMS microfluidic devices

One could argue that the primary vehicle that has driven the growth and advancement of microfluidic technologies in the last 15 years[43] can be attributed to the simple, accessible methods available to prototype and develop novel microfluidic designs—namely soft lithography using PDMS.[153] The process of fabricating PDMS microfluidic devices involves 5 primary steps: (1) design concept that has been translated into a 2D mask file; (2) the spinning of a photo-curable liquid polymer called photoresist (we use a material called SU8) onto a polished silicon wafer; (3) transposing the design onto the spun-on photoresist by masking ultraviolet (UV) light using the mask created in the first step; (4) the development of the SU8 master into a mold by removing uncured photoresist using a basic solution; and (5) pouring liquid PDMS onto the mold to create the microfluidic device (a

negative image of the mold). Following these five basic steps, a designer has the ability to conceive of a new microfluidic concept and prototype new devices within 3-5 days depending on the details of the design. Even faster techniques such as 3D RPT printing or micro-machining using CNC mills can also be used for microfluidic device fabrication, however these methods can be expensive and create rough surfaces that make optical imaging difficult or impossible. The following section briefly outlines the process of fabricating PDMS devices, but does not offer a detailed treatment of the process as these methods are widely reviewed in textbooks and the scientific literature.

3.2.1 Step-by-step fabrication process

The first step of the design process is creating a computer aided design (CAD) file of the mask (Figure 1). The purpose of the mask is to define, in two dimensions, the features of the mold that will form in that layer of photoresist (e.g. microchannels, ports, descriptive text, etc). Areas that are in black do not allow UV light to pass through, while transparent areas of the mask that represent the design features permit the transmittance of UV radiation.

A three dimensional (3-D) structure is created by adding additional layers of photoresist that can be cured by additional 2-D masks. Layer-by-layer, the designer adds or subtracts features in order to add complexity to the microfluidic device (e.g. channels or fluid access ports). The thickness of the photoresist layer defines the

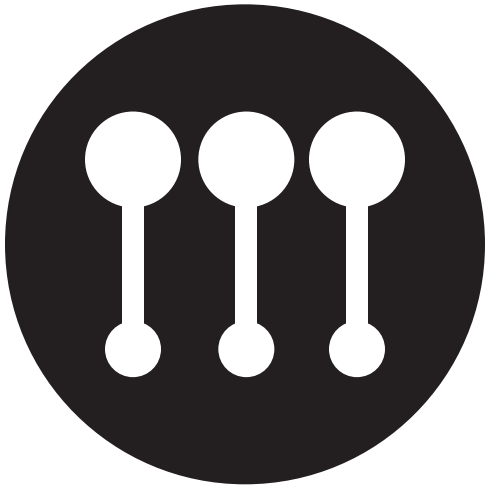

Figure 3.1 2-D mask for the first layer of a microfluidic device. The areas in black block the UV light and areas in white are transparent when printed and transmit UV.

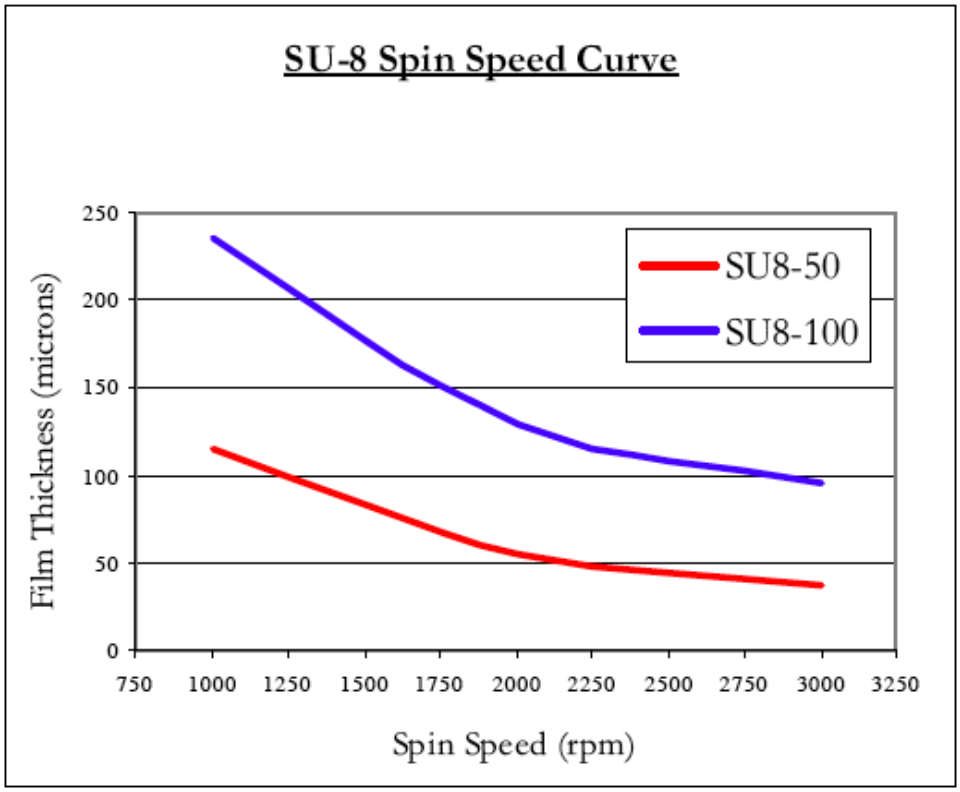

Figure 3.2 Thickness of photoresist is defined by the spin speed of the spinner and the viscosity of the resist. SU8-50 is a lower viscosity photoresist than SU8-100, hence the displacement of the SU8-50 curve below the SU8-100 curve for identical spin speeds. Source: obtained from microchem.com on February 2, 2013.

height of the microfluidic features exposed in that layer, and that thickness is determined by the viscosity of the photoresist and the spin speed of the spinner (Figure 2). Following the spinning step, a soft bake step is required to evaporate the solvent and densify the thin film. For the SU8 masters presented in this document, the soft-bakes were raised from room temperature to a temperature of 95 ℃ at a controlled ramp rate of 250 ℃/hr (or ~4 ℃/min). The time of the soft bake is determined by the thickness of the photoresist (thicker resist layers take more time). However, I found that an increase of roughly 50%-100% should be added to the specification outlined by Microchem for the soft-bake time. Once the soft-bake has been completed, the layer may be exposed by UV light to define the microfluidic features for that layer (Figure 3A). Following the exposure, a post-exposure bake should be performed to selectively cross-link the UV-exposed portions of the polymer. This step

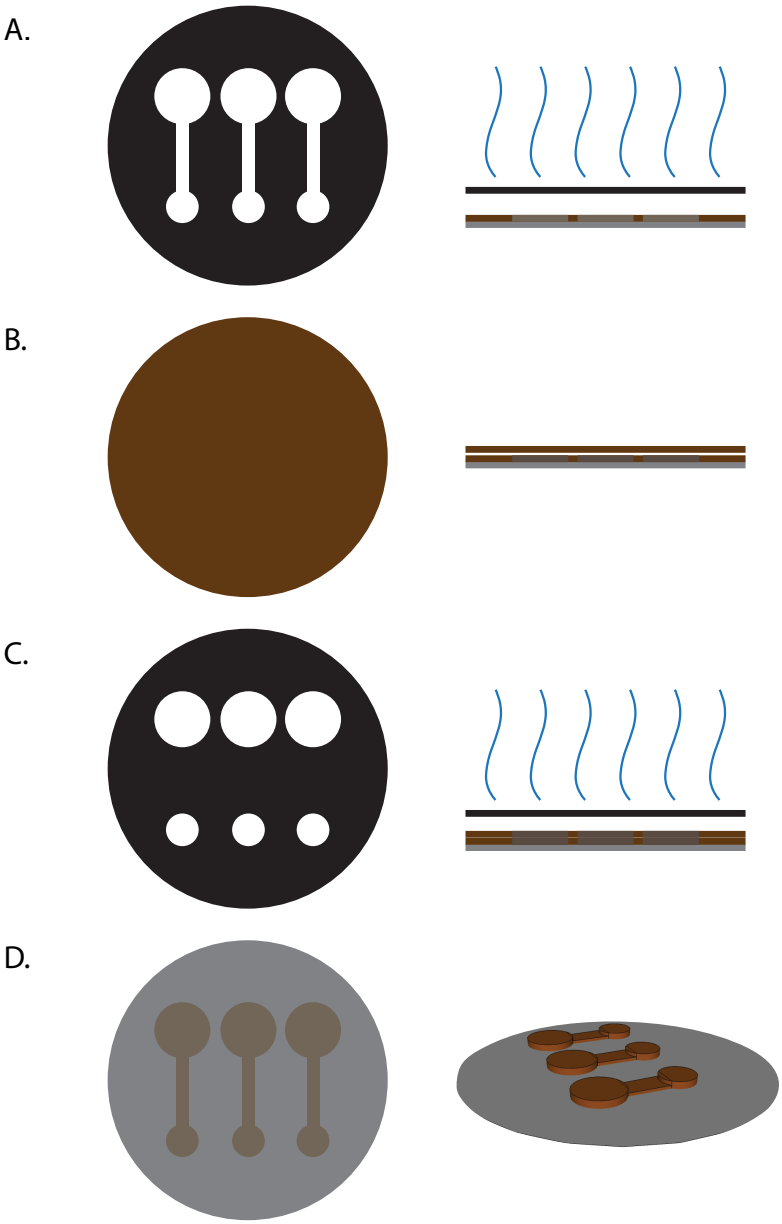

Figure 3.3 Additional steps to SU8 RPT; top view on the left and side view on the right. (A) Selective exposure of SU8 layer defines microfluidic features. **(B)** Spin on additional layer of photoresist to add more features and complexity to your microfluidic design. **(C)** In the second layer, only the circular features will be exposed with UV light; these features will ultimately become through-hole fluid access ports. Note that the connecting rectangle (the microchannel) does not appear in the second layer, which means that this feature is defined in height by the thickness of the first SU8 layer. **(D)** Unexposed SU8 has been developed away, yielding a

finished SU8 mold that can be used to make PDMS devices. Note the taller port features that appeared in two SU8 layers compared to the shorter microchannel that only appeared in one SU8 layer.

should be performed at 95 ℃ (usually for 20-45 minutes), and like the soft-bake step, the wafer should be allowed to controllably increase and decrease in temperature to mitigate thermal stresses in the material and increase the structural integrity of the mold. Once this post-exposure bake has been completed and the features have been defined for that layer, the process can be repeated to add additional layers to the device (Figure 3B-D). Lastly, the mold is created by immersing the wafer-SU8 structure in a developer solution that selectively removes SU8 that has not be exposed by UV light (Figure 3E), leaving only the design features of the device.

This simple and accessible method of rapid prototyping microfluidic designs allows for rapid design iterations and is relatively cheap and accessible for academic research. However, PDMS is not the ideal choice for commercial applications due is poor manufacturing scalability[154]; and more importantly for our lab, PDMS is not entirely compatible when working with cells. We attempted to address some of these concerns by offering an alternative approach to microfluidic device fabrication.

3.3 Fabrication of Polystyrene microfluidic devices

Although PDMS has been a highly versatile material for the development of novel microfluidic technologies, there are significant drawbacks to using PDMS in biology research (see detailed description in Chapter 1). PDMS has been shown to leach uncross-linked oligomers into solution[50], which is highly undesirable when working with cell culture systems. Furthermore, PDMS has been shown to absorb small hydrophobic molecules such as hormones, steroids, and growth factors.[52] For many years the microfluidics community has been unaware of these drawbacks of PDMS in some cases, or ignored these warning signs in others since they are inconvenient problems to deal with.[59] In order to use a new material system that addresses some of the compatibility problems of PDMS with cell biology, we designed a thermoplastic fabrication process using standard hot embossing and thermal bonding techniques. The method allows microfluidic engineers to create microfluidic designs using their standard PDMS rapid prototyping workflow, but then extends the capability to create molds for thermoplastic fabrication (Figure 4). The following sections describe the fabrication process for creating

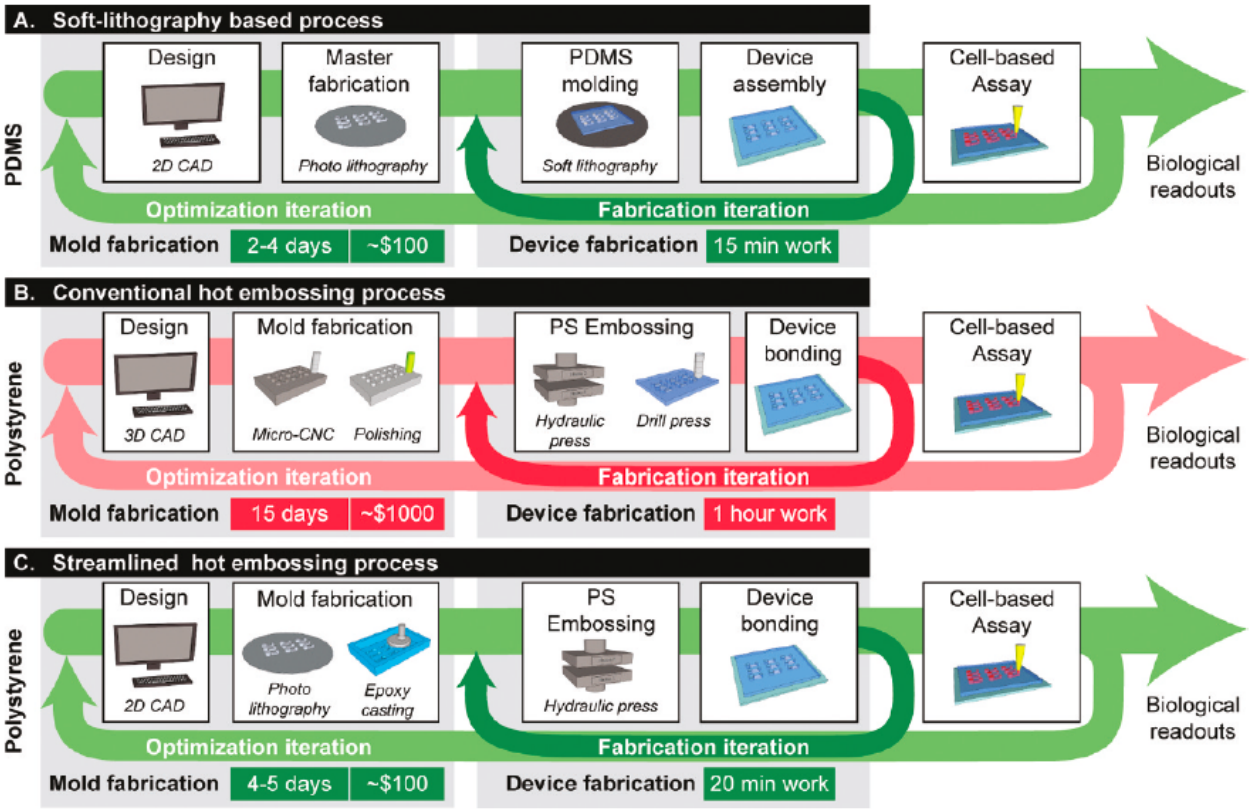

Figure 3.4 Microfabrication process workflows: comparing PDMS to thermoplastics. (A) PDMS-based soft lithography process. Turnaround time from computer mask design to completed master mold is ~2-4 days. Costs include mask, wafer, and SU8 photoresist. **(B)** Current thermoplastic-based microfabrication process. Approximately 10-15 days is required from design to usable mold; 1 h is required for embossing, bonding, and drilling access ports (for a platform containing 50-100 ports). Costs include mold machining and polishing. **(C)** Streamlined thermoplastic-based microfabrication process. Mold fabrication time is similar to that in method **(A)** with an additional epoxy casting step. Costs are similar to those for method A with the additional cost of the epoxy. Devices were fabricated more quickly by use of a through-hole embossing method that eliminated manual removal of access ports.

microfluidic molds; performing hot embossing on polystyrene (and by extension, other thermoplastics); and enclosing microfluidic channels using thermal bonding (content taken and adapted with permission from an original publication in *Analytical Chemistry*; see "Copyright permissions" for details). Lastly, this chapter describes efforts underway to improve the limit for thermal bonding features with high aspect ratios or low feature heights (e.g. ~6-8 μm).

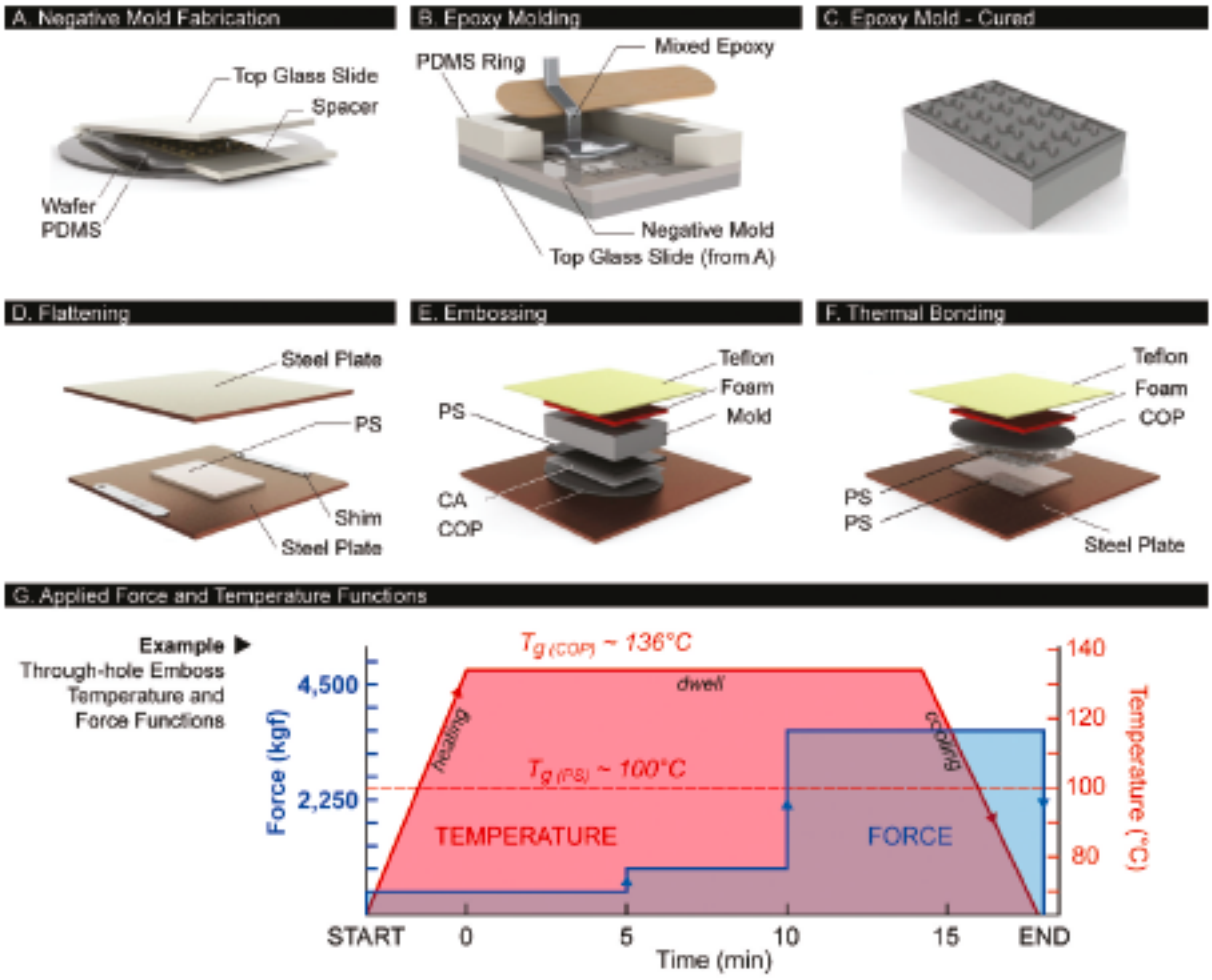

Process	Step	Force (lbf)	Force (kgf)	Pressure (MPa)	Temperature (°C)	Time (min)
Flattening - PS	1	1,000	450	1.15	135	2
	2	5,000	2,250	5.75		2
	3	15,000	6,800	17.25		3
Flattening - COP pellets	1	1,000	450	1.15	155	5
	2	10,000	4,500	11.5		10
Reflattening - COP sheets	1	1,000	450	1.15	155	2
	2	5,000	2,250	5.75		2
	3	15,000	6,800	17.25		3
Emboss - non-through-hole	1	2,000	900	2.3	125	15
Emboss - through-hole	1	1,000	450	1.15	135	3
	2	2,000	900	2.3		3
	3	8,000	3,600	9.2		8
Bonding	1	3,000	1,350	3.45	90	30

Figure 3.5 Polystyrene microfabrication process. (A) Fabrication of a PDMS slab of uniform thickness to replicate the SU8 master. **(B)** Casting of the epoxy in a PDMS cavity composed of the replicate of the SU8 mold and a PDMS ring. **(C)** Cured epoxy mold. **(D)** Flattening of the PS sample to a desired thickness by use of metal shims. **(E)** Hot

embossing of the PS sheet for through-hole fabrication (remove CA and COP for non-through-hole approach). **(F)** Thermal bonding of two PS sample pieces. **(G)** Fabrication recipes for different hydraulic press procedures. Pressure is nominal value calculated on the basis of mold surface area of 50 x 75 mm. Force-temperature functions used for through-hole embossing are shown as an example. Temperature curve consists of heating, dwell, and cooling phases. In the dwell phase, force may be successively ramped over time. During cooling, the final applied force during dwell was maintained to prevent sink marks in the embossed part.

3.3.1 Epoxy Mold Fabrication

The first two steps in our process for thermoplastic fabrication were equivalent to those for the soft lithography process described earlier in the chapter, namely, (1) the design and printing of photomasks and (2) the fabrication of a master mold from SU-8 photoresist (Microchem, Newton, MA). Briefly, SU-8 photoresist was spin-coated on a silicon wafer (WRS Materials, San Jose, CA) to the desired film thickness, prebaked, exposed to UV light (EXFO, Mississauga, Canada), postbaked, and finally developed in propylene glycol monomethyl ether acetate (PG-MEA; Sigma, St. Louis, MO). Draft angles on tall features were made by aligning the UV light-guide at an angle of 30-35º from normal and manually rotating the wafer on a turning plate during exposure. Exposure doses were doubled to account for the angled exposure and the rotation.

A negative mold of uniform thickness was made in PDMS (Dow Corning, Midland, MI) from the SU8 master using typical curing parameters (10:1 mixing ratio of elastomer base and curing agent, 90 ℃, 1 h) (Figure 5A). Uniformity of the layer thickness was critical and was achieved by laying a large glass slide on top of two 2.5-mm thick spacers. The PDMS slab was gently demolded from the wafer without detaching from the large glass slide, thereby preventing shrinkage of the features. A 15-mm tall PDMS ring was laid around the features to form a cavity into which a thermocurable epoxy (EC-415; see Materials and Preparation) was poured and allowed to fill the negative-relief features of the PDMS mold (Figure 5B). Air bubbles trapped in the mold features were dislodged manually with a sharp tool (e.g. dental tools or toothpicks). Desiccating the PDMS mold prior to pouring the epoxy reduced the incidence of these bubbles. Following manufacturer's specifications, the epoxy was cured for 24 h on a 40 ℃ hot plate, followed by a four-stage heat treatment (93 ℃ for 2 h; 121 ℃ for 2 h; 149

℃ for 2 h; 177 ℃ for 2 h) in an oven and subsequent cooling to ~60 ℃ before removal from the oven. The result was a solid positive-relief epoxy mold that replicated the original SU8 master (Figure 5C).

3.3.2 Materials and Preparation

PS raw materials were purchased from Goodfellow (Cambridge, MA) in various stock thicknesses, including 1.2 mm thick stock sheets (ST313120, amorphous), as well as 50, 125, and 250 μm thick stock films (ST311050, ST311125, and ST311250, respectively; biaxially oriented). Thick stock sheets can be precut to size with a razor blade or a laser cutting machine (Jinan Artsign Ltd., Jinan City, China), whereas thinner stock films can be cut to size with scissors. After cutting, PS sample pieces were either used as is, at 1.2 mm thickness, or flattened to other desired thicknesses by use of a hydraulic heated press (see Hot Embossing). The PS sample was placed between two mirror-finished stainless steel plates (McMaster-Carr, Elmhurst, IL) to ensure optical transparency. Note that over time these plates can deform and scratch, and should promptly be replaced with this occurs. Two metal shims (feeler gauge set; Grainger, Chicago, IL) were used as spacers on opposite sides of the PS part to ensure uniform desired thickness (Figure 5D). Parameters used in the PS flattening protocol are listed as part of Figure 5G. As an alternative method to flattening PS sheets, desired thicknesses were also attained by stacking the appropriate PS films together; for example, a 475 μm thick PS layer could be achieved by stacking one 250 μm, one 125 μm, and two 50 μm layers together. This is a much faster and more convenient approach during the hot embossing process. Cyclo-olefin polymer (COP) sheets were purchased from Ajedium Films (Ajedium, Solvay Solexis Inc., Newark, DE) as 610 μm thick sheets made from Zeonor COP (1420R grade). We tested three different epoxies to determine the material most suitable for our applications and our processing requirements: (1) Conapoxy FR-1080 (Cytec Industries Inc., Olean, NY); (2) RenCast 4037 (Freeman Manufacturing, Avon, OH); and (3) EC-415 (Adtech Plastic Systems, Madison Heights, MI). The strongest of the three materials was EC-415, since the material strength is increased by aluminum microparticles. Like most composite materials, EC-415 benefits from the "rule of mixtures", whereby the strength properties of the microparticles proportionably contribute to the overall strength of the material, while ductility is somewhat preserved by the matrix material (in this case, the epoxy).

3.3.3 Hot Embossing

Hot embossing was carried out by use of a programmable hydraulic press with heated platens (Model 3889, Carver Press, Wabash, IN). Two different approaches were used for embossing microfeatures into PS, the choice of which was dependent on the nature of the features. The first approach embossed the pattern into the PS without penetrating the material (i.e., the non-through-hole embossing approach). In this approach, the hydraulic press platens were first heated to an initial temperature of 125 ℃, ~25 ℃ above the glass transition temperature of PS. The PS sample was then loaded into the press in an arranged stack consisting of (from bottom to top) (1) a mirror-finished stainless steel plate; (2) PS sample; (3) epoxy mold; (4) 1 mm thick silicone rubber (McMaster- Carr, Elmhurst, IL) to more uniformly distribute the pressure; and (5) ~380 μm thick Teflon film (McMaster-Carr, Elmhurst, IL; Figure 5E). After loading, the press was closed with an applied force of 900 kgf (kilogram-force) (2000 lbs) for 15 min (Figure 5G, non-through-hole emboss). An in-house cooling system, consisting of a water chiller (Model ER301, Elkay, Oak Brook, IL; available from McMaster-Carr) and water pump, was connected via tubing to the platens of the hydraulic heated press in order to accelerate the cooling step in the recipe. Once cooled to ~70 ℃, the press was opened, and the PS sample was carefully demolded from the epoxy mold.

The second approach was used to emboss the pattern into the PS with penetration of the material at specific locations (i.e., the through-hole embossing approach). With respect to microsystem designs, through-holes are needed as access ports to the microsystem pattern. In this approach, the platens were first heated to 135 ℃ prior to loading the arranged stack containing the PS sample. The arranged stack was similar to the non-through-hole approach but consisted of an additional 610 μm thick COP sheet and a cellulose acetate film (Cheap Joe's, Boone, NC) between the stainless steel plate and the PS sample. An automated embossing recipe (Figure 5G, through-hole emboss) was applied to the stack via the hydraulic press. Cooling and demolding steps were similar to the non-through-hole approach. Note that although PS is able to reflow at these temperatures, the sample needed to be thinner than the height of the tallest mold features by ~100 μm to achieve complete

penetration of the mold; the feature heights of the mold can very from one side to the other, so the shortest feature should be taken for the 100 µm subtraction.

3.3.4 Thermal Bonding of PS Devices

To form enclosed PS devices, thermal diffusion bonding was applied to top and bottom PS sample pieces. Depending on the design, the bottom PS sample was either a simple flat sheet without features (plain substrate) or a PS layer consisting of embossed features; the top PS part was a PS layer containing microchannels and through-hole access ports. In both cases, the top and bottom PS samples were blow-dried with compressed air and arranged in a stack consisting of (from bottom to top) (1) stainless steel plate, (2) bottom PS layer, (3) top PS layer, (4) COP sheet, (5) silicone rubber, and (6) Teflon film. The hydraulic press was preheated to 90 C for 10 min, after which the stack was loaded and the press was closed with the required force and for the required time (Figure 5F). The platens were cooled to ~70 C before the bonded PS device was removed from the press. Different applied forces and bonding times were tested to determine optimal bonding parameters (see Bond Strength Characterization). In separate experiments, thermal bonding was also tested after sonication (10 min, 50 C) and oxygen plasma treatment (30 sccm, 60 W, 12 s) on the PS samples.

3.3.5 Bond Strength Characterization

Bond strength was quantified by a crack propagation method and surface energy calculation as an approximation.[155] Briefly, a 50 µm thick metal shim was inserted between two bonded PS layers, resulting in delamination of the bonded pieces in the form of a propagating crack line. The inserted shim and crack region were imaged together on an Olympus SZX16 stereoscope (Olympus, Center Valley, PA), and the delamination length (i.e., average distance between inserted shim and propagation crack line) was measured by ImageJ software (NIH) (Figure 5D). Shorter delamination lengths corresponded to higher surface bond energies, referred to as bond strength (joules per square meter) hereafter. We tested a minimum of three independently bonded devices (n = 3) for nine different sets of bonding parameters (900, 1350, and 1800 kgf applied force, each at 15, 30, and 60 min, with no surface treatment) to determine trends associated with force and time. From these data, one set of parameters was chosen (1350 kgf applied force, 30 min) for further analysis of bond strength with different surface treatments (sonication and oxygen plasma).

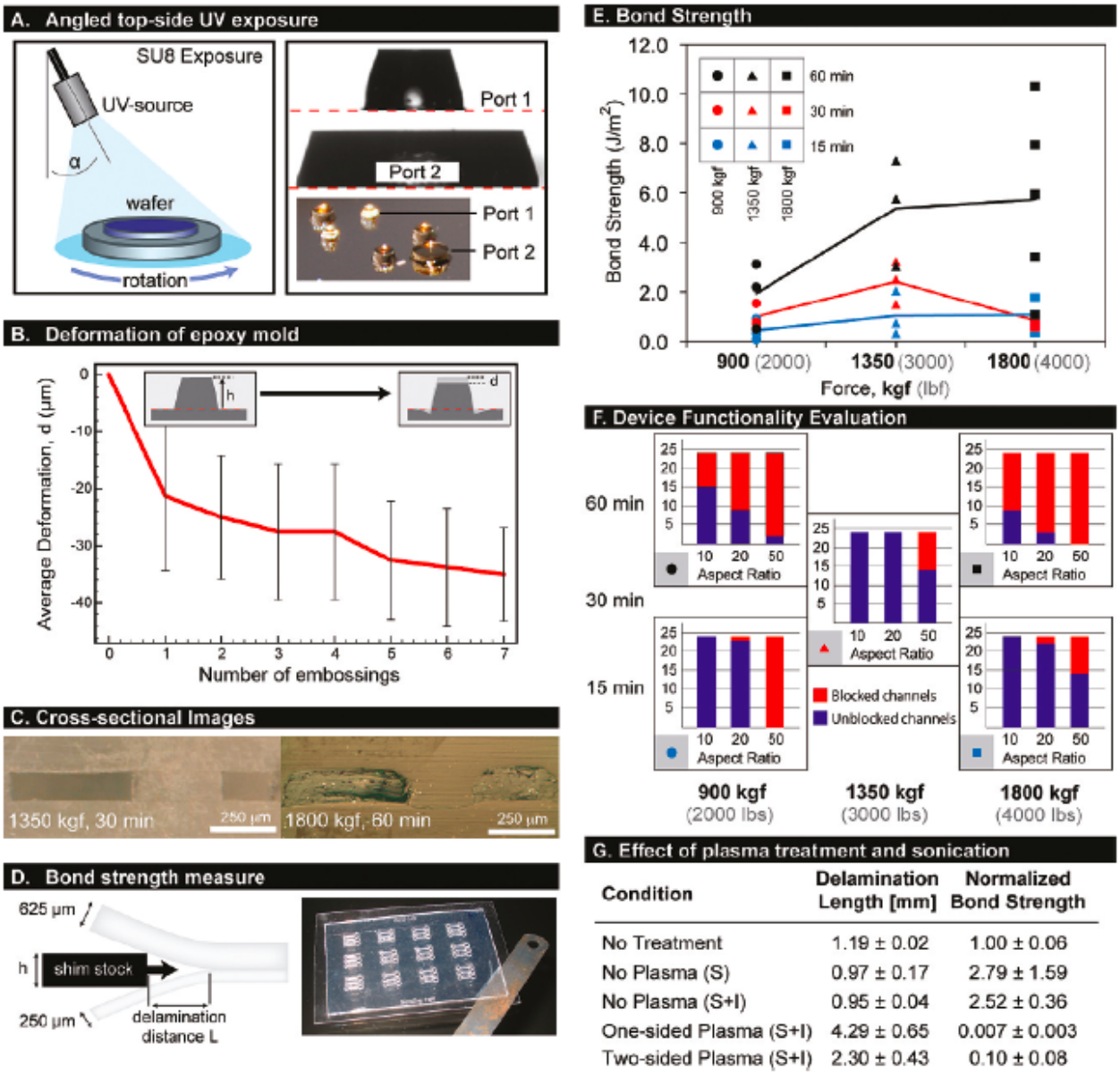

G. Effect of plasma treatment and sonication

Condition	Delamination Length [mm]	Normalized Bond Strength
No Treatment	1.19 ± 0.02	1.00 ± 0.06
No Plasma (S)	0.97 ± 0.17	2.79 ± 1.59
No Plasma (S+I)	0.95 ± 0.04	2.52 ± 0.36
One-sided Plasma (S+I)	4.29 ± 0.65	0.007 ± 0.003
Two-sided Plasma (S+I)	2.30 ± 0.43	0.10 ± 0.08

Figure 3.6 (A) UV exposure for SU-8 features with draft angles with rotation. **(B)** Deformation of the epoxy mold after repeated through-hole embossing. **(C)** Cross-sectional images for optimal bonding condition (1350 kgf, 30 min) and suboptimal condition (1800 kgf, 60 min) that led to significant channel deformation. **(D)** Schematic and image of bond strength test. **(E)** Bond strength results determined by crack propagation method. Nine conditions were tested, all at least in triplicate (all data points shown to indicate data spread). **(F)** Evaluation of device functionality by counting the number of blocked channels after bonding with a given set of parameters. All 24 microchannels for each aspect ratio were measured (heights of bars) and categorized as blocked (red) or unblocked (blue). **(G)** Effect of sonication and

oxygen plasma treatment on bond strength (values normalized to no treatment control). n = 3 for all conditions tested. Values represent average ± SD. S = sonication; I = incubation at 37 C, 5% CO_2.

3.3.6 Cross-Section Analysis

Cross-section analysis was performed on three representative sets of bonding parameters to illustrate how bonding parameters affected cross-sectional shape of microchannels. Bonded devices were cut near the desired cross-sectional plane on a VC-50 precision diamond saw (Leco, St. Joseph, MI). The use of a diamond saw was critical to achieve a highly precise cut and minimize the heat affected zone (HAZ) that occurs with more crude cutting tools. The cut samples were wet-sanded to a glossy finish with 800- followed by 1200-grit sandpaper. After the desired finish was achieved, the sectioned sample was sonicated in deionized water (10 min, 60 ℃) and dried. Imaging was performed on an Olympus SZX16 stereoscope.

3.3.7 Evaluation of Device Functionality

Bond quality and microchannel cross-sectional deformation were further evaluated by testing whether fluid flow was blocked in microchannels after thermal bonding. We designed a microsystem containing microchannels of three different (width-to-height) aspect ratios (AR = 10, 20, and 50), all with the same height of 10 µm. Twelve microsystems were placed in a 3 x 4 array on a single 50 x 75 mm device and fabricated by the through-hole embossing method. The device was then bonded with five of the nine sets of bonding parameters tested for bond strength: (1) 900 kgf, 15 min; (2) 900 kgf, 60 min; (3) 1350 kgf, 30 min; (4) 1800 kgf, 15 min; and (5) 1800 kgf, 60 min. Tests were conducted by flowing colored dye into each microchannel on the device and counting the number of blocked microchannels.

3.4 Results

The embossing and bonding protocols described in the previous section enabled simple fabrication of through-hole microfluidic devices devices in polystyrene. By extension, this technique could be applied to other thermoplastics such as COP and PMMA, with modifications to the temperature, pressure, and time parameters. Note that COP is used as a backing material for the through-hole emboss step, so automated through-holes are

more challenging if COP is used instead of PS since another backing material with an even higher T_g than COP should be used.

We characterized the embossing and bonding processes in order to understand the limitations of the methods described (Figure 6). The angular exposure of UV light reliably produced tapered features that greatly assisted in the demolding process (Figure 6A). This was especially critical for tall features such as ports, which could otherwise be prone to "T-topping"—or wider dimensions at the top of the feature compared to the base—during the SU8 photolithography process. We then characterized the deformation that occurs to the epoxy mold and found that significant shortening in feature height was observed in early hot embossing trials, and then began to asymptote after ~10 embosses to a ~30 μm decrease in feature height (Figure 6B). The elevated temperature and pressure likely accelerates the deformation process on the epoxy mold, before the material begins strain hardening due the cyclical stresses applied to the material.

We also characterized the thermal bond strength for a variety of parameters (time, pressure) and feature geometries (Figure 6C-F). As expected, an increase in pressure and time often positively correlated with an increase in bond strength (Figure 6E), though channel collapse or deformation was sometimes observed for longer bonding times. For these tests, the temperature was held constant at 90 ºC (below the glass transition temperature of PS), as this temperature provided the most robust bonding properties while limiting feature deformation. Unfortunately, even at 90 ºC the microchannels with higher aspect ratios (20-50) collapsed due to material deformation (Figure 6F). Sonicating the pieces of polystyrene greatly increased the bond strength by removing particulate matter on the surface of the PS that can obstruct the bond (Figure 6G), but the improvements were not significant enough to lower the bonding temperature and prevent microchannel collapse. Therefore, we sought alternative solutions such as plasma treating the surface to locally reduce the activation energy required for bonding of the materials, although this can also decrease the bond strength (Figure 6G). The following section describes an ongoing effort to improve the bonding of low feature heights and higher aspect ratios, which may be important for certain microfluidic features such as "diffusion channels" and cell migration applications (both described in Chapter 2).

3.5 Hot embossing low feature heights and high aspect ratios

In order to improve bonding of polystyrene microfluidic devices with small features or high aspect ratios, we had to develop strategies to reduce material deformation during the bonding process. This was already partially achieved by thermally bonding devices at 90 ºC, well below the glass transition temperature for polystyrene (~100-105 ºC). Unfortunately, even at 90 ºC, the temperature and pressure we use to achieve reliable bonding and enclosure of the microchannels lead to significant channel collapse under certain circumstances (Figure 6F). The collapse of microchannels is due largely to the added temperature and pressure required to achieve bonding over the entire device; since the platens in the hydraulic press are uneven and the epoxy mold itself is uneven, the pressure is non-uniformly applied to the surfaces of the two pieces of polystyrene at the bonding interface. There is no practical solution for addressing the unevenness of the platens and mold, so other strategies to reduce material deformation are needed. The approach we chose was to move as far away in temperature from the T_g to reduce bulk flow of the material, or if possible decrease the pressure applied during the bonding process. For robust bonding to occur, the activation energy required to form intermolecular bonds at the PS-PS bonding interface must be reduced.

To achieve bonding at temperatures even further below T_g we attempted plasma treatment-assisted (PTA) thermal bonds. An oxygen plasma treatment (45 sccm for 2 min, 3 min pumping with gas off, 30 W, 30 s) transforms the chemistry of the surface to a higher oxidative state and reduces the contact angle of liquids on the thermoplastic surface.[156] This strategy of functionalizing the plastic surface to reduce bonding temperature has been successfully applied in the past for microfluidic devices made with PMMA and COC, two classic thermoplastic materials used for microfluidic devices.[157] The following is a brief summary of the parameter-space we investigated for the polystyrene bonding trials:

- Performed over 100 emboss and bonds with and without plasma treatments
- Kept plasma treatment largely constant (recipe above), although we did try to achieve an upper limit of plasma treatment by over-treating devices. Over-treating led to exceptionally poor boding
- Attempted aspect ratios up to 80:1

Figure 3.7 Summary of plasma assisted bonding trials. (A) Legend describing rough criteria for characterizing bonds at different temperatures and pressures. **(B)** "Ideal" bonding conditions between two PS devices that have been sonicated (no hot embossing). **(C)** Bonding for "real world" conditions, where one piece of PS has been embossed and is non-uniform in height, and the other piece of polystyrene is a flat sheet.

- Lowest feature height attempted was 8 μm
- Temperature ranges from 65-120 ºC tested
- Pressure ranges from 100 – 20,000 lbs tested
- Low pressure, high temperature anneals tested to solidify bonds and induce hydrophobic recovery

3.5.1 Results

The results of the bonding trials are summarized in Figure 7. For a detailed and raw account of these bonding trials, including post-bond photos; experimental details; and commentary; request the digital notebook file from Dave Beebe. In short, none of the bonding parameters attempted produced reliable yields for the bonded devices. Figure 7B. shows that the "ideal" bonds with two pieces of flat polystyrene perform better than the "real-world" thermally embossed devices. This result was expected since the thickness uniformity of the polystyrene is decreased significantly after the thermal embossing process, leading to a non-uniform pressure distribution during the bonding process. Note that the plasma treated device bonded at 5000 lbs and 80 ºC produced an excellent bond under "ideal" circumstances, but the deformation from the embossing procedure significantly reduced the quality of the bond. This result suggests that the two competing factors—the surface defects produced by the embossing process and the need for a uniformly flat surface for the bond—are sufficiently incompatible that thermally bonding small features is not achievable with reasonable yields.

3.5.2 What does this mean for bonding low-feature heights in PS?

The overwhelming conclusion that one should draw from this study is that bonding small or high-AR features is exceptionally challenging for thermoplastic microfluidic devices. Other common strategies for bonding such as solvent bonding or adhesive bonding are likely to draw criticism when used with cells. Furthermore, these methods are also not ideal for short feature heights. Solvent bonding is a destructive process, and erodes material off of the plastic surface beyond the allowable tolerances for 6-8 μm features. Adhesive bonding requires the adhesive to be coated on the surface, which would fill in the small features that one wishes to bond; compatibility issues with cells also arise when considering that adhesives would likely leach out into the cell media.

All materials have limitations in properties, manufacturability, etc, and polystyrene is not immune to this fact. At least for now, one limitation of using PS for microfluidic devices is that the engineer must live with a reduced lower limit in feature size, and an upper limit in aspect ratio. Perhaps PDMS, or even glass, are more appropriate material choices when feature fidelity is a critical constraint on the device design. Alternatively, one might consider other methods to hot embossing for stamping the microfluidic features into the PS; these alternatives should mitigate the deformation that occurs during the embossing process, leading to bonding behavior that more closely follows the improved "ideal" bonding case. CNC milling is one potential solution that meets this criteria, however the roughness left on the channel ceiling after the milling process precludes devices fabricated in this fashion to be used with optical microscopy. For many investigators that rely heavily on optical imaging, this constraint would be a non-starter. Additionally, since only fluorescence imaging would be useful with CNC milled devices, PS would be a poor choice of material due to its autofluorescent properties that can occur after being heat-treated.[66] Ultimately it is up to the engineer to take all of these limitations into consideration before deciding what material choice is best for any given application.

3.6 Conclusion

This chapter has outlined basic techniques for fabricating microfluidic devices using PDMS and polystyrene. The methods for fabricating PS devices have their limitations, primarily with bonding small features, and those limitations should be taken into account when considering what material to use for a given application. Plasma-assisted thermal bonds showed some promising signs to mitigate channel collapse for PS bonding, but ultimately the non-uniformity in both the thickness of the PS and pressure distribution caused by the non-parallel platens necessitate alternative approaches to fabricating devices with sub-10 – 20 μm features.

3.7 Acknowledgements

I would like to acknowledge Edmond Young, Erwin Berthier, David Guckenberger, Jolene Enge, and Adan Gutierrez for contributions they made to the development of the polystyrene fabrication procedures. We acknowledge financial support from the Wisconsin Innovation & Economic Development Research Program (IEDR; E.K.S.); the National Institutes of Health National Cancer Institute (NIH-NCI, Grant CA137673); the Korea

Research Foundation Grant (KRF-2008-220-D00133) (D.J.B.); the Natural Sciences and Engineering Research Council of Canada (NSERC) postdoctoral fellowship (E.W.K.Y.); and the Morgridge Institute for Research (MIR) doctoral scholarship (E.B.).

3.8 Copyright Permission

Chapter 4

Microfluidic kit-on-a-lid: a versatile platform for neutrophil chemotaxis assays

4.1 Introduction

As discussed in Chapter 2, cell chemotaxis is central to biological processes such as wound healing[95], innate immunity[96], and cancer progression.[97,98] The Boyden chamber assay, developed in 1962[16], marked the first advance in engineering platforms that enabled systematic *in vitro* measurements of a cell's response to chemotactic factors. Since the introduction of the Boyden chamber, other methods have been developed for studying cell chemotaxis such as the Dunn[18], Zigmond[17], under-agarose[133], and micropipette-based[134] assays; however, these techniques limit the types of biological and clinical questions that can be addressed. Furthermore, these assays require lengthy blood draws and cell purification protocols[78] that depend upon tens of milliliters of blood to conduct an experiment. This limitation makes assaying neutrophil chemotaxis challenging for circumstances in which milliliters of blood are not easily obtainable, such as for infants or small animals.

Within the last decade, microfluidic platforms have demonstrated the ability to control the spatio-temporal properties of chemical gradients in a precise and reproducible way.[21,143,158,159] In some microfluidic applications the measurement of neutrophils has been used for clinical diagnostics[27,76], demonstrating the potential for translation of microfluidic methods into a clinical setting. However, few examples exist of microfluidic techniques being utilized in hematology research. While the published microfluidic platforms meet the technical requirements for neutrophil chemotaxis assays, they can be difficult to operate; require specialized equipment not typically found in biology laboratories[26]; are tailored for specific applications; and can be limiting in experimental throughput. Furthermore, the vast majority of microfluidic chemotaxis assays do not leverage the ability to use minute volumes of reagents and still rely on time consuming and extensive cell purification methods.[78] The persistence of traditional chemotaxis techniques in the hematology research community is perhaps evidence of some of these limitations for modern microfluidic approaches. Consequently, no dominant

microfluidic chemotaxis platform has emerged that facilitates new avenues of research and is accessible to hematology investigators.

Here we present a comprehensive microfluidic solution, dubbed Kit-on-a-lid-assay (KOALA) for chemotaxis, that performs neutrophil purification from nanoliter volumes of blood in minutes; generates repeatable chemotactic gradients; and does not require specialized equipment to operate. The platform makes possible the study of neutrophil chemotaxis in infants or small mammals, and is particularly useful for dynamic phenomena that need repeated sampling over multiple time-points. These features permit new applications; make the assay accessible to a broad audience of investigators; and significantly shortens the time from the start of sample collection to analysis (Figure 1a). The versatility of the KOALA platform was demonstrated through several applications that are challenging or impossible using traditional techniques. Importantly, all the work presented here was performed using only a micropipette and optical microscope, and no other external equipment was required.

4.2 Results

In the KOALA platform, the neutrophil purification and gradient generation are decoupled in a microfluidic base and a multi-function lid, respectively. The neutrophil purification is performed in microchannels that are located in the base by utilizing a capture technique first reported in a flow-based system.[75] Briefly, neutrophils are captured on a polystyrene surface functionalized by P-selectin, and subsequent washing steps remove the other components of the whole blood. Fluid handling is based on passive pumping techniques, avoiding the need for external active pumping systems.[12] The lid has two primary functions: 1) to house the reagents required to generate the gradient of chemoattractant and 2) to prevent evaporation and flow, which is detrimental to the proper formation of a soluble gradient in live-cell microscopy experiments.[53] Following the neutrophil capture, the chemotaxis assay is initiated by placing the lid onto the base, thereby allowing a chemoattractant in the lid to controllably diffuse into the microchannel. During the experiment the lid can easily be removed, providing fluidic access to the channels or allowing for the application of different lids.

The versatility and enabling potential of the KOALA platform was demonstrated through several applications that are challenging or impossible using traditional techniques. Flexibility of the experimental design was significantly improved with the ability to perform different functions of the assay in different locations, such as capturing mouse neutrophils in the vivarium; culturing cell monolayers in a cell culture hood and incubator; and initiating the gradient at a microscopy facility. The ease of use, variability of applications, and time savings are summarized in Figure 1. First, a monolayer of human umbilical vein endothelial cells (HUVECs) was cultured and subsequently used to capture neutrophils from whole blood (Figure 1b). Second, the KOALA platform enabled repeated neutrophil chemotaxis experiments on small mammals using ~150 nL of whole blood per microchannel (Figure 1c). This sample volume requirement is the lowest reported for leukocyte purification and chemotaxis, and at least four orders of magnitude lower than traditional purification methods currently used in hematology research.[78] Finally, traditional 2D or 3D migration (Figure 1d,e) are both possible with the KOALA platform because the gradient generation from the lid is functionally independent of the cell preparation that is performed in the base microchannels.

4.2.1 Modeling fluid dynamics in microchannels

The method for purifying neutrophils from whole blood relies on pumping media through the KOALA microchannels following the capture of neutrophils on the functionalized plastic or activated endothelium. Therefore, we utilized a previously developed analytical model[160] in order to characterize the range of shear stress generated by passive pumping in the microchannels. In brief, the flow rate in the microchannels is controlled by the pressure generated by the surface tension of the liquid at the input port and the fluidic resistance of the microchannel. The flow rate was calculated for both microchannel geometries presented in this work using Laplace equation (Equation 1) to define the pressure drop at the input port, combined with the Washburn equation (Equation 2) for determining the fluidic resistance of a microchannel with rectangular cross-section (see Materials and Methods). The flow rate in the microchannels was calculated using Equations (1) and (2) and numerical simulation (Figure 2). For the 180 μm tall microchannels, which were used for neutrophil capture on endothelial cells, the shear stress averaged 12 dyn/cm^2. This value is in the physiological range of the shear stresses measured in aorta and capillaries[161], and below shear stress values causing damage to the cell

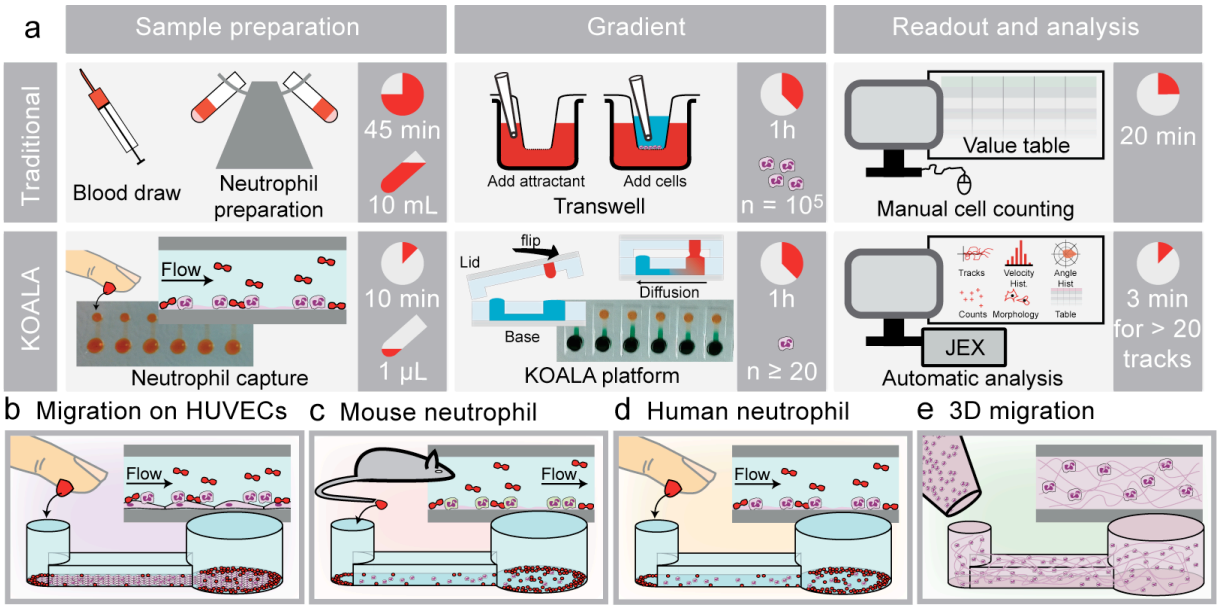

Figure 4.1 Overview of the KOALA platform. (a) Comparison of the purification and chemotaxis protocols for the KOALA platform and Transwell assay. Note that other traditional assays that utilize live-cell imaging (i.e. Micropipette-based assays) take many hours to manually track the same number of cells that can be tracked with automated JEX tracking in 3 minutes. **(b-e)** Applications of the KOALA platform for neutrophil chemotaxis including neutrophils migrating on endothelial cells **(b)**; a 2D chemotaxis assay for neutrophils obtained from mice **(c)**; a 2D chemotaxis assay for human primary neutrophils captured and sorted from a drop of whole blood; **(d)** and neutrophil chemotaxis in a 3D matrix **(e)**. Note: traditional purification methods and sample volumes shown in 1a are required for 3D neutrophil chemotaxis.

monolayer.[162] We found that for the 80 µm tall microchannels, which were used for neutrophil capture on P-selectin coated polystyrene, the shear stress averaged 0.1 dyn/cm^2. These results show that the KOALA microchannels are well-suited for use with cell monolayers and neutrophil sorting from whole blood.

4.2.2 Developing and characterizing KOALA and automated tracking

The ability to generate a stable and controllable chemical gradient for the duration of the experiment in a user-friendly way was central to the development of the KOALA platform. Computer simulation suggested that we would have good diffusion and gradient formation of our chemoattractant using the proposed hydrogel-based

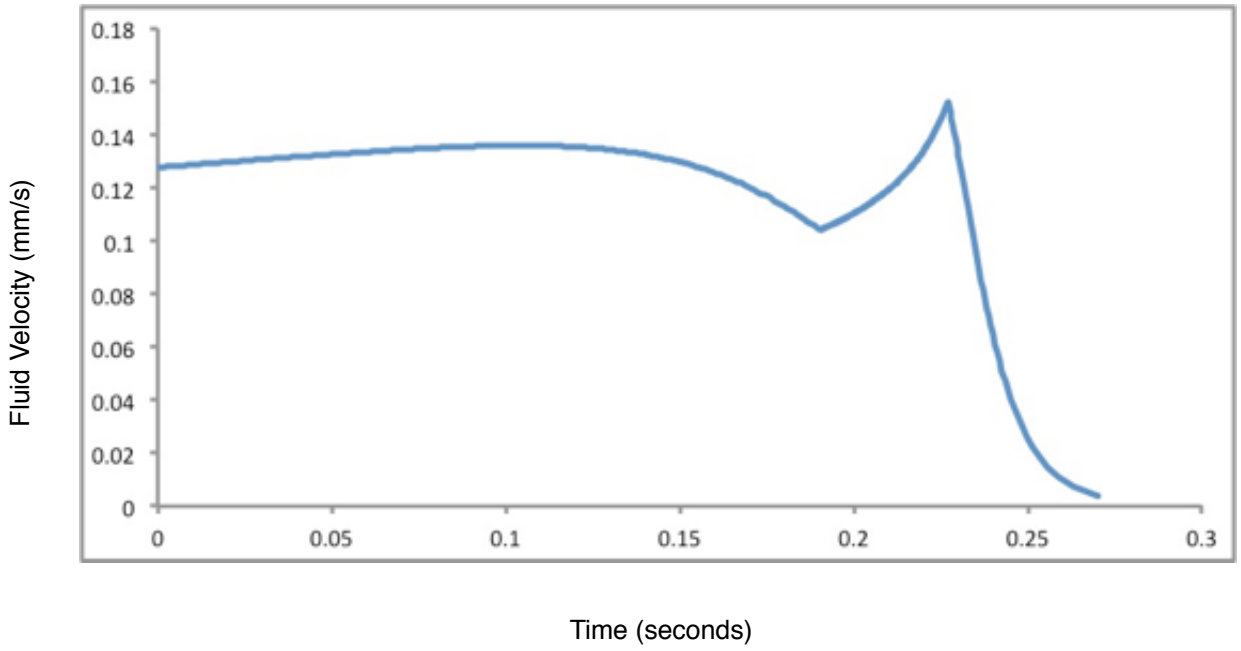

Figure 4.2 Velocity profile at the center of the microchannels for the base component of the KOALA device. The fluid velocity at the center of the microchannel was approximately 0.12 mm/s, yielding a flow rate of 26 µL/s. The velocity profile is stable for the most part of the flow, which lasts for about ¼ of a second, with a brief spike towards the end. The spike occurring at the end of the analysis window is the result of a transition between two phases of the analytical model.

delivery method (Figure 3a). Using fluorescent dye to monitor the profile of the gradient, we found that the KOALA platform generates and maintains a chemical gradient for at least two hours (Figure 3b). These results correlated closely with the predicted gradient determined using numerical simulation (Figure 3c). We found that delivering the source of chemoattractant using a laden hydrogel was a simple and repeatable method. Furthermore, we observed that the lid and hydrogel delivery method nearly eliminates flow and evaporation during a typical neutrophil chemotaxis experiment (Supplemental Video 1), which are common problems for static flow chemotaxis devices.

A second requirement of the KOALA device was the ability to purify neutrophils from whole blood on-chip, following the capture of neutrophils on the P-selectin coated microchannels. This eliminates the need for

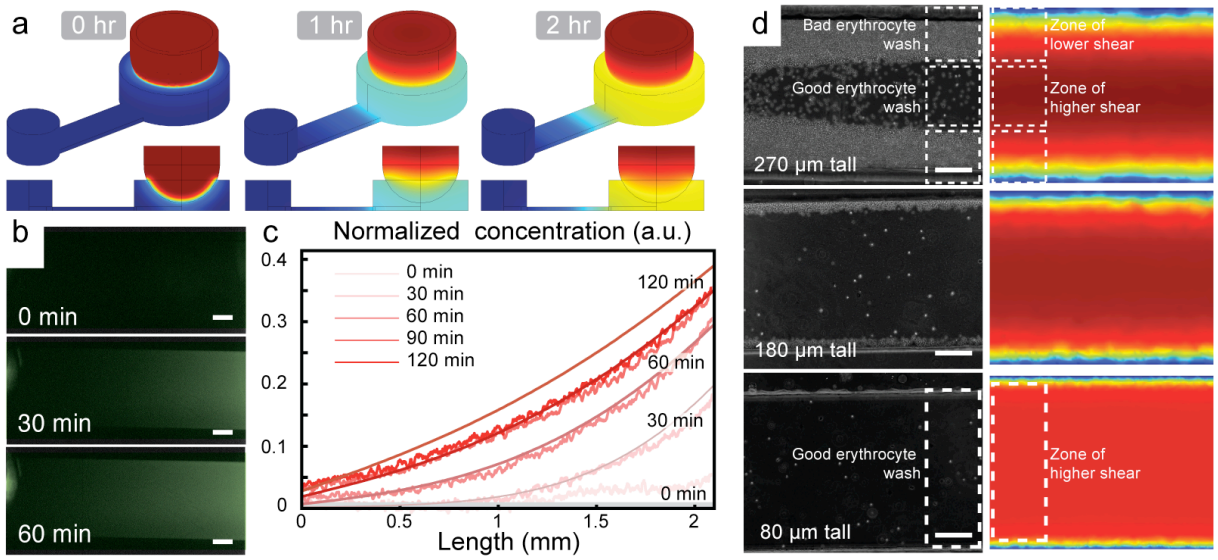

Figure 4.3 Characterization of the chemical gradient generation and neutrophil sorting for the KOALA platform. (a) COMSOL simulations of the diffusion of a chemoattractant loaded in a hydrogel sphere in the lid of the assay, dipping into a microfluidic channel in the base. **(b)** Fluorescent microscopy images of an AlexaFluor dye diffusing into the microchannel in the base of the KOALA platform. **(c)** Comparison of the concentration profiles between the experiments and the numerical simulations. **(d)** COMSOL simulation of the shear stress in microchannels of different heights and comparison with the efficacy of the whole blood washing. Scale bars for **b,d** are 100 μm; phase contrast images acquired using Slidebook software with an Olympus IX-81 microscope using 4x (NA=0.13) **(b)** and 10x (NA=0.30) **(d)** objectives at 37ºC. Additional details on imaging in Materials and Methods section under "Microscopy."

extensive purification protocols. In order to minimize undesirable erythrocyte contamination, we characterized the washing efficiency in the microchannels for various aspect ratios (Figure 3d). We determined that the aspect ratio of the microchannel has a strong impact on the washing efficiency and we found that channel dimensions of 800 μm by 80 μm (aspect ratio of 10:1) was an optimal channel geometry that minimized erythrocyte contamination (Figure 3d). Furthermore, we found that the KOALA microchannels captured a sufficient number of neutrophils in the field of view of a microscope to obtain statistically relevant tracking information (Figure 4). Additionally, we calculated the efficiency of neutrophil capture using KOALA by counting fluorescently tagged

neutrophils in whole blood before and after washing (Figure 4). We found that the KOALA neutrophil sorting technique captures ~80% of human primary neutrophils.

Finally, in order to manage the large quantities of cell migration data, collaborators Erwin Berthier and Jaw Warrick developed a tracking algorithm, dubbed Je'Xperiment (JEX), to analyze large sets of phase contrast timelapse data (Figure 5). Within 3 minutes, the software was able to track the neutrophils and output properties of each cell such as its speed, chemotactic index (CI), and directional velocity (Equations 3-5, respectively). The automated algorithm produced comparable results to manual tracking using the "cell tracking" plugin of ImageJ in only a fraction of the time (Figure 5).

4.2.3 Neutrophil chemotaxis for different slopes of chemical gradient

In order to determine how the slope of the chemical gradient affected neutrophil chemotaxis, we developed a KOALA device with multiple channel lengths to vary the steepness of the chemical gradient (Figure 6a);

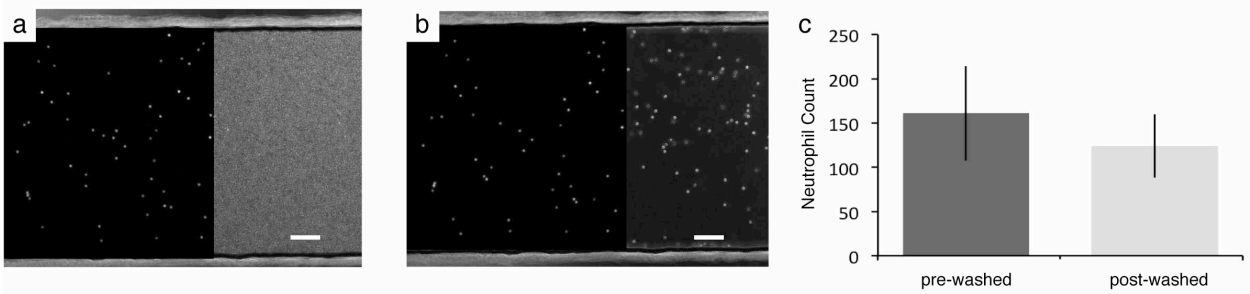

Figure 4.4 Capture efficiency of human neutrophils using the KOALA technique. (a,b) Phase contrast Micrographs of whole blood in the base microchannels prior to the washing step **(a)** and after the washing step **(b)**. Fluorescent neutrophils within the blood are superimposed on the phase contrast images to show the location of neutrophils. **(c)** Average neutrophil counts pre and post washing within the microchannels. Neutrophils capture on average with 80% efficiency on the P-selectin substrate. Scale bars 100 μm; phase contrast and fluorescent images acquired using Slidebook software with an Olympus IX-81 microscope using a 10x objective (NA=0.30) at 37°C. Additional details on imaging in Materials and Methods section under "Microscopy."

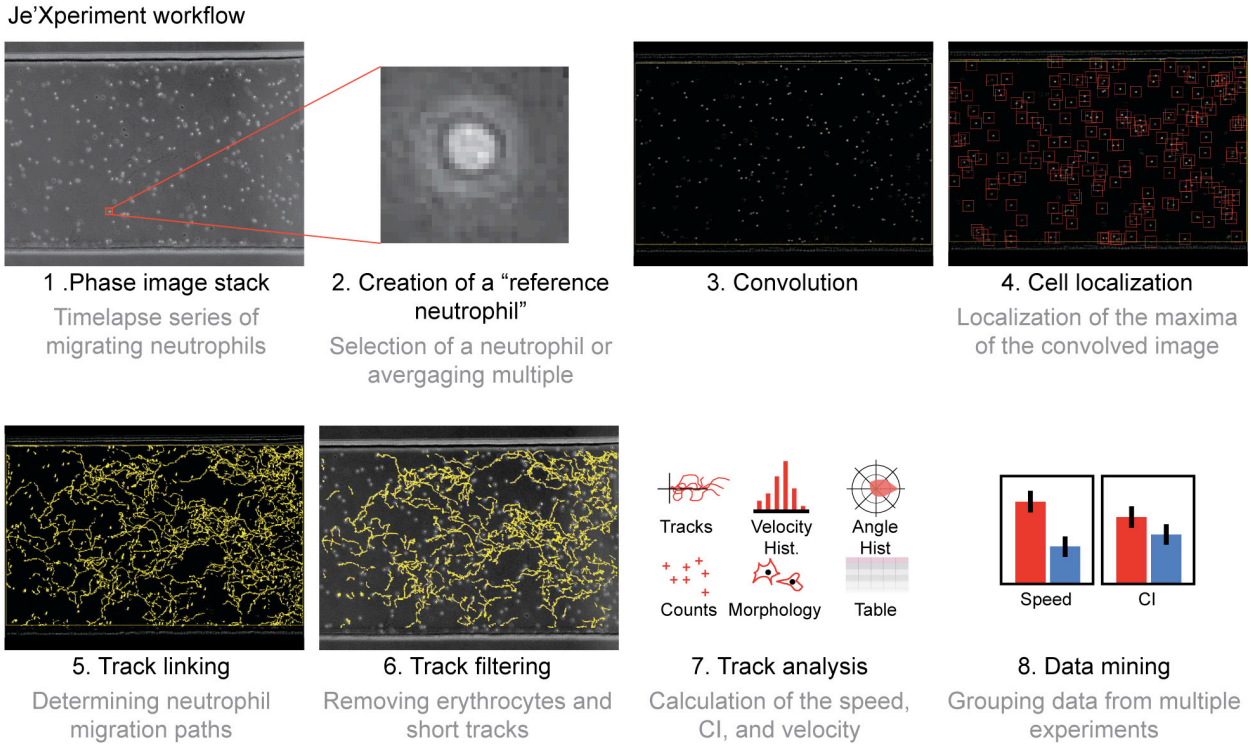

Figure 4.5 Je'Xperiment analysis workflow. JEX begins with the initial image in the timelapse (1); then the user selects a target cell (2); then the software performs a convolution (3) and locates the cells based on the convolved image (4). The cells are tracked from frame to frame (5), and filtering can be applied to further remove erythrocytes or cells that were not well-tracked (6). The software outputs a list of position vectors for each track and automatically yields outputs of interest (7), and has an interface to compare data over multiple samples and outputs (8).

furthermore, a dose response varying the source chemoattractant concentration was performed to measure the chemotaxis response for each channel length (Figure 6b; for raw data

and standard error, see Tables 1-3 in Appendix A). As expected, the random migration speed increased as the channel length decreased, and little neutrophil movement was observed for shallow slope chemical gradients in the longer channels (Figure 6c). A similar trend was observed with the chemotactic index, however this output quickly reached a roughly constant value as the channel length decreased (Figure 6d). Interestingly, the chemotaxis velocity reached a maximum value at an intermediate channel length for higher chemoattractant

dose conditions, but then decreased as the channel length decreased (Figure 6e). These results demonstrate that a microchannel length of 3 mm – the length chosen for the experiments shown in this work – enables robust neutrophil chemotaxis under a range of chemoattractant doses. Supplemental Videos 2 and 3 show examples of 2D human neutrophil chemotaxis in 3 mm long microchannels, using source concentrations of 500 nM fMLP and 0 nM fMLP (control), respectively.

4.2.4 Neutrophil chemotaxis on an endothelial cell substrate

In order to study the different adherent and migratory states neutrophils exhibit under inflammatory conditions in the blood vessel, we developed the KOALA platform to conduct neutrophil capture and chemotaxis on an endothelial cell substrate (ECS). Because the KOALA approach only requires a micropipette to operate and is easily transportable, we were able to integrate a confluent endothelial cell monolayer into the chemotaxis assay. The confluent endothelial cell monolayer could then be activated by IL1-β to express E-selectin (Figure 7a); this process mimics the inflammatory cascade *in vivo*, and allows for the capture of circulating neutrophils on the endothelial surface as the whole blood passes through the microchannel. Note that unstimulated HUVECs did not capture neutrophils using our KOALA platform, as expected (Figure 7a).

Following the neutrophil capture, a gradient of chemoattractant was formed in the microchannels by placing the lid onto the base, initiating the ECS neutrophil chemotaxis assay (Figure 7b; Supplemental Video 1; control – i.e. no chemoattractant – in Supplemental Video 4). When analyzing the area of randomly selected neutrophils that were captured on the ECS, we observed a bimodal distribution of the neutrophils that could be characterized by distinct morphological differences (Figure 8a). One neutrophil morphology appeared darker and more spread on the endothelium when observed under phase contrast microscopy while the other neutrophil morphology was more compact and lighter in appearance (Figure 7c). We termed these two neutrophil morphologies as "Type I" and "Type II" henceforth for reference. The Type I neutrophil morphology had less than half the area of Type II neutrophils as they appeared under phase contrast (Figure 7b). Analysis of the migration behavior of Type I and II neutrophils showed significantly different migratory phenotypes (Figure 7d-h). Type I cells displayed a significantly more directional chemotactic response than Type II cells (Figure 7d,g). By contrast, the Type II morphology was highly spread, had limited directionality (Figured 7c,d,g), and was

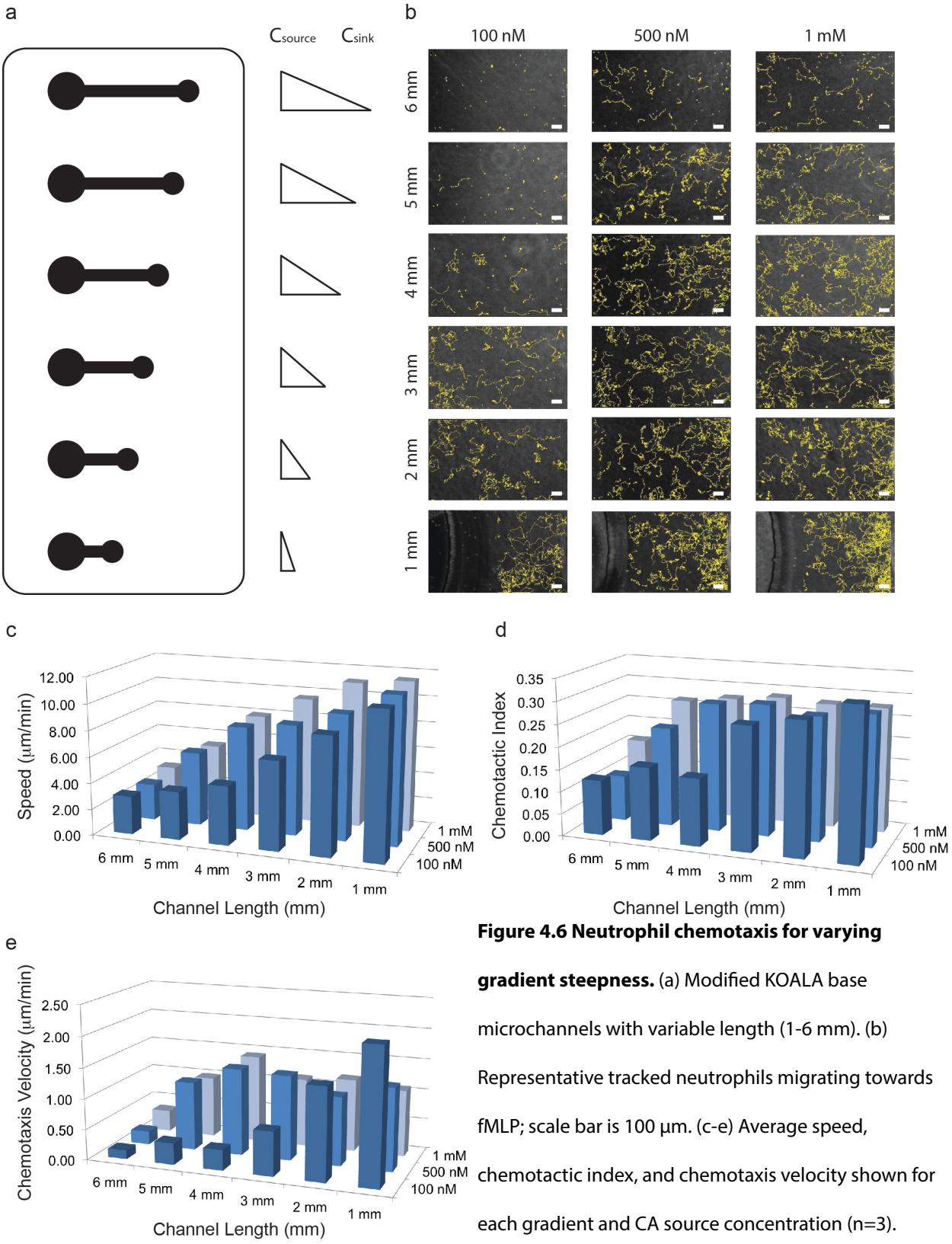

Figure 4.6 Neutrophil chemotaxis for varying gradient steepness. (a) Modified KOALA base microchannels with variable length (1-6 mm). (b) Representative tracked neutrophils migrating towards fMLP; scale bar is 100 μm. (c-e) Average speed, chemotactic index, and chemotaxis velocity shown for each gradient and CA source concentration (n=3).

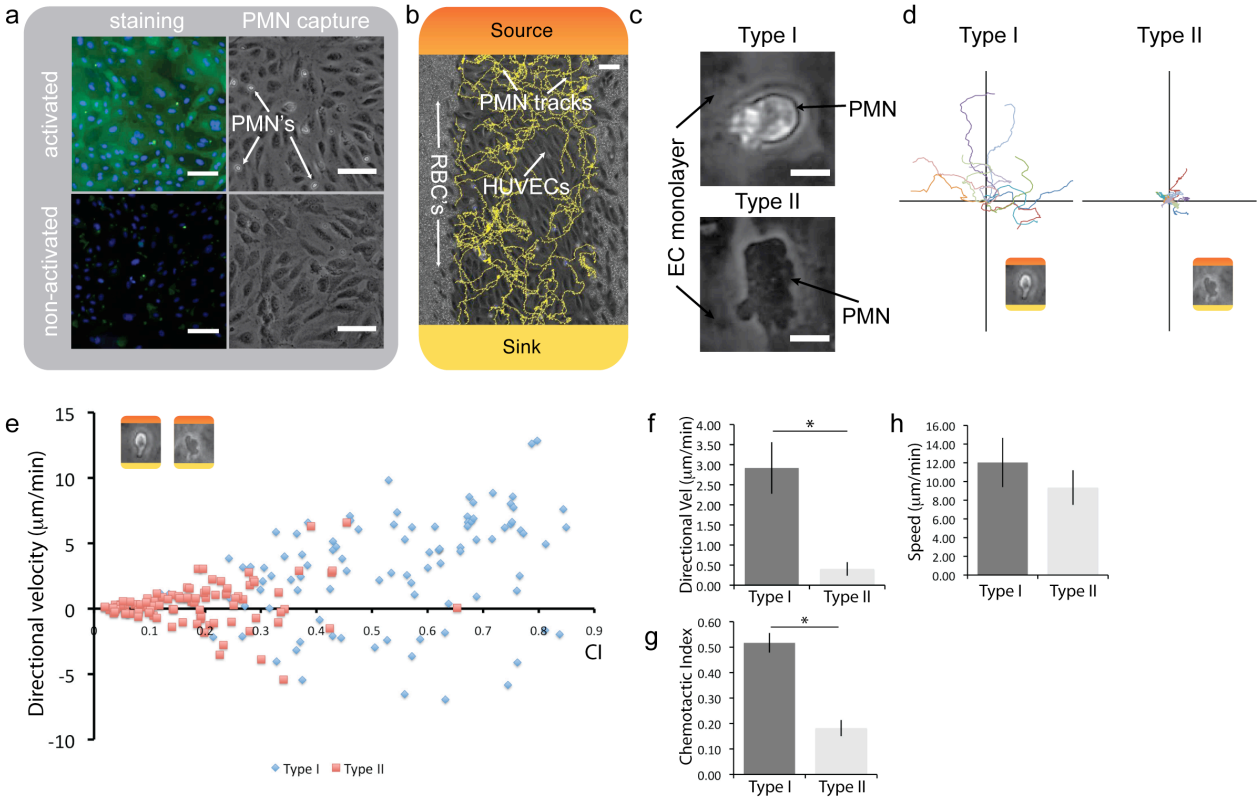

Figure 4.7 Capture and migration of human primary neutrophils on endothelial cells. **(a)** Staining for E-selectin on a HUVEC monolayer and corresponding polymorphonuclear leukocyte (PMN) capture from whole blood. **(b)** PMN migration on HUVECs with red blood cells (RBC's) on the side; automated tracks generated with JEX; colors represent the formation of the chemical gradient – red indicates maximum chemoattractant source concentration and yellow indicates the chemoattractant concentration in the sink. **(c)** Micrographs showing Type I and Type II neutrophil morphologies (also see Supplemental Video 5). **(d)** Representative tracks of each neutrophil phenotype transposed to the origin. **(e)** Representative individual neutrophil tracks of chemotactic index and directional velocity towards the chemoattractant, illustrating the differences in chemotactic function. **(f,g)** Type I phenotype is significantly more directional and has a higher velocity towards the chemoattractant than Type II (*p<0.05; n=3); **(h)** no significant difference in random migration speed between the two neutrophil phenotypes (n=3). Direct comparisons of neutrophil chemotaxis with controls shown in Figure A1 in Appendix A; 100 µm for **a,b**; 10 µm for **c**; error bars show s.e.m.; phase contrast images acquired using Slidebook software with an Olympus IX-81 microscope using a 10x objective (NA=0.30) at 37ºC, except for micrographs shown in **c**.

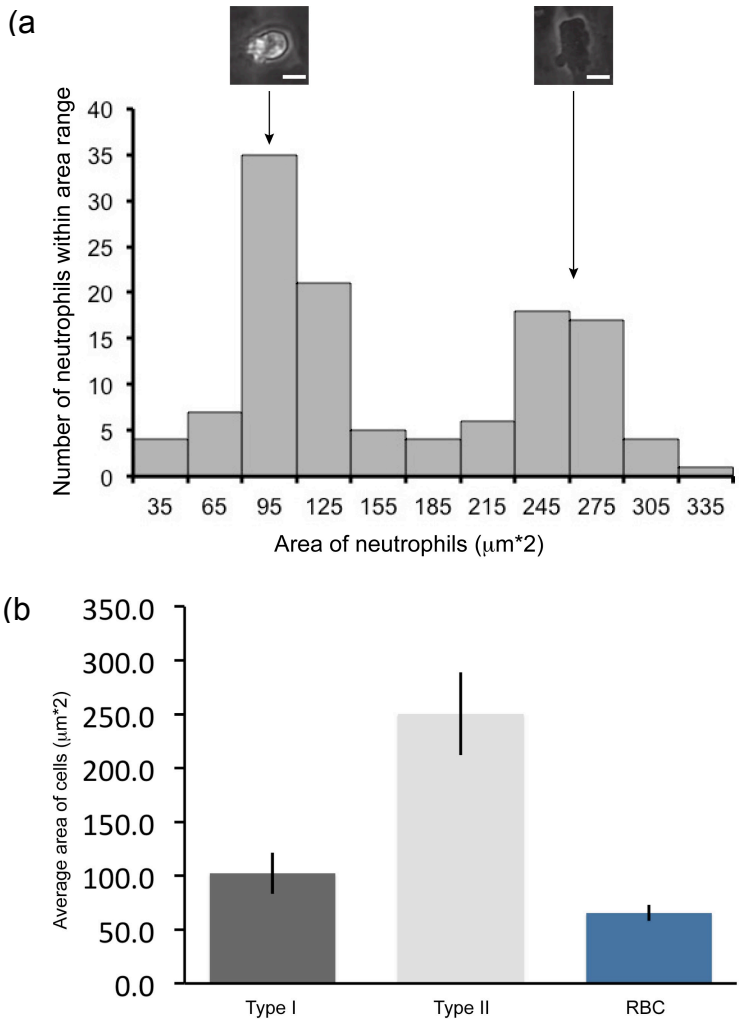

Figure 4.8 Area of Type I and Type II neutrophils as they appear under phase contrast microscopy. (a) Area histogram of randomly selected neutrophils showing a bimodal distribution of area the area of neutrophils; at each mode we observe two distinct neutrophil morphologies, which we termed Type I and II for reference. **(b)** The average area for the different neutrophil morphologies are shown, along with the average area of red blood cells (RBC) for reference. The standard deviation is reported for each area measurement. The area was measured for 59 Type I, 52 Type II, and 25 RBC's over 6 microchannels.

predominantly observed at the endothelial cell junctions (Supplemental Video 5). The Type I phenotype had a significantly higher directional velocity than Type II (Figure 7e,f); however, Type I neutrophils did not have a significantly higher random migration speed than Type II (Figure 7h). In control experiments, neutrophils migrated randomly on the ECS, which is in contrast with the 2D and 3D applications of the KOALA platform where neutrophils were immobile when no chemical gradient was present. As expected, neutrophils migrated significantly less directionally, with lower speed and much lower chemotaxis velocity than cells in a chemical gradient (Figure A2 in Appendix A; Supplemental Videos 1,4). Finally, we observed that neutrophils exhibit both Type I and Type II phenotypes in roughly even proportions at the beginning of the timelapse, and Type II neutrophils transition to Type I progressively during the timelapse over a span of 90 minutes (Figure 9).

4.2.5 Neutrophil adhesion and migration from arthritic mice

The protocol for neutrophil sorting and migration was modified in order to probe the adhesion and chemotactic behavior of neutrophils obtained from mice (see Methods and Materials). We show that the KOALA approach allows for repeated evaluation of the neutrophil adhesion and chemotaxis properties of the animal by acquiring whole blood from a small tail vein puncture without requiring animal sacrifice. Consistent with neutrophil chemotaxis assays for mice reported in the literature[163], mouse neutrophils required higher concentrations of chemoattractant than their human analogue in order to activate and migrate (Figure 4a). Additionally, we did not observe a significant difference in the migration speed, CI, or chemotaxis velocity between the doses of chemoattractant (Figure 10a-c).

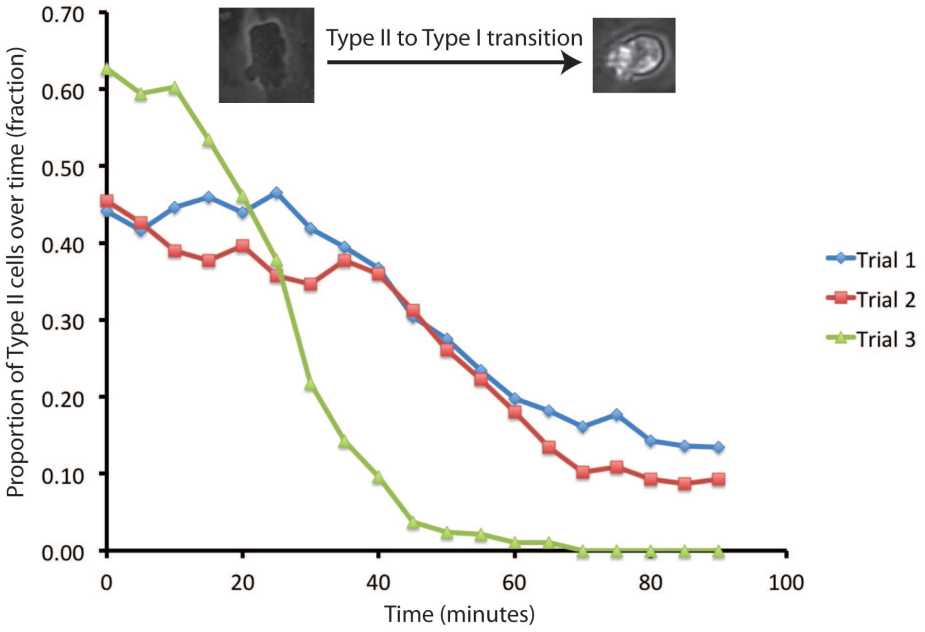

Figure 4.9 Characterizing the transition of neutrophil morphology from Type II to Type I over time. The neutrophils begin roughly evenly split between Type I and Type II morphologies; however, Type II cells transition to Type I after about 30-45 minutes into the timelapse session. Slight increases in proportion of Type II cells are not due to neutrophils changing from Type I to Type II, but rather due to neutrophils of each type entering and leaving the analysis window. Each trial shows analysis on one representative microchannel for a 90 minute timelapse session (n=3 total).

Once we optimized the KOALA platform for mouse neutrophils, we demonstrated its utility and sensitivity for the characterization of neutrophil adhesion and chemotaxis properties in a mouse disease model. We obtained neutrophils from mice that spontaneously develop arthritis due to over-expression of human

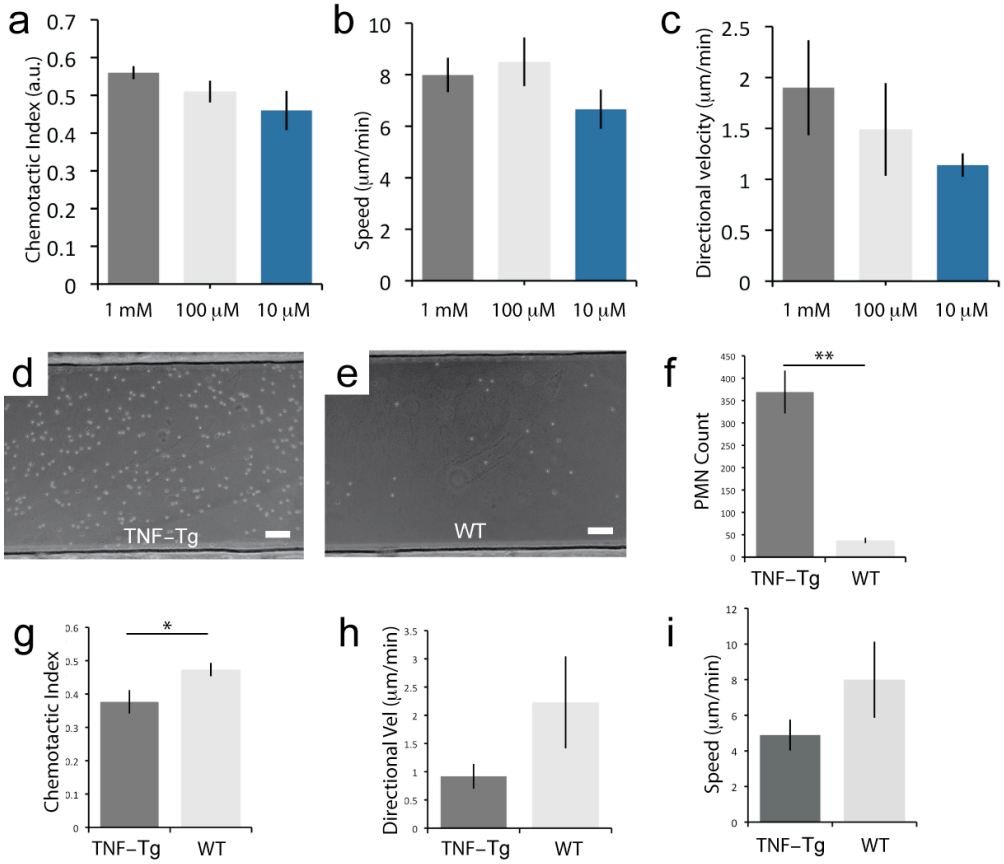

Figure 4.10 Capture and migration of mouse neutrophils from whole blood for TNF-Tg and WT mice. (a-c) Chemoattractant (fMLP) dose response for neutrophils obtained from WT mice from a tail vein puncture, showing the chemotactic index, speed, and directional velocity (n=3). **(d,e)** Representative micrographs of neutrophil capture out of whole blood for arthritic (TNF-Tg) and WT mice. **(f-i)** Difference in the number of neutrophils adhering to the P-selectin substrate, chemotactic index, directional velocity, and speed for neutrophils from TNF-Tg and WT mice [**p<0.01 and *p<0.05; n=5 (**f**) and 3 (**g-i**)]. Note: no observable migration for control (no fMLP). 100 μm for **d,e**; error bars show s.e.m.; phase contrast images acquired using Slidebook software with an Olympus IX-81 microscope using a 10x (NA=0.30) objective at 37ºC.

TNFα[164,165] (Supplemental Videos 6,7). We found that neutrophils from these mice displayed a strong increase in adhesion (Figure 10d-f) and a significant decrease in directionality (Figure 10g) compared to controls. Additionally, we observed a trend towards decreased speed and directional velocity for neutrophils from arthritic mice compared to wild type (Figure 10h,i). We observed that roughly one order of magnitude more neutrophils from arthritic mice adhered to P-selectin coated microchannels, as would be expected (Figure 10d-f). Furthermore, we saw a significant decrease in directionality (Figure 10g) of neutrophils from arthritic mice compared to controls, as well as a trend towards decreased speed and chemotaxis velocity for neutrophils from arthritic mice compared to wild type mice (Figure 10h,i).

4.2.6 3D neutrophil chemotaxis

In addition to 2D embodiments of neutrophil chemotaxis, the KOALA platform can be employed to study migration in 3D matrices with minimal modification of loading protocols. This was accomplished by flowing and polymerizing a hydrogel containing purified neutrophils into the microchannels. We show that neutrophil migration and automated tracking is readily achievable by analyzing the 2D projected migration path of the cells (Figure 5a; Supplemental Video 8). We observed that neutrophils in the presence of a chemoattractant could migrate directionally in the 3D matrix, whereas cells in the control channels (no chemoattractant) were completely immobile (Figure 11a,b). Additionally, we compared the 2D and 3D migration of human neutrophils in the presence of 100 nM fMLP gradient (Figure 11c-e). Neutrophils migrating in 3D showed a trend of migrating with a slightly higher speed than the 2D case, while being slightly less directional in their migration path. These results demonstrate that KOALA can be used to directly compare 2D and 3D neutrophil chemotaxis, which may be relevant for different physiological conditions.

4.3 Discussion

In this study, we report a microfluidic neutrophil chemotaxis platform that reduces sample volume requirements by orders of magnitude compared to traditional techniques such as Boyden and Dunn assays. The KOALA platform provides increased functionality and allows for new applications by decoupling the gradient generation and migration aspects of the microfluidic platform. Using this approach, the chemoattractant

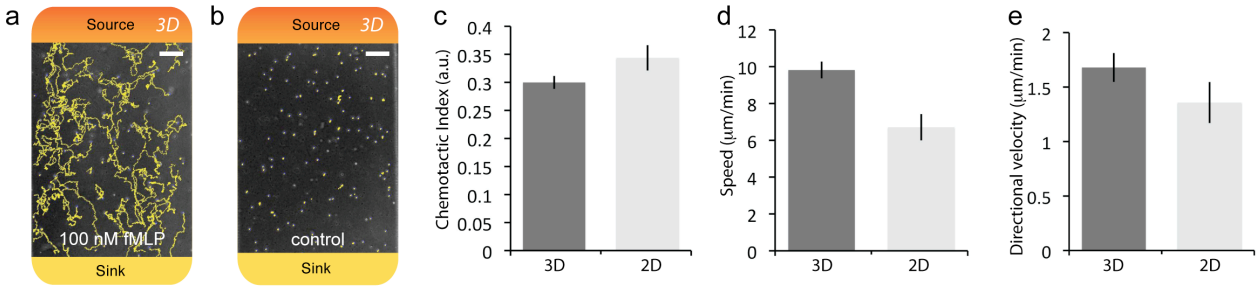

Figure 4.11 Migration of purified human neutrophils in a 3D collagen matrix. (a,b) Neutrophils tracked using JEX analysis, migrating in a 100 nM gradient of fMLP compared to no observable migration in the control (gel with no chemoattractant); colors represent the formation of the chemical gradient – red indicates maximum chemoattractant source concentration and yellow indicates the chemoattractant concentration at the sink. **(c-e)** Comparison of neutrophil migration in a 100 nM gradient of fMLP for the 2D and 3D embodiments of the KOALA platform, showing the chemotactic index, speed, and directional velocity. Note that standard purification protocols were used for 3D migration experiments (see Materials and Methods). 100 μm for **a,b**; error bars show s.e.m.; phase contrast images acquired using Slidebook software with an Olympus IX-81 microscope using a 10x objective (NA=0.30) at 37ºC.

conditions and the neutrophil migration environment can be controlled without the protocol for one negatively influencing the other. The KOALA chemotaxis platform utilizes a hydrogel to controllably diffuse the chemoattractant into the microchannels without inducing undesired flows, thereby increasing reliability of the gradient generation. The use of hydrogels has been shown to provide a semi-permeable structural material for microfluidic devices that can mediate the transfer of soluble factors.[166] In the KOALA platform, the hydrogel prevents unintended flow of the chemoattractant into the microchannel during the initial contact of the lid and base. Instead, the chemoattractant controllably diffuses into the microchannels due to the concentration gradient that exists between the source and sink.

The techniques utilized by the KOALA platform to form a chemical gradient and purify neutrophils differ significantly from traditional neutrophil chemotaxis methods, making direct quantitative comparisons challenging. For example, the gradient profile and cell microenviroment in KOALA devices vary greatly from

those of traditional methods such as the Boyden or micropipette-based assays. Additionally, the purification method employed by KOALA removes potentially harmful steps that are common in traditional purification protocols, such high-shear centrifugation, which has been shown to affect neutrophil function[167], and the cell lysis step for eliminating erythrocytes[168], which can induce harmful osmolarity shock. We show that our microfluidic approach reliably captures neutrophils efficiently (Supplemental Figure 2), and produces a linear chemical gradient (Figure 2a-c), enabling neutrophil chemotaxis in a range of chemical microenvironments (Supplemental Figure 5). This novel lid-based approach of delivering the chemotactic gradient makes the KOALA platform amendable to studying neutrophil chemotaxis in multiple contexts, including 2D and 3D systems, over an endothelium, and in both human and mouse models.

We report the first *in vitro* microfluidic assay that enables the direct monitoring of neutrophil chemotaxis on an endothelial cell substrate (ECS). This embodiment of the KOALA platform permits investigators to probe endothelial-leukocyte interactions that result in different phenotypes adopted by neutrophils. Importantly, the decoupling of the cell manipulation and gradient generation (base and lid, respectively) enables the investigator to culture endothelial cell monolayers and access the neutrophils and endothelial cells for further immunocytochemistry at any point during the assay by simply removing the lid. The ECS neutrophil chemotaxis assay revealed that neutrophils adopt two primary phenotypes in contact with endothelial cells, which had the appearance of being more compact or highly spread under phase contrast microscopy (Type I and II, respectively). We observed that most of the Type II cells transitioned to Type I cells during the course of a time-lapse session, whereby they adopted the migratory behavior and morphology observed in the initially Type I cells (Supplemental Video 5; Supplemental Figure 9). The Type I phenotype was significantly more directional than Type II and displayed higher migration velocity in the direction of the chemoattractant (Figure 3d-g). Type II phenotypes were commonly found at intercellular junctions, whereas the Type I phenotype was observed in all locations on the cell membrane. This spatial organization may be the result of increased cell stiffness at the intercellular junctions, which is known to elicit a more spread morphology.[169] Another possibility is that the presence of transmigratory molecules (e.g. ICAM1 and VCAM1) that are preferentially expressed at these locations[111] may cause the neutrophils to adopt a more adherent phenotype, resulting in the observed spread

morphology. These experiments demonstrate that neutrophils exhibit multiple morphologies and variable chemotactic behavior when they are captured on cytokine-stimulated endothelial cells, and further studies are needed to determine the mechanisms of these neutrophil phenotypes. The KOALA platform equips investigators with a simple tool to explore these interactions, which were difficult or impossible to study in the past.

The KOALA platform is the first demonstration of an assay capable of sorting, capturing, and purifying neutrophils obtained from mouse blood without sacrificing the animal. An immediate consequence of our technique is that animal waste for investigators may be reduced because the sacrifice of several animals is not required to perform each neutrophil chemotaxis experiment. This is achievable because nanoliter volumes of blood are sufficient to purify neutrophils for each microchannel in the KOALA platform, resulting in a total blood draw of 3 µL filling 15-30 microchannels. To the authors' knowledge, this sample volume requirement is one order of magnitude lower than the lowest achieved for leukocyte sorting and chemotaxis (<1 µL vs. 80 µL of diluted blood[75]). Importantly, the repeated measurement of neutrophil adhesion and chemotaxis for the same animal allows for the monitoring of neutrophil activity on mouse disease models in which the disease phenotypes may take long periods of time to develop or where multiple sampling is advantageous.

As a demonstration of the neutrophil capture technique using a tail vein blood draw, we assessed the function of neutrophils obtained from chronically inflamed mice (TNF-Tg) and compared them to WT. In mouse arthritis models, chronic inflammation is observed, and neutrophils specifically are central to the pathogenesis of this disease.[170] Using the KOALA platform, we observed a ~10 fold increase in the number of neutrophils that adhered to the P-selectin coated surface for TNF-Tg mice compared to WT; furthermore, neutrophils from chronically inflamed mice trended towards slower migration speeds and were significantly less directional compared to neutrophils from WT mice. Investigators have shown that, for mice not experiencing chronic inflammation, ~20-70 neutrophils should be present within one field of view of our microchannels.[171,172] Our average neutrophil capture falls within that range for WT mice, but is exceeded by roughly one order of magnitude for TNF-Tg mice (Figure 4d-f). Thus, the neutrophil count data suggests that TNF-Tg mice display strong neutrophilia, consistent with previous reports.[170] These experiments demonstrate the pertinence of the KOALA technique and validate the use of the platform for studying neutrophils in the context of mouse

inflammatory disease models. For the first time, this technique allows researchers to observe the development of disease phenotypes in mice over time, providing greater insight into the dynamics of symptom development. Furthermore, therapies such as antileukoproteinase-based treatments that target neutrophil adhesion to the endothelium[173] can be systematically studied while monitoring neutrophil function over time. More generally, the KOALA platform can be employed to study any disease where neutrophil adhesion and migration are central to the pathogenesis of the disease.

A growing body of work shows that cellular migration in a 3D matrix displays significantly altered phenotypes compared to 2D migration.[174-176] Therefore, an important requirement of the KOALA platform is to have the ability to characterize neutrophil migration in 2D and 3D. Indeed, we demonstrate that the assay can be utilized to conduct direct comparisons between protein-coated 2D substrates and 3D extra cellular matrix environments. We observe that neutrophils migrate faster towards the chemoattractant in 3D compared to 2D, confirming a trend that has been suggested by Kirsi *et al.* observed for migrating fibroblasts[177]; however, in contrast to the latter study, we do not observe a higher migration directionality for 3D compared to 2D. Using the KOALA platform, investigators have the opportunity to study neutrophil chemotaxis in 2D and 3D, while subjecting the cells to comparable chemical gradient profiles and geometries. These features allow hematology researchers to investigate neutrophil chemotaxis in multiple microenvironments and uncover differences in phenotypes that may have been masked by biases inherent to a 2D *in vitro* system.

In summary, we have developed and characterized a microfluidic chemotaxis platform that incorporates on-chip neutrophil purification; a novel lid-based gradient generation; and demonstrates gains in function, operability, and versatility. Importantly, the assay significantly reduces the difficulty of performing challenging experiments involving long-term cell cultures, animal/patient samples, and time-lapse microscopy. To demonstrate this, we analyzed the morphology and migration of neutrophils on a HUVEC monolayer; neutrophil chemotaxis from a tail vein puncture of chronically inflamed mice; and 3D neutrophil migration. The 50-10,000 fold reduction in blood requirements we achieved enables small mammal studies, where collection of more than microliters of blood usually requires sacrificing the animal. The KOALA chemotaxis platform achieved increased

functionality and simplicity of operation compared to standard techniques, making the assay well suited for widespread adoption in hematology research laboratories.

4.4 Materials and Methods

4.4.1 SU-8 mold and PDMS fab

The microfluidic base and lid of the KOALA platform were fabricated using soft lithography methods with Poly-dimethylsiloxane (Sylgaard 164, Dow Corning, Salzburg, MI). First, multilayer molds were created using SU-8 negative photoresist (Microchem, Newton, MA). In brief, pattern designs were created using Adobe Illustrator (Adobe, San Jose, CA) and printed on film (Imagesetter, Madison WI). A first layer was spun according to the manufacturer's specifications on a 150 mm diameter silicon wafer (WRS, San Jose, CA) using SU-8 50 to achieve 80 µm thickness or SU-8 100 for thicknesses of 180 and 270 µm. The photoresist was baked on hot plate and a Omnicure 1000 UV light source (EXFO, Quebec, Canada) was used to transfer the pattern to the photoresist. After a post-exposure baking step, the second, 400 µm thick, layer was spun on the wafer and patterned. The mold was then developed for 4 hours in SU-8 developer (PGMEA, 537543, Sigma, St Louis, MO) and washed with acetone and iso-propyl alcohol. PDMS was prepared in a ratio of 10:1 base to cross-linking agent, degassed in vacuum, and poured over the SU-8-silicon mold on a hot plate. A transparency (Cheap Joe's, Boone, NC), a layer of silicone (McMaster Carr, Eimhurst, IL), and a 5 kg weight, were placed on top of the mold, and baked at 80 degrees celsius for 4 hours. The base and lid of the KOALA device were adhered to tissue culture treated plastic from an Petri-dish (NUNC, Portsmouth, NH) prior to use. Photolithography masks used by the authors to fabricate devices is available upon request.

4.4.2 COMSOL modeling

A 3D model of the microchannel was developed using the COMSOL numerical simulation software (COMSOL, Burlington, MA). For the diffusion analysis a 3 mm diameter hemisphere - the size of the hydrogel bead placed in the KOALA lid - was drawn in the large port of the passive pumping microchannel and its initial concentration set to 1 with a diffusion coefficient of 100 µm2*s-1, corresponding to the diffusion rate of Alexa488 in hydrogel. A diffusion coefficient of 300 µm2*s-1 was used for all the low viscosity fluid-filled parts of the microchannel. Using

the diffusion simulation package with the GMRES solver, a time-dependent simulation was performed over 120 min, and the value of the concentration of chemoattractant was outputted for a horizontal plane placed 10 µm above the floor of the channel. Cross-section profiles taken along the axis of the channel were quantitatively analyzed. For the shear rate analysis, the incompressible Navier-Stokes simulation package was employed with an inlet pressure of 100 Pa and an outlet pressure of 0. A steady-state solution for the flow was found using the UMF pack solver and the value of the shear stress was plotted on floor of the microchannel.

4.4.3 Gradient characterization

The stability of the gradient and the validity of the numerical simulation were verified experimentally using a source concentration of 1 µM AlexaFluor488 dye (Molecular Probes, Carlsbad, CA) prepared in Matrigel (356231, BD Bioscience). A 3 µL drop of gel was placed in every location of the lid of the KOALA platform and polymerized in a humidified incubator. The channels in the base were filled with PBS and the lid was placed into contact with the base. Fluorescent timelapse microscopy was performed using a 4x objective at intervals of 10 min for a duration of 90 min at 37°C in an environmental-control chamber; an IX-81 microscope (Olympus, Tokyo, Japan) was used to capture the images, which were then analyzed using the imageJ software with a line scan with a width of 70 pixels. The concentration was normalized to the concentration observed when filling the channel with stock fluorescent solution.

4.4.4 Preparation of hydrogel-chemoattractant mixture

N-formyl-methionine-leucine-phenylalanine (fMLP; F3506-10MG, Sigma-Aldrich, St. Louis, MO) was suspended in dimethyl sulfoxide (DMSO; D2650; Sigma-Aldrich, St. Louis, MO) at 10 mM and stored at -80°C. The hydrogel-chemoattractant (H-CA) mixture consisted of fMLP and Matrigel, mixed in a 1:1 ratio to a final gel concentration of 4 mg/mL. The H-CA mixture was prepared before each chemotaxis experiment. For all doses of chemoattractant, the fMLP dilution was performed in PBS (Invitrogen, Grand Island, NY) prior to mixing with the hydrogel.

4.4.5 Endothelial cell culture

Human umbilical vein endothelial cells (HUVECs) were purchased from Lonza (Walkersville, MD), and regularly cultured on tissue culture-treated flasks pre-coated with 1.5 µg/cm2 of bovine plasma fibronectin (FN) (Sigma-

Aldrich, St. Louis, MO). HUVECs were maintained in EGM BulletKit media (CC-3124; Lonza) consisting of EBM-2 basal medium supplemented with 2% fetal bovine serum (FBS), bovine brain extract with heparin, hEGF, hydrocortisone, and gentamicin/Amphotericin B. HUVECs were fed every other day, passaged every 3 to 4 days at 90% confluence, and only passages 4-6 were used in microchannel experiments. To prepare HUVEC monolayers, microchannels were first primed with 10 µL PBS followed by 3 µL FN at 100 µg/mL. Microchannels were incubated at 37°C for 1 h in humidified trays to allow FN adsorption to the bottom substrate. After incubation, FN was replaced twice with 3 µL HUVEC media. HUVECs were seeded at 4,000 cells/µL 1.25 µL per microchannel, and allowed to adhere and culture until confluency (48 h). HUVEC microscale cultures were either used in neutrophil experiments when confluent. Activated HUVEC monolayers in microchannels were induced with 10 µg/mL interleukin-1β (IL-1β) for 4 h before performing neutrophil capture.

4.4.6 Neutrophil capture from whole blood on HUVECs

After obtaining consent at the time of the blood draw, whole blood was obtained from a lancet puncture on the finger of a self-reported healthy donor. The human subject protocol was approved by the University of Wisconsin Center for Health Sciences Human Subjects Committee. In brief, the skin was thoroughly cleaned with an alcohol swab and a disposable lancet (Safety Lancet, 02-675-160, Fischer Scientific) was lightly pressed against the skin and actuated. The first drop of blood was discarded and the finger pressed to obtain a drop of blood of about 5-10 µL on the bottom of a flat sterile petri-dish. 3 µL of blood was pipetted into a reservoir containing 18 µL of PBS and mixed gently. Following IL-1β stimulation, neutrophils were captured out of dilute whole blood in preparation of performing the chemotaxis assay. 1 µL of dilute whole blood was passed through each microchannel two times, with each pass 30 seconds apart. After allowing neutrophils to capture for 4 minutes, erythrocytes were removed by performing 3 washes with 3 µL of PBS, alternating the aspiration of PBS-blood mixture between the input and output ports. The PBS was replaced twice with 3 µL of EGM BulletKit media (CC-3124, Lonza) with 20 mM HEPES (25-060-CI; Mediatech, Manassas, Va).

4.4.7 Modeling fluid dynamics in microchannels

Using Equations (1) and (2), an analytical model and a numerical simulation was performed to calculate the flow rate in the microchannels of the KOALA platform. The dimensions used in the analytical model were: a volume of

3 µL of fluid dispensed on the input port of the channel of length 3 mm, width 0.8 mm and height 200 µm; the input port had a diameter of 1.5 mm and the output port is assumed to have a much larger diameter than the input port.

4.4.8 Neutrophil chemotaxis for varying gradient slopes

In order test neutrophil chemotaxis for different slopes of the chemical gradient, we fabricated a separate KAOLA device using methods described in SU-8 mold and PDMS fab. The base microchannels had lengths of 6, 5, 4, 3, 2, and 1 mm in order to change the slope of the chemical gradient; the height and width of the microchannels were 80 µm and 800 µm, respectively; the input and output ports had diameters of 1.5 mm and 2.5 mm, respectively, with heights of 600 µm. The neutrophil sorting and image capture was performed as described in the Washing efficiency characterization section. Four doses of fMLP were tested: 0 M (control),100 nM, 500 nM, 1 mM. Each dose was tested for three separate experiments (n=3). During each experiment, the neutrophil chemotaxis for each channel length was observed and automatically tracked using Je'Xperiment software.

4.4.9 Washing efficiency characterization

Different base microfluidic channels for the KOALA platform were fabricated according the methods described in the PDMS fabrication section with channel thicknesses of 80, 180, 270 µm. Each of these devices were coated for 30 min with 100 µg/mL human recombinant P-Selectin (R&D Biosystems, Minneapolis, MN). 3 µL of blood from a lancet puncture were collected and diluted in 18 µL of PBS and 1 µL of the latter solution was inserted into the microchannel base. Subsequently, the content of the microchannel were washed 3 times with 3 µL of PBS and images were taken on a IX-81 microscope using the 10X magnification objective.

4.4.10 Je'Xperiment tracking

Stacks of phase contrast images taken for each channel on the KOALA platform were exported into .tiff format and loaded into the Je'Xperiment software (available upon request). An automated algorithm was developed to track migrating neutrophils automatically. First, the user selects a representative neutrophil in one of the image stacks. Second, the algorithm performs a convolution on each image of the stack and identifies local maxima in the image produced. Maxima found are linked together into tracks by using an overall distance minimization strategy to find extensions of the tracks at each time-frame that minimize the overall displacement of the

neutrophils. Possible erythrocyte contaminants, wrongfully tracked particles, and dead or immobile neutrophils, are removed using a track filtering. The final tracks were analyzed to obtain their mean speed, chemotactic index, and directional velocity.

4.4.11 Comparing automated Je'Xperiment and ImageJ cell tracking

The accuracy of the automated software Je'Xperiment was assessed by comparison with experiments analyzed manually using the "Cell-tracker" plugin of ImageJ (http://rsbweb.nih.gov/ij/). Three channels coated with E-selectin and three channels coated with P-selectin were used to capture neutrophils and record their chemotaxis to fMLP. In each channel 5 neutrophils were selected and tracked manually as well as analyzed using JEX.

4.4.12 HUVEC immunostaining

Immunostaining was performed to verify presence of PECAM-1 at intercellular junctions, and upregulation of E-selectin upon activation using IL-1β. After 4 hours, HUVECs were fixed, permeabilized, and immunostained with either monoclonal anti-human E-selectin antibody (BBA1; R&D Systems Inc., Minneapolis, MN) or monoclonal mouse anti-human CD31 (MCA1738T; AbD Serotec., Oxford, UK) and Hoechst 33342 nuclear dye (H1399, Invitrogen, Carlsbad, CA). Images of the culture were acquired on a Nikon Eclipse Ti inverted fluorescence microscope coupled to a Nikon DS-QiMc CCD camera (Nikon Instruments, Melville, NY). A 10x objective (NA=0.30) was used for images shown in Figure 3a and a 20x objective (NA=0.50) was used for micrograph in Figure S3. NIS-Elements software (Nikon Instruments, Melville, NY) was used to capture and export the images in .tif format. A dry imaging medium was used for all captured images. ImageJ software was used to adjust the contrast of the images; the image processing was conducted uniformly across the entire image.

4.4.13 Tracking neutrophil chemotaxis on HUVECs

Stacks of phase contrast images taken for each channel on the KOALA platform were exported into .tif format and loaded into imageJ using the "import stack" tool. The imageJ plugin "Cell tracker" was used to track the migrating neutrophils on top of the endothelial cell monolayer. For each image stack, the two distinct morphologies of neutrophils were tracked using 10 cells of each phenotype tracked over at least 40 frames. 6 image stacks from 6 microfluidic channels were used for each repeat, and 3 independent repeats were

performed. The tracked images were outputted using imageJ, and the quantification of the migration speed, Chemotactic Index (CI) and directional velocity was performed using Excel (Microsoft, Redmond, WA).

4.4.14 Determining Type II to Type I transition

Neutrophils exhibiting the Type I and Type II morphologies were counted throughout a 90 minute timelapse to determine the proportions of each cell type over time. The "Cell counter" plugin of imageJ was used for cell counting. A representative channel was analyzed for three separate experiments. The neutrophils exhibiting Type I and Type II morphologies were counted every 5 minutes for the entire 90 minute timelapse. The proportion of Type II neutrophils at each point was calculated by dividing the number of neutrophils exhibiting a Type II morphology by the total number of cells counted in that frame (sum of Type I and Type II cell counts).

4.4.15 Measuring the area of Type I and Type II neutrophils

The area of the cells as seen under phase contrast microscopy was measured for neutrophils with Type I and Type II morphologies; the area of erythrocytes were also measured for reference. Once the correct scale was set in imageJ, the tracer tool and measure function were used to calculate the area of the cells. Representative neutrophils and erythrocytes across 6 microchannels were measured (52 Type II, 59 Type I, 25 erythrocytes).

4.4.16 Capture efficiency experiments

Neutrophils (at ~1x106 cells/mL density) were purified (details in "Human neutrophil purification") and then tagged with calcein-AM stain (L-3224; Invitrogen, Grand Island, NY). The calcein-AM was prepared by mixing 1 µL of calcein-AM with 1 mL of PBS. Cells were then placed into the diluted calcein-AM and incubated at 37°C for 15 minutes. 3 µL the tagged cells were then resuspended into 15 µL of whole blood and injected into the microchannels. Phase contrast and fluorescent images were taken of 5-6 microchannels prior to washing, and then the normal washing procedure was performed. Images of the microchannels were taken again after washing. Cells were counted manually using the imageJ plugin "Counter" for both the pre and post-wash channels. Count data from 5-6 channels were averaged, yielding an average count for a single experimental output (n=1). Three replicates (n=3) were performed. The capture efficiency was calculated by dividing the average number of neutrophils captured after washing was performed by the average number of neutrophils before washing was performed.

4.4.17 Mouse maintenance

TNF transgenic mice of the 3647 line were bred, cared for, and housed according to the University of Wisconsin Institutional Animal Care and Use Committee. Mice that were positive for the TNF transgene by Polymerase Chain Reaction (PCR) and littermate controls were used from 1.5 to 8 months of age.

4.4.18 Statistical analysis

Open source software, Mstat (http://www.mcardle.wisc.edu/mstat/) was used to perform statistical analysis on the data gathered. The Wilcoxon signed rank test (two-tailed, paired) was used to determine statistical significance. This test was used to determine the significant differences between categories where normality could not be assumed. Each output (chemotactic index, speed, directional velocity, and count) was individually measured for 2-6 microchannels and each channel output value was averaged to yield a single experimental output (n=1). Three (n=3) replicates were performed for all chemotaxis experiments. Five (n=5) replicates were performed for mouse neutrophil count data.

4.4.19 Mouse blood draw and neutrophil capture

Prior to the blood draw, microchannels were coated with 100 µg/mL concentration P-selectin (737-PS-050; R&D Systems, McKinley Place, Minneapolis, MN) for at least 30 minutes at 4°C. Mice were anesthetized using isofluorane until they did not experience pain from paw pinch and were then subjected to a tail snip. A 3 µL drop of blood was removed, which was then diluted into 18 µL PBS. 1 µL of dilute whole blood was passed through each microchannel two times, with each pass separated by 30 seconds. A minimum of 0.5 µL of dilute blood was tested to reliable fill the microchannel for neutrophil capture. After allowing neutrophils to capture for 4 minutes, erythrocytes were removed by performing 3 washes with 3 µL of PBS, alternating aspiration of PBS-blood mixture between the input and output ports. The PBS was replaced twice with 3 µL of Hanks Buffered Salt Solution (HBSS; 21-023-CV; Mediatech, Manassas, Va) with 20 mM HEPES. Supplemental Methods
Additional methods on fabrication of the KOALA microfluidic devices; characterization of the KOALA platform; mixing the chemoattractant and hydrogel; the culture of endothelial cells; staining protocols for immunocytochemistry; description of statistical analysis; mouse blood draw and neutrophil capture; and details regarding cell tracking techniques can be found in the Supplemental Materials.

4.4.20 Microscopy

For all time-lapse experiments, phase contrast images were taken using an Olympus IX-81 optical microscope (Olympus, Tokyo, Japan) with a 10x objective that had a numerical aperture (NA) of 0.30; the images were captured using a SPOT RT Monochrome CCD camera (Diagnostic Instruments, Inc, Sterling Heights, MI). For characterization of the chemical gradient using fluorescent dye, a 4x objective with NA=0.13 was used. The time-lapse experiments were conducted in an incubation chamber at 37°C; prior to the start of an imaging session, the samples were allowed to warm to 37°C for a minimum of 15 minutes. Slidebook software (Intelligent Imaging Innovations, Denver, CO) was used to capture the time-lapse images. The data was exported into .tif format prior to cell tracking. The imaging medium was dry for all images shown in this work. For HUVEC monolayer immunostaining, images were acquired on a Nikon Eclipse Ti inverted fluorescence microscope coupled to a Nikon DS-QiMc CCD camera (Nikon Instruments, Melville, NY); see additional details in Supplemental Methods. For higher resolution imaging of neutrophil morphologies, an Olympus IX-70 optical microscope (Olympus, Tokyo, Japan) with 20x objective set at 1.5x (30x effective) was used; The NA of the objective was 0.45 and a Hamamatsu camera (model C4742-80-12AG; Hamamatsu Photonics, Hamamatsu City, Japan) was used to capture the images using Metamorph software (Molecular Devices, Sunnyvale, CA).

4.4.21 Neutrophil migration on HUVECs

Following the neutrophil capture, a lid containing 100 nM fMLP was placed onto the base of the device, contacting the hydrogel-chemoattractant mixture (H-CA) to the output port of the migration channel. An image was taken every 30 seconds in each microchannel for 90 minutes.

4.4.22 Mouse neutrophil migration

Following the neutrophil capture, a lid containing various doses of H-CA was placed onto the base of the device, contacting the H-CA drop with the output port of the migration channel. Phase contrast images were taken with a 10x objective using an Olympus IX-81 optical microscope. An image was taken every 30 seconds in each microchannel for 120 minutes. For dose response experiments, fMLP concentrations of 1 mM, 100 μM, 10 μM, and 0 M control (gel only) were used. For TNF-Tg and WT mice migration experiments, 1 mM fMLP was used.

4.4.23 Human neutrophil purification

According to the manufacturer's recommendations, we purified peripheral blood neutrophils from human blood using Polymorphprep according to the manufacturer's recommendations (Nycomed, Sheldon, UK). All donors were self-reportedly healthy, and we obtained informed consent at the time of the blood draw. The human subject protocol was approved by the University of Wisconsin Center for Health Sciences Human Subjects Committee.

4.4.24 3D neutrophil migration

Following purification, human neutrophils were suspended in a 3D matrix by mixing 3 µL of cells at a density of ~1x106 cells/mL into 18 µL of Type I rat collagen (354249; BD Biosciences) to a final concentration of 5 mg/mL. The cell-collagen mixture was incubated at 37°C for 15 minutes, alternating the microfluidic device orientation between upside-down and right-side-up, until gel was solidified. Sacrificial deionized water (DI) was placed around the device to mitigate evaporation. A lid containing 3 µL H-CA mixture was placed onto the base and time-lapse image acquisition was performed as previously described.

4.4.25 Equations

We used an analytical model for estimating the flow rate in a microchannel generated by passive pumping. An important assumption of the model is a negligible pressure at the output port, which we can reasonably assume in this case given the much larger output port diameter. The pressure drop generated by surface tension is determined using the Laplace equation (1), where γ is the interfacial energy of water and air, R(t) is the radius of curvature of the input drop through time, and ΔP is the pressure drop between the input and output of the channel. The flow rate generated by a given pressure drop in a microfluidic channel of rectangular cross-section can be written as a function of ΔP using the Washburn equation (2), where η is the viscosity of the fluid, L is the length of the channel, λ is the aspect ratio of the channel, w is the width of the channel, h is the height of the channel, and Q(t) is the flow rate through time.

(1)
$$\Delta P_{in\ channel} = \frac{2\gamma}{R(t)}$$

(2) $$\Delta P_{in\ channel} = \frac{8\eta L g(\lambda)}{w^3 h} Q(t)$$

The speed, chemotaxis index (CI), and directional velocity of a tracked neutrophil were calculated using Equations (3-5), where n is the number of frames of the timelapse image, ti is the time interval between frames i-1 and i, ∂xi and ∂yi are the displacements along the x and y axis respectively between times i-1 and i, and ΔT is the time interval between the first and last frame of the timelapse.

The speed, chemotaxis index (CI), and directional velocity of a tracked neutrophil were calculated using equations (3-5), where n is the number of frames of the timelapse image, ti is the time interval between frames i-1 and i, ∂xi and ∂yi are the displacements along the x and y axis respectively between times i-1 and i, and ΔT is the time interval between the first and last frame of the timelapse.

(3) $$Speed = \sum_{i=1}^{n} \frac{\sqrt{\delta x_i^2 + \delta y_i^2}}{n \delta t_i}$$

(4) $$CI = \frac{\sqrt{(x_n - x_0)^2 + (y_n - y_0)^2}}{\sum_{i=1}^{n} \sqrt{\delta x_i^2 + \delta y_i^2}}$$

(5) $$Directional\ velocity = \frac{1}{n \Delta T} \sum_{i=1}^{n} \delta x_i$$

4.5 Acknowledgments

The work was made possible by funding from an Innovation & Economic Development Research Program grant (E.K.S) and a Morgridge Institute of Research fellowship (E.B). This work was also supported by NIH R01 EB010039 (D.J.B, E.K.S). M.A.S. was supported by a Rheumatology Scientist Development Award from the American College of Rheumatology Research and Education Fund. We wish to thank Prof. Kollias and the Alexander Fleming Biomedical Sciences Research Institute for providing the arthritic mouse line, and Jay Warrick for his contributions in developing the basis of the JEX software.

4.6 Copyright permission

Chapter 5

Characterizing asthma from a drop of blood using neutrophil chemotaxis

5.1 Introduction

Asthma is a chronic inflammatory disorder of the lungs that is associated with airway hyperresponsiveness (AHR) and obstructed airflow[117], affecting more than 300 million people worldwide.[121] Over the last 30 years, asthma prevalence has increased significantly in many populations, with some indications that prevalence may be reaching a plateau in the developed world.[117,122] Significant progress has been made in identifying primary mediators involved in the pathophysiology of asthma. Several cell types such as T helper cells (T_H1/T_H2), dendritic cells, mast cells, macrophages, eosinophils and neutrophils play central roles in the pathology of asthma.[115,116,127,178] Additionally, various cytokines that regulate the leukocyte trafficking–such as interleukins (IL), interferon gamma (IFN-γ), and tumor necrosis factor-alpha (TNF-α) – have been identified and targeted in drug therapies. The recruitment of leukocytes to the lungs, particularly eosinophils and neutrophils, is central to the pathogenesis of asthma. Increased numbers of eosinophils are prominently observed in the lung tissue and bronchoalveolar lavage (BAL) fluid for most asthmatics.[116] Neutrophils play a more critical role in severe asthma, where elevated counts of eosinophils are often not observed in the BAL fluid.[179] An overview of the role of neutrophils in asthma is shown in Fig. 1A. Although significant progress has been made in uncovering mediators in the pathology of asthma, these gains have not yet greatly improved our ability to define clinically relevant phenotypes of asthma in patients.

Asthma is diagnosed clinically by physicians, informed by the patient's medical history; spirometry tests that measure lung function; reversibility of AHR; along with several other potential metrics.[180] These diagnostic techniques measure the effects of the inflammatory response in the lung by assessing airway constriction; nitric oxide production; and the resulting clinical symptoms. However, all of these diagnostic tests require patient compliance, which can be challenging when diagnosing children or the elderly.[181] Additionally, many asthma

diagnostic tests partially rely on the patient experiencing clinical symptoms that are variable during or around the visit to the physician. Perhaps these common characteristics of current diagnostic techniques contribute to difficulties in diagnosing asthma, particularly in certain subpopulations. For example, in a recent Canadian study involving ~500 obese and non-obese subjects, Aaron *et al.* found that ~30% of the test subjects had been falsely diagnosed with asthma by physicians.[125] Additionally, it is well established that the elderly are consistently under-diagnosed for asthma.[123,124] Therefore, additional tools are needed to improve the diagnosis of asthma. Furthermore, current asthma assessments do not inform the clinician of disease severity, expected clinical course, and risk of exacerbations.

In order to improve characterization of asthma in the clinic, we have developed a handheld microfluidic chip that can identify functional measures of asthma from a drop of whole blood. Microfluidic systems have several characteristics that make them well-suited for clinical use, including low sample volume requirements [6,26]; simple integration with automated fluid handling systems[182]; and diffusion-dominant laminar fluidic phenomena that allow for precise control of a cell's microenvironment.[86,142,143] Indeed, microfluidic-based tools are increasingly being utilized in clinical research for diagnostic purposes.[3,27,60,76,87,183-185] Neutrophils have been used to diagnose clinical conditions in human patients based on proteomic and genomic analysis[76] and chemotaxis behavior[27,159], demonstrating that assays measuring cell function can be used for diagnostics. In this work, we assay the neutrophil chemotactic function in a blind study in order to identify quantitative domains that can be used to discriminate asthma from non-asthmatic allergic rhinitis. This approach of directly measuring the effector cell in the pathology of asthma differs from traditional diagnostic tests, which measure the variable effect of inflammation on airway constriction (Fig. 1B,C). Importantly, we developed methods to simplify the sample preparation, assay protocol, and data analysis that offer significant time savings over traditional macroscale[16,17,134] and microscale[143] chemotaxis techniques, allowing for the translation of the technology into the clinic. We analyzed 34 patients, and discovered that neutrophil chemotaxis can be used to discriminate asthma from non-asthmatic, allergic rhinitis patients with sensitivity and specificity of 96% and 73%, respectively. The results of the clinical application of our microfluidic device represent a first step demonstration of how

asthma can potentially be diagnosed and managed based on cellular function, rather than largely by clinical observations.

5.2 Results

We adapted a microfluidic neutrophil chemotaxis platform that we previously developed[28] in order to assay the neutrophil function of mildly asthmatic and non-asthmatic patients in a clinical setting. Briefly, the diagnostic chip has two primary components: (1) a functionalized migration channel in the base, where the rapid neutrophil purification and chemotaxis are performed, and (2) a multi-function lid that houses all the reagents required for the diagnostic test and mitigates evaporation, which can be detrimental for long-term open microfluidic experiments.[53] The purification is accomplished using a P-selectin-coated polystyrene surface, whereby whole blood is pumped into the microchannels allowing neutrophils to bind to the P-selectin, and other components of the whole blood (e.g. erythrocytes, plasma, etc.) are removed using subsequent laminar flow wash steps.[75] In our assay, the blood and reagents are passively pumped through the microchannels[12], enabling all of the fluid handling steps using only a micropipette and requiring no external pumping systems. Once the purification is complete, a lid containing a hydrogel-chemoattractant mixture (H-CA) is placed onto the base component, contacting the H-CA drop with the migration channel and initiating the chemotaxis experiment (Fig. 1B; reference 28). For step-by-step instructions on performing the diagnostic assay, see Appendix B. Following a timelapse capture of the neutrophil chemotaxis, the data is automatically tracked and analyzed using custom tracking software, dubbed Je'Xperiment (JEX), eliminating the need for onerous manual cell tracking . Three outputs were measured to characterize the neutrophil chemotactic function: the absolute migration speed (independent of the direction the cells move); the chemotactic index (displacement of the cell throughout the timelapse divided by its total path length); and chemotaxis velocity (speed of the cell in the direction of increasing concentration of chemoattractant). The diagnostic microfluidic chip was employed in a clinical setting to assay the neutrophil chemotactic function of mildly asthmatic and non-asthmatic patients in order to elucidate possible diagnostic domains between the two patient groups.

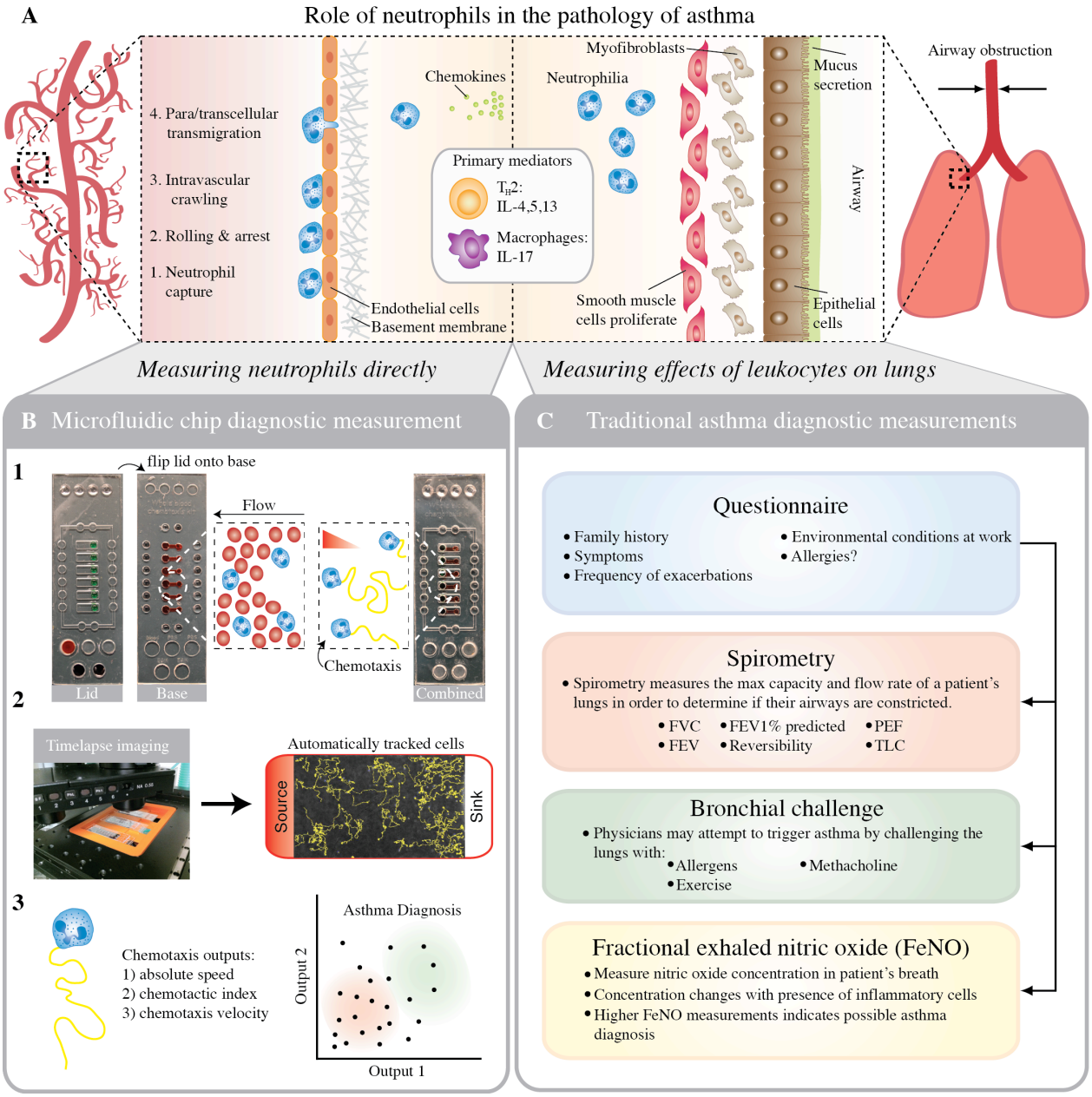

Figure 5.1 Overview of different diagnostic techniques and the role of neutrophils in the pathology of asthma. (**A**) Summary of the role of neutrophils in the pathology of asthma, showing neutrophil adhesion and transendothelial migration; chemotaxis mediated by macrophages and T-helper cells; and neutrophilia in the lung tissue that leads to airway remodeling and airflow obstruction. (**B**) Proposed microfluidic method for phenotyping asthma patients by measuring upstream of the asthma pathology with rapid neutrophil sorting and chemotaxis (1); automated high-throughput microscopy and automated cell tracking (2); and asthma diagnosis on the basis of chemotaxis outputs (3). (**C**) Traditional clinical asthma diagnostic methods occur

downstream of the asthma pathology by measuring the effect of leukocyte inflammation on airway obstruction, nitric oxide output, or clinical symptoms.

5.2.1 Characterizing neutrophil isolation and chemotaxis

We sought to characterize the neutrophil capture technique for blood samples obtained from the clinic. Using the protein-based neutrophil sorting procedure, we found that ~89% of neutrophils remained on the surface following subsequent wash steps (Fig. 2A). Furthermore, we found that the surface could be enriched with neutrophils by simply passing whole blood through the microchannels multiple times prior to the washing procedure (Fig. 2B); this was advantageous if neutrophil capture was particularly low and more neutrophils were required to obtain meaningful chemotaxis data.

Following the neutrophil isolation, we characterized the migration of human neutrophils in a linear chemotactic gradient using the potent chemoattractants, interleukin-8 (IL-8) and formyl-Methionyl-Leucyl-Phenylalanine (fMLP; Fig. 2C); Supplemental Video 1). For all control experiments (i.e. gel and media, no chemoattractant), neutrophils remained unactivated and there was no observable migration (Supplemental Video 2). Additionally, we compared neutrophil chemotaxis for neutrophils on a P-selectin and E-selectin substrates in order to determine the effects of different capture proteins on the neutrophil chemotaxis function in a linear gradient of fMLP (Fig. 2D). No significant differences were observed in the chemotaxis outputs, indicating that either protein coating could be used for the purification and chemotaxis. For the assay of patient samples, we used 100 μg/mL P-selectin for the substrate coating and 100 nM fMLP for the source of chemoattractant, as we observed robust neutrophil capture and chemotaxis using these experimental conditions. In order to obtain sufficient neutrophil enrichment from clinical samples, blood was passed through the microchannels two times prior to neutrophil purification.

5.2.2 Measuring neutrophil chemotactic function for asthmatic and non-asthmatic patients

After we characterized the neutrophil chemotaxis assay using human blood samples, we employed the microfluidic device in a clinical setting to analyze the neutrophil function for a cohort of patients that were

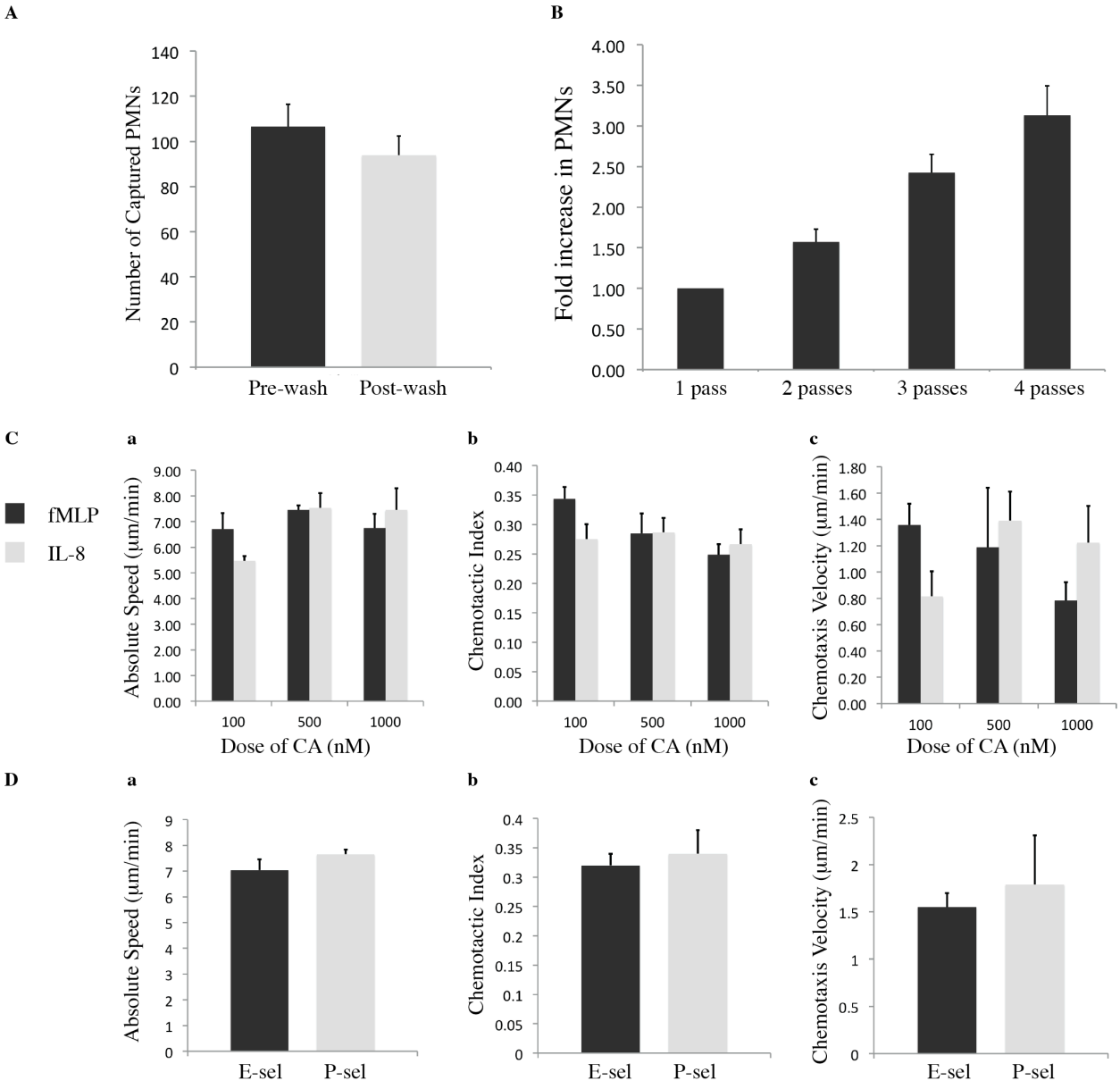

Figure 5.2 Characterization of diagnostic chip for performing neutrophil chemotaxis from a drop of blood. (**A**) Capture of neutrophils, or polymorphonuclear leukocytes (PMN's), from clinical blood samples before and after laminar flow wash steps; capture efficiency was 89% (n=4). (**B**) Increase in neutrophil capture on P-selectin-coated microchannels with additional passes of blood across the microchannel substrate (n=3). (**C**) Chemoattractant (CA) dose response for neutrophils obtained from healthy human patients, measuring the absolute migration speed (a), chemotactic index (b), and chemotaxis velocity (c); timelapse imaging for 120 minutes (n=3). Note: no observable neutrophil migration in controls (gel without CA). (**D**) Neutrophil chemotaxis in a linear gradient of fMLP with a source concentration of 100 nM; timelapse imaging for 90 minutes (n=3).

clinically characterized as asthmatic or non-asthmatic (Table 1). The absolute migration speed, chemotactic index, and chemotaxis velocity for all the patients are shown in Fig. 3A (see "Calculating chemotaxis outputs" in Materials and Methods). The absolute migration speed and chemotactic index of the neutrophils did not differ significantly by asthma status (p=0.33 and p=0.49, respectively). However, the chemotaxis velocity for asthmatic patients was significantly reduced compared to non-asthmatic patients (p=0.002). To our knowledge, this is the first report of a difference in neutrophil chemotaxis between asthmatic and non-asthmatic patients.

In addition to determining the patients' neutrophil chemotaxis function, patients were characterized using several other measures commonly employed in the clinic, such as FEV_1 %Predicted, FEV_1/FVC ratio, eosinophil count (Eos#), %Reversibility, and Fraction of exhaled nitric oxide (FeNO). Comparisons between our

Table 5.1: Characteristics of Study Subjects

Characteristic	Asthma (n=23)	No Asthma (n=11)
Age* (range), yr.	36 (20-52)	33 (20-48)
Men, No.	13	8
Blood EOS count, #/mm^3	293 (60)	242 (73)
FEV_1, %Predicted	91.2 (18.6)	104.2 (31.4)
FEV_1/FVC, ratio	0.772 (0.161)	0.802 (0.242)
Reversibility, %	7.66 (.951)	3.60 (0.945)
FeNO, ppb	47.0 (9.79)	24.5 (7.34)
Allergic, No. (%)	22 (95.6)	10 (90.9)
Current asthma symptoms, No. "Yes"	1	0

Average value shown with s.e.m. in (---), unless otherwise indicated.
*Age reported for patient's baseline characterization.

neutrophil chemotaxis outputs and spirometry measurements did not reveal any correlations that could be used to confirm or invalidate our test (Figures B1-5 in Appendix B). However, the comparison of neutrophil chemotaxis velocity with FeNO measurements – an emerging clinical marker that positively correlates with the number of

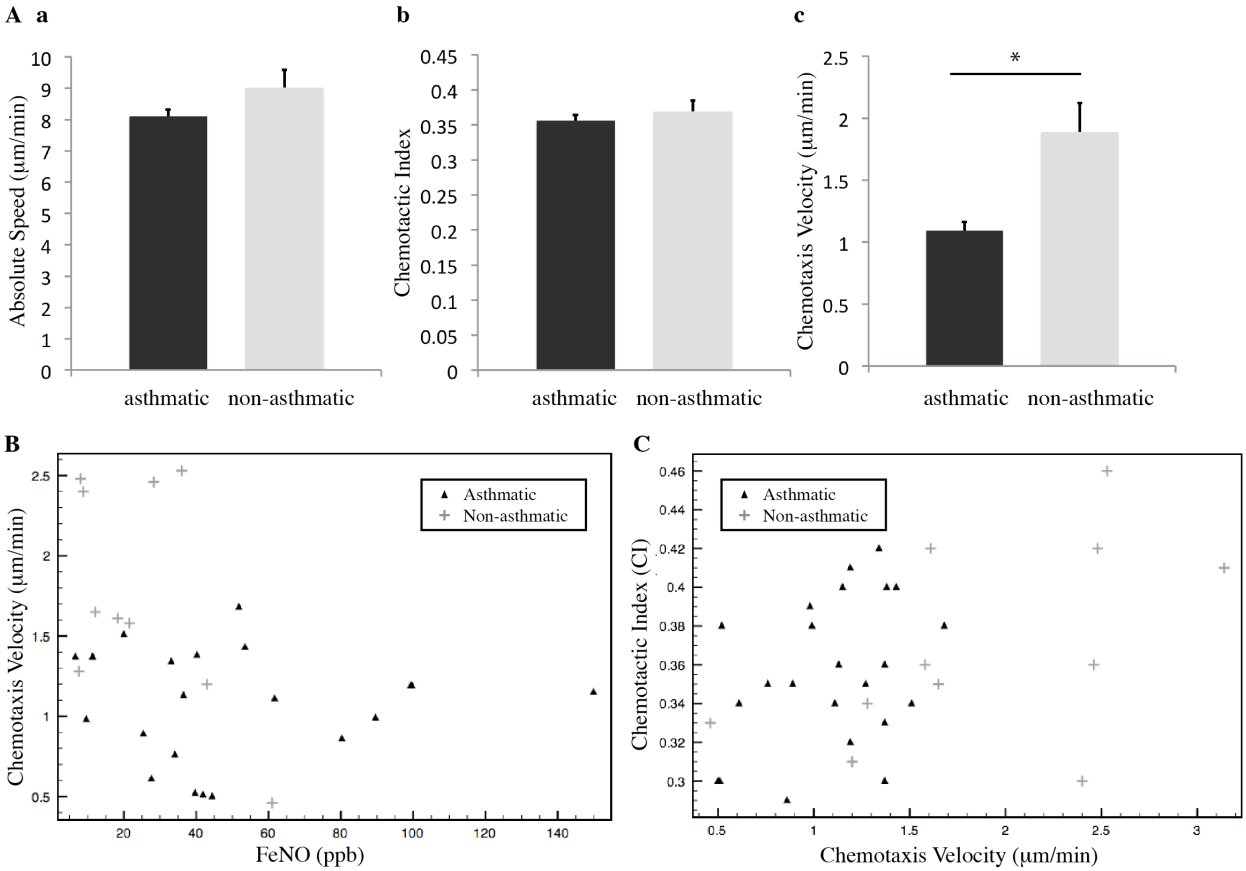

Figure 5.3 Neutrophil chemotaxis for blood samples obtained from the clinic and comparison with FeNO measurements. (**A**) No statistically significant difference in neutrophil migration speed (i) and chemotactic index (ii) for asthmatic and non-asthmatic patients; neutrophil chemotaxis velocity (iii) is significantly lower for asthmatic patients (n=23) compared to non-asthmatic patients (n=11);*P=0.002. (**B)** Comparison of neutrophil chemotaxis velocity and an emerging clinical diagnostic test (FeNO), showing higher neutrophil chemotaxis velocity for non-asthmatic patients correlating with lower FeNO values. (**C**) Diagnosis based on multiple chemotaxis outputs, as shown in Figure 1B; other chemotaxis outputs (CI and absolute migration speed) do not improve diagnostic performance. All chemotaxis data tracked and analyzed with JEX. Error bars show s.e.m.

inflammatory cells present in the lungs – revealed an increase in neutrophil velocity at lower values of FeNO (Fig. 2B); the absolute neutrophil migration speed and chemotactic index did not show similar correlations (Fig. B6). Importantly, patients with increased neutrophil chemotaxis velocity had measures of FeNO below the typical diagnostic cutoff point (20-40 ppb) that clinicians often use to diagnose asthma.[186-189]

5.2.3 Determining chemotaxis domains for asthmatic from non-asthmatic patients

Following the identification of the neutrophil chemotaxis velocity as a potential biomarker for asthma, we examined the receiver operator characteristics (ROC) of the chemotaxis velocity data in order to determine the optimal domains to discriminate the patient groups (Fig. 4A). We observed that using a chemotaxis velocity of 1.545 µm/min as the threshold for diagnosis of asthma, this biomarker correctly identified 22 of 23 asthma subjects (sensitivity 95.7%, 95% confidence interval 87.0-100.0) and 8 of 11 non-asthma subjects (specificity 72.7%, 95% confidence interval 45.5-100.0). The other chemotaxis measures – chemotactic index and migration speed – had poor sensitivity and specificity due to the non-significance in these outputs between asthmatic and non-asthmatic patients (Fig. 3A,B). Finally, we compared the sensitivity and specificity[190] of our diagnostic test to other quantitative tests reported in the literature (Fig. 4B; Table B1 in Appendix B). We found that our neutrophil

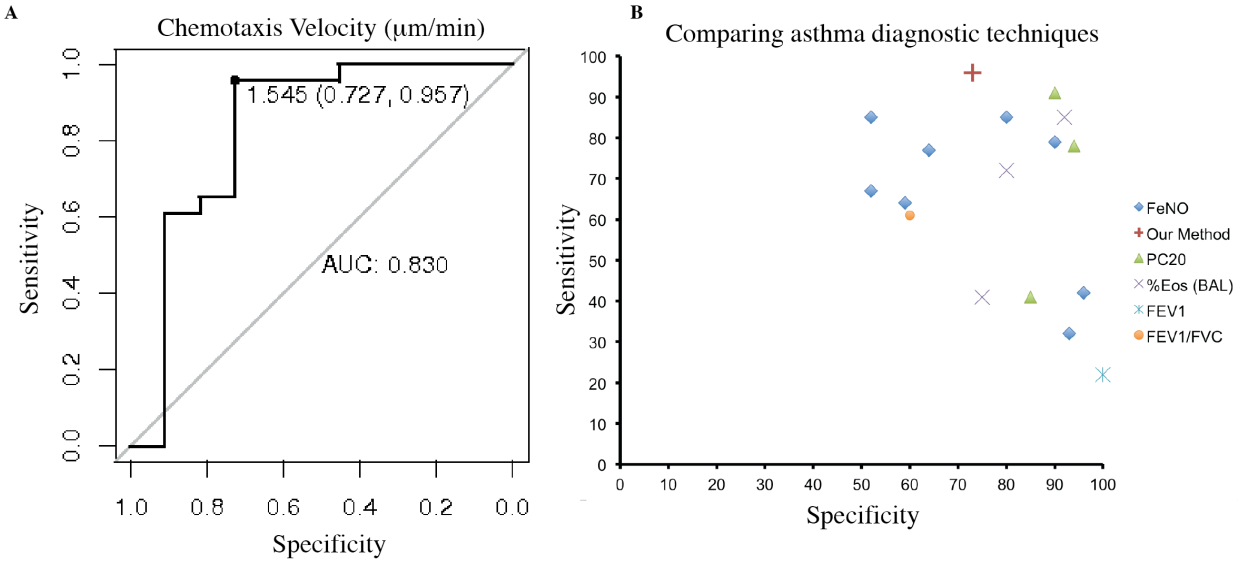

Figure 5.4 Performance of microfluidic assay compared to traditional methods. (**A**) Receiver operator characteristic (ROC) curve for the neutrophil chemotaxis velocity patient data, showing the optimal sensitivity and specificity at a diagnostic cutoff of 1.545 µm/min. (**B**) Comparison of our method to techniques reported in the literature (see Table BI for in Appendix B for additional details).

chemotaxis diagnostic marker is amongst the most sensitive measures reported, although not as specific as other diagnostic methods.

5.3 Discussion

Asthma is a complex and heterogeneous disease with multiple phenotypes, and accurately diagnosing the severity and/or phenotype of asthma continues to present difficulties for physicians.[123-125] The varying phenotypes of asthma has led some to suggest that it is a syndrome, or multiple distinct diseases that share common symptoms.[115,117] In current clinical practice, there is no single test that physicians rely on to diagnose asthma, but rather a series of tools that are both qualitative and quantitative in nature (Fig. 1C). Most quantitative diagnostic tests currently in use measure the physiological effects of inflammatory cells – such as neutrophils and eosinophils – on the lungs, which is in contrast to our direct measurement of neutrophil function.[191] One method that has been proposed for defining the different phenotypes of asthma is by the predominant inflammatory cell type involved – eosinophilic (elevated eosinophil counts), neutrophilic (elevated neutrophil counts), and paucigranulocytic (normal neutrophil and eosinophil counts).[115,116,192] However, this method of categorizing the patient groups does not take into account the functional status of these inflammatory cells. Mild asthma has been linked most strongly with eosinophils, while neutrophils have been implicated in the pathology of severe asthma. Interestingly, we observed that neutrophils obtained from mild asthmatic patients exhibit impaired chemotactic responses in a linear gradient of chemoattractant compared to neutrophils from non-asthmatic patients (Fig. 3A). To our knowledge, this is the first time altered neutrophil chemotactic function has been linked to asthma.

One possible explanation for the decrease we observed in neutrophil chemotaxis velocity for asthmatic patients is an increase in adhesion between asthmatic neutrophils and the P-selectin substrate coating the microchannels in our diagnostic chip. Dang *et al.* have reported that leukocytes from allergic-asthmatic patients exhibit higher surface expression of P-selectin glycoprotein ligand-1 (PSGL-1)[193], which mediates neutrophil binding to P-selectin.[194] Therefore, our diagnostic assay may be detecting an increase in neutrophil adhesion to the substrate, resulting in reduced neutrophil chemotaxis velocity towards the chemoattractant. Importantly,

this result could not easily be observed by performing a cell count of leukocytes in the peripheral blood or BAL, as has largely been done in past studies.[189,195,196] We show that our microfluidic chip and automated readout method is sensitive enough to detect these differences in neutrophil function, which can then be used as a basis for classifying asthma. Given this capability of our microfluidic device to measure functional activities of inflammatory cells that correspond to clinical features of disease, we propose that analyses of neutrophils on alternate substrates or the analysis of other inflammatory cells such as eosinophils using our method will provide a composite measure for enhanced identification of clinically relevant phenotyping of asthma.

Our proposed method has several features that enabled its translation into a clinical setting. First, a focus on user-friendly operation; transportability; scalable thermoplastic fabrication; and rapid sample processing and data analysis were central to the design of the assay. The fluid handling in our system does not require any external pumps or tubing, and the lid-based method of generating a gradient of chemoattractant enables the robust and repeatable implementation of the technique. Once the sample processing is completed in the clinic, the device can easily be transported to a microscopy facility to conduct the automated imaging and analysis. An important distinction between our approach and other clinical diagnostic methods, such as spirometry or questionnaires, is that our technique does not rely on patient compliance. Our method objectively probes the chemotactic function using neutrophils obtained from a drop of blood, rather than testing clinical symptoms that may or may not be present during the patient's visit. Indeed, nearly all patients in this study were not experiencing symptoms of asthma during their baseline characterization (Table 1). ROC analysis indicated that using an optimal neutrophil chemotaxis velocity of ~1.55 μm/min, our method achieved sensitivity and specificity of 96% and 73%, respectively. This performance compares favorably to other diagnostic tests reported in the literature (Fig. 4C; Table B1). Additionally, we observed a correlation between higher neutrophil chemotaxis velocity and lower FeNO values for patients in our study (Fig. 2B), further validating the efficacy of the microfluidic diagnostic test. Note that the sensitivity of our assay is significantly higher than diagnosing asthma based on the spirometry and FeNO measurements of these patients (Fig. 2B; Figures B1-5). For example, if a cutoff value of 30 ppb is chosen for diagnosis on the basis of FeNO measurements, 40% (6/15) of asthmatic

patients would be characterized as non-asthmatic. These results are a first demonstration of how neutrophil chemotaxis – and more generally, a readout based on effector cell function – can potentially be used to classify asthma, rather than relying solely on clinical symptoms. Furthermore, since our tool provides a quantitative readout, it is interesting to consider the possibility that this tool can also serve as a measure for disease severity. Thus, another potential clinical application is the routine measurement of neutrophil chemotaxis velocity in asthma patients to determine the level of asthma control, or more importantly, risk for future exacerbations of asthma.

In order to further validate our method, additional studies are required to determine how much the specificity of our test is influenced by other inflammatory diseases. Chronic obstructive pulmonary disease (COPD) is an example of a disease that driven by neutrophil inflammation.[114] In general, COPD is difficult to distinguish from severe asthma using existing quantitative clinical tests since the symptoms closely resemble each other; in our study, COPD was an exclusion criterion, so the study subjects were asthmatic, non-asthmatic, allergic, or some combination (Table 1). In practice, our diagnostic technique would likely be used in combination with existing clinical protocols to make the diagnosis, rather than exist as a standalone test. Furthermore, the information-rich readout provided by cell migration analysis allows for the comprehensive study of neutrophil dysfunction that occurs for other inflammatory diseases. For example, we have previously utilized a similar chemotaxis technology to analyze neutrophils obtained from an arthritic mouse model[164], a disease where neutrophil inflammation is known to regulate dysfunction.[170] In this study we observed a ~10 fold increase in neutrophils from arthritic mice adhering to the substrate; a significant decrease in neutrophil directionality; but no significant difference in chemotaxis velocity compared to wild-type mice.[28] Importantly, the neutrophil defect observed in this prior study differs significantly from the asthmatic neutrophil phenotype characterized in this work, suggesting that differences in neutrophil function could be observed to differentiate other inflammatory disorders from asthma. Our method minimizes the training, equipment, and labor requirements necessary to perform these assessments, making the characterization of other inflammatory diseases possible.

In conclusion, we report a comprehensive microfluidic solution for discriminating asthma from non-asthmatic, allergic rhinitis patients based on the chemotactic function of patient's neutrophils. The technology is handheld and easily transportable; can purify neutrophils from whole blood obtained from a lancet puncture within five minutes; and reports whether a patient is asthmatic or non-asthmatic with sensitivity of 96% and specificity of 73%. Importantly, the user-friendly design features of the assay enabled the application of the technology in a clinical setting, and we identified a previously unknown correlation between reduced neutrophil chemotaxis velocity and asthmatic patients. This work suggests that neutrophil chemotaxis may be a potential biomarker for asthma, though additional studies are required to investigate whether the specificity is reduced in broader populations.

5.4 Materials and Methods

5.4.1 Study Subjects

Peripheral blood and related clinical data was obtained from normal or asthmatic donors ranging in age from 18 to 55 years. Informed consent was obtained before participation and the study was approved by the University of Wisconsin Health Sciences Institutional Review Board, Protocol Numbers H 2008–0096 and 2010-3071.

5.4.2 Clinical diagnosis of asthma and allergy

Allergic individuals are defined as having a skin test positive to at least one of 12 aeroallergens. Asthmatic individuals are defined as having at least a six month history of asthma based on clinical findings such as cough, wheeze and shortness of breath. Additionally asthmatics may be currently taking the following medications; inhaled short acting B-agonist (as needed and < 6 puffs/day during an acute cold), low dose inhaled corticoid steroids, Advair, and/or a daily non-steroid controller medication.

5.4.3 Human blood draw and neutrophil isolation for capture experiments

Neutrophils were prepared from heparinized peripheral blood obtained from adult donors. Neutrophils were isolated by density fractionation over Percoll 1.090 g/ml. The cell pellets were collected and contaminating red

blood cells were lysed by hypotonic lysing. Purified neutrophils were on average >95% pure and the contaminating cells were eosinophils.

5.4.4 FeNO measurements

FeNo measurements were collected just prior to blood draw. FeNO values were measured during a 10-15 sec. exhalation using the NIOX-MINO (Aerocrine Inc; Morrisville, NC) analyzer, according to the manufacture's instruction. Briefly, patients were instructed to be seated with no nose clip, and to fully exhale away from mouthpiece. Patients then inhaled on the mouthpiece, maintaining a tight lip seal, to near total lung capacity over approximately 2- 3 secs. Once total lung capacity was achieved, patients were instructed to slowly exhale keeping a constant flow for 10-15 sec. while continuing to maintain a tight lip seal. FeNO value was obtained by only one measurement, according to the manufacturer's instruction.

5.4.5 Spirometry measurements

Spirometry was performed and analyzed according to currently approved American Thoracic Society Guidelines (ATS).[197] Briefly, Forced expiratory volume for 1 second (FEV1) and Forced vital capacity (FVC) were collected using a Nspire KOKO spirometer (nSpire Health, Inc.; Longmont, CO), and the best FVC and FEV1 values from three reproducible measurements were used. FEV1 % predicted was determined using NHANES III derived data. Reversibility was determined by change in FEV1 or FVC after 4 puffs of albuterol were administered and the subject rested for 10 minutes.

5.4.6 Device fabrication in PDMS and polystyrene

Microfluidic devices were fabricated out of both Poly-dimethylsiloxane (PDMS) and Polystyrene. The master for the microfluidic base and lid of the diagnostic chip were fabricated using soft lithography methods with PDMS (Sylgaard 164, Dow Corning, Salzburg, MI). First, multilayer molds were created using SU-8 negative photoresist (Microchem, Newton, MA). Briefly, pattern designs were created using Adobe Illustrator (Adobe, San Jose, CA) and printed on film (Imagesetter, Madison WI). A first layer was spun according to the manufacturer's specifications on a 150 mm diameter silicon wafer (WRS, San Jose, CA) using SU-8 50 to achieve 80 μm thickness.

The photoresist was baked on hot plate and a Omnicure 1000 UV light source (EXFO, Quebec, Canada) was used to transfer the pattern to the photoresist. After a post-exposure baking step, the second, 400 µm thick, layer was spun on the wafer and patterned. The mold was then developed for 4 hours in SU-8 developer (PGMEA, 537543, Sigma, St Louis, MO) and washed with acetone and iso-propyl alcohol. PDMS was prepared in a ratio of 10:1 base to cross-linking agent, degassed in vacuum, and poured over the SU-8-silicon mold on a hot plate. A transparency (Cheap Joe's, Boone, NC), a layer of silicone (McMaster Carr, Eimhurst, IL), and a 5 kg weight, were placed on top of the mold, and baked at 80 degrees celsius for 4 hours. The base and lid of the diagnostic device were adhered to non-tissue culture treated plastic from an Petri-dish (NUNC, Portsmouth, NH) prior to use. Photolithography masks used by the authors to fabricate devices are available upon request. For polystyrene devices, hot embossing fabrication techniques were utilized as previously described.[64] A mold for the lid of the diagnostic device was rapid prototyped (FineLine Prototyping; Raleigh, NC) from a source file created by SolidWorks (Dassault Systèmes SolidWorks Corporation; Waltham, MA), and then converted into an epoxy mold for hot embossing.[64]

5.4.7 Preparation of hydrogel-chemoattractant mixture

N-formyl-methionine-leucine-phenylalanine (fMLP; F3506-10MG, Sigma-Aldrich, St. Louis, MO) was suspended in dimethyl sulfoxide (DMSO; D2650; Sigma-Aldrich, St. Louis, MO) at 10 mM and stored at -80°C. The hydrogel-chemoattractant (H-CA) mixture consisted of fMLP and Matrigel, mixed in a 1:1 ratio to a final gel concentration of 4 mg/mL. The H-CA mixture was prepared before each chemotaxis experiment. For all doses of chemoattractant, the fMLP dilution was performed in PBS (Invitrogen, Grand Island, NY) prior to mixing with the hydrogel.

5.4.8 Neutrophil sorting from whole blood and chemotaxis assay

The human subject protocol was approved by the University of Wisconsin Center for Health Sciences Human Subjects Committee. The diagnostic chip was coated with human recombinant P-selectin (R&D Biosystems, Minneapolis, MN) at 4ºC for at least 30 minutes. After obtaining ~150 µL from the asthma clinic (see subsection, "Human blood draw"), 3 µL of the whole blood was pipetted into a reservoir containing 18 µL of PBS and mixed

gently. Neutrophils were captured out of dilute whole blood in preparation of performing the chemotaxis assay by pumping 1 µL of dilute whole blood through each microchannel two times, with each pass 30 seconds apart. After allowing neutrophils to capture for 4 minutes, erythrocytes were removed by performing 3 washes with 3 µL of PBS, alternating the aspiration of PBS-blood mixture between the input and output ports. The PBS was replaced twice with 3 µL of EGM BulletKit media (CC-3124, Lonza) with 20 mM HEPES (25-060-CI; Mediatech, Manassas, Va). The lid containing the H-CA and the microchannels were placed in a humidified container at 37°C for 5 minutes prior to placing the lid onto the base and initiating the chemotaxis assay. For all chemotaxis experiments in the diagnostic assay, 100 nM fMLP and 0 nM fMLP (gel only control) were used.

5.4.9 Calculating chemotaxis outputs

The neutrophil chemotaxis outputs for this work were calculated the same as described in Chapter 5. The absolute speed, chemotactic index (CI), and chemotaxis velocity (or directional velocity towards the formation of the gradient of chemoattractant) of a tracked neutrophil were calculated using Equations 1-3, where n is the number of frames of the timelapse image, t_i is the time interval between frames i-1 and i; ∂x_i and ∂y_i are the displacements along the x and y axis, respectively, between times i-1 and i; and ΔT is the time interval between the first and last frame of the timelapse.

(1) $$Speed \ = \ \sum_{i=1}^{n} \frac{\sqrt{\delta x_i^2 + \delta y_i^2}}{n \delta t_i}$$

(2) $$CI \ = \ \frac{\sqrt{(x_n - x_0)^2 + (y_n - y_0)^2}}{\sum_{i=1}^{n} \sqrt{\delta x_i^2 + \delta y_i^2}}$$

(3) $$Directional \ velocity \ = \ \frac{1}{n \Delta T} \sum_{i=1}^{n} \delta x_i$$

5.4.10 Microscopy

For all time-lapse experiments, phase contrast images were taken using an Olympus IX-81 optical microscope (Olympus, Tokyo, Japan) with a 10x objective that had a numerical aperture (NA) of 0.30; the images were

captured using a SPOT RT Monochrome CCD camera (Diagnostic Instruments, Inc, Sterling Heights, MI). The time-lapse experiments were conducted in an incubation chamber at 37°C; prior to the start of an imaging session, the samples were allowed to warm to 37°C for a minimum of 15 minutes. Slidebook software (Intelligent Imaging Innovations, Denver, CO) was used to capture the time-lapse images. The data was exported in .tif format and processed using JEX. The imaging medium was dry for all images shown in this work.

5.4.11 Capture efficiency experiments

Neutrophils (at ~1x10^6 cells/mL density) were purified (details in "Human neutrophil purification") and then tagged with Calcein-AM stain (L-3224; Invitrogen, Grand Island, NY). The Calcein-AM was prepared by mixing 1 µL of Calcein-AM with 1 mL of PBS. Cells were then placed into the diluted Calcein-AM and incubated at 37°C for 8 minutes. 3 µL the tagged cells were then resuspended into 15 µL of whole blood and injected into the microchannels. Phase contrast and fluorescent images were taken of 6 microchannels prior to washing, and then the normal washing procedure was performed. Images of the microchannels were taken again after washing. Cells were counted manually using the imageJ plugin "Counter" for both the pre and post-washed channels. Count data from 6 channels were averaged, yielding an average count for a single experimental output (n=1). Three replicates (n=3) were performed. The capture efficiency was calculated by dividing the average number of neutrophils captured after washing was performed by the average number of neutrophils before washing was performed.

5.4.12 Neutrophil enrichment on the microfluidic device

Following the neutrophil tagging steps outlined in, "Capture efficiency experiments," whole blood was injected with tagged neutrophils into eight P-selectin-coated microchannels. Additional blood was passed through microchannels, separated by 30 seconds, with sets of two microchannels receiving an additional whole blood sample. Therefore, the first set of microchannels received 1 µL of whole blood each, the second set of two microchannels received 2 µL of whole blood each, the third set of two microchannels received 3 µL of whole blood each, and the fourth set of two microchannels received 4 µL of whole blood each. After allowing neutrophils to capture for 4 minutes, erythrocytes were removed by performing 3 washes with 3 µL of PBS,

alternating the aspiration of PBS-blood mixture between the input and output ports. Cells were counted manually using the imageJ plugin "Counter."

5.4.13 Statistical analysis

The associations between asthma diagnosis and chemotaxis outputs (speed, chemotactic index, and chemotaxis velocity) were examined using the Wilcoxon rank sum test. The sensitivity and specificity for asthma diagnosis at varying thresholds of chemotactic velocity were summarized using the receiver operator characteristic (ROC) curve. The optimal chemotaxis velocity threshold for asthma diagnosis was chosen to maximize the sum of specificity and sensitivity. Confidence intervals for sensitivity and specificity were constructed using 2000 stratified bootstrap replicates.[198] Each chemotaxis output was individually measured for 3-6 microchannels per subject, and the channel output values were averaged to yield a single value for each subject. Analyses were conducted using Mstat version 5.5 (http://www.mcardle.wisc.edu/mstat/) and R version 2.14 (R Core Team (2012). R: A language and environment for statistical computing. R Foundation for Statistical Computing, Vienna, Austria. ISBN 3-900051-07-0, URL http://www.R-project.org/) A two-sided p-value less than 0.05 was regarded as significant.

5.5 Acknowledgements

We would like to thank Jay Warrick for his contribution in developing the foundation of JEX. The work was made possible by funding from an Innovation & Economic Development Research Program grant (E.K.S) and a Morgridge Institute of Research fellowship (E.B). This work was also supported by NIH R01 EB010039 (D.J.B, E.K.S). The facility providing asthma patient samples and data was funded by a National Institute of Health Program Project Grant HL088584.

5.6 Disclosure of Conflicts of Interest

D.J.B. has an ownership interest in BellBrook Labs, LLC which has licensed technology presented in this chapter. E.K.S., E.B. and D.J.B. have filed a patent application based on technology presented in this work.

5.7 Copyright permission

The work presented here is currently in submission; therefore copyright permissions are currently not required to present this work in my dissertation.

Chapter 6

Other useful neutrophil assays and applications

6.1 Introduction

Prior to this chapter I have presented versatile methods for performing neutrophil chemotaxis assays, and applied these technologies to research and clinical applications. This chapter will maintain the theme of methods for neutrophil purification and analysis, but provide preliminary data for other assays currently in development. Furthermore, other applications that would benefit from KOALA chemotaxis technology will be discussed in significant detail. The data presented in this chapter is all preliminary, and provides some foreword-looking guidance for other ways that microfluidics can be useful for neutrophil research.

6.2 Neutrophil sorting from whole blood using IFAST

In addition to conducting studies that characterize neutrophil chemotactic function, it is useful to interrogate cells for proteomic and genomic information. The utility of having a simple device that can easily capture neutrophils from whole blood for genetic or protein analysis was recently demonstrated by Toner, *et. al.*[76] In this study, neutrophils from burn patients and healthy donors were captured with CD66b specific antibodies in a closed microfluidic cartridge; these devices were operated by untrained personnel and had high capture efficiency and clearly resolved, time-dependent transcriptional events that evolved during the patient's healing process. This technology was also applied to analyze BAL fluid from asthmatic patients[77], showing the versatility of the approach for a variety of applications. The method to purify neutrophils from whole blood that I have been presented in previous chapters could potentially be extended to proteomic and genomic analysis, but these channels randomly fix neutrophils on the surface and do not allow for the cells to be transported to multiple locations. This is not ideal for some applications, particularly when a higher concentration of the cells are desired or the user wishes to conserve the whole blood while extracting the neutrophils.

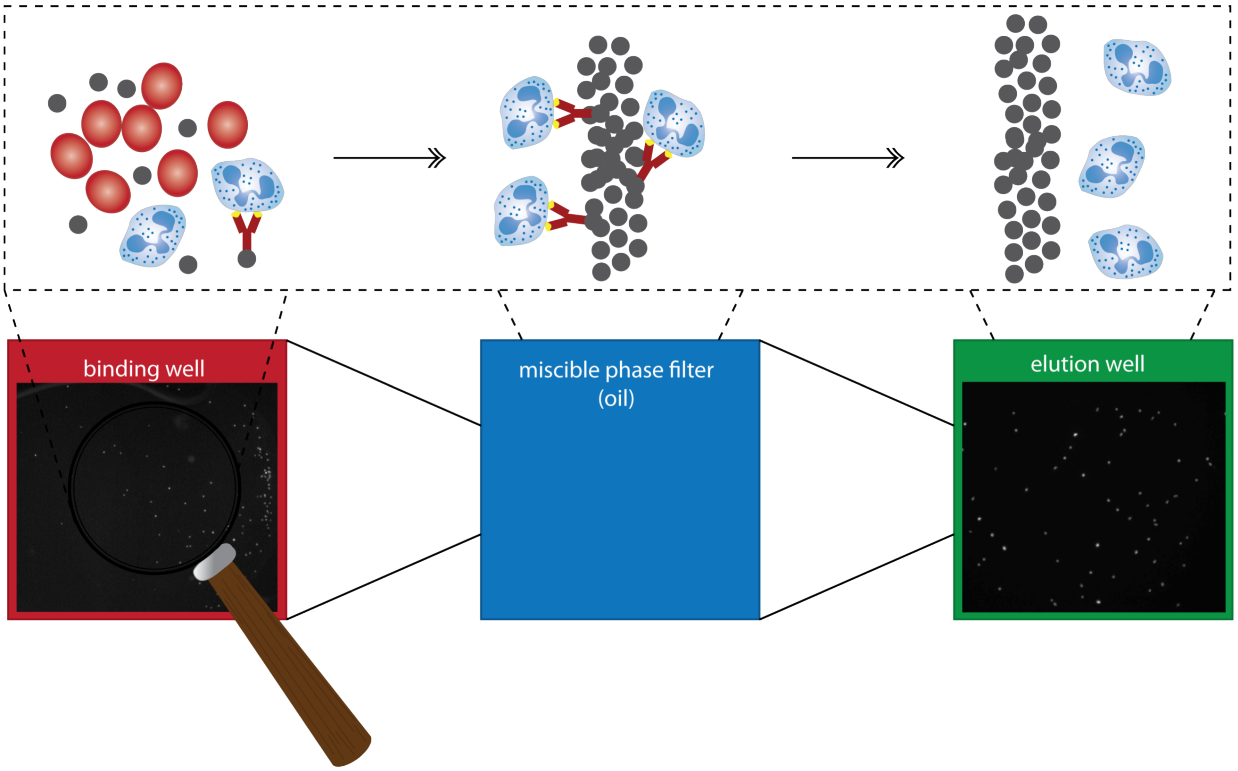

Figure 6.1 Schematic illustrates processing for purifying neutrophils from whole blood using CD66b specific antibodies. After an hour of binding the beads to the antibodies (30 min) and the antibodies to the cells neutrophils (30 min), a magnet is used to pull the cells through the miscible phase filter, leaving behind RBC's and then dispersed in the elution well. The fluorescent images show calcein-dyed neutrophils for determining purification efficiencies. For already purified neutrophils (shown in figure) the capture efficiency is ~95% (n=3). For neutrophils captured out of whole blood, the efficiencies are much lower (~30-40%).

To solve this problem, we applied another cell sorting technology from our lab[79,80] that still meets the sample volume and rapid purification performance of the KOALA platform. The technique—dubbed Immiscible Filtration Assisted by Surface Tension (IFAST)— is an alternative approach that utilizes hydrophilic and hydrophobic chambers to separate cells that are specifically bound to beads and ultimately pulled across (Figure 1). In this case, we used a CD66b-specific antibody that was attached to functionalized magnetic beads, and then the beads were dispersed into the whole blood, specifically binding neutrophils (and a small number of

eosinophils). After binding, the neutrophils were dragged across an oil phase with a magnet, while leaving behind (though still conserving) all the erythrocytes, plasma, and other components of whole blood. Once the cells have been sorted, one can interrogate them for molecular information and potentially correlate this with chemotaxis data gathered at similar time-points.

Preliminary results indicate that the capture efficiency of neutrophils that have already been purified from whole blood is ~95% (n=3) using this technique. This result establishes a theoretical upper limit for what ideally could be achieved using this method, since capturing cells from whole blood only reduces the efficiency due to non-specific chemical and physical obstructions. Indeed, subsequent trials that attempted to capture calcein-dyed neutrophils spiked in whole blood reduced the capture efficiency to ~30-40% (n=3)—well below acceptable limits. Clearly, further development is required before this technique could be reliably used for rapid neutrophil purification. Adjustments that would likely improve capture efficiency include: (1) using biotinylated beads; (2) adjusting capture time, temperature, and mixing rate; and (3) adjust the heparin concentration in whole blood. Once the capture efficiency is improved, an investigator would have complimentary rapid neutrophil purification techniques that could be employed together to perform a different assays at roughly the same time.

6.3 A neutrophil oxidative burst assay for research and clinical applications

Once a neutrophil has been recruited during an inflammatory response to a wounding site[111], one of its primary functions when the cell encounters a pathogen is to engulf and degrade the foreign object.[199] Upon recognizing a pathogen, the neutrophil undergoes a series of biophysical and biochemical changes that allow the cell to contort its plasma membrane around the pathogen until the object is fully engulfed (see Figure 2.1 in Chapter 2). After the pathogen has bean encapsulated, a membrane-bound enzyme called nicotinamide adenine dinucleotide phosphate–oxidase (NADPH–oxidase) begins to reduce oxygen species, increasing the production of 0_2^- and ultimately H_20_2, a process that is often referred to as "oxidative–" or "respiratory bursts." Once the pathogen has been phagocytosed and is encapsulated in a phagosome, the neutrophil undergoes

degranulation, rapidly releasing reactive oxygen species (ROS) to destroy the pathogen. In some rare cases, the host may have a genetic or other type of defect that prevents oxidative bursts, resulting in recurrent bacterial and fungal infections.[200] This condition, called chronic granulomatous disease (CGD), results from dysfunctional NADPH–oxidase machinery, which prevents the host from properly destroying pathogens when infected. CGD occurs in one out of every 250,000 patients[201], and is likely fatal if not diagnosed and properly treated.

Currently CGD is diagnosed using one of two methods: (1) with flow cytometry to identify fluorescently labeled phagocytes; and (2) a nitro blue tetrazolium (NBT) test, which yields a "blue score" that positively correlates with NADPH–oxidase, thereby acting as a surrogate marker for ROS production. Both of these methods are effective at diagnosing CGD, however flow cytometry is more expensive; time consuming; and not always available (especially in low-resource settings). Improvements have been made to the NBT assay that allows the user to test from whole blood, however these tests can sometimes yield ambiguous results and still miss some variants of CGD.[202] We sought to adapt the neutrophil sorting techniques used in the KOALA neutrophil chemotaxis assay to create a fast, cheap, and reliable oxidative burst assay that can be performed using blood obtained from a lancet puncture. The technique can be performed using two pipetting steps, and can report a result in ~45 minutes. This method could potentially be applied to the diagnosis of CGD in the clinic, or used in a research setting for the measurement of ROS production in neutrophils.

6.3.1 Methods

Oxidative burst assay

The base component of the KOALA assay described in Chapters 3 and 4 was used for the oxidative burst assay (no lid required). 100 µg/mL human recombinant P-selectin was pre-coated in the microchannels for 30 minutes at 4 ℃. Note that channels can be coated, dried, and the devices frozen (-20 ℃) at an earlier time-point to further automate the assay. A lancet puncture was then performed and the whole blood diluted in PBS at a ratio of 1:6. The dilute whole blood was then pumped through the microchannels twice (once also acceptable if capture was sufficient). After 3 minutes, 5 µL of the multi-reagent solution (DHR and +/–PMA, in PBS) was pumped through

the microchannels and allowed to incubate for 30 minutes at room temperature. The channels were then placed on an automated microscope stage and imaged using fluorescence microscopy and phase contrast.

Reagents

Dihydrorhodamine 123 (DHR) and Hoechst 33342 nuclear dye were purchased from Molecular Probes (Eugene, OR, USA) and were stored at -20 ℃. Phorbyl 12-myristate 13-acetate (PMA) and Diphenyleneiodonium chloride (DPI) were purchased from Sigma Aldrich (Milwaukee, WI, USA). PMA was dissolved in DMSO at a stock solution concentration of 1.6mM and stored at -20 ℃. DPI was dissolved in de-ionized water at a concentration of 10mM, and stored at room temperature. All reagents for the neutrophil sorting assay are identical to those used in Chapters 3 and 4.

Image Analysis

Image J was used to analyze fluorescent images. Fluorescent images from the Hoechst stain were used to identify all cells present within the viewing window. After background subtraction using a rolling ball (radius = 50 pixels), nuclei were identified by thresholding. The binarized features were dilated using a 3x3 mask since Hoechst only captures the cell region. The analyze particles command was used to select the objects regions. Object regions identified within the Hoechst image was used to select regions within the DHR fluorescent image containing the cells. Mean DHR fluorescent values within a cell structure and the sum of all pixels within the cells was calculated.

6.3.2 Preliminary results

We have validated that this simple method of neutrophil sorting and staining accurately and reliably reports ROS production in healthy donors in under 45 minutes (Figure 2; n=2 donors). The Hoechst stain effectively targeted the neutrophils' nuclei, and this image was used to identify the cells in the field of view. The cells were then bound and tagged individually in ImageJ, and those borders were imported into the DHR image to visualize whether the neutrophils in the microchannels produced ROS. The assay correctly showed that neutrophils that were not activated by PMA were not generating ROS in significant quantities. However, there was a small baseline ROS production even in unactivated cells since the neutrophils are from healthy donors and not

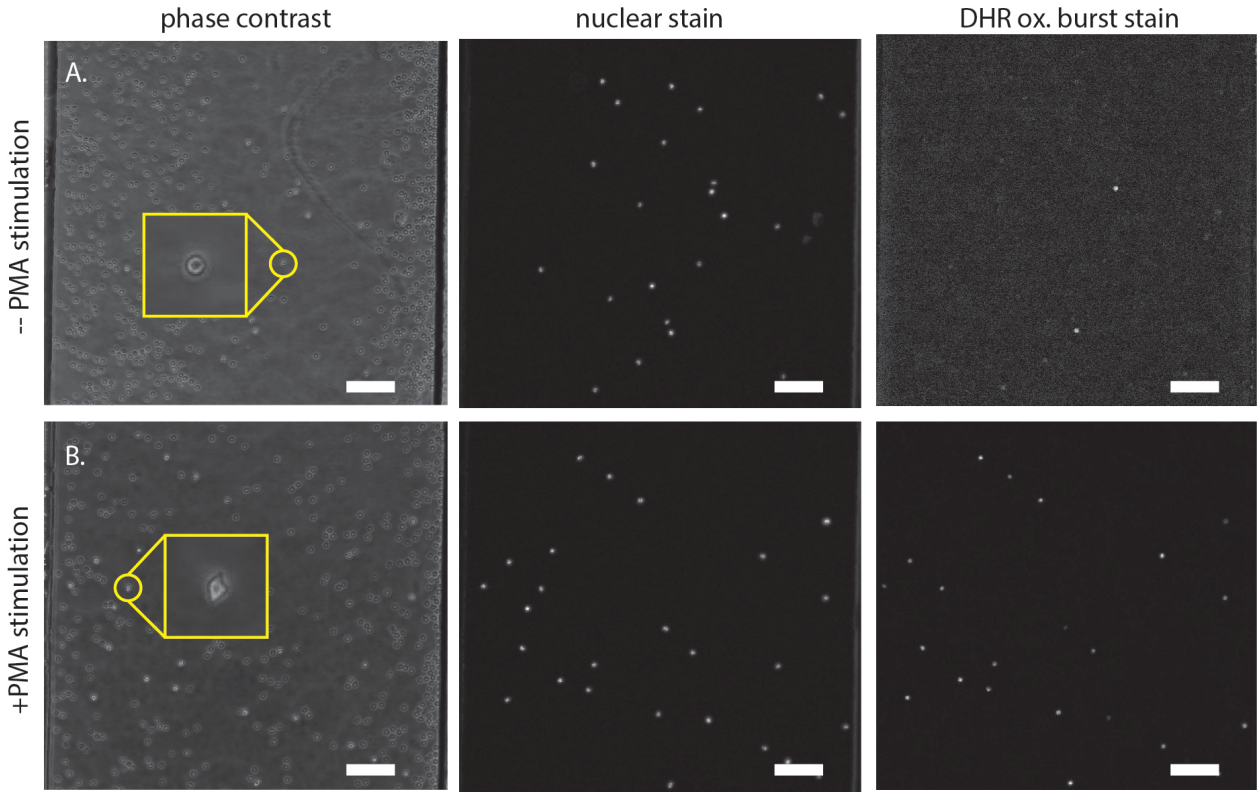

Figure 6.2 Phase contrast and fluorescent images of neutrophils from a healthy donor. The nuclear stain identifies the location of all the neutrophils in the field of view (FOV). The Dihydrorhodamine (DHR) stain reports the presence of hydrogen peroxide. **(A)** As expected, the neutrophils that have not been activated by phorbol myristate acetate (PMA) did not undergo oxidative bursts, whereas the PMA-activated neutrophils report ROS production **(B)**. Note the change in morphology of the activated and unactivated cells. Scale bar is 100 µm.

patients with CGD. We have conducted a dose response of the DHR reporter in order to obtain the best possible contrast between activated and non-activated cells (representative data in Figure 3; n=3 experiments have been completed). A dilution ratio of 1:500 (DHR in PBS) yields the highest contrast and was used for subsequent experiments.

In addition to performing these proof of concept and DHR characterization experiments, we have also initiated dose response trials on an inhibitor that blocks NADPH–oxidase (DPI) in order to mimic CGD in healthy donors. Preliminary experiments (n=2) have revealed that DPI effectively blocks ROS production, and the DHR

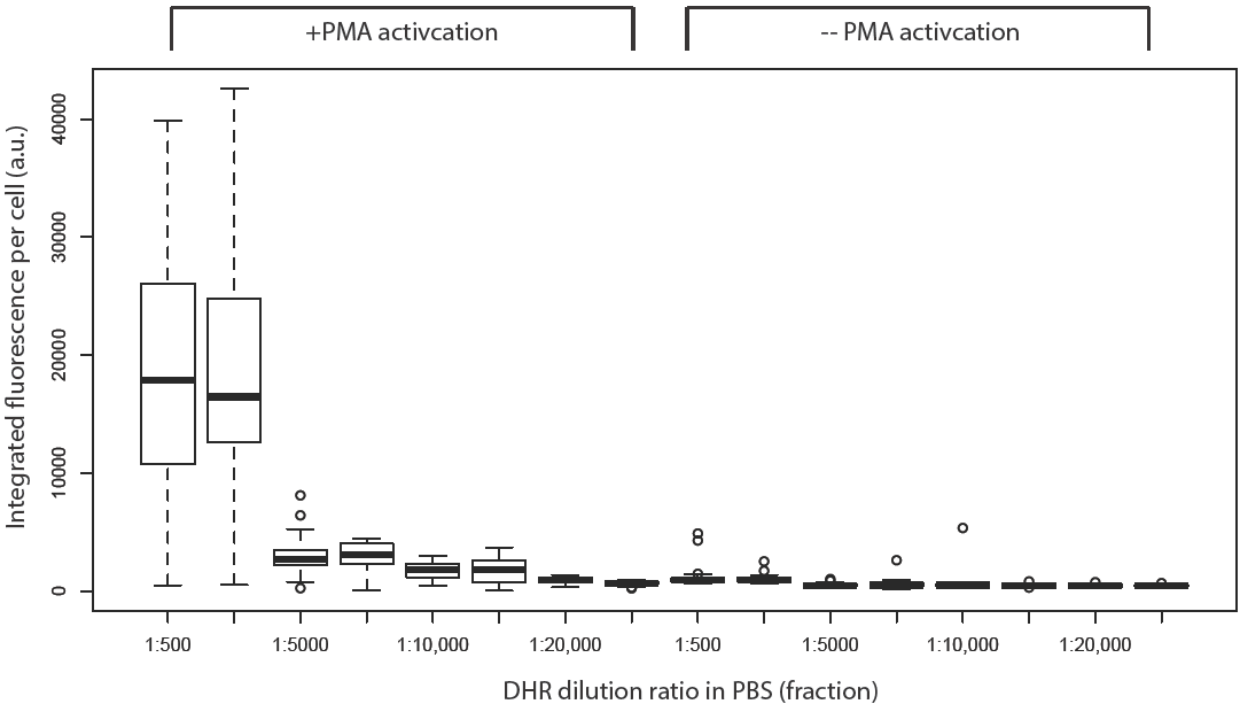

Figure 6.3 Representative dose response curve for the DHR reporter for activated and non-activated neutrophils. The 1:500 dilution of DHR in PBS provides the highest contrast between the two neutrophil activations states. As expected, neutrophils without PMA activation exhibit little or no ROS production, whereas significant ROS is observed for activated cells. Two channels per dose; box plots show the median (center line), 25th and 75th percentiles, and standard deviation. Note that some spontaneous activation does occur in neutrophils for healthy individuals. Subsequent experiments with an inhibitor (DPI) that block ROS (mimicking CGD) show even less ROS production than unstimulated neutrophils, whether the inhibited cells have been stimulated or not.

reports an even lower fluorescence intensity for PMA-activated, NADPH inhibited cells, compared to non-PMA activated healthy donors. These early results indicate that we can effectively mimic CGD *in vitro* following a human lancet puncture. Furthermore, the test performed in Figure 2 was conducted by a user with one single training session, demonstrating the user-friendliness and simplicity of the technique.

Additional experiments are still envisioned to complete the development of the assay. First, we will conduct a dose response on the PMA activation to test whether the contrast between "CGD patients" (DPI

inhibited) and healthy donors can be improved even further. Second, we have obtained a neutrophil-like cell line (PLB-985) that have a knock-down for genes that encode functions for ROS production, once again providing another way to mimic CGD. The "disease" cells will be compared with controls. Lastly, we will examine ways to automate the assay by freezing down and vacuum sealing the reagents; pre-coating the channels with P-selectin; adjust the inter-microchannel spacing so a multi-micropipette can be used to pump all the channels in parallel; fabricate the devices using CNC milling and hot embossing the devices in polystyrene since optical clarity is not required; and explore fluid handling methods that eliminate the need for a micropipet entirely.[93] Note that we have compared the fluorescence readout in glass and polystyrene microfluidic devices to ensure the autofluorescence of PS dose not impede the assay[66]; indeed, there was no noticeable difference in assay sensitivity between the two materials. These preliminary results demonstrate that somewhat complex and time-consuming oxidative burst assays can be dramatically simplified, requiring only minimal modifications to the neutrophil sorting techniques used in the KOALA neutrophil chemotaxis assays.

6.4 The influence of lifestyle factors on neutrophil function

Neutrophils are involved in a complex equilibrium of immune protection and autoimmune damage. While the recruitment of neutrophils to a wound or infection is critical to the healing process and immune protection, a large or prolonged response can lead to healing deficiencies, scaring and tissue damage. The ability to measure the amplitude of a response for a specific patient in an *in vitro* wound model, and the variation of this response when the patient is subjected to certain activities/diet, could bring valuable insight into the physiology of the innate immune system. As discussed in Chapters 4 and 5, traditional neutrophil chemotaxis assays require large volumes of blood and a long purification process.[78] This lengthy purification process has been shown to affect neutrophil function[167] and strictly limits the number of draws possible from a single patient. The KOALA platform largely eliminates these drawbacks as it has the capability to purify neutrophils from a lancet puncture in less than 5 minutes and easily setup a biomolecular gradient of chemokines for the chemotaxis assay. In this case, KOALA permits truly novel studies that were not possible in the past because they were unsafe (require too much blood), or did not benefit from the dramatically improved time resolution that KOALA can achieve for

neutrophil chemotaxis. Therefore, we are interested in assaying the chemotactic function of neutrophils surrounding discrete "lifestyle factor" events that are believed to affect, in one way or another, the innate immune system but are not well understood.

6.4.1 Brief review of the literature and hypotheses

Using traditional cell biology assays, researchers have identified several factors that may play important roles in regulating neutrophil function. Lifestyle and diet factors, amongst others, have been shown to impact neutrophil count, migration, and biochemical function. For example, sleep deprivation has been linked with higher neutrophil count[203], despite a known immunodepressive effect. Physical exercise shows increase in neutrophil count and increase in neutrophil degranulation.[204] Diet factors, such as caffeine and ethanol ingestion have been linked with neutropenia and reduced neutrophil migration and oxidative bursts. Building on this research, we intend to probe the role of these lifestyle factors on neutrophil migration. We have several questions we would like to answer:

- *How does moderate to strenuous cardiovascular exercise influence the migratory behavior of neutrophils in healthy patients?*
    - Hypothesis: Exercise induces a rise in neutrophil count and decrease in chemotaxis velocity due to increased tissue damage, more activated platelets, and other effects described in prior studies. The literature shows:
        - The effects of exercise and caffeine on leukocyte count have been investigated[205], however these studies were limited in scope due to the blood sampling method and assays available.
        - Intense exercise may cause bronchial epithelial damage, inducing a strong response in neutrophil activity[206].
- *How does limited sleep for one night or several nights in a row affect neutrophil function? What is the effect when combining sleep deprivation with exercise or caffeine intake?*
    - Hypothesis: Sleep deprivation induces a decrease in neutrophil adhesion possibly but not limited to diminished ICAM-1/LFA-1 interaction. The literature shows:

- Cytokines regulating sleep (e.g. TNF-α and IL-1) may be altered, increasing chance of infection.[207]
- A significant increase in neutrophil count was observed after 3 days of sleep restriction (four hours) compared to a control group.[203]

- *Heavy alcohol consumption has long been linked to problems with immunity. How does moderate to heavy ethanol ingestion affect neutrophil behavior? How does it affect neutrophil function over time? Are there consumption levels where the effect is positive?*
  - Hypothesis: Ethanol consumption induces an increase of neutrophil adhesion and decrease in chemotactic response possibly linked to the production of pro-inflammatory cytokines. The literature shows:
    - Increased expression in the neutrophil adhesion molecule ICAM-1 is observed in mice exposed to ethanol and subsequently burned (although burning could certainly account for this increase). The ethanol and burn combination increased the morbidity rate amongst these mice compared to mice with no ethanol exposure.[208]
    - Alcoholic liver disease (ALD) results, in part, from infiltration of activated neutrophils into the liver, causing tissue damage after acute alcohol exposure.[209]
    - Phelps *et al.* and others have shown significantly reduced motility for patients that have ingested ethanol.[210]
- *How does moderate caffeine consumption affect neutrophil adhesion, migration, and morphology?*
  - Hypothesis: Exposure to chronic and/or high doses of caffeine will reduce the inflammatory response of neutrophils, thereby decreasing neutrophil migration velocity. Previous studies have shown:
    - Caffeine consumption alters the cyclic AMP/protein kinase pathway, which inhibits expression of the pro-inflammatory cytokine TNF-α.[211]
    - The adenosine A_{2A} receptor expression from platelets increases following caffeine consumption, promoting an anti-inflammatory effect.[212]

- Caffeine ingestion has been found to reduce neutrophil migration in a transwell assay (after *in-vivo* ingestion) at clinically relevant concentrations.[210]

All of these studies indicate that various lifestyle factors significantly alter immune function in humans. However, these studies were limited in scope due to experimental constraints from the assays that were used by the investigators. The time and expense of performing traditional chemotaxis assays also inherently (albeit indirectly) limits the number of patients that can be sampled. To date, most studies testing neutrophil function on human patients have included a small number of subjects with few or no repeats (ref. 213 — 8 subjects; ref. 203 —17 subjects; ref. 205 — 20 subjects). The KOALA platform leverages ultra-low volume blood sampling to enable highly time-resolved neutrophil tracking surrounding a "lifestyle factor" event, along with automated imaging and analysis. This combination of rapid neutrophil purification procedures with an easy-to-use device enables frequent sampling and large quantities of data acquisition, permitting studies that were simply not achievable using traditional methods. Results from the prior studies that use traditional neutrophil analysis techniques show measurable differences in neutrophil counts, protein expression, and chemotaxis; one would anticipate seeing definitive trends in our studies using a modern microfluidic approach, given the technological improvements the KOALA platform provides.

6.4.2 Proposed methods for lifestyle factors study

This section details how one could potentially undergo the lifestyle factors study. Each lifestyle factor is addressed, and values for the "dose" of the lifestyle factor are suggested based on comparable studies in the literature. Figure 4 details a proposed workflow for the study.

Caffeine ingestion: Subjects would be exposed to various doses of caffeine from common commercially available products, in the limit of 600 mg (approx. equivalent to the caffein intake from a large 20 oz coffee) per day. After selection and consent, a control assay should be performed on the subject to establish their baseline neutrophil chemotaxis function. In the following hour, subjects would be provided with a disclosed dose of caffeine in the form of a commercially available drink (e.g. Starbucks™ coffee, Coca Cola™). After the caffein ingestion, lancet punctures would be performed regularly to measure the evolution of neutrophil function.

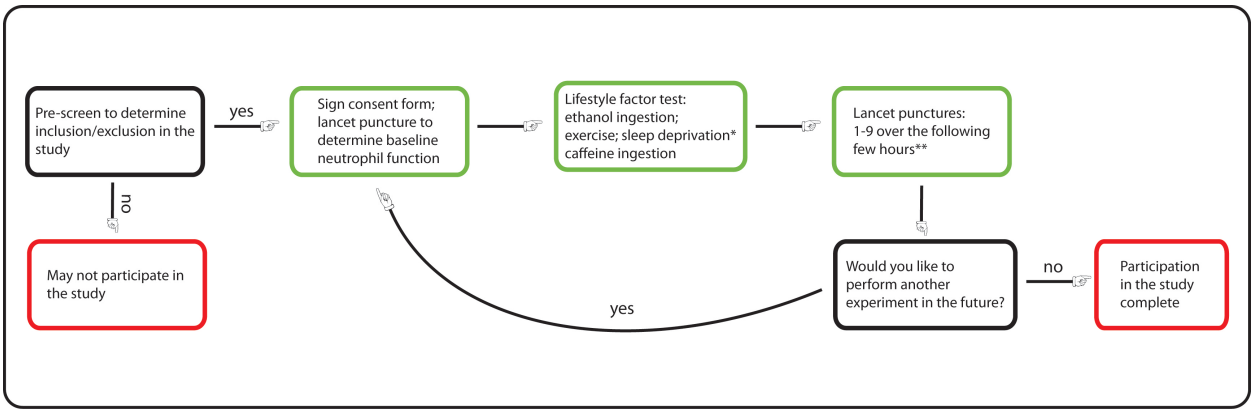

Figure 6.4 Schematic illustrating sequence of events for a subject participating in a lifestyle factor experiment. *The sleep deprivation experiment requires a change (Δ) measurement; therefore, the subject must be first tested at night and in the morning after little or no sleep. Then a separate experiment would then be conducted with the same time-points, only allowing a "normal" (e.g. 7-9 hours) amount of sleep and comparing the two Δ values. **The number of lancet punctures should be determined before beginning the experiment. The highest number of lancet punctures that should be performed in a day would likely be ~5 times over several hours. The upper limit of 9 lancet punctures accounts for the possibility of lancet punctures at much later time-points (e.g. 24-48 hours after the initial experiment).

Exercise: Subjects would execute a defined exercise routine on a stationary bike, determined by their average heart rate (maximum average of 160 bpm and absolute maximum of 190 bpm) and duration of exercise (maximum 30 min); frequent sampling of the donors' lactic acid content may also be included to further characterize the exercise level throughout the session. After selection and consent, a control assay should be performed on the subject to measure their baseline neutrophil chemotaxis function. In the following hour, subjects would ride the exercise bike, and their heart rate and general status should be assessed continuously. Subjects would be required to "cool down" for a minimum of 5 minutes. Within the 10 minutes following the exercise lancet punctures should be performed once, or regularly over multiple time-points to measure the evolution of neutrophil function.

Ethanol: All subjects should be tested with a breathalyzer to ensure a starting breath alcohol level of zero, and a lancet puncture should be performed to assess baseline neutrophil function. The subjects would then be

given 1.5 oz of 86 proof liquor mixed in with a "mixer" on ice. Subjects would be permitted to consume the drink at their own pace, although no slower than one drink per hour. Before being served a subsequent drink, subjects should undergo breath alcohol testing and examination for signs of intoxication by a supervising researcher. Participants should not be permitted further alcohol containing drinks once their breath alcohol level surpasses 0.08 mg/dL or signs of clinical intoxication became evident (slurred speech, balance instability, alteration of mental status). Once the minimum breath alcohol level is reached, lancet punctures should be performed regularly to measure the evolution of neutrophil function. Subjects should be required to stay within the facility until breath alcohol levels are below 0.08 mg/dL, and should not be permitted to drive upon leaving the session.

Sleep deprivation: Two sleep deprivation procedures could be investigated, testing the effects of acute and chronic sleep deprivation on neutrophil function. The first procedure consists of a 30 hour period without sleep. The first lancet puncture should be performed in the afternoon, 6-10 hours after awakening. The subject would be asked to avoid sleeping the following night and the investigators would confirm donor compliance the following morning. The following day a second lancet puncture should be performed 30 hours after awakening. The second procedure induces chronic sleep deprivation defined by 3 consecutive nights with 4 hours of sleep. The first lancet puncture would be performed on the first day of the test and the second lancet puncture would be performed on the 4th day. Sleep deprivation may induce a temporary decrease in cognitive ability, and a difficulty to perform mentally taxing tasks. During the sessions, research supervisors should assess the subjects state and will propose the subject rest within the research facilities if required. Additionally, commercially available sleeping monitors could be worn to characterize the quality of sleep.

6.4.3 Preliminary results for neutrophil chemotaxis and exercise study

Preliminary pilot testing was conducted to test the effects of exercise on neutrophil chemotactic function. The KOALA device and neutrophil sorting procedures described in Chapter 4 were used for the neutrophil chemotaxis assay.

Experimental design

The source of chemoattractant was 100 nM fMLP (or gel without CA for the control). Prior testing of neutrophil chemotactic function revealed significant variation in function throughout the day, as expected (Figure 5).

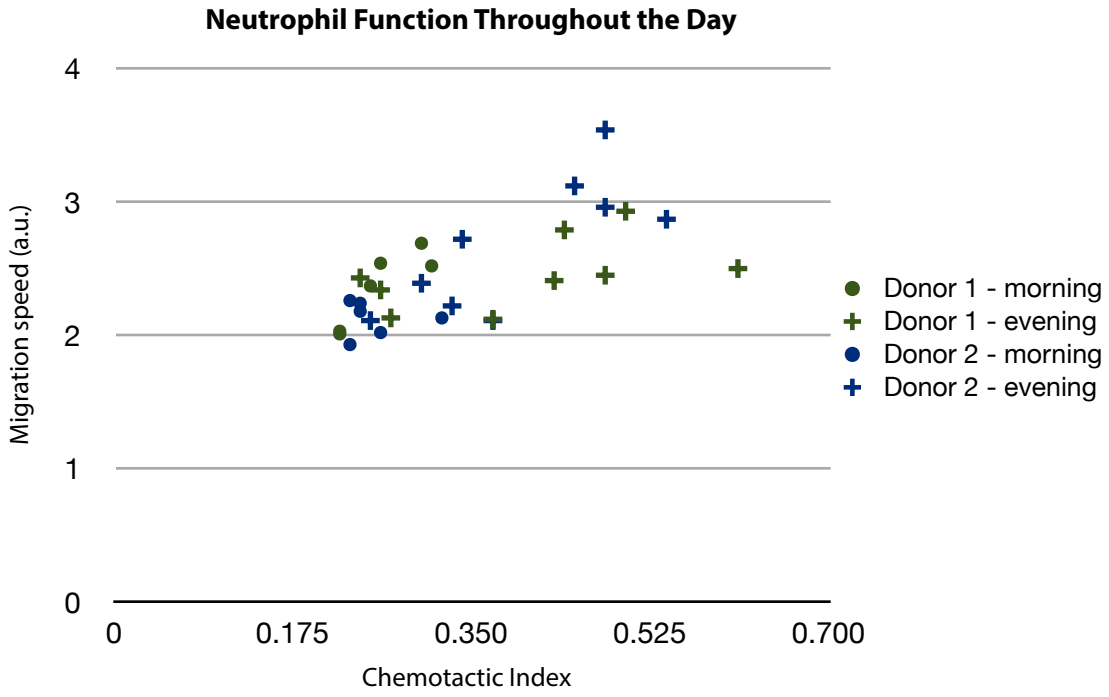

Figure 6.5 Neutrophil function throughout the day. Graph shows increasing chemotactic index and migration velocity for the two donors tested throughout the day (n=4 repeats). CA source was 100 nM fMLP. Channels coated with 100 μg/mL for 1 h.

Therefore, we were interested in obtaining the change in neutrophil function surrounding the exercise session. For each experiment, three lancet punctures were performed over a period of several hours. The first lancet puncture and purification was performed ($t=T_1$) prior to the exercise session, and following purification in KOALA, the device was placed in a microscope incubator set at 37 ℃ for 45 minutes with the lid placed on the device; thus, the gradient was forming during this time, but the neutrophils were not being monitored with timelapse microscopy yet. Following this first purification, a rigorous exercise session was performed on a Schwinn, variable resistance exercise bike for 30 minutes (estimated maximum heart rate of 160-185 bpm based on prior experience). Heart rate or lactic acid tracking was not performed for these experiments, although should be considered for future studies. Immediately following the exercise session, another lancet puncture and blood purification was performed ($t=T_2$); the second sample was placed in the incubator at 37 ℃ for 45 minutes with the lid placed on the device. Timelapse microscopy was initiated on the first sample 45 minutes after T_1

(microscopy setup described in Chapters 4 & 5). One hour after the completion of the exercise session, a third lancet puncture and purification was performed ($t=T_3$). The 45 minute timelapse imaging sessions were separated by one hour, with 15 minutes between sessions for positioning and focusing on each microchannel.

Results

Preliminary results for the exercise trials are shown in Figure 6. The analysis of the change in neutrophil function over time shows a marked decrease in neutrophil chemotaxis velocity and increase in directionality. Further, this result demonstrates that these changes occur on a relatively short time-scale, and that the chemotaxis readouts provided by KOALA are sensitive enough to detect changes in neutrophil function on this time-scale. Controls that measure the change in neutrophil function without exercise over this these time-points still need to be conducted in order to verify that the lifestyle factor caused the change in function. Furthermore, it would be

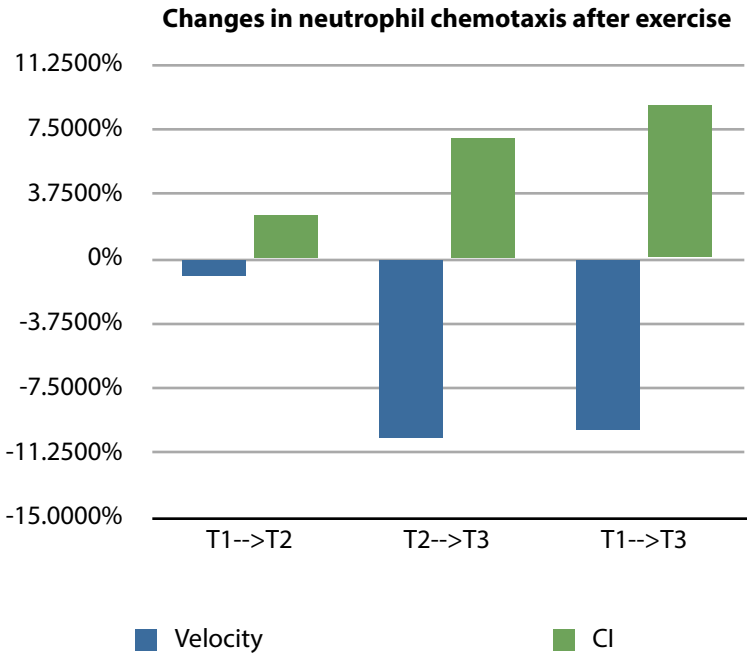

Figure 6.6 Neutrophil function after an exercise session. Graph shows average change in neutrophil chemotactic index (green) and chemotaxis velocity (blue) following an exercise session for one donor (n=6 repeats). CA source was 100 nM fMLP. Channels coated with 100 μg/mL overnight prior to the start of the experiment. No observable migration for controls. Note that error bars are not shown because the graph displays the change in average chemotaxis values, which cannot be easily represented by S.D. or S.E.M.

interesting to test neutrophil chemotaxis in a uniform concentration of chemoattractant in order to asses differences between chemotaxis and chemokinesis. Nonetheless, these preliminary results represent a promising first demonstration of how these lifestyle factor experiments can be conducted.

6.5 Conclusion

This chapter discussed additional *in vitro* tools currently in development that can potentially contribute to the study of neutrophils in both a research and clinical context. Furthermore, an outline was presented for a study that could leverage the beneficial aspects of the KOALA chemotaxis method to potentially provide novel insight into how common dietary and wellness choices affect the innate immune system. Importantly, all of the assays discussed in this chapter—KOALA; the oxidative burst assay; and rapid cell sorting with IFAST—can be used in concert to provide the investigator with a powerful set of tools to perform neutrophil studies.

6.6 Acknowledgements

I would like to thank Jay Warrick and Erwin Berthier for their contribution in developing the foundation of JEX. The work was made possible by funding from an Innovation & Economic Development Research Program grant (E.K.S). This work was also supported by NIH R01 EB010039 (D.J.B, E.K.S, F.M.H.). Farsh Moussavi-Harami contributed to the design and analysis of the oxidative burst assay and experiments presented in this chapter.

6.7 Disclosure of Conflicts of Interest

D.J.B. has an ownership interest in BellBrook Labs, LLC which has licensed technology presented in this manuscript. E.K.S., E.B. and D.J.B. have filed a patent application based on technology presented in this work. E.K.S., F.M.H., D.J.B. and A.H. have disclosed additional technology that has been presented in this chapter to WARF and reserve the right to file a patent application.

6.8 Copyright permissions

All work presented in this chapter is unpublished; therefore copyright permissions are currently not required to present this work in my dissertation.

Chapter 7

Developing a biomimetic wound-on-a-chip

7.1 Introduction

All the microfluidic technologies presented to this point were designed with the intention of replacing or enhancing standard cell biology or clinical diagnostic assays. However, as discussed in Chapter 1, there is a new class of microfluidic technologies that have been designed with fundamentally different goals. These so called "organ-on-a-chip" devices integrate multiple advancements in microscale technologies into a single system. This class of technologies aim to recapitulate *in vivo* organ function while maintaining *in vitro* control over the design and execution of the assay.[91] Ultimately, these systems may be employed in drug discovery and research applications, curtailing the use of animal models and enabling more experimental control for the researcher. The final chapter of my dissertation focuses on developments underway in the MMB lab that aim to contribute to this emerging area of research through the development of a "wound-on-a-chip" device.

In addition to stimulating neutrophils with recombinant chemoattractants such as IL-8 or fMLP, an opportunity exists to perform novel wounding assays, with the wound acting as the source for neutrophil migration. In this scheme, one cultures a cells in 2D or 3D (e.g. epithelial cells and/or fibroblasts) in one or more chambers of a multi-culture microfluidic device, and monitors the chemotaxis of neutrophils toward the cells after a wounding event. The wound can be as simple a scratch (mimicking traditional wounding assays), or other types of wounds such as tribological wounding, chemical wounding, laser wounding, electrical wounding, or exposure to ultra-violate light. These wounding assays would provide insight into the kinetics and mechanisms of wounding that are currently poorly understood, with the ability to leverage a powerful screening approach.

The following sections describe the technology platform currently in development and some preliminary results. In order to simplify the problem, the wounding component and the neutrophil extravasation component of the assay have been developed separately and in parallel. This means that parts of the technology

are in different stages of development, as will be evident from the preliminary results. However, this approach has allowed for a more rapid progress of the neutrophil extravasation model.

7.2 Neutrophil extravasation from a microfluidic biomimetic blood vessel

The process of neutrophil recruitment to a site of inflammation can be described by three primary stages: (1) tethering and capture of neutrophils on an activated area of the endothelium; (2) firm arrest and and intravascular crawling prior to transendothelial cell migration (TEM) across the blood vessel; and (3) chemotaxis towards the wound or site of infection.[111,214,215] Neutrophil extravasation is dependent upon several factors biophysical and biochemical factors that determine whether the cells can efficiently emigrate from the blood stream. The stiffness of the matrix surrounding the blood vessel has been shown to strongly influence neutrophil TEM.[216,217] Additionally, ligand expression such as ICAM-1[216,218], PECAM-1[111], and MAC-1[219] are important for the extravasation process. Most neutrophil TEM studies have been conducted using a modified Boyden Chamber assay design, or intravitial microscopy; but these assays are not ideal because intravital microscopy can be difficult and expensive to perform, and modified Boyden Chambers do not faithfully recapitulate *in vivo* conditions of the blood vessel.

Recently several microsystem engineering groups have demonstrated blood vessel-on-a-chip models that have been applied to diagnostic[87,89] and research[220] applications. Furthermore, others have shown neutrophil or neutrophil-like TEM assays using macroscale[216] and microscale assays.[221] However, none of these methods integrate biophysical, chemical, and geometric considerations into a comprehensive neutrophil extravasation model that mimics *in vivo* function. This section details efforts underway in our lab to develop this comprehensive solution for applications in research and drug discovery.

7.3 Methods

Devices were fabricated in PDMS using standard lithography discussed in previous chapters. Please refer to earlier chapters for procedures such as SU8 master fabrication; PDMS mixing ratios and curing time and temperature; and plasma treatment protocols.

7.3.1 Preparation of the hydrogel solution

A hydrogel consisting of extracellular matrix (ECM) proteins made of a final concentration of 6.0 mg/mL Type I collagen (rat tail, BD Biosciences, Bedfrod, MA, USA), and 25% Matrigel (BD Biosciences, Bedford, MA, USA) was used experiments. Prior to each experiment, roughly 133 µL of hydrogel solution was made and placed on ice until it was needed for creating the lumen. To make the hydrogel, 1.6 µL of a neutralizing basic solution (5.0 N NaOH) was added to 20 µL of 5x PBS. This solution was then added to 78.4 mL of the collagen I, and left on ice for about 5 minutes. Finally 33 µL of Matrigel was added to the hydrogel solution and the solution was set on ice until it was needed.

7.3.2 Creating lumen structures

Prior to patterning lumens, devices were oxygen-plasma-treated to bond the PDMS channels to a glass surface (the inside of a glass-bottom Petri dish, MatTek, Ashland, ME, USA), and to render the inside of the chambers hydrophilic. The bonding procedure should not include an elevated temperature step to solidify the PDMS-glass bond since the glass bottom on the Petri dish can fall off from this process. The devices were coated with either 200 µL/mL fibronectin (Fn) or 1 mg/mL Poly-D-Lysine (PDL) to increase the adhesion of the hydrogel to the microchannel walls; this helps to ensure media does not convect through from side channels during an experiment. PDL coatings were performed the night before an experiment for 2-4 hours, followed buy a 24 hour baking step in a dry oven at 80 ℃. The Fn coating was performed on the same day as the experiment; after 20 min Fn coating at room temperature, the Fn solution was aspirated from the microchannels. A previously described method called viscous finger patterning was performed to create lumen through a hydrogel.[222] Briefly, the above hydrogel solution was pumped into a microchannel, and then media was pumped through the hydrogel, driven by surface tension (Figure 1a). Once the lumens were formed, the channels were placed in an incubator while the endothelial cells were being passaged (minimum of 10 minutes).

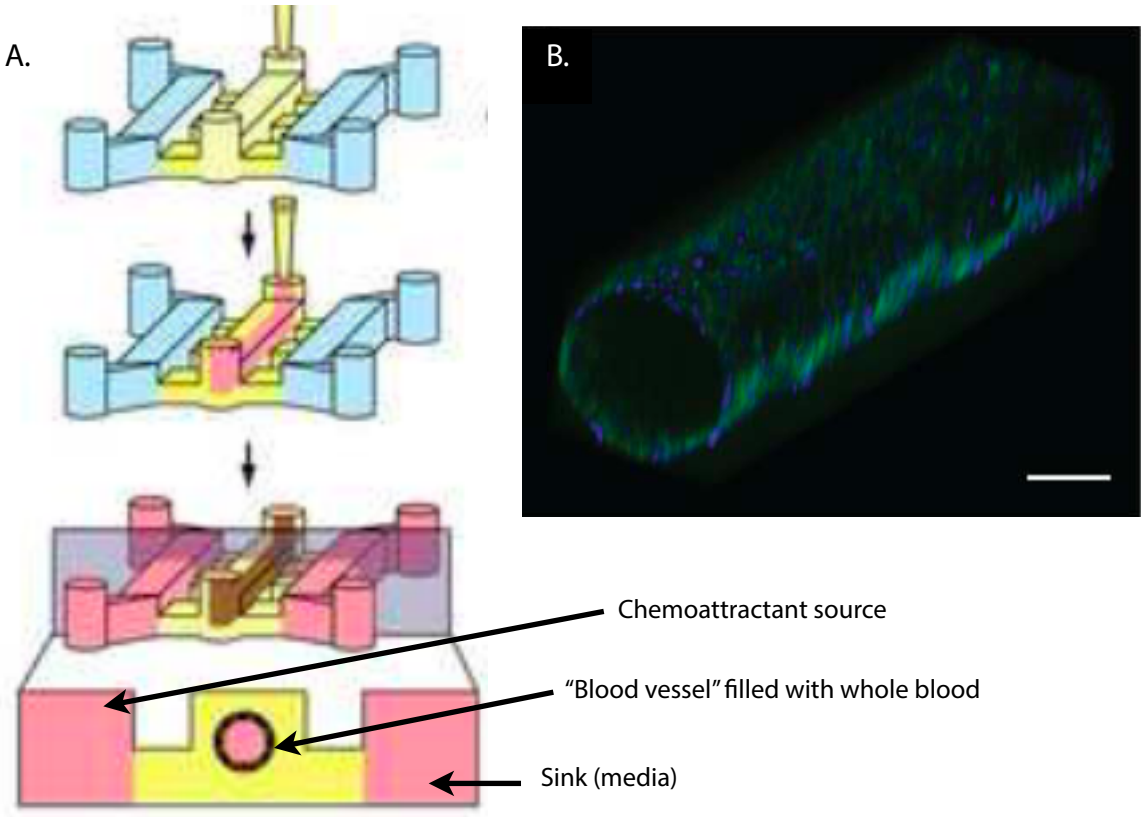

Figure 7.1 Schematic and data showing the creation of a blood vessel-like model surrounded by ECM. (A) Lumens are created in a hydrogel by first filling the center channel in a multi-channel microfluidic device. Once the liquid "pins" at the edge of the migration/diffusion channels, media is pumped through the center of the hydrogel, creating a 3D cylindrical space in the hydrogel. Following incubation to solidify the hydrogel, endothelial cells and media are passively pumped through the lumen and continuously rotated on a motor for even cell seeding. **(B)** Confocal microscopy image showing the stained EC's; scale bar is 100 μm. Schematic and image are provided courtesy of Lauren Bischel, who developed this method. The images were taken and adapted from the original source with permission.

7.3.3 Lining lumen with endothelial cells

For the studies presented in this chapter, HUVECs were used to line the lumen. The lumens were created by using one of two methods. (1) Seeding the channels four times, rotating the device 90º every 15 minutes; or (2) the devices were placed on rotating motor, and the cells were seeded once. The latter option was used for all recent

experiments (and for data presented in this chapter). Once the cells have been passaged, the cells were resuspended in media to a concentration of 40,000 cells/μL. 2 μL of the cell solution was passively pumped into the lumens, and the Petri dish was securely attached to the motor (BBQ Rotisserie Variable Speed Reversible Brushless Gear Motor, Wondermotor, CA, USA); placed in an incubator; and turned on at 2 RPM for 30 min to 60 minutes to allow for cell attachment to the lumen. Then, the devices were removed from the motor and placed in an incubator for a minimum of 2 hours before being perfused with fresh media via passive pumping to rinse unattached cells. After 24-48 hours, the endothelial cells had formed cell-cell junctions around the interior of the lumen (example shown in Figure 1b).

7.3.4 Activation protocols and blood seeding

The endothelial cells need to be stimulated by various cytokines in order to induce the expression of ligands important for neutrophil capture and TEM. Briefly, the endothelial cells were activated with TNFα (R&D systems; Minneapolis, MN; 210-TA-010) at concentrations of 10–50 ng/mL; activation was started between 12–24 hours prior to the seeding of whole blood or purified neutrophils. 10 ng/mL of IL1-β was added to the TNFα solution 4 hours prior to blood or neutrophil seeding. The activations were either performed directly within the lumen, or occasionally in the adjacent "chemoattractant channel" to more closely mimic *in vivo* stimulation. The cell seeding was performed with either whole blood with Calcein dye for the visualization of neutrophils; whole blood with fluorescently-labeled purified neutrophils; or fluorescently labeled purified neutrophils. For the whole blood draw, the procedure was performed after obtaining consent, and whole blood was obtained from a lancet puncture on the finger of a self-reported healthy donor. The human subject protocol was approved by the University of Wisconsin Center for Health Sciences Human Subjects Committee. In brief, the skin was thoroughly cleaned with an alcohol swab and a disposable lancet (Safety Lancet, 02-675-160, Fischer Scientific) was lightly pressed against the skin and actuated. The first drop of blood was discarded and the finger pressed to obtain a drop of blood of about 5-10 μL on the bottom of a flat sterile petri-dish. 3 μL of blood was pipetted into a reservoir containing 9 μL of HUVEC media and mixed gently. The blood was then mixed 1:1 with Calcein AM dye that had been diluted from stock at a ratio 1:500 in HUVEC media. For purified neutrophil preparation, see

Chapter 5. Once fresh media replacements were performed to remove activation reagents, 2 µL of the blood/ neutrophil samples were placed in the lumens for the TEM experiment. The devices were either left horizontally in the incubator; tilted slightly towards the chemoattractant channel (for gravity-assisted TEM); or tilted 90° towards the chemoattractant source so the neutrophil TEM and chemotaxis were oriented parallel to the formation of the chemical gradient. For the source of chemoattractant, 100 nM – 2 µM fMLP was used.

7.3.5 Imaging for neutrophil extravasation from blood vessels

Imaging was conducted on an Olympus IX-81 microscope at 37 ℃ (see Chapters 4-6). Phase contrast and fluorescent images were taken at predetermined time-points, including z-stack images when endpoint analysis was performed. For timelapse imaging, images were acquired every 30–60 seconds for up to 5 hours. Timelapse imaging was usually performed immediately after seeding the blood in the lumens. Endpoint analysis was

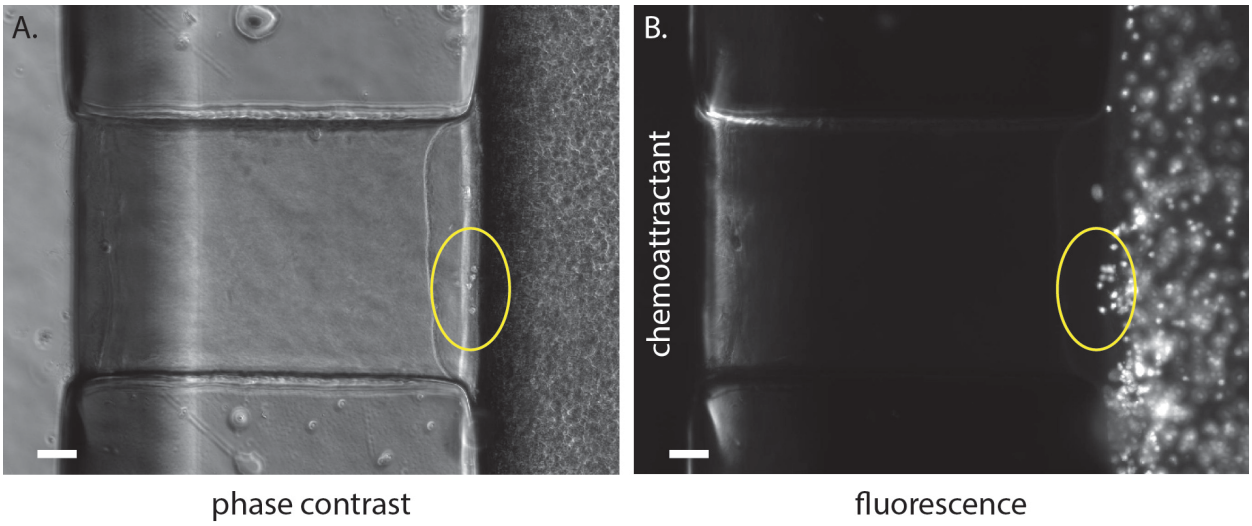

Figure 7.2 Purified neutrophil extravasation from EC-lined lumen into collagen ECM. (A) Phase contrast image with several neutrophils having extravasated from the "blood vessel" into the migration channel. **(B)** Fluorescent image showing neutrophils in different focal planes. The circled area near the migration channel is in focus. 2 µM fMLP chemoattractant on left channel; 6.0 mg/mL collagen in migration channel; scale bar 100 µm; Image taken 12 hours after 25 ng/mL TNFα stimulation.

performed between 12–24 hours after blood seeding. Note that beyond 48 hours, the HUVECs are likely starved of reagents and the neutrophils are unhealthy, necrotic, apoptotic.

7.4 Preliminary results

We have observed neutrophil extravasation out of the endothelial-cell lined lumen and into the surrounding extracellular matrix. This process has been observed in real-time using timelapse microscopy, as well as using endpoint image analysis (i.e. imaging the channels after a predetermined amount of time). Neutrophils extravasated from the lumen most often when they had already been purified from whole blood via density centrifugation methods. Figure 2 shows an example of purified neutrophils that have been fluorescently tagged leaving the lumen and migrating towards an increasing concentration of a chemoattractant. This image was taken 12 hours after the endothelial cells were stimulated with TNFα, which up-regulates the expression of transmigratory proteins such as PECAM-1.[111] Note that after 12 hours, the gradient of fMLP had likely disappeared since it diffuses on a much faster timescale than the extravasation and migration occur. We modeled this diffusion process experimentally in the lumen device with an Alexa Fluor 488 dye, and discovered that the gradient in concentration was significantly reduced after 2-3 hours between the source and sink (Supplementary Video 1). Furthermore, it is noteworthy that the neutrophils have only started migrating in the diffusion channel, but have likely traveled ~200-300 μm from the lumen (vertically and horizontally) over a period of 12 hours. This yields an average migration rate of ~15-25 μm/hr, which is well below the anticipated migration rate of neutrophils in 3D (see Chapter 4). The diminished neutrophil chemotaxis velocity can likely be attributed to the elimination of the chemical gradient early in the experiment (Supplementary Video 1). The neutrophils likely traveled the full distance while a gradient in the chemoattractant still existed, and then lost directionality as the sink became saturated with chemoattractant (Supplementary Video 2). In addition to observing purified neutrophils extravasate from the lumen, we have also observed neutrophils in whole blood exit the lumen (Figure 3). This result was less common than observing purified neutrophil extravasation, likely because the neutrophil concentration is far lower in whole blood samples. Additionally, the neutrophils are not

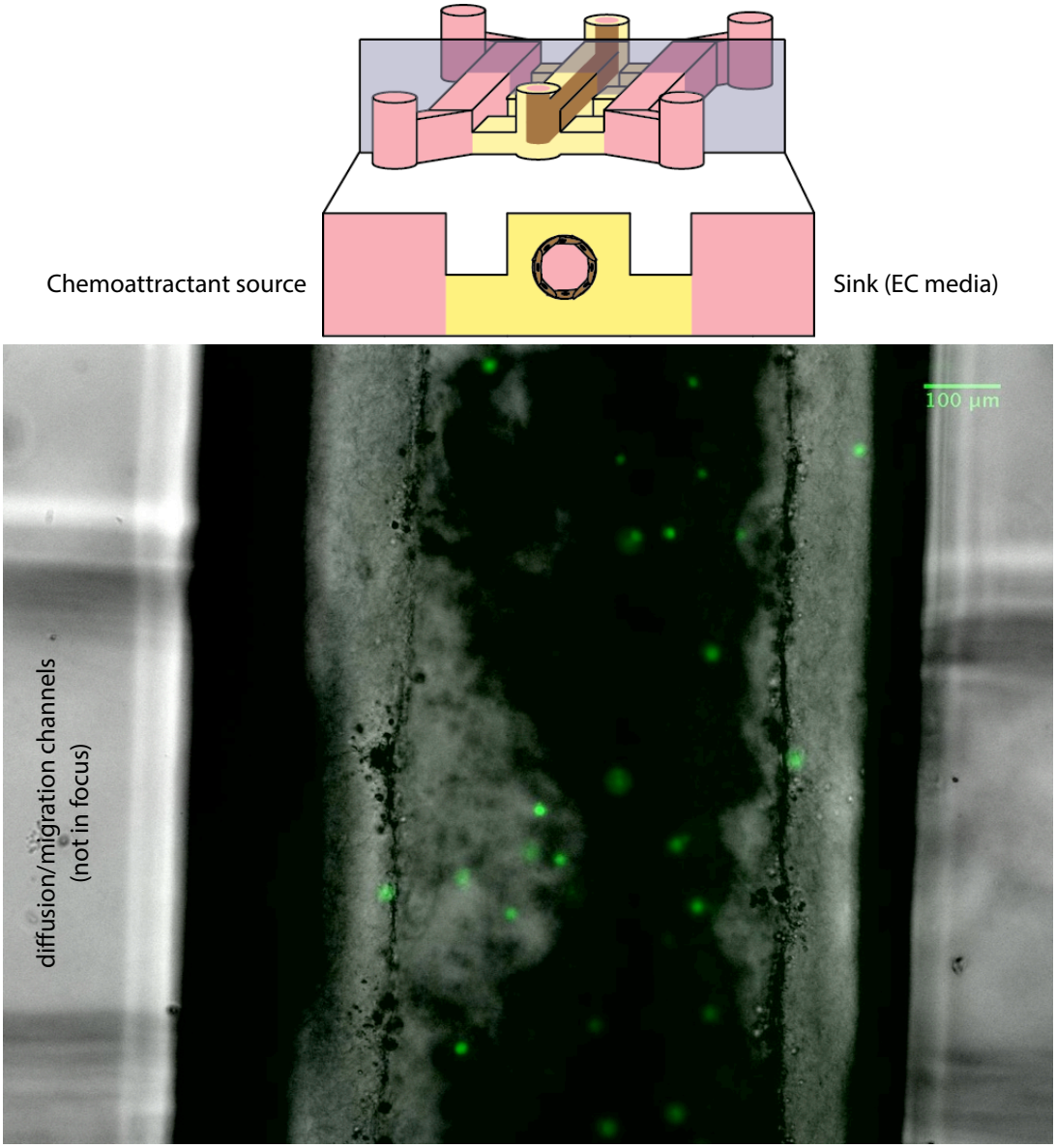

Figure 7.3 Neutrophil extravasation from blood vessel microfluidic device. Neutrophils tagged with Calcein dye (shown in green) extravasate out of an EC-lined lumen into the extracellular matrix. Whole blood was obtained from a lancet puncture. Phase contrast image with superimposed fluorescence image of neutrophils. Schematic above the image illustrates the experimental setup.

be able to sense chemoattractant concentration gradients when surrounded by whole blood (Supplementary Videos 3 & 4), though haptotaxis and durotaxis signals are much more relevant for intraluminal crawling and TEM

in vivo since blood flow can disrupt chemokine gradients.[223]

Despite having observed neutrophil TEM in this *in vitro* wounding model in some instances, the assay does not consistently work as intended. Yield can be low (~50%) when fabricating the lumens initially, which makes it more challenging to perform the experiment. Additionally, the endothelial cells did not always withstand the activation protocols, and can look markedly less healthy or dead prior to the blood cell seeding. Lastly, the mechanical properties of the surrounding hydrogel, largely dictated by the viscous fingering protocols, may not be ideal for neutrophil TEM. These problems and others still need to be solved as they currently limit the reliability and performance of the assay.

7.5 Neutrophil response to *in vitro* cell wounds

The most popular wounding assay performed in cell biology is known as the "scratch assay", and the simplicity of the name accurately reflects the nature of the method. When one wishes to perform a scratch assay, the investigator simply cultures a confluent monolayer of cells, usually in a plastic petri dish, scratches the cells with a micropipette tip, and then watches the "wound closure" over time.[224] While this method is extraordinarily simple and accessible, it has poor reproducibility; usually is conducted in 2D, limiting its physiological relevance; and does not correlate wounds with the inflammatory response of leukocytes. Over the last decade, other wounding methods have been developed that aim to improve upon the repeatability of the scratch assay, such as using PDMS stencils for monitoring cell migration[95,109,225]; continuous flow patterning of trypsin to selectively remove cells[226]; electrical wounding[227]; high-throughput stamp wounding[228]; and other methods. However, none of these techniques attempt to measure the response of neutrophils to wounded cells. Zebrafish[229,230] and murine[231] models have been used to correlate wounding dynamics with neutrophil response, revealing important mechanistic insights into the role or neutrophils in wound healing. Experiments conducted in these more sophisticated *in vivo* models highlight the benefits of correlating wounding dynamics with the response of inflammatory cells. Thus, we aim to develop a comprehensive *in vitro* wounding model that integrates neutrophil

Table 7.1 Summary of wounding experiments with preliminary results

Experiment	Conditions	Readout	Results
Wounding cells with ultraviolet light	Wounded BEAS-2B; HUVECs. Control wrapped in foil. 30 second to 15 minute UV exposure. UVB and UVC radiation	Live/Dead stain (L/D)	Cells rarely died, even after 15 minute exposure. 24 hours post-exposure, cells still healthy.
wounding cells with beads and magnetic particles	Lateral flow patterning device used to shear HUVECs w/ beads. Wounding w/ PMPs and magnet below the microchannel	Phase contrast image of wound size	Not enough shear to damage cells. PMP patterning dominated by magnet, so the particles could not reliably pattern a "wounding strip."
Wounding w/ Hyper/hypotonic salt solutions	HUVECs and BEAS-2B exposed to salt rich (10x PBS) or deionized water. 1-5 minute exposure times. Simple straight microchannels used.	Live/Dead stain	Cells looked unhealthy w/ hypertonic wound, but still lived. DI wounds killed cells, but lysed cells difficult to measure w/ L/D.
Scratch assays in open microfluidic chambers and multi-well plates	P200 pipet tip used to create circular or straight-line scratches. Cells in mono-culture (2D/3D). Human mammary fibroblasts & normal dermal fibroblasts; and HUVECs tested. Measured cell conditioned media, or cond. media and cell lysate; 6-24 hrs post-wound	Phase contrast image of wound; timelapse tracking of neutrophils in KOALA	No measurable neutrophil response detected. Neutrophil morphology and lack of motility identical to negative controls. Positive controls (100 nM fMLP) always induced neutrophil chemotaxis, indicating the assay functioned properly.
Conditioned media from Cancer cells to study cancer as "over-healing wound"	Cancer cells kept in culture for up to 5 days. Conditioned media tested. Cell types: MDA231 breast cancer cells; LnCaP prostate cancer cell line	Phase contrast image of cancer cells; timelapse tracking of neutrophils in KOALA	No measurable neutrophil response detected, except for some motility following 5 days of culture for MDA231 (w/out feeding, so may have been cell degradation)

response with different types and magnitudes of wounds in order to study innate immunity in a more physiologically relevant manner.

We have explored a variety of cell wounding technologies but have yet to reliably measure neutrophil chemotaxis in response to a wound. A brief summary describing some of these efforts is provided in Table 1.

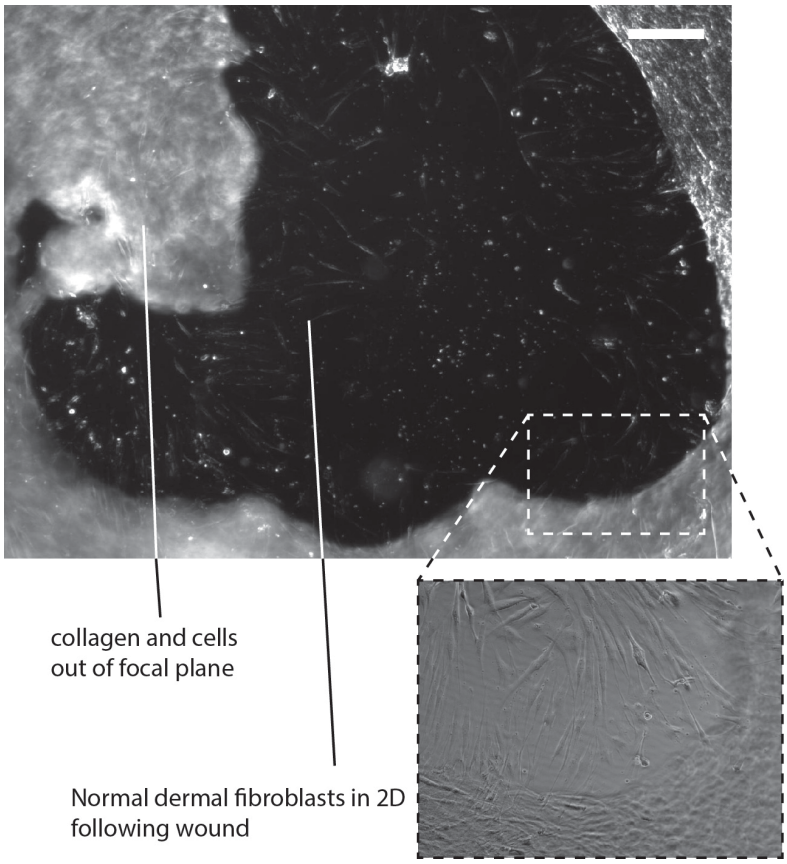

Figure 7.4 Bright field image of normal dermal fibroblasts following micropipet wound. The image was taken 24 hours following a circular scratch wound with a p200 micropipet tip. Collagen and cells removed from the wound can be seen in the upper left corner. Inset shows zoomed in view of fibroblasts that have proliferated and migrated in 2D. This experiment was carried out within a well of a 48-well plate. The scale bar on upper right shows is 100 μm.

Several different types of wounds have been explored, including wounding with ultraviolet (UV) light; wounding with salt-rich (10x PBS) and low-salt (deionized water) solutions; shearing cells with laminar flow-patterned[92] beads or paramagnetic particles (PMP's); scratch wounds of cells in 2D and 3D; and co-culture of cancer cells or their conditioned media with purified neutrophils (to model cancer as an "over-healing wound").

These methods have not stimulated convincing neutrophil chemotaxis. The most common method of wounding performed in these experiments was a simple scratch assay of cells cultured in 2D or 3D (Figure 4). Once the cells were wounded, a period of time was allowed to pass for the release of inflammatory cytokines in the media.

After the pre-determined amount of time had had elapsed, the conditioned media or media and cell lysate were tested in the KOALA assay for chemotaxis. Other attempts were made to directly measure a neutrophil response following a scratch wound in a microfluidic co-culture device, however the device did not sufficiently withstand convection between the co-culture chambers. For measuring neutrophil response to cancer cells, either the conditioned media was measured in KOALA, or the cancer cells were cultured directly in the lid in 3D to act as the source of chemoattractant. However, the cells cultured in the lid contracted heavily on the surrounding 3D matrix, and changing the curvature such that the drop of gel could no longer contact the neutrophil channels in the base. The gel contraction problem was reduced when higher ratios of Matrigel were mixed in with collagen, although constraining extracellular matrix properties to allow for the proper function of the KOALA chemotaxis assay is not an acceptable compromise. Evidently, more assay designs and cell combinations need to be explored before the wounding portion of the assay can reliably generate an inflammatory response.

7.6 Conclusion

The development of a biomimetic "wound-on-a-chip" device is still in its early stages, though not without promising preliminary results. On the neutrophil extravasation side of the model, we have observed neutrophil TEM out of whole blood and into the surrounding ECM, albeit with some inconsistency. The assay development strategies going forward should involve the testing the biophysical, biochemical, and geometric parameter spaces of the assay. For testing the biophysical microenvironment, different ECM densities and stiffness values should be tried since this is known to strongly influence neutrophil TEM. However, the challenge with changing the physical properties of the gel is that this also alters the structural design and integrity of the assay. Additionally, the constant flow of blood in the lumen should also be explored in the future, since shear forces are known to affect the morphology endothelial cells directly, as well as the bonds they form with neutrophils and subsequent TEM. Further trials should also be conducted on the activation protocols of the endothelial cells, though this has been tested relatively thoroughly thus far and the values used are consistent with those that have been reported in the literature. Finally, geometric confinement of the neutrophils may significantly aid in neutrophil TEM since this is often how neutrophils leave the blood stream *in vivo*. Unfortunately, viscous

fingering cannot effectively pattern lumens on the size-scale of capillaries, which means other methods will be required to make smaller vessels, such as angiogenisis through lithographically-constrained microchannels.[220]

The cell wounding portion of the assay still needs considerable improvement before it can be integrated with the *in vitro* blood vessel component of the model. A wide variety of wound and cells types have been explored so far, but none have induced a detectable neutrophil chemotactic response. It is not yet clear why neutrophils are not able to respond to wounded cells *in vitro*. One possible culprit is that the experiments to-date have only been conducted in mono-culture, and perhaps the correct combination of different cell types is required using multi-culture designs to generate the necessary signaling proteins. Furthermore, improvements should be made in device designs to accommodate direct measurement of the neutrophil response in co-culture with the wounded cells. This setup has been attempted in the past by separating two chambers with a hydrogel barrier, but convection was still a significant issue due to the pressure imbalance between the two chambers. Other device designs should be used to mitigate the convection issue, such as utilizing a short channel height for the connection diffusion channels (see Chapter 2; example in reference 159). The technical issues surrounding the wounding assay are far from insurmountable. Going forward, efforts should be placed in determining what biological conditions are required to generate an inflammatory response from neutrophils *in vitro*, since technical problems in the assay are relatively easy to solve.

7.7 Supplementary video captions

Video 7.1 Modeling of a chemical gradient in the lumen device. Diffusion of fluorescent dye modeling small chemoattractants such as fMLP. The timelapse is 120 minutes long. The source of Alexa Fluor 488 is located at the top of the video. Fluorescent images acquired using Slidebook software with an Olympus IX-81 microscope using a 4x objective at 37°C.

Video 7.2 Purified neutrophils extravasating from an endothelial cell-lined lumen. Human neutrophils on extravasating from the "blood vessel" towards 2 μM fMLP. Early in the experiment a neutrophil leaves the lumen in the upper migration channel; later in the timelapse, neutrophils extravasate into the lower migration channel.

The timelapse is 120 minutes long. Phase contrast images acquired using Slidebook software with an Olympus IX-81 microscope using a 10x objective (NA=0.30) at 37ºC.

Video 7.3 Fluorescently tagged neutrophils in whole blood. Human neutrophils migrating towards 100 nM fMLP on P-selectin-coated polystyrene in KOALA. The neutrophils have not been purified from whole blood, and do not migrate well. The timelapse is 60 minutes long. The source of chemoattractant is located on the right side of the video. Fluorescent images acquired using Slidebook software with an Olympus IX-81 microscope using a 10x objective (NA=0.30) at 37ºC.

Video 7.4 Fluorescently tagged neutrophils purified from whole blood. Human neutrophils migrating towards 100 nM fMLP on P-selectin-coated polystyrene in KOALA. The neutrophils have been purified from whole blood, and chemotaxis is much more persistent than in the non-purified channels. The timelapse is 60 minutes long. The source of chemoattractant is located on the right side of the video. Fluorescent images acquired using Slidebook software with an Olympus IX-81 microscope using a 10x objective (NA=0.30) at 37ºC.

Video 7.5 Example of human neutrophils in response to NDF cells in KOALA. Human neutrophils on P-selectin-coated polystyrene, with hydrogel and mixed with conditioned media from NDF cells cultured in a 3D collagen matrix, 6 hours after a scratch wound. Neutrophils show no movement throughout the timelapse. The timelapse shown is 60 minutes long, although the cells were monitored for 5 hours. Phase contrast images acquired using Slidebook software with an Olympus IX-81 microscope using a 10x objective (NA=0.30) at 37ºC.

Video 7.6 Example of human neutrophils in response to HMF cells in KOALA. Human neutrophils on P-selectin-coated polystyrene, with hydrogel and mixed with conditioned media from HMF cells cultured in a 3D collagen matrix, 6 hours after a scratch wound. Neutrophils show no movement throughout the timelapse. The timelapse shown is 60 minutes long, although the cells were monitored for 5 hours. Phase contrast images acquired using Slidebook software with an Olympus IX-81 microscope using a 10x objective (NA=0.30) at 37ºC.

7.8 Acknowledgments

I would like to thank Lauren Bischel for training on creating endothelial cell-lined lumen structures. The lumen patterning; hydrogel preparation protocols; and initial lumen devices were provided by Lauren. I also wish to acknowledge Lindsy Boateng from the Huttenocher lab for collaborating with me on the experiments that tested neutrophil response to MDA231 cells. Lastly, I wish to acknowledge Adan Guitirrez and Sara Montanez for providing me with LnCap, HMF, and NDF cells.

7.9 Copyright permissions

Concluding remarks

The work I have presented in this document aims to provide new capabilities for biology and clinical investigators to study neutrophils in the context of disease. The design of these new microscale assays emphasized achieving significant gains in experimental capability, while not sacrificing operability by untrained personnel. Indeed, one could argue that the KOALA neutrophil chemotaxis assay is easier to use in many ways than traditional macroscale methods. The KOALA platform was applied to study both research and clinical questions, demonstrating the utility of the technique. The success of these projects was strongly aided by the beneficial collaborations that were formed between our lab and external biology and clinical groups on campus.

In order to further increase the impact of novel techniques being developed by microfluidics engineers, both the biology and engineering communities should continue to pursue close collaborations. In addition to providing individual, hands-on attention to these external groups, the microfluidics field must continue to innovate on the design, manufacturing, and packaging of microfluidic tools in order to export these devices with reasonable scale. Furthermore, engineers should focus on developing comprehensive solutions that solve real problems in the biology and medical communities. Considering the compelling advantages microfluidic technologies offer for many problems in cell biology, the potential impact the field can have on mainstream biology research and clinical diagnostics remains promising.

Bibliography

1.Beebe, D. J., Mensing, G. A. & Walker, G. M. Physics and Application of Microfluidics in Biology. *Annual Review of Biomedical Engineering* **4,** 261–286 (2002).

2.Hansen, C. & Quake, S. R. Microfluidics in structural biology: smaller, faster em leader better. *Curr. Opin. Struct. Biol.* **13,** 538–544 (2003).

3.Yager, P. *et al.* Microfluidic diagnostic technologies for global public health. *Nature* (2006).

4.El-Ali, J., Sorger, P. & Jensen, K. Cells on chips. *Nature* (2006).

5.Craighead, H. Future lab-on-a-chip technologies for interrogating individual molecules. *Nature* (2006).

6.Whitesides, G. M. The origins and the future of microfluidics. *Nature* **442,** 368–373 (2006).

7.MANZ, A., GRABER, N. & WIDMER, H. M. Miniaturized Total Chemical-Analysis Systems - a Novel Concept for Chemical Sensing. *Sensors and Actuators B-Chemical* **1,** 244–248 (1990).

8.Reyes, D. R., Iossifidis, D., Auroux, P.-A. & Manz, A. Micro Total Analysis Systems. 1. Introduction, Theory, and Technology. 1–14 (2002). doi:10.1021/ac0202435

9.Whitesides, G. M. Cool, or simple and cheap? Why not both? *Lab Chip* **13,** 11 (2012).

10.Blow, N. Microfluidics: in search of a killer application. *Nat Methods* **4,** 665–668 (2007).

11.Becker, H. Hype, hope and hubris: the quest for the killer application in microfluidics. *Lab Chip* **9,** 2119 (2009).

12.Walker, G. A passive pumping method for microfluidic devices. *Lab Chip* **2,** 131–134 (2002).

13.Lee, S. H. *et al.* Capillary based patterning of cellular communities in laterally open channels. *Anal Chem* **82,** 2900–2906 (2010).

14.Berry, S. M., Alarid, E. T. & Beebe, D. J. One-step purification of nucleic acid for gene expression analysis via Immiscible Filtration Assisted by Surface Tension (IFAST). *Lab Chip* **11,** 1747 (2011).

15.Anna, S. L., Bontoux, N. & Stone, H. A. Formation of dispersions using 'flow focusing' in microchannels. *Applied Physics Letters* **82,** 364 (2003).

16.Boyden, S. The chemotactic effect of mixtures of antibody and antigen on polymorphonuclear leucocytes. *J Exp Med* (1962).

17.Zigmond, S. H. Ability of polymorphonuclear leukocytes to orient in gradients of chemotactic factors. *The Journal of Cell Biology* **75,** 606–616 (1977).

18.Zicha, D., Dunn, G. A. & Brown, A. F. A new direct-viewing chemotaxis chamber. *Journal of Cell Science* **99 (Pt 4),** 769–775 (1991).

19.Muinonen-Martin, A. J. A., Veltman, D. M. D., Kalna, G. G. & Insall, R. H. R. An improved chamber for direct visualisation of chemotaxis. *PLoS ONE* **5,** e15309–e15309 (2010).

20.Keenan, T. M. & Folch, A. Biomolecular gradients in cell culture systems. *Lab Chip* **8,** 34–57 (2008).

21.Irimia, D. Microfluidic Technologies for Temporal Perturbations of Chemotaxis. *Annual Review of Biomedical Engineering* **12,** 259–284 (2010).

22.Kamholz, A. E. & Yager, P. Theoretical Analysis of Molecular Diffusion in Pressure-Driven Laminar Flow in Microfluidic Channels. *Biophys J* **80,** 155–160 (2001).

23.Ismagilov, R. F., Stroock, A. D., Kenis, P. J. A., Whitesides, G. & Stone, H. A. Experimental and theoretical scaling laws for transverse diffusive broadening in two-phase laminar flows in microchannels. *Applied Physics Letters* **76,** 2376 (2000).

24.Jeon, N. L. *et al.* Generation of Solution and Surface Gradients Using Microfluidic Systems. *Langmuir* **16,** 8311–8316 (2000).

25.Irimia, D., Geba, D. A. & Toner, M. Universal Microfluidic Gradient Generator. *Anal Chem* **78,** 3472–3477 (2006).

26.Paguirigan, A. L. & Beebe, D. J. Microfluidics meet cell biology: bridging the gap by validation and application of microscale techniques for cell biological assays. *Bioessays* **30,** 811–821 (2008).

27.Butler, K. L. *et al.* Burn injury reduces neutrophil directional migration speed in microfluidic devices. *PLoS ONE* **5,** e11921 (2010).

28.Sackmann, E. K. *et al.* Microfluidic kit-on-a-lid: a versatile platform for neutrophil chemotaxis assays. *blood* **120,** e45–e53 (2012).

29.Jowhar, D., Wright, G., Samson, P. C., Wikswo, J. P. & Janetopoulos, C. Open access microfluidic device for the study of cell migration during chemotaxis. *Integr Biol (Camb)* **{2},** {648–658} (2010).

30.Kilby, J. MINIATURIZED ELECTRONIC CIRCUITS. (1959).

31.Noyce, R. N. SEMICONDUCTOR DEVICE-AND-LEAD STRUCTURE. (1959).

32.WILDING, P., PFAHLER, J., BAU, H. H., ZEMEL, J. N. & KRICKA, L. J. Manipulation and Flow of Biological-Fluids in Straight Channels Micromachined in Silicon. *Clin. Chem.* **40,** 43–47 (1994).

33.VANDEPOL, F., WONNINK, D., ELWENSPOEK, M. & FLUITMAN, J. A Thermo-Pneumatic Actuation Principle for a Microminiature Pump and Other Micromechanical Devices. *Sensors and Actuators* **17,** 139–143 (1989).

34.VANLINTEL, H., VANDEPOL, F. & BOUWSTRA, S. A Piezoelectric Micropump Based on Micromachining of Silicon. *Sensors and Actuators* **15,** 153–167 (1988).

35.Esashi, M., Shoji, S. & Nakano, A. Normally closed microvalve and mircopump fabricated on a silicon wafer. *Sensors and Actuators* **20,** 163–169 (1989).

36.Harrison, D. J., MANZ, A., FAN, Z. H., LUDI, H. & WIDMER, H. M. Capillary Electrophoresis and Sample Injection Systems Integrated on a Planar Glass Chip. *Anal Chem* **64,** 1926–1932 (1992).

37.Effenhauser, C. S., Manz, A. & Widmer, H. M. Glass chips for high-speed capillary electrophoresis separations with submicrometer plate heights. *Anal Chem* **65,** 2637–2642 (1993).

38.Chiem, N. H. & Harrison, D. J. Microchip systems for immunoassay: an integrated immunoreactor with electrophoretic separation for serum theophylline determination. *Clin. Chem.* **44,** 591–598 (1998).

39.Li, P. & Harrison, D. J. Transport, manipulation, and reaction of biological cells on-chip using electrokinetic effects. *Anal Chem* **69,** 1564–1568 (1997).

40.Duffy, D. C. D., McDonald, J. C. J., Schueller, O. J. O. & Whitesides, G. M. G. Rapid Prototyping of Microfluidic Systems in Poly(dimethylsiloxane). *Anal Chem* **70,** 4974–4984 (1998).

41.Aumiller, G. D., Chandross, E. A., Tomlinson, W. J. & Weber, H. P. Submicrometer resolution replication of relief patterns for integrated optics. *Journal of Applied Physics* **45,** 4557–4562 (1974).

42.Masoli, M., Washizu, M. & Nanba, T. Novel method of cell fusion in field constriction area in fluid integration circuit. *IEEE Trans. Ind. App.* **25,** 732–737 (1989).

43.Berthier, E., Young, E. W. K. & Beebe, D. Engineers are from PDMS-land, Biologists are from Polystyrenia. *Lab Chip* **12,** 1224–1237 (2012).

44.CHAUDHURY, M. K. & Whitesides, G. M. Direct Measurement of Interfacial Interactions Between Semispherical Lenses and Flat Sheets of Poly(Dimethylsiloxane) and Their Chemical Derivatives. *Langmuir* **7,** 1013–1025 (1991).

45.Morra, M. *et al.* On the Aging of Oxygen Plasma-Treated Polydimethylsiloxane Surfaces. *J Colloid Interface Sci* **137,** 11–24 (1990).

46.Yang, M. T., Fu, J., Wang, Y.-K., Desai, R. A. & Chen, C. S. Assaying stem cell mechanobiology on microfabricated elastomeric substrates with geometrically modulated rigidity. *Nat Protoc* **6,** 187–213 (2011).

47.Choi, C. K., Breckenridge, M. T. & Chen, C. S. Engineered materials and the cellular microenvironment: a strengthening interface between cell biology and bioengineering. *Trends in Cell Biology* **20,** 705–714 (2010).

48.Quake, S. R. From Micro- to Nanofabrication with Soft Materials. *Science* **290,** 1536–1540 (2000).

49.Unger, M. A. Monolithic Microfabricated Valves and Pumps by Multilayer Soft Lithography. *Science* **288,** 113–116 (2000).

50.Regehr, K. J. *et al.* Biological implications of polydimethylsiloxane-based microfluidic cell culture. *Lab Chip* **9,** 2132–2139 (2009).

51.Lee, J. N., Park, C. & Whitesides, G. M. Solvent Compatibility of Poly(dimethylsiloxane)-Based Microfluidic Devices. *Anal Chem* **75,** 6544–6554 (2003).

52.Toepke, M. W. & Beebe, D. J. PDMS absorption of small molecules and consequences in microfluidic applications. *Lab Chip* **6,** 1484 (2006).

53.Berthier, E., Warrick, J., Yu, H. & Beebe, D. J. Managing evaporation for more robust microscale assays. Part 1. Volume loss in high throughput assays. *Lab Chip* **8,** 852–859 (2008).

54.Wu, M.-H. M., Dimopoulos, G. G., Mantalaris, A. A. & Varley, J. J. The effect of hyperosmotic pressure on antibody production and gene expression in the GS-NS0 cell line. *Biotechnol Appl Biochem* **40,** 41–46 (2004).

55.deZengotita, V., Kimura, R. & Miller, W. M. Effects of CO2 and osmolality on hybridoma cells: growth, metabolism and monoclonal antibody production. *CYTOTECHNOLOGY* **28,** 213–227 (1998).

56.Heo, Y. S. *et al.* Characterization and Resolution of Evaporation-Mediated Osmolality Shifts That Constrain Microfluidic Cell Culture in Poly(dimethylsiloxane) Devices. *Anal Chem* **79,** 1126–1134 (2007).

57.Futai, N., Gu, W., Song, J. W. & Takayama, S. Handheld recirculation system and customized media for microfluidic cell culture. *Lab Chip* **6,** 149 (2006).

58.Chang, W.-J., Akin, D., Sedlak, M., Ladisch, M. R. & Bashir, R. Poly (dimethylsiloxane)(PDMS) and silicon hybrid biochip for bacterial culture. *Biomed Microdevices* **5,** 281–290 (2003).

59.Mukhopadhyay, R. When PDMS isn't the best. *Anal Chem* **79,** 3248–3253 (2007).

60.Chin, C. D. *et al.* Microfluidics-based diagnostics of infectious diseases in the developing world. *Nature Medicine* **17,** 1015–1019 (2011).

61.Becker, H. & Heim, U. Hot embossing as a method for the fabrication of polymer high aspect ratio structures. *Sensors and Actuators A: Physical* **83,** 130–135 (2000).

62.Martynova, L. *et al.* Fabrication of plastic microfluid channels by imprinting methods. *Anal Chem* **69,** 4783–4789 (1997).

63.Goral, V. N., Hsieh, Y.-C., Petzold, O. N., Faris, R. A. & Yuen, P. K. Hot embossing of plastic microfluidic devices using poly(dimethylsiloxane) molds. *J Micromech Microeng* **21,** 017002 (2010).

64.Young, E. W. K. *et al.* Rapid Prototyping of Arrayed Microfluidic Systems in Polystyrene for Cell-Based Assays. *Anal Chem* **83,** 1408–1417 (2011).

65.Wang, Y. *et al.* Benchtop micromolding of polystyrene by soft lithography. *Lab Chip* **11,** 3089 (2011).

66.Young, E. W. K., Berthier, E. & Beebe, D. J. Assessment of Enhanced Autofluorescence and Impact on Cell Microscopy for Microfabricated Thermoplastic Devices. *Anal Chem* **85,** 44–49 (2013).

67.Nilghaz, A. *et al.* Flexible microfluidic cloth-based analytical devices using a low-cost wax patterning technique. *Lab Chip* **12,** 209 (2011).

68.Lode, von, P. Point-of-care immunotesting: Approaching the analytical performance of central laboratory methods. *Clinical Biochemistry* **38,** 591–606 (2005).

69.Martinez, A. W., Phillips, S. T., Whitesides, G. M. & Carrilho, E. Diagnostics for the Developing World: Microfluidic Paper-Based Analytical Devices. *Anal Chem* **82,** 3–10 (2010).

70.Carrilho, E., Martinez, A. W. & Whitesides, G. M. Understanding Wax Printing: A Simple Micropatterning Process for Paper-Based Microfluidics. *Anal Chem* **81,** 7091–7095 (2009).

71.Martinez, A. W., Phillips, S. T., Wiley, B. J., Gupta, M. & Whitesides, G. M. FLASH: A rapid method for prototyping paper-based microfluidic devices. *Lab Chip* **8,** 2146 (2008).

72.Abe, K., Suzuki, K. & Citterio, D. Inkjet-Printed Microfluidic Multianalyte Chemical Sensing Paper. *Anal Chem* **80,** 6928–6934 (2008).

73.Olkkonen, J., Lehtinen, K. & Erho, T. Flexographically Printed Fluidic Structures in Paper. *Anal Chem* **82,** 10246–10250 (2010).

74.Apilux, A., Ukita, Y., Chikae, M., Chailapakul, O. & Takamura, Y. Development of automated paper-based devices for sequential multistep sandwich enzyme-linked immunosorbent assays using inkjet printing. *Lab Chip* **13,** 126 (2012).

75.Agrawal, N. & Toner, M. Neutrophil migration assay from a drop of blood. *Lab Chip* **8,** 2054–2061 (2008).

76.Kotz, K. T. *et al.* Clinical microfluidics for neutrophil genomics and proteomics. *Nature Medicine* **{16},** {1042–U142} (2010).

77.Warner, E. A. *et al.* Microfluidics-based capture of human neutrophils for expression analysis in blood and bronchoalveolar lavage. *LABORATORY INVESTIGATION* **{91},** {1787–1795} (2011).

78.Bach MK, B. J. Single-step separation of red blood cells, granuloctyes and mononuclear leukocytes on discontinuos density gradients of Ficoll-Hypaque. *Experimental Cell Research* **61,** 387–396 (1970).

79.Berry, S. M., Strotman, L. N., Kueck, J. D., Alarid, E. T. & Beebe, D. J. Purification of cell subpopulations via immiscible filtration assisted by surface tension (IFAST). *Biomed Microdevices* **13,** 1033–1042 (2011).

80.Berry, S. M., Maccoux, L. J. & Beebe, D. J. Streamlining Immunoassays with Immiscible Filtrations Assisted by Surface Tension. *Anal Chem* **84,** 5518–5523 (2012).

81.Cressey, D. Pfizer slashes R&D. *Nature* **470,** 154 (2011).

82.DiMasi, J. A., Hansen, R. W. & Grabowski, H. G. The price of innovation: new estimates of drug development costs. *Journal of Health Economics* **22,** 151–185 (2003).

83.Cressey, D. Traditional drug-discovery model ripe for reform. *Nature* **471,** 17–18 (2011).

84.Paul, S. M. *et al.* How to improve R&D productivity: the pharmaceutical industry's grand challenge. *Nat Rev Drug Discov* (2010). doi:10.1038/nrd3078

85.Kimura, H., Yamamoto, T., Sakai, H., Sakai, Y. & Fujii, T. An integrated microfluidic system for long-term perfusion culture and on-line monitoring of intestinal tissue models. *Lab Chip* **8,** 741 (2008).

86.Huh, D. *et al.* Reconstituting organ-level lung functions on a chip. **328,** 1662–1668 (2010).

87.Tsai, M. *et al.* In vitro modeling of the microvascular occlusion and thrombosis that occur in hematologic diseases using microfluidic technology. *J. Clin. Invest.* **122,** 408–418 (2012).

88.Bischel, L. L., Young, E. W. K., Mader, B. R. & Beebe, D. J. Tubeless microfluidic angiogenesis assay with three-dimensional endothelial-lined microvessels. *Biomaterials* **34,** 1471–1477 (2013).

89.Wood, D. K., Soriano, A., Mahadevan, L., Higgins, J. M. & Bhatia, S. N. A Biophysical Indicator of Vaso-occlusive Risk in Sickle Cell Disease. *Sci Transl Med* **{4},** (2012).

90.Jang, K.-J. & Suh, K.-Y. A multi-layer microfluidic device for efficient culture and analysis of renal tubular cells. *Lab Chip* **10,** 36 (2010).

91.Huh, D., Hamilton, G. A. & Ingber, D. E. From 3D cell culture to organs-on-chips. *Trends in Cell Biology* **21,** 745–754 (2011).

92.Berthier, E., Warrick, J. & Casavant, B. Pipette-friendly laminar flow patterning for cell-based assays. *Lab Chip* (2011).

93.Berthier, E. *et al.* Kit-On-A-Lid-Assays for accessible self-contained cell assays. *Lab Chip* **13,** 424–431 (2013).

94.Ahn, A. C., Tewari, M., Poon, C.-S. & Phillips, R. S. The Limits of Reductionism in Medicine: Could Systems Biology Offer an Alternative? *Plos Med* **3,** e208 (2006).

95.Poujade, M. *et al.* Collective migration of an epithelial monolayer in response to a model wound. *Proc Natl Acad Sci USA* **104,** 15988–15993 (2007).

96.Nathan, C. Neutrophils and immunity: challenges and opportunities. *Nat Rev Immunol* **6,** 173–182 (2006).

97.Condeelis, J., Singer, R. H. & Segall, J. E. The great escape: when cancer cells hijack the genes for chemotaxis and motility. *Annu. Rev. Cell Dev. Biol.* **21,** 695–718 (2005).

98.Müller, A. *et al.* Involvement of chemokine receptors in breast cancer metastasis. *Nature* **410,** 50–56 (2001).

99.Roussos, E. T., Condeelis, J. S. & Patsialou, A. Chemotaxis in cancer. *Nature Reviews Cancer* **11,** 573–587 (2011).

100.Adler, J. CHEMOTAXIS IN BACTERIA. *Annual Review of Biochemistry* 341–354 (1975).

101.Parent, C. A. Making all the right moves: chemotaxis in neutrophils and Dictyostelium. *Current Opinion in Cell Biology* **16,** 4–13 (2004).

102.Affolter, M. & Weijer, C. J. Signaling to Cytoskeletal Dynamics during Chemotaxis. *Developmental Cell* **9,** 19–34 (2005).

103.Sozzani, S., Allavena, P., Vecchi, A. & Mantovani, A. Chemokines and dendritic cell traffic. *J. Clin. Immunol.* **20,** 151–160 (2000).

104.Robertson, M. J. Role of chemokines in the biology of natural killer cells. *J Leukoc Biol* **71,** 173–183 (2002).

105.Pixley, F. J. & Stanley, E. R. CSF-1 regulation of the wandering macrophage: complexity in action. *Trends in Cell Biology* **14,** 628–638 (2004).

106.Mosser, D. M. & Edwards, J. P. Exploring the full spectrum of macrophage activation. *Nat Rev Immunol* **8,** 958–969 (2008).

107.Van Haastert, P. J. M. P. & Devreotes, P. N. P. Chemotaxis: signalling the way forward. *Nature Reviews Molecular Cell Biology* **5,** 626–634 (2004).

108.Iglesias, P. A. & Devreotes, P. N. Navigating through models of chemotaxis. *Current Opinion in Cell Biology* **20,** 35–40 (2008).

109.Fong, E., Tzlil, S. & Tirrell, D. A. Boundary crossing in epithelial wound healing. *Proc Natl Acad Sci USA* **107,** 19302–19307 (2010).

110.Martin, P. & Leibovich, S. J. Inflammatory cells during wound repair: the good, the bad and the ugly. *Trends in Cell Biology* **15,** 599–607 (2005).

111.Ley, K., Laudanna, C., Cybulsky, M. I. & Nourshargh, S. Getting to the site of inflammation: the leukocyte adhesion cascade updated. *Nat Rev Immunol* **7,** 678–689 (2007).

112.Soehnlein, O. & Lindbom, L. Phagocyte partnership during the onset and resolution of inflammation. *Nat Rev Immunol* **10,** 427–439 (2010).

113.Murphy, G., Caplice, N. & Molloy, M. Fractalkine in rheumatoid arthritis: a review to date. *Rheumatology* **47,** 1446–1451 (2008).

114.Barnes, P. J. Neutrophils find smoke attractive. *Science* **330,** 40–41 (2010).

115.Wenzel, S. E. Asthma: defining of the persistent adult phenotypes. *Lancet* **368,** 804–813 (2006).

116.Fahy, J. V. Eosinophilic and neutrophilic inflammation in asthma: insights from clinical studies. *Proc Am Thorac Soc* **6,** 256–259 (2009).

117.Eder, W., Ege, M. J. & Mutius, von, E. The asthma epidemic. *N. Engl. J. Med.* **355,** 2226–2235 (2006).

118.Chambers, A. F., Groom, A. C. & MacDonald, I. C. Metastasis: Dissemination and growth of cancer cells in metastatic sites. *Nature Reviews Cancer* **2,** 563–572 (2002).

119.Roussos, E. T. *et al.* Mena invasive (MenaINV) promotes multicellular streaming motility and transendothelial migration in a mouse model of breast cancer. *Journal of Cell Science* **124,** 2120–2131 (2011).

120.Condeelis, J. & Pollard, J. W. Macrophages: Obligate Partners for Tumor Cell Migration, Invasion, and Metastasis. *Cell* **124,** 263–266 (2006).

121.Masoli, M., Fabian, D., Holt, S., Beasley, R.Global Initiative for Asthma (GINA) Program. The global burden of asthma: executive summary of the GINA Dissemination Committee report. *Allergy* **59,** 469–478 (2004).

122.James, A. L. *et al.* Changes in the prevalence of asthma in adults since 1966: the Busseltion health study. *European Respiratory Journal* **35,** 273–278 (2010).

123.Enright, P. L., McClelland, R. L., Newman, A. B., Gottlieb, D. J. & Lebowitz, M. D. Underdiagnosis and undertreatment of asthma in the elderly. Cardiovascular Health Study Research Group. *Chest* **116,** 603–613 (1999).

124.Urso, D. L. Asthma in the Elderly. *Current Gerontology and Geriatrics Research* **2009,** 1–5 (2009).

125.Aaron, S. D. *et al.* Overdiagnosis of asthma in obese and nonobese adults. *CMAJ* **179,** 1121–1131 (2008).

126.Serra-Batlles, J., Plaza, V. & Morejon, E. Costs of asthma according to the degree of severity. *European Respiratory Journal* **12,** 1322–1326 (1998).

127.Lloyd, C. M. & Hessel, E. M. Functions of T cells in asthma: more than just T(H)2 cells. *Nat Rev Immunol* **10,** 838–848 (2010).

128.Haldar, P. *et al.* Mepolizumab and Exacerbations of Refractory Eosinophilic Asthma. *N. Engl. J. Med.* **360,** 973–984 (2009).

129.Nair, P. *et al.* Mepolizumab for prednisone-dependent asthma with sputum eosinophilia. *New England Journal of Medicine* **360,** 985–993 (2009).

130.Wilkinson, P. C., Borel, J. F., Stecher-Levin, V. & Sorkin, E. Macrophage and Neutrophil Specific Chemotactic Factors in Serum. *Nature* **222,** 244–247 (1969).

131.Schiffmann, E., Corcoran, B. & Wahl, S. N-Formylmethionyl Peptides as Chemoattractants for Leucocytes. *Proc Natl Acad Sci USA* **72,** 1059–1062 (1975).

132.Tseng, H.-Y. *et al.* A Microfluidic Study of Megakaryocytes Membrane Transport Properties to Water and Dimethyl Sulfoxide at Suprazero and Subzero Temperatures. *BIOPRESERVATION AND BIOBANKING* **{9},** {355–362} (2011).

133.Nelson, R. D., Quie, P. G. & Simmons, R. L. Chemotaxis under agarose: a new and simple method for measuring chemotaxis and spontaneous migration of human polymorphonuclear leukocytes and monocytes. *The Journal of Immunology* **115,** 1650–1656 (1975).

134.Gerisch, G. & Keller, H. U. Chemotactic reorientation of granulocytes stimulated with micropipettes containing fMet-Leu-Phe. *Journal of Cell Science* **52,** 1–10 (1981).

135.Foxman, E. F., Campbell, J. J. & Butcher, E. C. Multistep navigation and the combinatorial control of leukocyte chemotaxis. *The Journal of Cell Biology* **139,** 1349–1360 (1997).

136.Foxman, E. F., Kunkel, E. J. & Butcher, E. C. Integrating conflicting chemotactic signals. The role of memory in leukocyte navigation. *JOURNAL OF CELL BIOLOGY* **147,** 577–588 (1999).

137.Heit, B. An intracellular signaling hierarchy determines direction of migration in opposing chemotactic gradients. *The Journal of Cell Biology* **159,** 91–102 (2002).

138.Lauffenburger, D. A. D. & Zigmond, S. H. S. Chemotactic factor concentration gradients in chemotaxis assay systems. *Journal of Immunological Methods* **40,** 45–60 (1981).

139.Wilkinson, P. C. Assays of leukocyte locomotion and chemotaxis. *Journal of Immunological Methods* **216,** 139–153 (1998).

140.Wei, S. H., Parker, I., Miller, M. J. & Cahalan, M. D. A stochastic view of lymphocyte motility and trafficking within the lymph node. *Immunol. Rev.* **195,** 136–159 (2003).

141.Xiao, Z., Zhang, N., Murphy, D. B. & Devreotes, P. N. Dynamic distribution of chemoattractant receptors in living cells during chemotaxis and persistent stimulation. *The Journal of Cell Biology* **139,** 365–374 (1997).

142.Squires, T. & Quake, S. Microfluidics: Fluid physics at the nanoliter scale. **77,** 977–1026 (2005).

143.Jeon, N. L. *et al.* Neutrophil chemotaxis in linear and complex gradients of interleukin-8 formed in a microfabricated device. *Nature Biotechnology* **20,** 826–830 (2002).

144.Chung, B. G. *et al.* Human neural stem cell growth and differentiation in a gradient-generating microfluidic device. *Lab Chip* **5,** 401 (2005).

145.Song, L. *et al.* Dictyostelium discoideum chemotaxis: Threshold for directed motion. *Eur J Cell Biol* **85,** 981–989 (2006).

146.Wang, S.-J., Saadi, W., Lin, F., Minh-Canh Nguyen, C. & Li Jeon, N. Differential effects of EGF gradient profiles on MDA-MB-231 breast cancer cell chemotaxis. *Experimental Cell Research* **{300},** {180–189} (2004).

147.Wong, A., Perez-Castillejos, R., Love, C. & Whitesides, G. Partitioning microfluidic channels with hydrogel to construct tunable 3-D cellular microenvironments. *Biomaterials* **29,** 1853–1861 (2008).

148.Berthier, E., Surfus, J., Verbsky, J., Huttenlocher, A. & Beebe, D. An arrayed high-content chemotaxis assay for patient diagnosis. *INTEGRATIVE BIOLOGY* **{2},** {630–638} (2010).

149.Domenech, M. *et al.* Cellular observations enabled by microculture: paracrine signaling and population demographics. *Integr Biol (Camb)* **1,** 267 (2009).

150.Solomkin, J. S. J., Nelson, R. D. R., Chenoweth, D. E. D., Solem, L. D. L. & Simmons, R. L. R. Regulation of neutrophil migratory function in burn injury by complement activation products. *Ann Surg* **200,** 742–746 (1984).

151.Kurkchubasche, A. G., Panepinto, J. A., Tracy, T. F., Jr, Thurman, G. W. & Ambruso, D. R. Clinical features of a human Rac2 mutation: A complex neutrophil dysfunction disease. *The Journal of Pediatrics* **139,** 141–147 (2001).

152.Díaz-González, M. & Baldi, A. Fabrication of Biofunctionalized Microfluidic Structures by Low-Temperature Wax Bonding. *Anal Chem* **84,** 7838–7844 (2012).

153.McDonald, J. & Whitesides, G. Poly (dimethylsiloxane) as a material for fabricating microfluidic devices. *Acc. Chem. Res* (2002).

154.Becker, H. It's the economy…. *Lab Chip* **9,** 2759 (2009).

155.Maszara, W., Goetz, G. & Caviglia, A. Bonding of silicon wafers for silicon-on-insulator. *Journal of Applied Physics* **64,** 4943–4950 (1988).

156.Henry, A. C. *et al.* Surface Modification of Poly(methyl methacrylate) Used in the Fabrication of Microanalytical Devices. *Anal Chem* **72,** 5331–5337 (2000).

157.Tsao, C., Hromada, L., Kumar, P. & DeVoe, D. Low temperature bonding of PMMA and COC microfluidic substrates using UV/ozone surface treatment. *Lab Chip* **7,** 499–505 (2007).

158.Toetsch, S., Olwell, P., Prina-Mello, A. & Volkov, Y. The evolution of chemotaxis assays from static models to physiologically relevant platforms. *Integr Biol (Camb)* **1,** 170 (2009).

159.Berthier, E., Surfus, J., Verbsky, J., Huttenlocher, A. & Beebe, D. An arrayed high-content chemotaxis assay for patient diagnosis. *Integr Biol (Camb)* **2,** 630–638 (2010).

160.Berthier, E. & Beebe, D. J. Flow rate analysis of a surface tension driven passive micropump. *Lab Chip* **7,** 1475 (2007).

161.Papaioannou, T. G. & Stefanadis, C. Vascular wall shear stress: basic principles and methods. *Hellenic J Cardiol* **46,** 9–15 (2005).

162.Stathopoulos, N. A. & Hellums, J. D. Shear stress effects on human embryonic kidney cells in Vitro. *Biotechnol Bioeng* **27,** 1021–1026 (1985).

163.Hartt, J. K., Barish, G., Murphy, P. M. & Gao, J. L. N-formylpeptides induce two distinct concentration optima for mouse neutrophil chemotaxis by differential interaction with two N-formylpeptide receptor (FPR) subtypes. Molecular characterization of FPR2, a second mouse neutrophil FPR. *J Exp Med* **190,** 741–747 (1999).

164.Douni, E. *et al.* Transgenic and knockout analyses of the role of TNF in immune regulation and disease pathogenesis. in *J Inflamm* **47,** 27–38 (1996).

165.Li, P. & Schwarz, E. M. The TNF-alpha transgenic mouse model of inflammatory arthritis. *Springer Seminars in Immunopathology* **25,** 19–33 (2003).

166.Cheng, S., Heilman, S., Wasserman, M. & Archer, S. A hydrogel-based microfluidic device for directed cell migration. *Lab Chip* **7,** 763–769 (2007).

167.Fukuda, S. & Schmid-Schonbein, G. Centrifugation attenuates the fluid shear response of circulating leukocytes. *J Leukoc Biol* **72,** 133–139 (2002).

168.Lang, F., Lang, K. S., Lang, P. A., Huber, S. M. & Wieder, T. Osmotic shock-induced suicidal death of erythrocytes. *Acta Physiol (Oxf)* **187,** 191–198 (2006).

169.Oakes, P. W. *et al.* Neutrophil morphology and migration are affected by substrate elasticity. *blood* **114,** 1387–1395 (2009).

170.Németh, T. & Mócsai, A. The role of neutrophils in autoimmune diseases. *Immunol Lett* (2012). doi:10.1016/j.imlet.2012.01.013

171.Boxio, R. Mouse bone marrow contains large numbers of functionally competent neutrophils. *J Leukoc Biol* **75,** 604–611 (2004).

172.Serrander, L., Skarman, P. & Rasmussen, B. Selective Inhibition of IgG-Mediated Phagocytosis in Gelsolin-Deficient Murine Neutrophils. *J Immunol* **165,** 2451–2457 (2000).

173.Sehnert, B., Gierer, P., Burkhardt, H.10. Modulation of granulocyte-endothelium interactions by antileukoproteinase: inhibition of anti-type II collagen antibody-induced leukocyte attachment to the synovial endothelium. *Arthritis Res Ther* **8,** R95–R95 (2006).

174.Doyle, A. D., Kutys, M. L., Yamada, K. M.6. Microenvironmental control of cell migration: Myosin IIA is required for efficient migration in fibrillar environments through control of cell adhesion dynamics. *Journal of Cell Science* (2012). doi:10.1242/jcs.098806

175.Doyle, A. D., Wang, F. W., Yamada, K. M.4. One-dimensional topography underlies three-dimensional fibrillar cell migration. *The Journal of Cell Biology* **184,** 481–490 (2009).

176.Blow, N. Cell migration: our protruding knowledge. *Nat Methods* **4,** 559–594 (2007).

177.Hakkinen, K. M. K., Harunaga, J. S. J., Yamada, K. M. K.4. Direct comparisons of the morphology, migration, cell adhesions, and actin cytoskeleton of fibroblasts in four different three-dimensional extracellular matrices. *CORD Conference Proceedings* **17,** 713–724 (2011).

178.Nakagome, K. & Nagata, M. Pathogenesis of airway inflammation in bronchial asthma. *Auris Nasus Larynx* **38,** 555–563 (2011).

179.Wenzel, S. E. *et al.* Bronchoscopic evaluation of severe asthma. Persistent inflammation associated with high dose glucocorticoids. *Am J Respir Crit Care Med* **156,** 737–743 (1997).

180.Menzies, D., Jackson, C., Mistry, C., Houston, R. & Lipworth, B. J. Symptoms, spirometry, exhaled nitric oxide, and asthma exacerbations in clinical practice. *Annals of Allergy, Asthma & Immunology* **101,** 248–255 (2008).

181.Dombkowski, K. J., Hassan, F., Wasilevich, E. A. & Clark, S. J. Spirometry use among pediatric primary care physicians. *Pediatrics* **126,** 682–687 (2010).

182.Puccinelli, J. P., Su, X. & Beebe, D. J. Automated high-throughput microchannel assays for cell biology: Operational optimization and characterization. *JALA* **15,** 25–32 (2010).

183.Young, E. W. K. *et al.* Microscale functional cytomics for studying hematologic cancers. *blood* **119,** e76–85 (2012).

184.Wood, D. K., Soriano, A., Mahadevan, L., Higgins, J. M. & Bhatia, S. N. A Biophysical Indicator of Vaso-occlusive Risk in Sickle Cell Disease. *Sci Transl Med* **4,** 123ra26–123ra26 (2012).

185.Issadore, D. *et al.* Ultrasensitive Clinical Enumeration of Rare Cells ex Vivo Using a Micro-Hall Detector. *Sci Transl Med* **4,** 141ra92–141ra92 (2012).

186.Schneider, A., Tilemann, L. & Schermer, T. Diagnosing asthma in general practice with portable exhaled nitric oxide measurement–results of a prospective diagnostic study. *Respiratory Research* **10,** (2009).

187.Dupont, L. J., Demedts, M. G. & Verleden, G. M. Prospective evaluation of the validity of exhaled nitric oxide for the diagnosis of asthma. *Chest* **123,** 751–756 (2003).

188.Miedinger, D. D. *et al.* Diagnostic tests for asthma in firefighters. *Chest* **131,** 1760–1767 (2007).

189.Fortuna, A. M., Feixas, T., González, M. & Casan, P. Diagnostic utility of inflammatory biomarkers in asthma: exhaled nitric oxide and induced sputum eosinophil count. *Respir Med* **101,** 2416–2421 (2007).

190.Altman, D. G. & Bland, M. J. Diagnostic tests 1: sensitivity and specificity. *BMJ* **308,** 1552 (1994).

191.Busse, W. W. What is the best pulmonary diagnostic approach for wheezing patients with normal spirometry? *Respir Care* **57,** 39–39 (2012).

192.Simpson, J. L. J., Scott, R. J. R., Boyle, M. J. M. & Gibson, P. G. P. Differential proteolytic enzyme activity in eosinophilic and neutrophilic asthma. *Am J Respir Crit Care Med* **172,** 559–565 (2005).

193.Dang, B. B., Wiehler, S. S. & Patel, K. D. K. Increased PSGL-1 expression on granulocytes from allergic-asthmatic subjects results in enhanced leukocyte recruitment under flow conditions. *J Leukoc Biol* **72,** 702–710 (2002).

194.Moore, K. *et al.* P-Selectin Glycoprotein Ligand-1 Mediates Rolling of Human Neutrophils on P-Selectin. *The Journal of Cell Biology* **128,** 661–671 (1995).

195.Md, M. T. A.-S., Phd, A. B., Msc, D. P. & Md, R. O. Variability of sputum inflammatory cells in asthmatic patients receiving corticosteroid therapy: A prospective study using multiple samples. *Journal of Allergy and Clinical Immunology* **125,** 1161–1163.e4 (2010).

196.Shaw, D. E. *et al.* Association between neutrophilic airway inflammation and airflow limitation in adults with asthma. *Chest* **132,** 1871–1875 (2007).

197.Miller, M. R. Standardisation of spirometry. *European Respiratory Journal* **26,** 319–338 (2005).

198.Robin, X. *et al.* pROC: an open-source package for R and S+ to analyze and compare ROC curves. *BMC Bioinformatics* **12,** 77 (2011).

199.Hurst, J. K. & Barrette, W. C. Leukocytic oxygen activation and microbicidal oxidative toxins. *Crit. Rev. Biochem. Mol. Biol.* **24,** 271–328 (1989).

200.Song, E. *et al.* Chronic granulomatous disease: a review of the infectious and inflammatory complications. *Clinical and Molecular Allergy* **9,** 10 (2011).

201.van den Berg, J. M. *et al.* Chronic Granulomatous Disease: The European Experience. *PLoS ONE* **4,** e5234 (2009).

202.Roesler, J. & Emmendorffer, A. Diagnosis of chronic granulomatous disease. *blood* **78,** 1387–1389 (1991).

203.Boudjeltia, K., Faraut, B. & Stenuit, P. Sleep restriction increases white blood cells, mainly neutrophil count, in young healthy men: A pilot study. *Vascular Health and Risk Management* **4,** 1467–1470 (2008).

204.Costa Ricardo, J. S. *et al.* No effect of a 30-h period of sleep deprivation on leukocyte trafficking, neutrophil degranulation. *European journal of Applied Physiology* **105,** 499–504 (2009).

205.Machado, M., Antunes, W. & Tamy, A. Effect of a Single Dose of Caffeine Supplementation and Intermittent-interval Exercise on Muscle Damage Markers in Soccer Players. *J Exerc Sci Fit* **7,** 91–97 (2009).

206.Chimenti, L. *et al.* Bronchial epithelial damage after a half-marathon in nonasthmatic amateur runners. *Am J Physiol Lung Cell Mol Physiol* **298,** L857–62 (2010).

207.Dickstein, J. B. & Moldofsky, H. Sleep, cytokines and immune function. *Sleep Med Rev* **3,** 219–228 (1999).

208.Bird, M. D., Morgan, M. O., Ramirez, L., Yong, S. & Kovacs, E. J. Decreased pulmonary inflammation after ethanol exposure and burn injury in intercellular adhesion molecule-1 knockout mice. *J Burn Care Res* **31,** 652–660 (2010).

209.Bode, C. & Bode, J. C. Activation of the innate immune system and alcoholic liver disease: effects of ethanol per se or enhanced intestinal translocation of bacterial toxins induced by ethanol? *Alcohol Clin Exp Res* **29,** 166S–71S (2005).

210.Phelps, P. & Stanislaw, D. Polymorphonuclear leukocyte motility in vitro. VI. Effect of pH, Temperature, ethyl alcohol, and caffeine, using a modified boyden chamber technic. *Arthritis & Rheumatism* **12,** 181–188 (1969).

211.Horrigan, L., Kelly, J. & Connor, T. Caffeine suppresses TNF-[alpha] production via activation of the cyclic AMP/protein kinase A pathway. *International immunopharmacology* (2004).

212.Varani, K., Portaluppi, F., Gessi, S. & Merighi, S. Caffeine intake induces an alteration in human neutrophil A 2A adenosine receptors. *Cellular and Molecular Life Sciences* **62,** 2350–2358 (2005).

213.Cooper, E. S., Berry, M. P., McMurray, R. G., Hosick, P. A. & Hackney, A. C. Core temperature influences on the relationship between exercise-induced leukocytosis and cortisol or TNF-alpha. *Aviat Space Environ Med* **81,** 460–466 (2010).

214.Schmidt, E. P., Lee, W. L., Zemans, R. L., Yamashita, C. & Downey, G. P. On, around, and through: neutrophil-endothelial interactions in innate immunity. *Physiology (Bethesda)* **26,** 334–347 (2011).

215.Williams, M. R., Azcutia, V., Newton, G., Alcaide, P. & Luscinskas, F. W. Emerging mechanisms of neutrophil recruitment across endothelium. *Trends Immunol* **32,** 461–469 (2011).

216.Stroka, K. M. & Aranda-Espinoza, H. Endothelial cell substrate stiffness influences neutrophil transmigration via myosin light chain kinase-dependent cell contraction. *blood* **118,** 1632–1640 (2011).

217.Rabodzey, A., Alcaide, P., Luscinskas, F. W. & Ladoux, B. Mechanical forces induced by the transendothelial migration of human neutrophils. *Biophys J* **95,** 1428–1438 (2008).

218.Yang, L., Froio, R., Sciuto, T. & Dvorak, A. ICAM-1 regulates neutrophil adhesion and transcellular migration of TNF-{alpha}-activated vascular endothelium under flow. *Blood* **106**, 584-592 (2005).

219.Phillipson, M. *et al.* Intraluminal crawling of neutrophils to emigration sites: a molecularly distinct process from adhesion in the recruitment cascade. *J Exp Med* **203,** 2569–2575 (2006).

220.Kim, S., Lee, H., Chung, M. & Jeon, N. L. Engineering of functional, perfusable 3D microvascular networks on a chip. *Lab Chip* **13,** 1489 (2013).

221.Han, S. *et al.* A versatile assay for monitoring in vivo-like transendothelial migration of neutrophils. *Lab Chip* **12,** 3861 (2012).

222.Bischel, L. L. L., Lee, S.-H. S. & Beebe, D. J. D. A practical method for patterning lumens through ECM hydrogels via viscous finger patterning. *J Lab Autom* **17,** 96–103 (2012).

223.Alcaide, P., Auerbach, S. & Luscinskas, F. W. Neutrophil Recruitment under Shear Flow: It's All about Endothelial Cell Rings and Gaps. *Microcirculation* **16,** 43–57 (2009).

224.Liang, C.-C., Park, A. Y. & Guan, J.-L. In vitro scratch assay: a convenient and inexpensive method for analysis of cell migration in vitro. *Nat Protoc* **2,** 329–333 (2007).

225.Ostuni, E., Kane, R., Ingber, D. & Whitesides, G. Patterning mammalian cells using elastomeric membranes. *Langmuir* (2000).

226.Murrell, M., Kamm, R. & Matsudaira, P. Tension, Free Space, and Cell Damage in a Microfluidic Wound Healing Assay. *PLoS ONE* **{6},** e24283 (2011).

227.Keese, C. R., Wegener, J., Walker, S. R. & Giaever, I. Electrical wound-healing assay for cells in vitro. *Proc Natl Acad Sci USA* **101,** 1554–1559 (2004).

228.Yarrow, J. C., Perlman, Z. E., Westwood, N. J. & Mitchison, T. J. A high-throughput cell migration assay using scratch wound healing, a comparison of image-based readout methods. *BMC Biotechnol* **4,** 21 (2004).

229.Yoo, S. K. & Huttenlocher, A. Spatiotemporal photolabeling of neutrophil trafficking during inflammation in live zebrafish. *J Leukoc Biol* **89,** 661–667 (2011).

230.Mathias, J. R. *et al.* Resolution of inflammation by retrograde chemotaxis of neutrophils in transgenic zebrafish. *J Leukoc Biol* **80,** 1281–1288 (2006).

231.McDonald, B. *et al.* Intravascular danger signals guide neutrophils to sites of sterile inflammation. **330,** 362–366 (2010).

List of Figures

Figure B.5 FeNO compared to neutrophil chemotaxis speed

Figure B6. Workflow of performing the microfluidic asthma characterization assay

List of Tables

Appendix A

Captions for Supplementary Videos A1-8 and Supplementary Figures A1-2.

Supplementary video captions

Video A1. Demonstration of the intraluminal crawling assay in KOALA. Human neutrophils migrating towards 100 nM fMLP on a HUVECs monolayer, tracked automatically with JEX. The timelapse is 90 minutes long. Note that the erythrocytes along the edge of the channel remain relatively static, showing the KOALA method enables a static flow, diffusion-dominant microenvironment; the erythrocytes are not completely washed because the culture of HUVECs in the microchannel requires taller microchannels that do allow for efficient cell sorting. The source of chemoattractant is located on the left side of the video. Phase contrast images acquired using Slidebook software with an Olympus IX-81 microscope using a 10x objective (NA=0.30) at 37ºC. Additional details in on imaging Materials and Methods section under "Microscopy."

Video A2. Example of human neutrophils migrating in a gradient of chemoattractant. Human neutrophils migrating towards 500 nM fMLP on P-selectin-coated polystyrene, tracked automatically with JEX. A channel length of 3 mm is shown, which represents the geometry used for all the embodiments of KOALA shown in this work. The timelapse is 90 minutes long. The source of chemoattractant is located on the left side of the video. Phase contrast images acquired using Slidebook software with an Olympus IX-81 microscope using a 10x objective (NA=0.30) at 37ºC. Additional details on imaging in Materials and Methods section under "Microscopy."

Video A3. Example of control (no chemoattractant) for 2D chemotaxis in KOALA. Human neutrophils in 2D on P-selectin-coated polystyrene, with hydrogel and media (no chemoattractant mixed in the hydrogel). Neutrophils show virtually no movement throughout the timelapse. Note that some erythrocyte movement is observable over the course of the timelapse, likely due to a temperature gradient in the microscope incubator causing slight fluid convection. The timelapse is 120 minutes long. The source, which in this case does not contain chemoattractant, is located on the left side of the video. Phase contrast images acquired using Slidebook

software with an Olympus IX-81 microscope using a 10x objective (NA=0.30) at 37ºC. Additional details on imaging in Materials and Methods section under "Microscopy."

Video A4. Demonstration of the intraluminal crawling assay in KOALA with no chemoattractant. Human neutrophils migrating towards 0 nM fMLP (control) on a HUVECs monolayer, tracked automatically with JEX. The timelapse is 90 minutes long. The source of chemoattractant is located on the left side of the video. Phase contrast images acquired using Slidebook software with an Olympus IX-81 microscope using a 10x objective (NA=0.30) at 37ºC. Additional details in on imaging Materials and Methods section under "Microscopy."

Video A5. Transient Type I and II neutrophil phenotypes on HUVECs. Zoomed in view of neutrophils migrating on HUVECs showing the cells switching between the transient Type I and II phenotypes; the video is 45 minutes long. The source of chemoattractant is located on the left side of the video. In most cases, neutrophils that adopted a Type II phenotype eventually adopted the behavior and morphology of originally Type I cells. Phase contrast images acquired using Slidebook software with an Olympus IX-81 microscope using a 10x objective (NA=0.30) at 37ºC. Additional details on imaging in Materials and Methods section under "Microscopy."

Video A6. WT mouse neutrophils in a gradient of chemoattractant. WT mouse neutrophils migrating on P-selecting coated polystyrene surface towards 1 mM fMLP, automatically tracked with JEX. The timelapse is 120 minutes long. The source of chemoattractant is located on the left side of the video. Phase contrast images acquired using Slidebook software with an Olympus IX-81 microscope using a 10x objective (NA=0.30) at 37ºC. Additional details on imaging in Materials and Methods section under "Microscopy."

Video A7. TNF-Tg mouse neutrophils in a gradient of chemoattractant. TNF-Tg mouse neutrophils migrating on P-selecting coated polystyrene surface towards 1 mM fMLP, automatically tracked with JEX. The timelapse is 120 minutes long. The source of chemoattractant is located on the left side of the video. Note that significantly more cells have been captured on the P-selectin coated surface than in Video S3. Phase contrast images acquired using Slidebook software with an Olympus IX-81 microscope using a 10x objective (NA=0.30) at 37ºC. Additional details on imaging in Materials and Methods section under "Microscopy."

Video A8. 3D human neutrophil chemotaxis. Neutrophils obtained from a human using a lancet puncture, migrating towards 100 nM fMLP in a 3D collagen matrix [5 mg/mL]. The source of chemoattractant is located on

the left side of the video. Note that several cells are in and out of the focal plane throughout the time-lapse session, however JEX software analyzes the cells' 2D projected path. The timelapse is 90 minutes long. Phase contrast images acquired using Slidebook software with an Olympus IX-81 microscope using a 10x objective (NA=0.30) at 37ºC. Additional details on imaging in Materials and Methods section under "Microscopy."

Figures

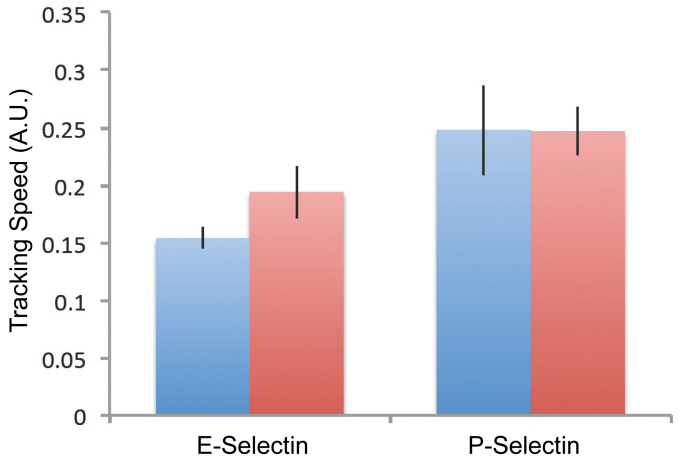

Figure A1. Je'Xperiment vs. ImageJ. Comparison of neutrophil chemotaxis speed from tracking data obtained automatically using Je'Xperiment and manually using the Cell-tracker plugin of ImageJ for neutrophils captured on a P/E-selectin coated substrate. Results show that automated tracking produces results equivalent to manual tracking for P-selectin. The difference for the E-selectin can reside in the decreased capture efficiency, and therefore a higher erythrocyte count that be tracked by JEX, which can lead to erroneous tracking.

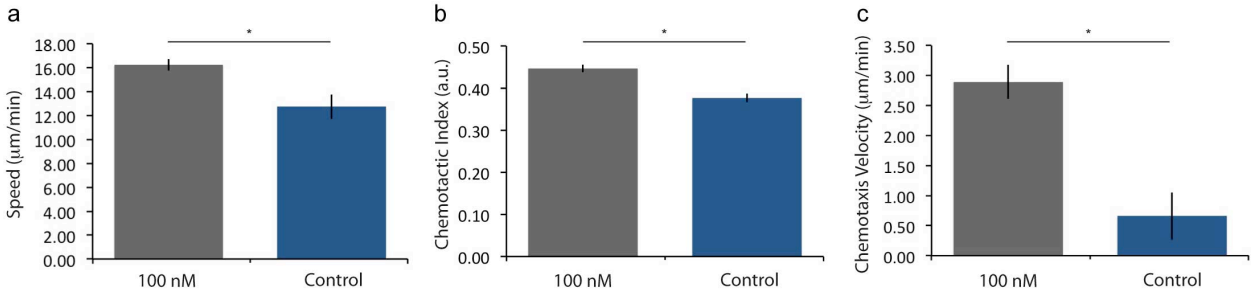

Figure A2. Comparing migration for neutrophils on ECS with a chemical gradient and control. (a-c) Average speed, chemotactic index, and chemotaxis velocity for neutrophils migrating on a monolayer of activated HUVECs with 100 nM gradient of fMLP and control (n=3). HUVECs were activated with IL1-β for 4 hours prior to neutrophil capture and purification from whole blood. All three chemotaxis outputs were significantly higher for neutrophils in a chemical gradient compared to controls, where slower, less directional migration was observed (*$p<0.05$).

Appendix B

Captions for supplementary videos; Supplementary Figures B1-6; and Table B1.

Supplementary video captions

Video B1- Example of human neutrophils from a clinical patient sample migrating in a gradient of chemoattractant. Human neutrophils migrating towards 100 nM fMLP on P-selectin-coated polystyrene. The timelapse is 90 minutes long. The source of chemoattractant is located on the left side of the video. Phase contrast images acquired using Slidebook software with an Olympus IX-81 microscope using a 10x objective (NA=0.30) at 37ºC.

Video B2- Example of control (no chemoattractant) of human neutrophils from a clinical patient sample. Human neutrophils on P-selectin-coated polystyrene, with hydrogel and media (no chemoattractant mixed in the hydrogel) as the source located on the left side of the video. Neutrophils show no movement throughout the timelapse. Note that some erythrocyte movement is observable over the course of the timelapse, likely due to a temperature gradient in the microscope incubator causing slight fluid convection. The timelapse is 90 minutes long. Phase contrast images acquired using Slidebook software with an Olympus IX-81 microscope using a 10x objective (NA=0.30) at 37ºC.

Figures

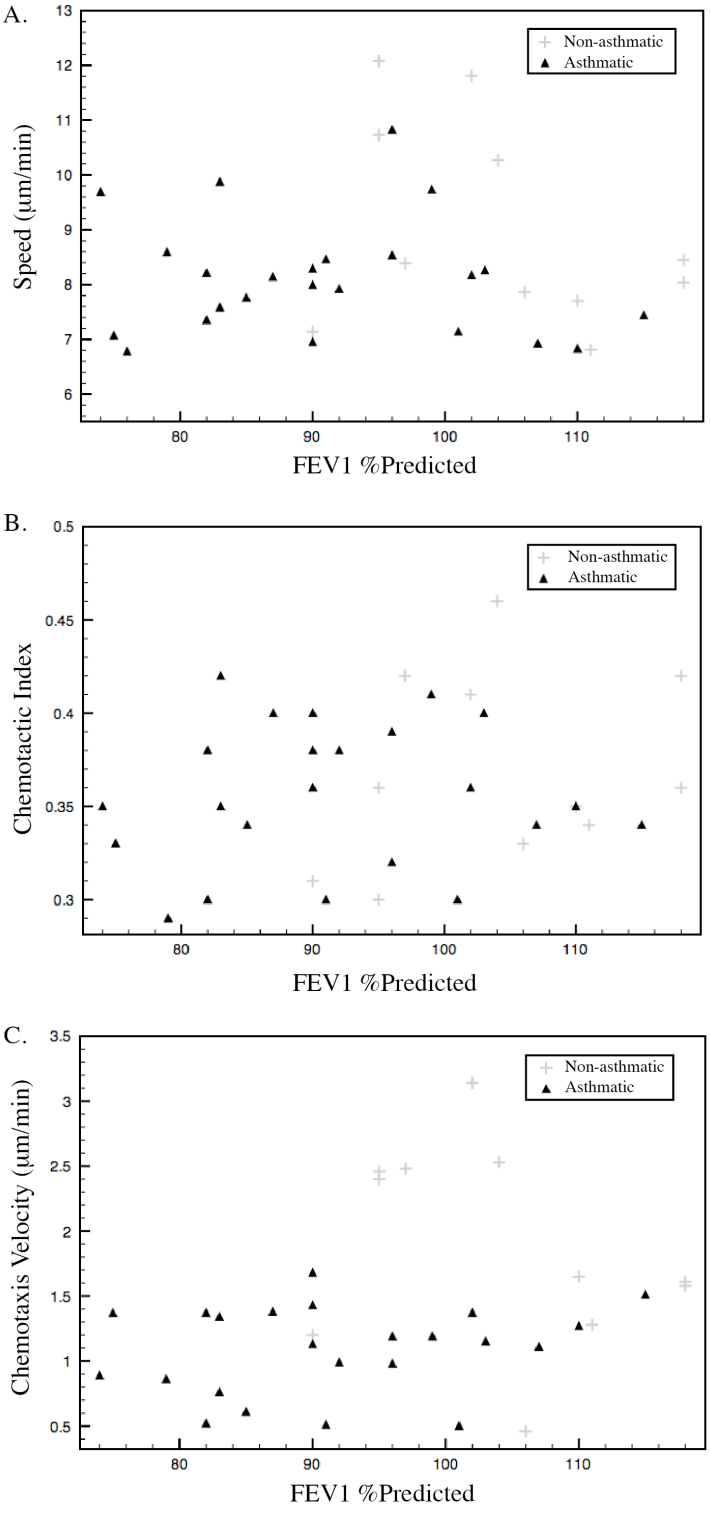

Figure B.1 FEV1 %Predicted compared to neutrophil chemotaxis speed (**A**), chemotactic index (**B**), and (**C**) chemotaxis velocity. The speed and chemotactic index do not show any correlations with FEV1 %Predicted for asthmatic and non-asthmatic patients. Patients with higher neutrophil chemotaxis appear to correlate with higher values of FEV1 %Predicted.

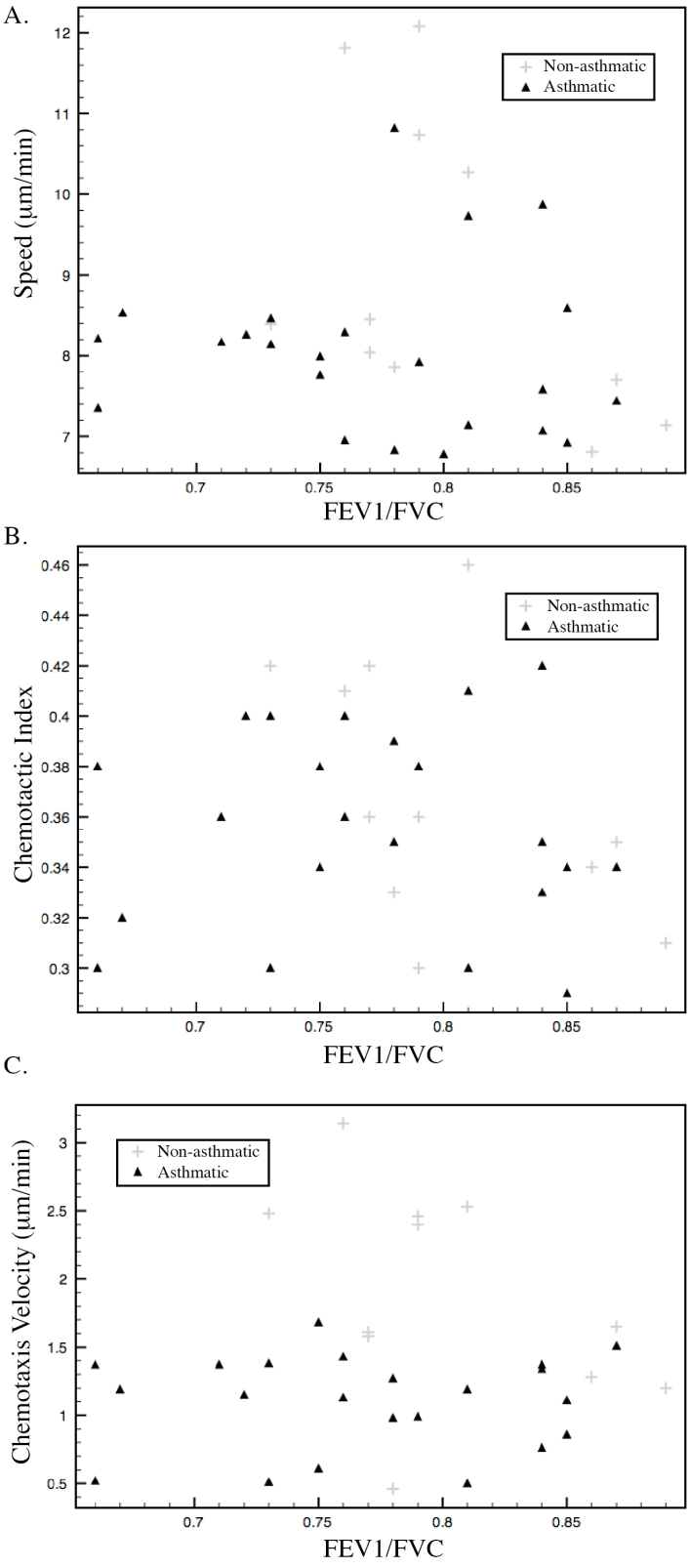

Figure B.2 FEV1/FVC compared to neutrophil chemotaxis speed (**A**), chemotactic index (**B**), and (**C**) chemotaxis velocity. No apparent correlations between the neutrophil chemotaxis outputs (**A-C**) and FEV1/FVC measurements. Asthmatic and non-asthmatic patients have spirometry measurements that span across the full range of FEV1/FVC values, and there are no apparent correlations between neutrophil chemotaxis and FEV1/FVC values.

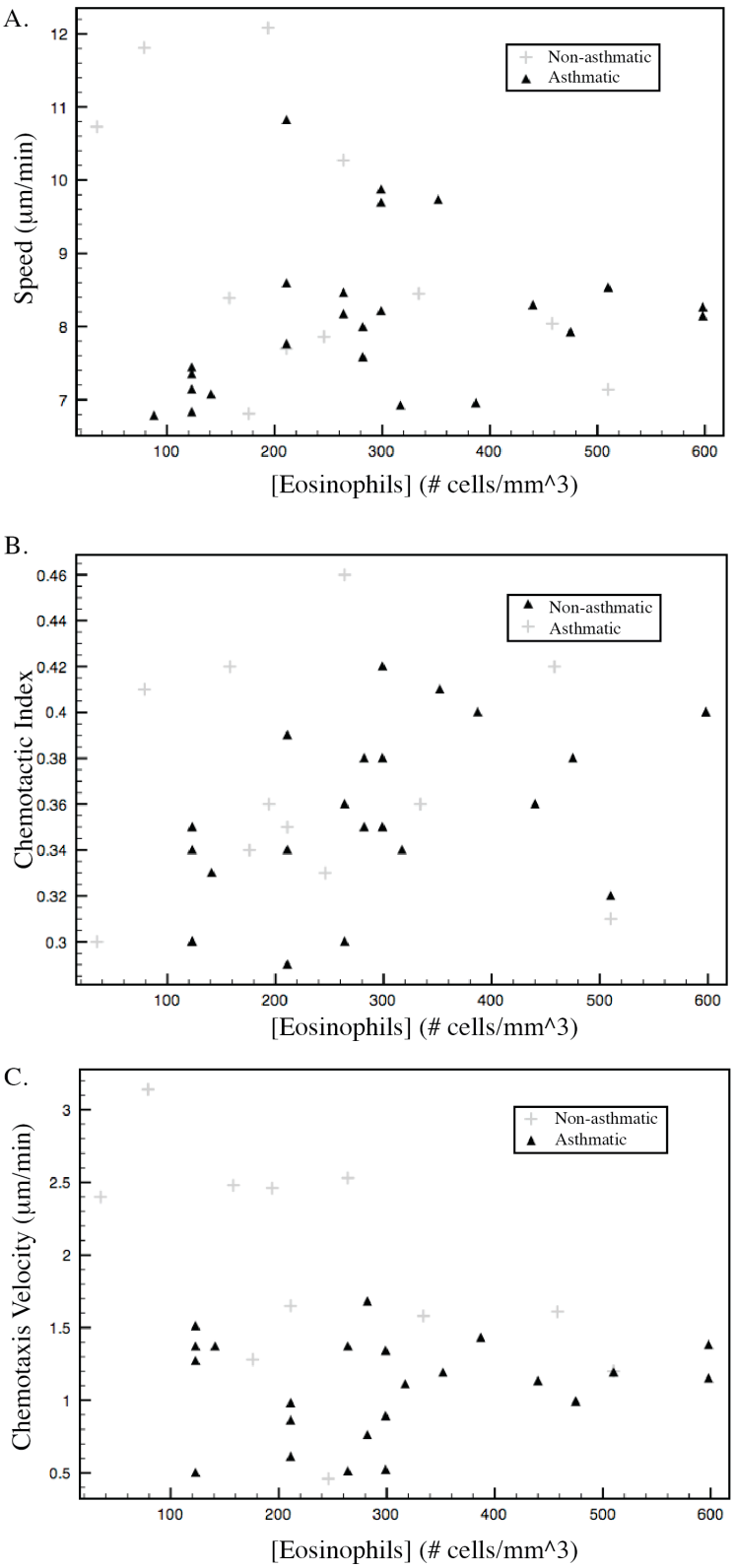

Figure B.3 Concentration of eosinophils in peripheral blood compared to neutrophil chemotaxis speed (**A**), chemotactic index (**B**), and (**C**) chemotaxis velocity. No apparent correlations between the neutrophil chemotaxis outputs (**A-C**) and eosinophil counts.

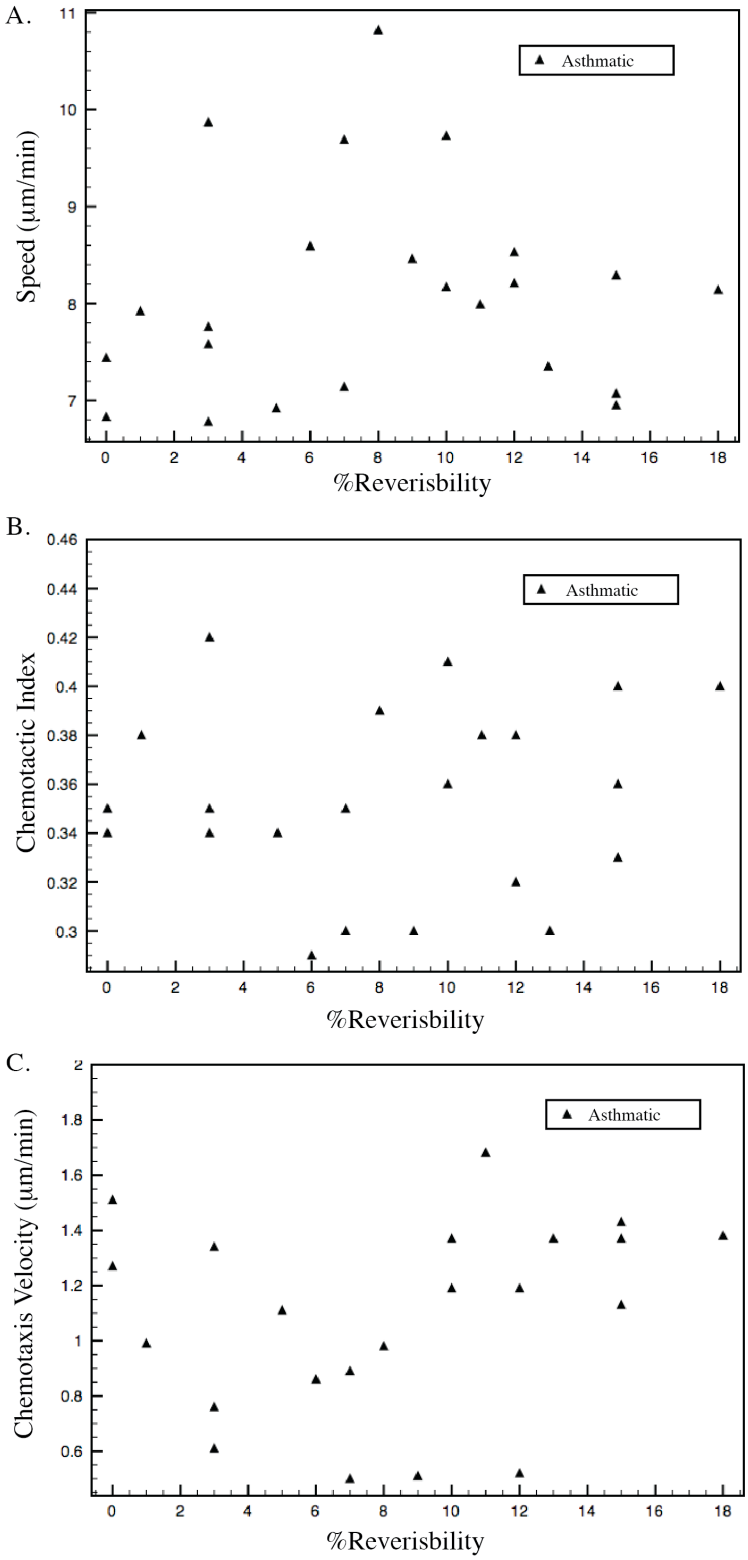

Figure B.4 %Reversibility compared to neutrophil chemotaxis speed (**A**), chemotactic index (**B**), and (**C**) chemotaxis velocity. Only asthmatic patients are reported since insufficient data is available for non-asthmatic patients.

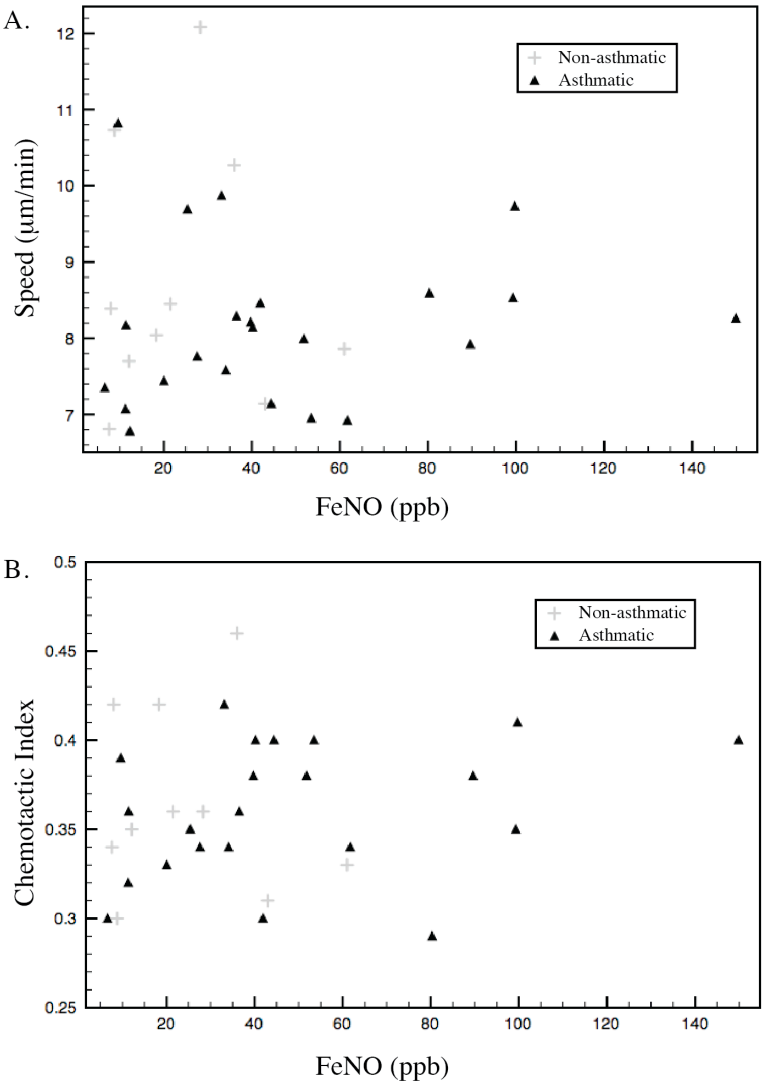

Figure B.5 FeNO compared to neutrophil chemotaxis speed (**A**) and chemotactic index (**B**). No apparent correlations between the neutrophil chemotaxis outputs and FeNO values.

Figure B6. Workflow of performing the microfluidic asthma characterization assay

Diagnostic chip base microchannels for neutrophil sorting & chemotaxis

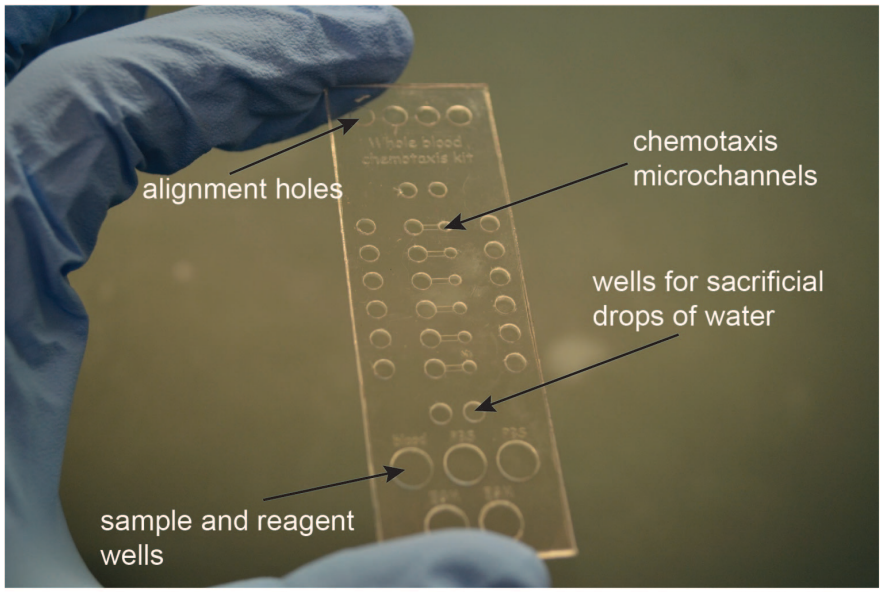

A) Image shows the features of the "base" component of the asthma diagnostic chip. Prior to performing the neutrophil sorting and chemotaxis, the microchannels should be coated with recombinant human P-selectin (see Materials and Methods). The channels should be rinsed with two replacements of PBS prior to flowing in dilute blood and initiating the assay.

Lid component of diagnostic chip for reagents and preventing evaporation

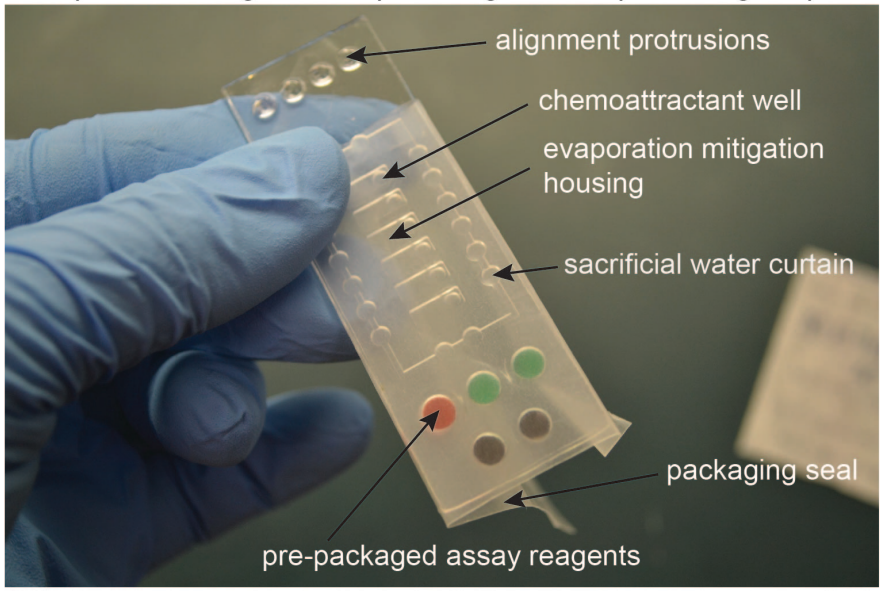

B) Image shows the features of the "lid" component of the asthma diagnostic chip, with the dyed liquid representing different reagents in the assay. The diagnostic assay can be pre-packaged by filling the lid with the required reagents to run the diagnotstic test. Reagents can be frozen down and sealed, allowing the user to simply remove the seal and thaw the reagents prior to initiating the assay.

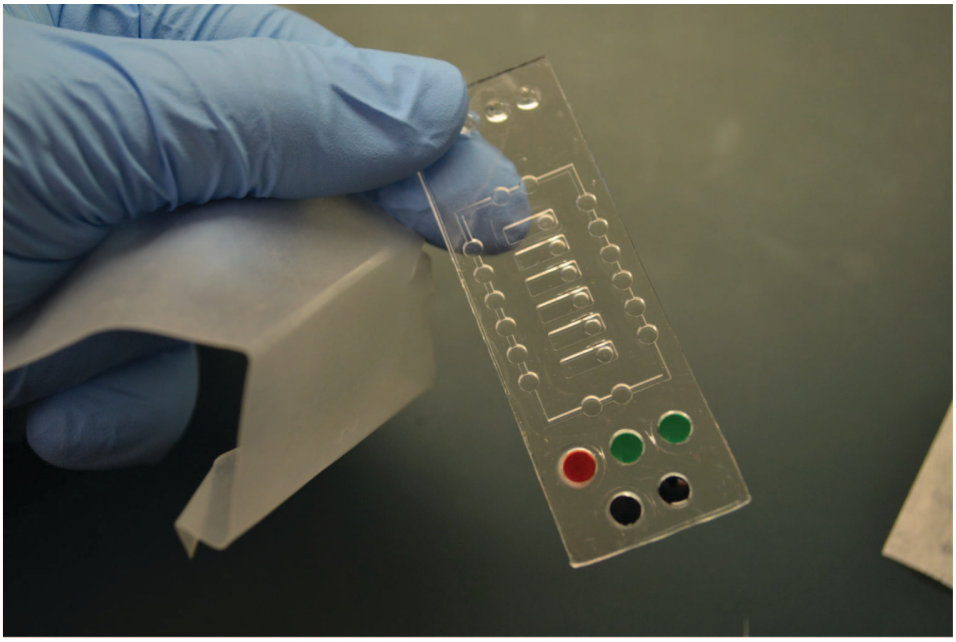

C) Remove the seal and allow the reagents to thaw at room temperature (1-2 minutes). The seal should be removed before the media has thawed to prevent reagents from adhering to the seal following the solid-to-liquid phase change.

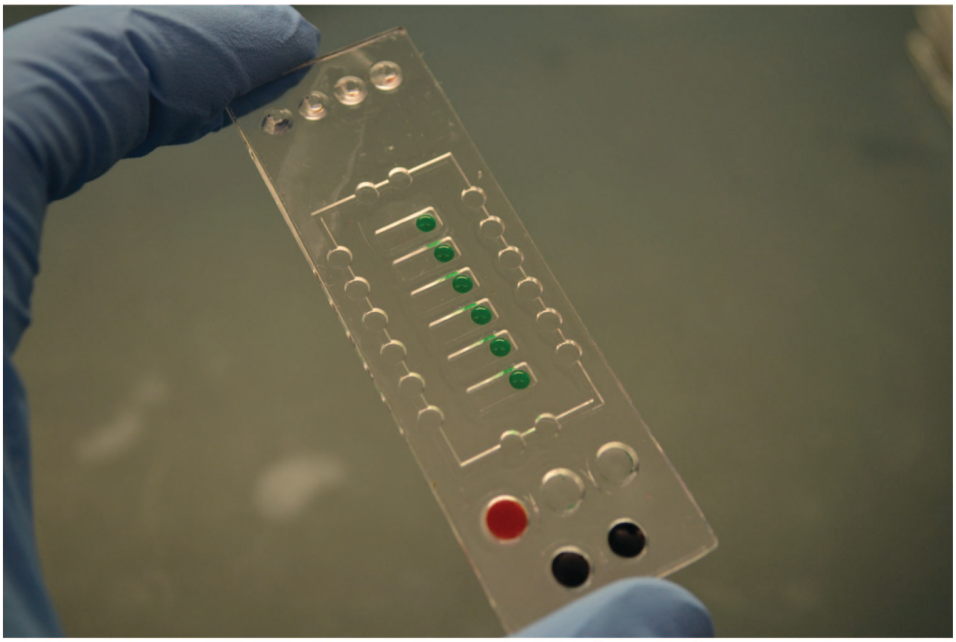

D) Pipet 3 μL drops of the hydrogel-chemoattractant (H-CA) mixture into the "chemoattractant well." If 3 μL drops do not realiably make contact to the output port drops of media in the base microchannels, larger volumes of H-CA should be used. The H-CA mixture is represented by the green liquid.

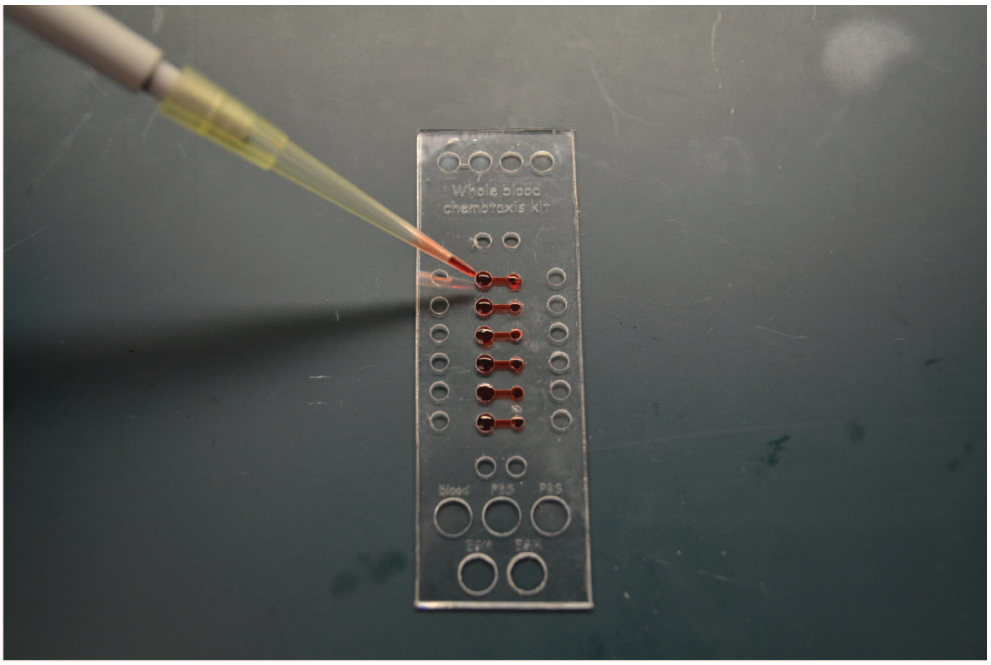

E) After performing a lancet puncture on the finger of the patient, dilute the whole blood into PBS in the vacant “blood” well (see Methods and Materials). Pump 1 μL of dilute blood into the microchannel for neutrophil capture. Blood can be passed through the microchannels multiple times to further enrich the surface with neutrophils. Perform several wash steps to remove erythrocytes from micorchannels.

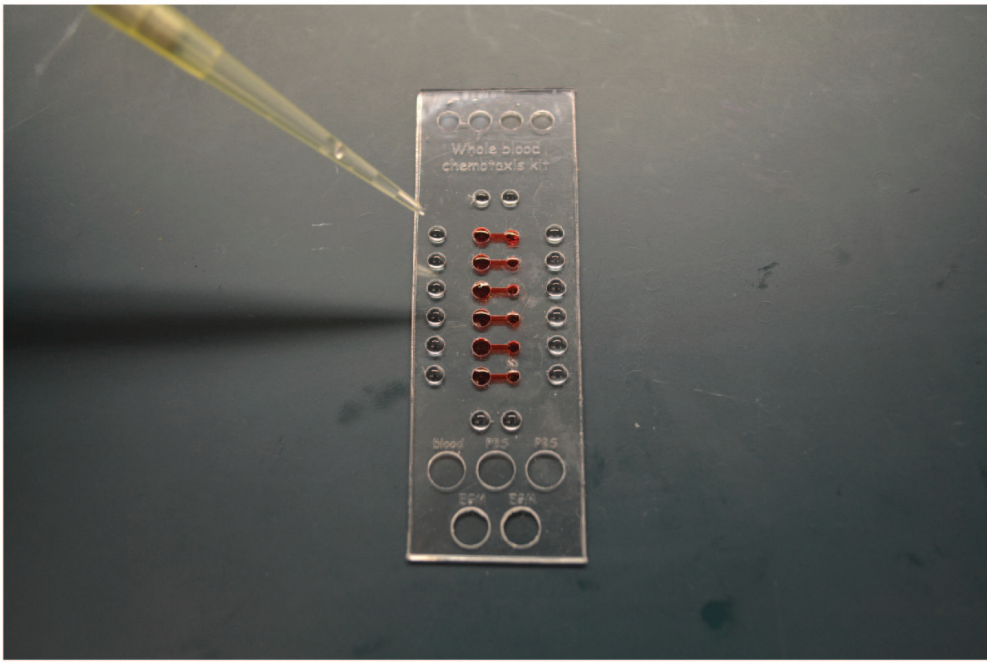

F) Pipet 6 μL drops PBS into the wells for sacrificial liquid. These drops help to mitigate evaporation during the timelapse imaging portion of the assay.

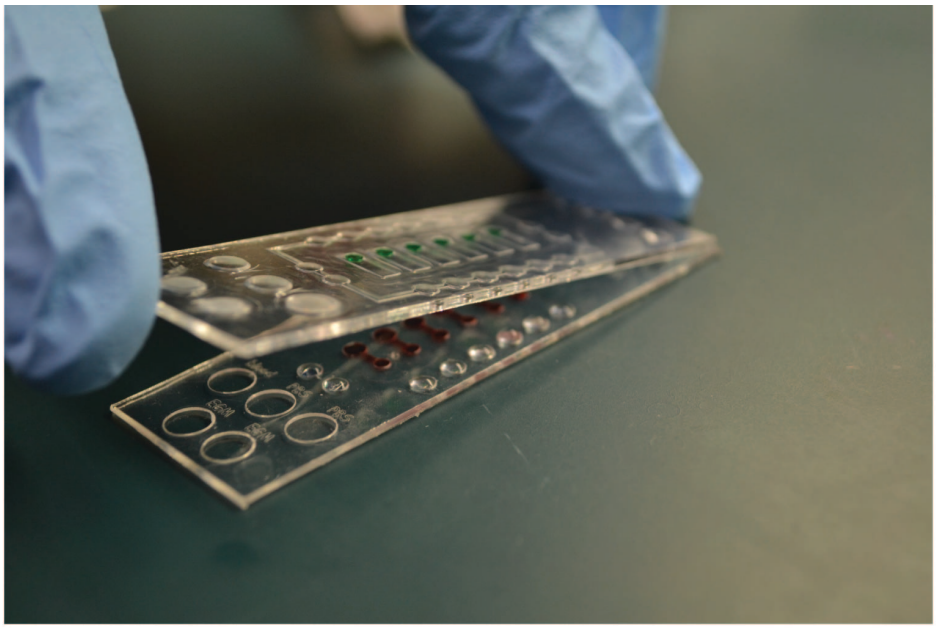

G) After heating up the lid and base of the diagnostic assay to 37 degrees celcius in an humidified chamber (~3 minutes), use the alignment protrusions and wells to place the lid onto the base. The H-CA (shown in green) should make contact with the media in the base microchannels, allowing for diffusion of the chemoattractant into the microchannels to form a chemical gradient.

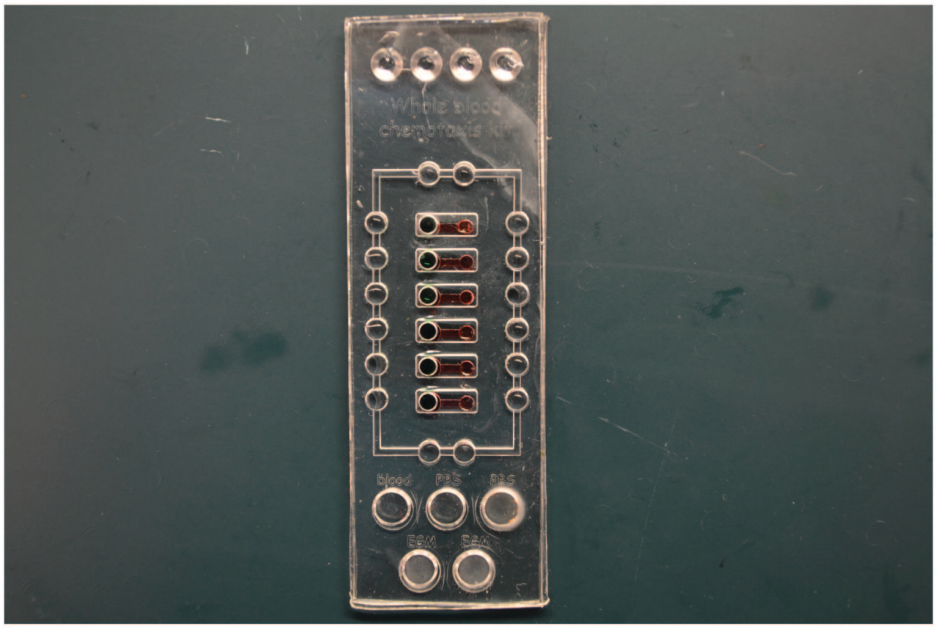

end

H) Image shows lid-base combination of the diagnostic assay. The liquid droplets of PBS in the sacraficial liquid wells will wick into the hydrophilic channels in the lid to form a “liquid curtain” to mitigate evaporation. Once the lid has been placed onto the base, the chip can be placed on a stage for timelapse imaging.

Table B1: Comparative diagnostic performance of other methods compared to microfluidic test

Diagnostic Test	Cutoff	Sensitivity	Specificity	Citation
FeNO (ppb)	46	32	93	Schneider, 2009.
	20	77	64	Fortuna, 2007.
	20	64	59	Miedinger, 2007.
	47	42	96	
	13	85	80	Dupont, 2003.
	19	85	52	Kostikas, 2008.
	40	79	90	Fukuhara, 2011.
	20	67	52	Menzies, 2008.
%Eos (BAL)	3	41	75	Fortuna, 2007.
	1	72	80	Hunter, 2002.
	5	85	92	Park, 1998.
PC20	8 mg/mL	91	90	Hunter, 2002.
	–	78	94	Miedinger, 2007.
	16 mg/mL	41	85	Fortuna, 2007.
FEV1	80	22	100	Fortuna, 2007.
FEV1/FVC	76.6%	61	60	Hunter, 2002.
Chemotaxis Test	1.545 (μm/min)	96	73	–